

AD-A092 264

SCIENTIFIC RESEARCH CENTER SANTA MONICA CA
THEORETICAL STUDIES OF LOW-LOSS OPTICAL FIBERS. (U)
SEP 80 W SPARKS, W FREDERICKS, D MILLS

F/6 20/6

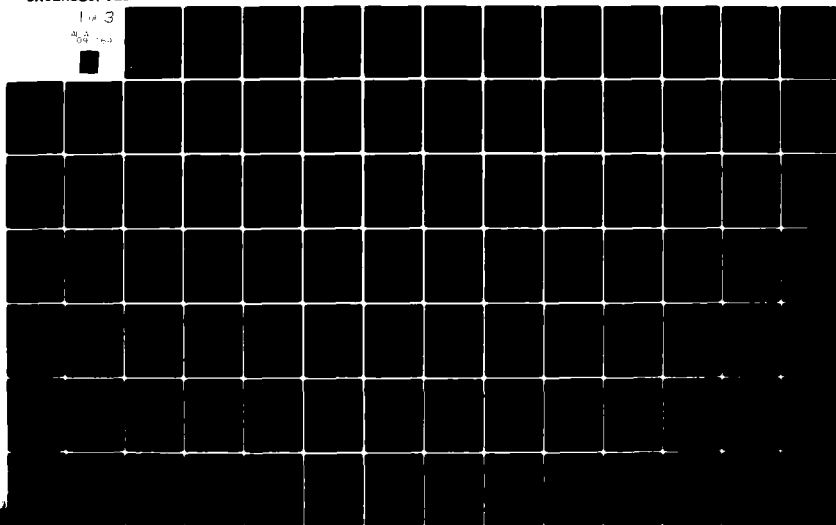
N00173-79-C-0361

UNCLASSIFIED

NL

1 of 3

AD-A092 264



LEVEL

(13)

AD A092264

THEORETICAL STUDIES OF LOW-LOSS OPTICAL FIBERS

M. Sparks

Prepared for
THE NAVAL RESEARCH LABORATORY
Washington, DC 20375

DTIC
DEC 1 1980

FINAL REPORT

Contract Number N00173-79-C-0361

15 August 1980

SCIENTIFIC RESEARCH CENTER
1640 Fifth Street
Suite 216
Santa Monica, CA 90401

DISTRIBUTION STATEMENT A
Approved for public release;
Distribution unlimited

DDC FILE COPY

8011 10 023

SA-PA-2-071

REPORT DOCUMENTATION PAGE		READ INSTRUCTIONS BEFORE COMPLETING FORM
1. REPORT NUMBER	2. GOVT ACCESSION NO. AD-A092264	3. RECIPIENT'S CATALOG NUMBER
4. TITLE (and Subtitle) THEORETICAL STUDIES OF LOW-LOSS OPTICAL FIBERS		5. TYPE OF REPORT & PERIOD COVERED Final 9/28/79 - 9/15/80
7. AUTHOR(s) M. Sparks, W. Fredericks, D. Mills and R. Warren.		6. PERFORMING ORG. REPORT NUMBER
9. PERFORMING ORGANIZATION NAME AND ADDRESS Scientific Research Center 1640 Fifth Street Santa Monica, CA 90401		8. CONTRACT OR GRANT NUMBER(s) N00173-79-C-0361
11. CONTROLLING OFFICE NAME AND ADDRESS Naval Research Laboratory Washington, DC 20375		10. PROGRAM ELEMENT, PROJECT, TASK AREA & WORK UNIT NUMBERS 11/15 21 001
14. MONITORING AGENCY NAME & ADDRESS (if different from Controlling Office) Defense Advanced Research Projects Administration 1400 Wilshire Boulevard Arlington, VA 22209		12. REPORT DATE 9/15/80
		13. NUMBER OF PAGES 217
		15. SECURITY CLASS. (of this report) unclassified
		15a. DECLASSIFICATION DOWNGRADING SCHEDULE
16. DISTRIBUTION STATEMENT (of this Report) unrestricted		
17. DISTRIBUTION STATEMENT (of the abstract entered in Block 20, if different from Report) unrestricted		
18. SUPPLEMENTARY NOTES		
19. KEY WORDS (Continue on reverse side if necessary and identify by block number) Absorption, crystals, extrinsic, far infrared, fibers, glasses, infrared, intrinsic, optical, scattering, theory.		
20. ABSTRACT (Continue on reverse side if necessary and identify by block number) Extrinsic scattering coefficients (with values as great as 1 to 100 dB/m for any one of seven scattering processes) and extrinsic absorption coefficients (β_{ab} (with impurity concentrations of either isolated impurity ions or molecules, or macroscopic inclusions as low as 10^{-3} to 10^{-4} parts per billion giving $\beta_{ab} = 10^{-2}$ dB/km) must be greatly reduced in order to attain an extinction coefficient $\beta_{ex} = 10^{-2}$ dB/km $= 2 \times 10^{-8}$ cm $^{-1}$, which is extremely low, but is a fairly modest goal for low-loss fibers. There are only a few candidate		

glasses, and current fabrication techniques of crystalline fibers give extinction as great as five orders of magnitude greater than 10^{-2} dB/km. Attaining, maintaining, and even measuring the high purity in both crystals and glasses is expected to be difficult. Impurity-absorption spectra and peak-absorption wavelengths of both infrared and visible/ultraviolet absorption are tabulated for use in identifying troublesome impurities. Experimental absorption coefficients in the infrared region are tabulated to establish the state of the art. Single-crystal alkali halides may be rendered useless as low-loss fiber materials by surface imperfections (steps) and fracture, both induced by bending. Plots of intrinsic-scattering- and absorption-coefficients, the so called V curves, which are compiled here, are useful in establishing the wavelength region in which intrinsic loss is negligible. But it is not necessary to operate at the minimum of the V curve because extrinsic scattering and absorption are expected to limit the loss. Values of the zero-dispersion-crossover wavelength λ_{D0} (at which $d^2n/d\lambda^2 = 0$) are tabulated because information-carrying fibers must be operated near λ_{D0} . The choice of the optimum operating wavelength involves compromises in view of the conflicts in the above requirements. The issues involved in the choice between single-crystal- and polycrystalline-fibers are identified even though the choice cannot be made with confidence at present, especially in view of the excessive scattering and absorption in both single-crystal- and polycrystalline-fibers. A new extrusion technique using a quartz capillary with a square exit, with hydrogen-chloride flushing and argon cooling, is proposed. Intrinsic Rayleigh plus Brillouin scattering has typical scattering coefficients at $1 \mu\text{m}$ ranging from 4×10^{-4} to 0.4 dB/km for the typical materials considered. Intrinsic Raman scattering can be much greater, by a factor of 40 in the examples, than the Brillouin scattering, which is sometimes tacitly assumed to set the intrinsic scattering limit. Scattering from vacancies or impurity ions, either isolated or in small clusters, is negligible, but scattering from extended imperfections can be great. Quenching or annealing temporarily changes clustering and scattering, but clustering and water or OH^- uptake cause scattering in alkali halides to increase with crystal age. It is shown that multiple scattering and scattering by the strain field around an impurity ion are negligible. Laser-damage thresholds are tabulated.

TABLE OF CONTENTS

	page
Abstract	5
A. Introduction	7
B. Scattering by Macroscopic Imperfections	13
C. Defect Chemistry of Alkali Halides and Their Optical Properties	31
D. Light Scattering by Point Defects in Insulating Crystals	70
E. Multiple Scattering	86
F. Tabulation of Infrared-Absorption Coefficients	101
G. V Curves of Absorption and Scattering	170
H. Extrinsic Absorption	179
I. Tabulation of Laser-Breakdown Thresholds of Solids	194
J. Optimum Frequency Range	201
K. Choice of Glass-, Polycrystalline-, or Single-Crystal-Fibers	206
L. Publications	212
M. Summary and Conclusions	213

Accession For	✓
RTIS	
INDEX	
Unrec'd	
Just	
By	
Date	

A

ABSTRACT

Extrinsic scattering coefficients (with values as great as 1 to 100 dB/km for any one of seven scattering processes) and extrinsic absorption coefficients β_{ab} (with impurity concentrations of either isolated impurity ions or molecules or macroscopic inclusions as low as 10^{-3} to 10^{-4} parts per billion giving $\beta_{ab} = 10^{-2}$ dB/km) must be greatly reduced in order to attain an extinction coefficient $\beta_{ex} = 10^{-2}$ dB/km $= 2 \times 10^{-8}$ cm $^{-1}$, which is extremely low, but is a fairly modest goal for low-loss fibers. There are only a few candidate glasses, and current fabrication techniques of crystalline fibers give extinction as great as five orders of magnitude greater than 10^{-2} dB/km. Attaining, maintaining, and even measuring the high purity in both crystals and glasses is expected to be difficult. Impurity-absorption spectra and peak-absorption wavelengths of both infrared and visible/ultraviolet absorption are tabulated for use in identifying troublesome impurities. Experimental absorption coefficients in the infrared region are tabulated to establish the state of the art. Single-crystal alkali halides may be rendered useless as low-loss fiber materials by surface imperfections (steps) and fracture, both induced by bending. Plots of intrinsic-scattering- and absorption-coefficients, the so-called V curves, which are compiled here, are useful in establishing the wavelength region in which intrinsic loss is negligible. But it is not necessary to operate at the minimum of the V curve because extrinsic scattering and absorption are expected to limit the loss. Values of the zero-dispersion-crossover wavelength

λ_{0d} (at which $d^2n/d\lambda^2 = 0$) are tabulated because information-carrying fibers must be operated near λ_{0d} . The choice of the optimum operating wavelength involves compromises in view of the conflicts in the above requirements. The issues involved in the choice between single-crystal- and polycrystalline-fibers are identified even though the choice cannot be made with confidence at present, especially in view of the excessive scattering and absorption in both single-crystal- and polycrystalline-fibers. A new extrusion technique using a quartz capillary with a square exit, with hydrogen-chloride flushing and argon cooling, is proposed. Intrinsic Rayleigh plus Brillouin scattering has typical scattering coefficients at $1 \mu\text{m}$ ranging from 4×10^{-4} to 0.4 dB/km for the typical materials considered. Intrinsic Raman scattering can be much greater, by a factor of 40 in the examples, than the Brillouin scattering, which is sometimes tacitly assumed to set the intrinsic scattering limit. Scattering from vacancies or impurity ions, either isolated or in small clusters, is negligible, but scattering from extended imperfections can be great. Quenching or annealing temporarily changes clustering and scattering, but clustering and water or OH^- uptake cause scattering in alkali halides to increase with crystal age. It is shown that multiple scattering and scattering by the strain field around an impurity ion are negligible. Laser-damage thresholds are tabulated.

A. INTRODUCTION

The purpose of the program is to perform theoretical analyses of fiber materials and fibers in order to determine the practical- and ultimate-intrinsic-limits of low-loss fibers. Potential uses of low-loss fibers include long-distance communications, power transmission, and such devices as various detectors. The most important limitations to attaining useful low-loss fibers are the losses--by absorption and particularly scattering--and dispersion, which limits the bandwidth in communications fibers. The emphasis of the program is on crystalline fibers, not necessarily because they were expected to be superior to glass fibers, but because analysis of crystalline fibers was badly needed.

The character of the study changed considerably since the study was first proposed. Originally, absorption and Brillouin scattering, displayed in V curves as discussed below, were discussed as intrinsic limits, and the practical limit was considered to be the purification of the materials to reduce the absorption. Since scattering in crystalline fibers, both polycrystalline and single-crystal, is a severe problem that must be solved before reducing the absorption will be useful, the scattering investigation became a major part of the program.

The loss, or attenuation, is characterized by the extinction coefficient $\beta_{ex} = \beta_{ab} + \beta_{sc}$, consisting of absorption β_{ab} and scattering β_{sc} contributions. The lowest loss attained to date is $\beta_{ex} = 0.3$ dB/km for a fused-silica fiber at $1.6 \mu\text{m}$. Other low attained values of current interest are 2 dB/km at $0.85 \mu\text{m}$ and 0.5 dB/km at $1.3 \mu\text{m}$. For commercially available fiber, 1.5 dB/km for 1 to $1.6 \mu\text{m}$ operation is considered standard-product performance.¹

Recall that $1 \text{ dB/km} = 2.3 \times 10^{-6} \text{ cm}^{-1}$, which is an extremely low loss.

The value of 0.3 dB/km is believed to be the intrinsic $1.6 \mu\text{m}$ value and the lowest attainable value at any wavelength for fused silica. After many years of research, the intrinsic limit of fused silica has been reached. Thus, other materials must be considered in order to obtain lower loss. Both glasses and crystalline materials are candidates. Crystalline materials have both potentially lower scattering and absorption, but severe technical problems must be overcome before the potential of crystalline fibers can be realized.

The goal of the Clearday program, as the low-loss fiber program of the Defense Advance Research Projects Agency is called, was originally to reduce the loss to such low values as 10^{-4} dB/km or even lower. Since such low values are now considered to be unrealistic for the near future, the goal is to reduce the loss as much as possible below these current values. For example, reduction in the loss by a factor of 30 would give $\beta_{\text{ex}} = 10^{-2} \text{ dB/km}$ as a typical goal.

In selecting low-loss materials, V curves are usually used.² The V curves are plots of the absorption coefficient and the scattering coefficient as functions of frequency, as illustrated by the tabulation of V curves in Sec. G. Even though the V curves have been considered extensively in the literature and are useful for glasses, they are perhaps more misleading than useful for crystalline materials at present. First, the scattering half of the V is the intrinsic Brillouin scattering. The low theoretical value of the Brillouin scattering in crystals was indeed one of the initial reasons for considering crystals for low-loss fibers. However, as shown in Secs. B through E, extrinsic scattering is currently

several orders of magnitude greater than the intrinsic Brillouin scattering. Reduction of the scattering in crystalline fibers, even single crystals, is a cardinal problem that must be solved in order to attain low-attenuation fibers.

Second, the dispersion (particularly $d^2n/d\lambda^2$, where n is the real part of the index of refraction and λ is the wavelength), rather than loss, often limits the use of fibers because signals carrying information necessarily have nonzero bandwidth and the different frequencies within the bandwidth travel at different velocities.

The importance of the material dispersion, as $d^2n/d\lambda^2$ will be called, can be seen as follows: The group velocity is

$$v_g = \frac{d\omega}{d\beta} = \frac{c}{d\beta/dk_{\text{vac}}} , \quad (1)$$

where $k_{\text{vac}} = 2\pi/\lambda$, λ is the wavelength in vacuum, $\omega = ck_{\text{vac}}$, and the propagation constant β (denoted by k in some references) determines the spatial phase ($E \sim \exp(i\beta z)$ for propagation along the z axis). Both the propagation characteristics of the fiber and wavelength dependence of the refractive index n determine the dependence of β on k_{vac} . The function $\beta(k_{\text{vac}})$ is complicated in general. However, by considering the effects of the propagation characteristics alone and the refractive-index dispersion alone, it can be shown that the refractive-index dispersion usually dominates the propagation-characteristic dispersion.³

The following calculation shows that the refractive-index dispersion is zero when the material dispersion $d^2n/d\lambda^2 = 0$. In order for the various frequency components of an information-carrying laser signal to arrive at the output-end of the fiber at the same time, the group velocity must

be independent of the frequency, that is, $dv_g/d\omega = 0$. For propagation of a plane wave in an infinite medium of dispersive refractive index $n(\lambda)$, the propagation constant is

$$\beta = nk_{\text{vac}} \quad (2)$$

Assuming an infinite medium is equivalent to formally neglecting the propagation characteristics of the fiber. The derivative of v_g in Eq. (1) is

$$\frac{dv_g}{d\omega} = \frac{1}{c} \frac{dv_g}{dk_{\text{vac}}} = - \frac{d^2(nk_{\text{vac}})/dk_{\text{vac}}^2}{(d\beta/dk_{\text{vac}})^2}.$$

The value of $dv_g/d\omega$ is zero at

$$d^2(nk_{\text{vac}})/dk_{\text{vac}}^2 = 0 \quad (3)$$

With $k_{\text{vac}} = 2\pi/\lambda$, where λ is the vacuum wavelength, it is easy to show that Eq. (3) is satisfied when

$$d^2n/d\lambda^2 = 0 \quad (4)$$

is satisfied. The wavelength at which $d^2n/d\lambda^2 = 0$ is called the zero-dispersion-crossover wavelength.

Third, the extremely low values of the extinction coefficients at the minima of the V curves for many crystalline materials surely cannot be attained in practice in the foreseeable future. In addition to the scattering limitations mentioned above, the purity of the crystals required to attain the low absorption is unrealistically low in at least most cases of interest. As discussed in Sec. H, impurity concentrations of only 10^{-4} part per billion

can give rise to a typical goal value of the absorption coefficient, $\beta = 10^{-2}$ dB/km. Even the measurements of both the impurity concentrations of 10^{-4} parts per billion and the absorption coefficient $\beta = 10^{-2}$ dB/km are beyond the current state of the art.

In high-power laser windows, absorption is usually more important than scattering because absorption leads directly to heating, which in turn leads to such failure as fracture, vaporization, plasma ignition, or optical distortion. By contrast, the total loss, including scattering as well as absorption, is believed to be the limiting factor in low-loss fibers.

There are many related topics that are not considered in the present investigation. These include: applications of fibers, refractive-index gradation, claddings, and guided-mode theory.

REFERENCES

1. C. K. Kao, "Future of Optical Fiber Systems for Undersea Applications,"
Sea Tech., p.13, (May 1980)
2. J. A. Harrington and M. Braunstein, "Scattering Losses in Single and
Polycrystalline Materials for Infrared Fiber Applications," unpublished.
3. Detlef Gloge, IEEE Trans. Microwave Theory Tech. MTT 23, 106-120 (1975).

B. SCATTERING BY MACROSCOPIC IMPERFECTIONS

In this section it is shown that scattering is the most serious problem limiting the operation of low-loss fibers of crystalline materials, both polycrystalline and single-crystal. Any one of the following extrinsic scattering processes can limit the total loss to values orders of magnitude in excess of the intrinsic value:

- surface imperfections,
- voids,
- macroscopic inclusions,
- dislocations,
- strains,
- grain boundaries in noncubic crystals,
- contaminated grain boundaries or imperfections, and
- impurities, especially in clusters.

All of these scattering mechanisms are potentially more severe in fibers than in bulk crystals because current processes of forming the crystalline fibers, such as extrusion, hot rolling, direct growth, and others induce sources of scattering. Values of the scattering coefficients β_{sc} that are calculated in the present section are listed in Table I. These very large values of β_{sc} --ranging from ~ 0.01 to ~ 100 dB/m--compared with the typical goal of 10^{-5} dB/m, clearly illustrate the severity of the scattering problem.

A complete formalism of the scattering problem is given in Sec. E. The simple estimates in the present section suffice for current use because the scattering is so strong that the simple estimates are sufficiently accurate to show that the scattering is overpowering.

First consider scattering by voids or macroscopic inclusions. The simple model of spherical particles of refractive index n_r and density N particles per unit volume imbedded in a host dielectric of refractive index n_H is used. The absorption coefficient for this Rayleigh-Mie scattering is well known.^{1,2,3} A typical scattering cross section σ_s of a single particle of radius a as a function of $k_H a$, where $k_H = n_H k$ with $k = 2\pi/\lambda$, is sketched in Fig. 1.

The particles of interest have $ka \gtrsim 1$; thus the scattering cross section is approximately equal to twice the geometrical cross section $\sigma_g = \pi a^2$. As an example of $ka \gtrsim 1$ being satisfied, solving $k_H a = 1$ for a gives

$$a = \lambda/2\pi n_H \quad (1)$$

with $n_H = 1.5$, Eq. (1) gives $a = 0.11\lambda$, and for $\lambda = 1 \mu\text{m}$, the value of a is $0.11 \mu\text{m}$. Particles with $a \lesssim \lambda/2\pi n_H$ have smaller cross sections, as seen in Fig. 1 and discussed below.

The scattering coefficient β_{sc} is

$$\beta_{sc} = \sigma_s N \quad (2a)$$

$$\cong 2\pi a^2 N, \quad \text{for } ka \gtrsim 1 \quad (2b)$$

$$\cong (4/27) (n_r^2 - n_H^2)^2 (k_H a)^4 \pi a^2 N, \quad \text{for } ka \lesssim 1 \quad (2c)$$

Equation (2a) is the standard expression for β_{sc} in terms of σ_s ; Eq. (2a) follows by setting $\sigma_s \cong 2\pi a^2$; and Eq. (2c) is the usual Rayleigh result.^{1,2,3} The factor of two in the cross section is discussed in standard texts.^{1,2} For a typical case of $1 \mu\text{m}$ - radius particles or voids spaced $200 \mu\text{m}$ apart, the density is

$$N = (1/200 \text{ } \mu\text{m})^3 = 1.2 \times 10^5 \text{ cm}^{-3},$$

and for $ka \gtrsim 1$ (that is, $\lambda \gtrsim 9.4 \text{ } \mu\text{m}$ for $n_H = 1.5$), Eq (2b) gives,

$$\beta_{sc} = 7.8 \times 10^{-3} \text{ cm}^{-1} = 3.4 \text{ dB/m}$$

Thus, the small concentration of 10^5 cm^{-3} of $1 \text{ } \mu\text{m}$ radius particles gives rise to a scattering coefficient that is five orders of magnitude greater than a typical goal of 10^{-2} dB/km . The concentration $1.2 \times 10^5 \text{ cm}^{-3}$ and radius $a = 1 \text{ } \mu\text{m}$ correspond to a fractional volume f_V of

$$\begin{aligned} f_V &= V_{\text{particles}}/V_{\text{sample}} = (4\pi/3)a^3N \\ &= 5.2 \times 10^7 = 0.52 \text{ ppm.} \end{aligned}$$

This small fractional volume corresponds to the very large value of 3.4 dB/m . The fiber must be essentially particle and void free in order to attain the goal of $\beta_{sc} \ll 1 \text{ dB/km}$.

In the calculation above, it was tacitly assumed that the scattering cross section σ_{sc} corresponds to scattering out of the fiber. This approximation is well satisfied for the purpose of the estimate because the scattering angle for a single sphere is approximately πn_Δ , where $n_\Delta = |n_H - n_r|$, as will be shown below. This approximate value gives a scattering angle of $\pi/2$ for $n_H = 1.5$ and $n_r = 1.0$. Even though the approximation breaks down for such a large scattering angle (because the scattering angles at the front and rear surfaces of the sphere were assumed to be equal), the estimate indicates that a single scattering is sufficient to scatter most of the rays outside the angle of total internal reflection.

Next consider the contribution to the scattering coefficient from surface imperfections on the fiber. Somewhat greater care is required to obtain reliable estimates for the surface-induced scattering than for the scattering by voids or inclusions in the bulk of the fiber. Nevertheless, in view of the overwhelming effect of scattering in the spherical-particle model above, it is intuitively obvious that the fiber surfaces must be essentially free of imperfections such as the "fish-scales" observed by Harrington and coworkers⁴ and voids or protrusions on the fiber surface.

Single-mode fiber operation is of interest in communications. Marcuse^{5,6,7} has shown that surface imperfections are a strong source scattering loss in single-mode operation of both round dielectric waveguides, including fibers, and dielectric-slab waveguides. For example, "the radiation losses caused by surface roughness of a fiber designed for single mode operation at 1 μm wavelength can be as high as 10 dB/km for an rms variation of the fiber wall of as little as 8 \AA ." This and other examples obtained for special cases of Marcuse's general results (as in Table I) clearly indicate that fiber surfaces must be nearly perfect in order to attain even the state-of-the-art values of 0.3 dB/km.

At the risk of oversimplification, the following simplified estimate explains the exceptionally strong scattering from large-diameter multimode scaley fibers fortuitously well. A typical scattering coefficient for a scaley fiber is

$$\beta_{\text{sc}} = 20 \text{ dB/m} \quad (3)$$

for a 250 μm -radius multimode potassium-chloride fiber.⁸

The strongly multimode-fiber irradiance is considered as a collection of rays that can be treated by ray tracing, with diffraction added formally.

A ray through the center of a circular fiber making a small angle θ with the fiber axis travels a transverse distance $2a_f$, where a_f is the fiber radius, in a distance L , where

$$\theta L \cong 2a_f. \quad (4)$$

The number of times that the ray reflects off the surface before the irradiance is reduced by a factor of $1/e$ is denoted n_B . For surface imperfections of dimension a (the radius of a hemispherical pit, for example) sufficiently large for $k_H a \gtrsim 1$ to be satisfied, the large-scattering cross section $\sigma_s \cong 2\pi a^2$ for a spherical void in an infinite medium suggests that the scattering is strong at the surface. Thus, a reasonable value of n_B is

$$n_B \cong 4, \quad \text{for } k_H a > 1. \quad (5)$$

Formally reducing the scattering by a factor of $(4/27)(n_H^2 - 1)^2(k_H a)^4 \equiv \epsilon$ for $k_H a \gtrsim 1$, according to Eq. (2c), gives the following equation for n_B

$$(1 - \epsilon)^{n_B/4} = 1/e \quad (6)$$

For $\epsilon \ll 1$, Eq. (6) gives

$$n_B \cong 4/\epsilon = 4[(4/27)(n_H^2 - 1)^2(k_H a)^4]^{-1} \quad (7)$$

Setting $\beta_{sc} = (n_B L)^{-1}$ and using Eqs. (4), (5), and (7) gives

$$\beta_{sc} = \theta/8a_f, \quad \text{for } k_H a \gtrsim 1 \quad (8a)$$

$$= (1/54)(n_H^2 - 1)^2(k_H a)^4 \theta/a_f, \quad \text{for } k_H a \gtrsim 1 \quad (8b)$$

The value of θ to be used in Eq. (8) is determined by the divergence and alignment of the incident laser beam, the deviation from straightness of the fiber, and diffraction. For the diffraction limit, the value of θ is formally

$$\theta = 1.2\lambda/2a_f \quad . \quad (9)$$

For the case of $a_f = 250 \mu\text{m}$, $\lambda = 10.6 \mu\text{m}$, and $k_H a > 1$, Eqs. (8a) and (9) give

$$\theta = 1.27 \times 10^{-2} \text{ rad} \quad (10)$$

$$\beta_{sc} = 0.254 \text{ cm}^{-1} = 55 \text{ dB/m} \quad (11)$$

in excellent agreement with the typical experiment value of $\beta_{sc} = 20 \text{ dB/m}$ in Eq. (3).

Next consider the optical scattering by dislocations. The order of magnitude of β_{sc} is obtained by the following simple estimate of the scattering by the stress field associated with a dislocation. The magnitude of the stress in the vicinity of an edge dislocation is⁹

$$\sigma_{\rho\rho} = \sigma_{\theta\theta} = - \frac{Gb}{2(1-\nu)} \frac{\sin\theta}{\rho} \quad (12)$$

$$\sigma_{\rho\theta} = \frac{Gb}{2(1-\nu)} \frac{\cos\theta}{\rho} \quad (13)$$

where G is the shear modulus, b is the Burgers-vector amplitude of the displacement, ν is the Poisson ratio, and ρ and θ are cylindrical coordinates.

For the order-of-magnitude estimate, the angle factors in Eqs. (12) and (13) are formally neglected, giving

$$\begin{aligned}\sigma &= Gb/2\pi(1 - \nu)\rho, \\ &\cong 1.4\sigma_c b/\rho\end{aligned}\quad (14)$$

where we used the typical value of $\nu = 0.3$ in the second equality. The stress reaches the critical value $\sigma_c = G/2\pi$ for which the lattice becomes unstable at the radius $\rho \cong b$. Thus, the model for the stress is basically valid at distances from the dislocation that are many times the lattice spacing b , which is not surprising in view of the severe lattice disruption at the dislocation itself.

As a further approximation, the stress field is approximated by an infinitely long cylinder of uniform stress. The radius a of the cylinder is chosen as the value ρ at which $\sigma = \sigma_c/10$. With this value of σ , Eq. (14) gives, with typical values of $\nu = 0.3$ and $b = 3 \text{ \AA}$,

$$a \cong 10b/(1 - \nu) \cong 4 \times 10^{-7} \text{ cm}.$$

The average stress in the cylinder is approximately

$$\begin{aligned}\langle \sigma \rangle &= \int_b^a d\rho \rho [\sigma_c b / (1 - \nu) \rho] / \int_b^a d\rho \rho \cong 2b\sigma_c / (1 - \nu)a \\ &= \sigma_c/5\end{aligned}$$

The index of refraction

$$n_r \cong 1 + q \langle \sigma \rangle \cong 1 + q\sigma_c/5 \quad (15)$$

then has a typical value

$$n_r \cong 1 + 3 \times 10^{-3}$$

for a typical value of $\sigma_c = G/2\pi = 3 \times 10^{11} (\text{dyne/cm}^2)/2\pi$ ($= 30 \text{ GPa}/2\pi = 4.4 \times 10^7 \text{ psi}/2\pi$) and a typical value of the strain-optic coefficient $q = 3 \times 10^{-13} \text{ cm}^2/\text{dyne}$ ($= 3 \times 10^{-12} \text{ Pa}^{-1}$).

The scattering cross section per unit length of a thin cylinder of index n_r and radius a , for $ka \geq 1$, is²

$$C = 2a \frac{\pi^2 (ka)^3}{4} \left(\frac{n_r^2 - 1}{n_r^2 + 1} \right)^2. \quad (16)$$

The scattering coefficient is²

$$\beta_{sc} = N_d C \quad (17)$$

where N_d is the number of cylinders per unit area (the dislocation density).

With $\lambda = 1.06 \text{ } \mu\text{m}$, $n_r^2 + 1 \cong 2$, and

$$\begin{aligned} n_r^2 - 1 &= (1 + q\sigma_c/5)^2 - 1 \\ &\cong 2q\sigma_c/5 = 6 \times 10^{-3}, \end{aligned} \quad (18)$$

Eq. (16) gives

$$\begin{aligned} C &= \frac{2(4 \times 10^{-7})\pi^2}{4} \left(\frac{2\pi 4 \times 10^{-7}}{1.06 \times 10^{-4}} \right)^3 \left(\frac{6 \times 10^{-3}}{2} \right)^2 \\ &= 2.4 \times 10^{-16} \text{ cm}. \end{aligned} \quad (19)$$

Since fibers are filled with a large number of dislocations generated by the manufacturing process, we choose the large value

$$N_d = 10^{12} \text{ cm}^{-2} \quad (20)$$

Substituting Eqs. (19) and (20) into Eq. (17) gives

$$\beta_{sc} = 2.4 \times 10^{-4} \text{ cm}^{-1} = 103 \text{ dB/km}$$

This estimated value of β_{sc} is sensitive to changes in the model, particularly the choice of the values of the parameters. Typical dislocation densities N_d range from 10^8 to 10^{12} cm^{-2} . The choice of the value of "a" is also rather sensitive because $C \sim a^4$. Finally, at the longer wavelength 10.6 μm , with $C \sim \lambda^{-3}$, $\beta_{sc} = 0.10 \text{ dB/km}$.

Next consider the scattering by the large inhomogeneous strains induced in crystalline materials by the fiber manufacturing process. The strains could be related to grains, but are not directly related to the grains in general. The inhomogeneities are modeled by a system of spheres of constant stress. The scattering of an individual sphere is estimated, then the total scattering angle is estimated as the random-walk value of $N_s^{1/2} \theta_1$, where N_s is the number of spheres and θ_1 is the average scattering angle for one sphere. When the total scattering angle is sufficiently large that the ray is no longer totally internally reflected, the ray is assumed to be lost by transmission out of the fiber.

Consider the scattering by a sphere of radius a and constant stress σ . The angle of incidence θ_i for a ray having impact parameter ℓ is

$$\theta_i = \sin^{-1} \ell/a. \quad (21a)$$

From Snell's law, the angle of refraction θ_r is given by

$$\theta_r = \sin^{-1} (n_r \sin \theta_i) = \sin^{-1} (n_r \ell/a) \quad . \quad (21b)$$

The deflection angle is

$$\theta_d = \theta_i - \theta_r \quad (21c)$$

Since the ray undergoes a second deflection upon leaving the sphere, the total scattering angle θ_1 for $\theta_1 \ll 1$ is

$$\theta_1 = 2(\theta_i - \theta_r)$$

With

$$n_r = 1 + n_\Delta,$$

Eqs. (21) give (22)

$$\begin{aligned} \theta_1 &\cong 2 \left| \sin^{-1} (\ell/a) - \sin^{-1} (\ell/a + n_\Delta \ell/a) \right| \\ &\cong 2 \left| \sin^{-1} (\ell/a) - \sin^{-1} (\ell/a) - n_\Delta (\ell/a) (1 - \ell^2/a^2)^{-1/2} \right| \\ &= 2n_\Delta \ell (a^2 - \ell^2)^{-1/2} \end{aligned}$$

For uniform illumination of the sphere, the probability of a ray having impact parameter between ℓ and $\ell + \ell_\Delta$ is

$$\frac{2\pi \ell \ell_\Delta}{\pi a^2} = 2 \frac{\ell \ell_\Delta}{a^2}$$

Thus, the expected scattering angle is

$$\begin{aligned}
\langle \theta_1 \rangle &= \int_0^a d\ell \ell \theta_1 / \int_0^a d\ell \ell \\
&= \int_0^a \frac{2n_\Delta \ell}{(a^2 - \ell^2)^{1/2}} \frac{2\ell d\ell}{a^2} \\
&= \int_0^a \frac{2n_\Delta}{a^2} \left(\frac{y}{a^2 - y} \right)^{1/2} dy \\
&= \int_0^1 2n_\Delta \left(\frac{t}{1-t} \right)^{1/2} dt \\
&= 2n_\Delta B\left(\frac{3}{2}, \frac{1}{2}\right)
\end{aligned}$$

$$\langle \theta_1 \rangle = 2n_\Delta \frac{\Gamma(\frac{3}{2})\Gamma(\frac{1}{2})}{\Gamma(2)} = \pi n_\Delta \quad (23)$$

The random-walk result for the expected scattering after N_s scatterings through angle $\langle \theta_1 \rangle$ is

$$\theta_{sc} \cong N_s^{1/2} \langle \theta_1 \rangle \quad (24)$$

Setting θ_{sc} (measured with respect to the fiber axis) equal to $\pi/2 - \theta_{TIR}$, where θ_{TIR} is the critical angle for total internal reflection (measured with respect to the normal to the surface of the fiber) gives

$$N_s = (\pi/2 - \theta_{cr})^2 / \langle \theta_1 \rangle^2 \quad (25)$$

For $n_r = 1.5$,

$$\theta_{cr} = \sin^{-1}(1/1.5) = 0.73 \text{ rad} = 41.8^\circ \quad (26)$$

Substituting Eqs. (23) and (24) into Eq. (25) gives

$$N_s = 7.2 \times 10^{-2} / n_{\Delta}^2 \quad (27)$$

For a distance $4a$ per scattering, the scattering length is

$$\beta_{sc}^{-1} = 4aN_s.$$

With Eq. (27), this gives

$$\beta_{sc} = 3.5n_{\Delta}^2/a \quad (28)$$

The change n_{Δ} in the index of refraction in Eq. (22) is obtained from the approximation

$$n \cong 1 + q\sigma$$

Comparison with Eq. (22) gives

$$n_{\Delta} = q\sigma \quad (29)$$

Substituting Eq. (29) into Eq. (28) gives

$$\beta_{sc} = 3.5q^2\sigma^2/a \quad (30)$$

For the typical value $q \cong 3 \times 10^{-12} \text{Pa}^{-1}$ and a very large value of $\sigma = \sigma_c = 5 \times 10^9 \text{Pa}$ the value of n_{Δ} is 1.5×10^{-2} , and Eq. (30), with $a = a_f/2 = 125 \mu\text{m}$, gives

$$\begin{aligned} \beta_{sc} &= 3.5(1.5 \times 10^{-2})^2 / 125 \times 10^{-4} \text{ cm} \\ &= 6 \times 10^{-2} \text{ cm}^{-1} = 30 \text{ dB/m} \end{aligned} \quad (31)$$

This large value of $\beta_{sc} = 30 \text{ dB/m}$ is attained for a fiber that is severely strained--to the limit of the theoretical strength. For a strain $\sigma = 10^4 \text{ psi} = 6.9 \times 10^7 \text{Pa}$, the corresponding value of β_{cs} is

$$\beta_{sc} = 400 \text{ dB/kM} \quad (32)$$

As a final example, a value of $\beta_{sc} = 10^{-2} \text{ dB/kM}$ corresponds to $\sigma = 0.024 \text{ psi} = 1.7 \times 10^3 \text{ Pa}$, which is an extremely small value. The examples illustrate that the fibers must be essentially strain free in order to attain the goal values of $\beta_{sc} \ll 0.1 \text{ dB/km}$.

Next consider scattering by crystalline grains. For the first case of noncubic crystals, a ray at non-normal incidence on a grain boundary is deflected because the index of refraction for the ray in the two grains is different because the direction of propagation with respect to the crystal axes is different. The scattering angle at a grain boundary is of the order of the difference n in the refractive indices of the two grains. For example, Snell's law is

$$\begin{aligned} n_r \sin \theta_i &= (n_r + n_\Delta) \sin (\theta_i - \theta_d) \\ &= (n_r + n_\Delta) [\sin \theta_i - \theta_d \cos \theta_i + \dots] \end{aligned}$$

Equating the zeroth-order terms gives the identity $n_r \sin \theta_i = n_r \sin \theta_i$, and equating the first-order terms and solving for θ_d gives

$$\theta_d = n_\Delta \tan \theta_i \quad (33a)$$

$$= n_\Delta, \quad \text{at } \theta_i = \pi/4. \quad (33b)$$

As shown in the similar calculation above, the average of $\theta_1 \equiv 2\theta_d$ over a sphere is

$$\langle \theta_1 \rangle = \pi n_\Delta. \quad (34)$$

Also, θ_{sc} is given in terms of $\langle \theta_1 \rangle$ by Eq. (24), and β_{sc} is given by Eq. (28). With $n_{\Delta} = 10^{-2}$, as a typical value of the difference between the indices for propagation along different directions in a noncubic crystal, and $a = a_f/2 = 125 \mu\text{m}$, Eq. (28) gives

$$\beta_{sc} = 2.8 \times 10^{-3} \text{ cm}^{-1} = 1.2 \text{ dB/m} \quad (35)$$

This large value of β_{sc} clearly demonstrates that noncubic polycrystalline fibers will have excessive scattering. They are not useful for low-loss fibers.

Next consider the scattering by crystalline grains in cubic crystals. Theoretically, perfect grain boundaries in cubic crystals do not cause scattering because the value of the index of refraction is independent of the angles between the wavevector of the radiation and the crystal axes. Contaminated grain boundaries can of course cause scattering, as discussed in Secs. C and D. Also, a constant strain can cause scattering at grain boundaries even in cubic crystals because cubic crystals are anisotropic in the strain-optic coupling. A constant stress on a polycrystalline sample of cubic material can also give rise to inhomogeneous strains as a result of the grain structure and the anisotropic elastic constants.

Scattering by impurities, clusters of impurities, voids, and contaminated grain boundaries or other contaminated imperfections are considered in Secs. C and D.

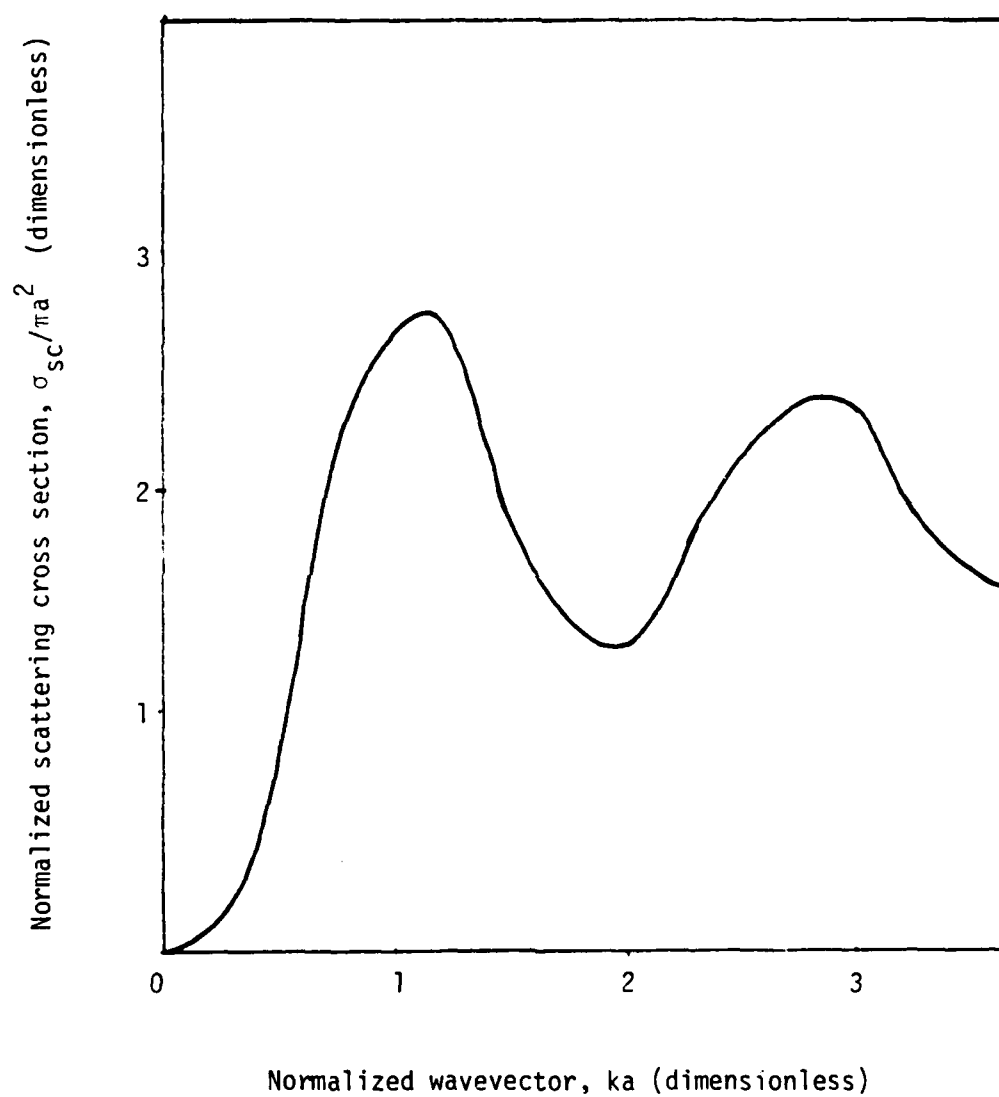
Table I. Tabulation of scattering coefficients estimated in Sec. B.

	β_{sc} (dB/m)	Conditions
voids or inclusions	1.7	typical values of $k_H a \lesssim 1$ ($\lambda \gtrsim 10 \mu\text{m}$), $a = 1 \mu\text{m}$, 200 μm spacing ($f_V = 0.5 \text{ ppm}$)
surface imperfections Marcuse single mode	0.01	very small value of $a = 8\text{\AA}$ at $\lambda = 1 \mu\text{m}$
	2.7	typical value of $a = 1 \mu\text{m}$, $\lambda = 10.6 \mu\text{m}$, $a_f = 37 \mu\text{m}$
surface imperfections multimode	55	typical values of $k_H s \gtrsim 1$, $\theta = 0.013 \text{ rad}$
dislocations	103	$\lambda = 1 \mu\text{m}$ and large value $N_d = 10^{12}$ dis- locations/ cm^2
strains	30	$k_H a \lesssim 1$ and limiting large value $\sigma = 5 \times 10^9 \text{ Pa}$
grain boundaries in noncubic materials	1.2	typical values of $\Delta n = 10^{-2}$ and $ka \gtrsim 1$
typical goal	10^{-5}	-----

FIGURE CAPTIONS

Figure 1. Schematic illustration of a typical extinction cross section for scattering by a sphere.

Figure 1. Schematic illustration of a typical extinction cross section for scattering by a sphere.



REFERENCES FOR SEC. B

1. H. C. Van de Hulst, Light Scattering by Small Particles, 2nd ed. (Wiley, New York, 1972).
2. M. Kerker, The Scattering of Light, 2nd ed. (Academic Press, New York, 1970).
3. E. U. Condon and H. Odishaw, Handbook of Physics, 2nd ed. (McGraw-Hill, New York, 1967).
4. J. A. Harrington and M. Braunstein, "Scattering Losses in Single and Polycrystalline Materials for Infrared Fiber Applications," unpublished.
5. D. Marcuse, "Mode Conversion Caused by Surface Imperfections of a Dielectric Slab Waveguide," Bell Syst. Tech. J. 48, 3187-3215 (1969).
6. D. Marcuse and R. M. Derosier, "Mode Conversion Caused by Diameter Changes of a Round Dielectric Waveguide," Bell Syst. Tech. J. 48, 3217-3232 (1969).
7. D. Marcuse, Bell Syst. Tech. J. 48, 3233-3242 (1969).
8. Dr. James Harrington, private communication, 1980.
9. C. Kittel, Introduction to Solid State Physics, 4th ed. (Wiley, New York, 1971) p. 678.

C. DEFECT CHEMISTRY OF ALKALI HALIDES AND THEIR OPTICAL PROPERTIES

W. J. Fredericks

Department of Chemistry
Oregon State University
Corvallis, Oregon 97331

Intrinsic-Brillouin and intrinsic-Rayleigh scattering, which determine the lowest possible scattering that can be attained in fiber materials, have typical scattering coefficients $\beta_{sc} = \beta_B + \beta_{int R}$ of $1 \times 10^{-9} \text{ cm}^{-1} = 4 \times 10^{-4} \text{ dB/km}$ for lithium fluoride to $8 \times 10^{-7} \text{ cm}^{-1} = 0.4 \text{ dB/km}$ for zinc selenide, both at wavelength $\lambda = 1 \text{ }\mu\text{m}$. The total intrinsic scattering coefficient, for Brillouin and intrinsic Raman scattering, can be much greater--by a factor of 40 in the examples considered--than the Brillouin scattering, in contrast to the tacit assumption made in the standard practice of using the Brillouin scattering in the V curves for crystalline materials. Electronic scattering from vacancies or impurity ions that are either isolated or in small clusters is negligible, but electronic scattering from extended imperfections, such as precipitates, grain boundaries, Suzuki phases, and dislocations can be great. The substantial variations in both the laser breakdown thresholds and the amount of scattering that is observed as various regions of a crystal are probed are explained in terms of the distributions of impurities and imperfections--which

change in time. Quenching temporarily reduces clustering, thereby reducing scattering and possibly isolated-spot laser damage; whereas annealing increases clustering, thereby increasing scattering and possibly isolated-spot laser damage. Clusters are expected to form in time even in quenched crystals, and OH^- and H_2O substantially penetrate alkali-halide crystals if they contain a few parts per million of divalent ions (which are used to strengthen alkali halides).

I. INTRODUCTION

The purpose of this report is to consider the effect of complex defects present in alkali halides on their optical properties. In spectral regions far removed from any optical-absorption band, the limiting transparency of a substance is determined by the amount of light it scatters. Light is scattered from any region that varies in polarizability from the neighboring region of the substance. Both intrinsic scattering and extrinsic scattering are considered. Sources of extrinsic scattering are discussed. Significant results are obtained, as summarized in Sec. V.

The sections of this report are as follows:

- I. Introduction
- II. Intrinsic Scattering
- III. Defect Chemistry of Alkali Halides
- IV. Defect Scattering
- V. Summary and Discussion

II. INTRINSIC SCATTERING

In this section it is shown: that even intrinsic scattering can limit the loss of fibers; that the scattering in even the best current bulk materials is greater than the intrinsic value; and that intrinsic Rayleigh scattering can be much greater than intrinsic Brillouin scattering in materials other than alkali halides.

The limiting case of low scattering occurs when only the thermal fluctuations in density cause scattering of light. Landau and Placzek¹ showed that the intensity of the intrinsic wavelength-unshifted Rayleigh-scattering light to the intensity of the intrinsic shifted Brillouin-scattered light was a constant, η_{LP} . This quantity, known as the Landau-Placzek ratio, is usually expressed as

$$\eta_{LP} = I_R/2I_B = \gamma - 1 = (\beta_T - \beta_S)/\beta_S, \quad (1)$$

where γ is the ratio of the specific heat capacity at constant pressure to that at constant volume and β_T and β_S are the isothermal and adiabatic compressibilities, respectively. Munster² provides a concise review of early development and also discusses later work³. Light scattering has been used to study many theoretical and practical problems, mostly in amorphous materials, which have been extensively reviewed^{4,5,6}.

Most discussions of scattering in crystalline solids have concerned

the hypothetical "pure, perfect crystal."^{7,8} For the present discussion, that case represents the ideal limit; all real crystals will exceed this limit. Landau and Lifshitz⁹ give a convenient expression for η_{LP} as

$$\eta_{LP} = c_{11} T (3\alpha_L)/c_p \quad (2)$$

where c_{11} is a component of the elastic tensor, α_L is the coefficient for thermal expansion and they assumed the index of refraction, n , is independent of temperature, T , at constant density, ρ , (i.e. $(\partial n/\partial T)_\rho = 0$). A more accurate expression has been given by Wehner and Klein¹⁰ as a modification of Landau's and Lifshitz's formula which considers the non-zero value of $(\partial n/\partial T)_\rho$ and from the fact that the transverse strain must vanish in a plane longitudinal wave. Instead a transverse stress is present. In their analysis they reduce these considerations to a dimensionless number, r , which can be evaluated from the elastic constants, the linear thermal expansion coefficient, the elasto-optic coefficients, $(\partial \epsilon/\partial u)_T$, and the thermo-optic coefficients, $(\partial \epsilon/\partial T)_u$, where u is a displacement. They show that the corrected scattering ratio η_{WK} is given as

$$\eta_{WK} = \eta_{LP} (1 - r)^2, \quad (3)$$

where r can be expressed as

$$r = \frac{1}{\alpha_L (1 + 2c_{12}/c_{11})} \frac{(\partial \epsilon_1 / \partial T)_u}{(\partial \epsilon_1 / \partial u)_T} \quad (4)$$

when the coefficients α_L and $(\partial \epsilon / \partial T)_p$ are for hydrostatic conditions and the fluctuations are uniaxial. The two thermo-optic coefficients can then be related by

$$(\partial \epsilon / \partial T)_u = (\partial \epsilon / \partial T)_p + \alpha_L \epsilon_1^2 (p_{11} + \partial p_{12}) \quad (5)$$

where ϵ_1 , p_{ij} are components of the dielectric constant and the elastic-optic (Pockels) coefficient tensors, respectively. Alternately, r can be evaluated from the index of refraction, n , if the appropriate coefficient are available. The corresponding relations are

$$r = \frac{1}{\alpha_L (1 + 2c_{12}/c_{11})} \frac{(\partial n_1 / \partial T)_p}{(\partial n_1 / \partial u_2)_T} \quad (6)$$

and the density-independent thermo-optic coefficient can be related to the pressure independent coefficient by

$$\left(\frac{\partial n}{\partial T}\right)_p = \left(\frac{\partial n}{\partial T}\right)_p + \frac{n^3 \alpha_L (p_{11} + 2p_{22})}{2} \quad (7)$$

when coefficients are for same conditions as in Eq. (5).

Wehner and Klein have evaluated r at room temperature for a variety of crystals. In Table I the ratio r_{WK} has been calculated for a few

selected substances. Most of the data for ϵ , n , p_{ij} and differential coefficients were for visible wavelength with the exception of silicon. The magnitude of the Brillouin scattering coefficient, β_B , can be estimated from Eq. (5)

$$\beta_B = \frac{\pi^2 \epsilon^4 kT}{2\lambda^4} \left\{ \frac{2(p_{12}^2 + p_{44}^2)}{c_{11} + c_{12} + 2c_{44}} + \frac{p_{44}^2}{c_{44}} \right\} \quad (8)$$

using the data in Table II and the relations $(p_{11} - p_{12})/2 = p_{44}$ and $(c_{11} - c_{12})/2 = c_{44}$ for cubic crystals. Then from the basic definition of the Landau-Placzek ratio the Rayleigh scattering coefficient can be estimated from the relation

$$\beta_R = 2\beta_B \eta_{WK} \quad (9)$$

The sum $\beta_R + \beta_B$ provides a measure of the limiting loss of light in a substance through non-absorption processes. At room temperature LiF and NaF are the most transparent of the substances considered here. However at other temperatures or in wavelength regions where the tails of absorption bands cause n or ϵ to vary this may not be so. The latter problem has been considered extensively¹². Temperature effects enter in a more subtle way. Pohl and Schwarz¹¹ discuss the exceptional case of NaF. The temperature dependence of η_{WK} and the Rayleigh scattering coefficient is determined by α_L , p_{ij} , n , or ϵ and $(\partial n/\partial T)_p$ or $(\partial \epsilon/\partial T)_p$. (See Eqs. (6) and (7)). They found α_L to vary from $30 \times 10^{-6} \text{ K}^{-1}$ at 200 K to $0.01 \times 10^{-6} \text{ K}^{-1}$ at 10 K and $(\partial n/\partial T)_p$ counteracts $(\partial n/\partial p)_T/(\partial p/\partial T)_p$. Sodium fluoride is the only alkali halide in

which this has been reported¹³. This unusual property causes the Rayleigh scattering to vanish when the contributions $(\partial n / \partial \rho)_T (\partial \rho / \partial T)$ and $(\partial n / \partial T)_\rho$ are equal and opposite.

Table II shows that for the alkali halides the magnitude of the Brillouin scattering exceeds that of the Rayleigh scattering. This has not been observed.^{8,14,15} The most probable cause of the failure to obtain the expected result is that these theories apply only to pure, perfect crystals and no such crystals can exist. All real crystals, even if pure, must have some form of defect structure to satisfy thermodynamic requirements. If they contain impurities, a rather complex collection of impurity-defect and impurity-impurity compounds can exist. Theimer and his associates^{16,17,18,19} recognized that defects and impurities could make a significant contribution to the Rayleigh scattering, but at that time neither quality crystals nor a detailed understanding of defect interactions were available.

III. DEFECT CHEMISTRY OF ALKALI HALIDES

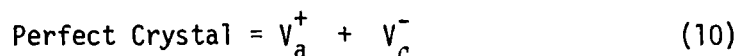
In discussing the effects of defect- and impurity-species on light scattering, it is convenient to retain the conventional subdivisions of intrinsic and extrinsic, but we will also need to distinguish between symmetric and unsymmetric species. First we need more general relations for defect species.

a. Intrinsic Defects. A pure crystal can be perfect only at zero Kelvin. Any pure real crystal must contain defects whose number is determined solely by the temperature with which the crystal is in equilibrium. Each chemical group of crystals will contain basic types of defects and their derivative species. The common basic defect in alkali halides consists of a vacant anion and vacant cation site, that is a Schottky defect. Each of the vacant sites (vacancies) bear an effective charge of a sign such that the vacant site attracts ions of the kind that normally occupy it. Thus, cation- and anion-vacancies are mutually attracted. When they occupy adjacent sites, the Coulomb energy is minimized and that configuration may be slightly more stable than two isolated vacancies. Such a configuration of oppositely charged vacancies is called a pair. Usually an adjacent pair is termed a nearest-neighbor pair, and when once removed a next-nearest-neighbor pair, and so forth.

In addition to Coulomb attraction, the energy of the host-defect system is lowered by the ions in sites adjacent to a vacancy or a pair shifting from their normal sites because their chemical bonds to the

missing ion no longer exist. This "relaxation" extends the defect into the lattice. Pairs tend to form clusters because they are dipolar species. This lowers both the electrostatic- and relaxation-energy of the system.

The various species of intrinsic defects can be represented by psuedo-chemical reactions denoting the formation of basic and compound defects. All intrinsic defect species can be represented by the psuedo-chemical reactions



and

$$\delta V_a^+ + \delta V_c^- = [(V_a V_c)_{\delta \zeta}] \quad , \quad (11)$$

where V_a and V_c represent anion and cation vacancies respectively. Brackets are used to indicate a complex defect species. Here δV 's are stoichiometry numbers, while subscript δ denotes the number of vacancy pairs in a cluster, and ζ indicates the type of pairs or clusters formed, that is nearest neighbor, next nearest neighbor, etc.

It has been shown that the concentrations of the various defects are related through a set of simple mass-action expressions,^{20,21} which are written to include all complex species as

$$a_a a_c = K_s = \exp (\Delta_s/k) \exp (-h_s/kT) \quad , \quad (12)$$

and

$$a_{\delta\zeta}/a_a^{\delta}a_c^{\delta} = K_{\delta\zeta} = z_{\delta\zeta} \exp(\Delta_{\delta\zeta}/k) \exp(-h_{\delta\zeta}/kT) \quad (13)$$

In these equations the thermodynamic activity, enthalpy and entropy of formation are represented as a , h and s , respectively. The mass-action constants are given as K , the subscripts denote species as given above with the additional subscript s to identify Schottky-defect equilibrium. The configuration entropy is z and the Boltzmann constant is k .

The experimental methods usually used to evaluate the thermodynamic quantities do not distinguish between the various compound defects, but simply separate charged defects from neutral defects on the assumption that all the neutral defects are $[(V_a V_c)_1]$, that is nearest-neighbor vacancy pairs.²² If species $[(V_a V_c)_1^2]$, $[(V_a V_c)_2^1]$ or $[(V_a V_c)_3^1]$ are stable in alkali halides, they have not been detected. Whatever species are present their activities are set by the temperature at which the defect system was equilibrated and are given by

$$a_{\delta\zeta} = K_{\delta} K_S^{\delta} \quad (14)$$

b. Extrinsic Defects. Even the best purification methods leave some foreign atoms in any real crystal. The defect species that these foreign atoms form depends on whether they incorporate substitutionally or interstitially in the host lattice, whether they are homovalent or aliovalent, and their ionicity with respect to the host lattice. Experimental evidence indicate that all common impurities in alkali

halides are substitutionally incorporated in the crystal.²² This situation gives rise to a relatively simple defect chemistry, which can be described by

$$\delta M_i^{+v} + v\delta V_c^- = [\{M_i(V_c)_v\}_\delta \zeta] \quad , \quad (15)$$

$$\delta A_i^{-v} + v\delta V_a^+ = [\{A_i(V_a)_v\}_\delta \zeta] \quad , \quad (16)$$

$$\delta \xi M_i^{+v} + \delta v A_j^{-\xi} = [\{(M_i)_\xi (A_j)_v\}_\delta] \quad , \quad (17)$$

$$\delta \xi M_i^{+v} + \delta v V_c^- + \delta \phi [M_h A_h] = [\{(M_i(A_h)_v)_\xi \cdot (M_h A_h)_\phi \cdot (M_h)_\xi v \cdot (V_c)_\xi v\}_\delta]_\downarrow \quad , (18)$$

and

$$\delta M_i + ED = [(M_i)_\delta ED]_\downarrow \quad . \quad (19)$$

Cations and anions are represented by M and A, respectively, i and j denote impurity species while h denotes the host species. With the exception of ζ , which specifies type of impurity-complex, the lower case Greek letters are stoichiometry or charge numbers. The impurity- or defect-charge is given as the excess or deficiency of charge at the lattice position. In these equations the cluster size, δ , has been factored from the stoichiometry numbers. When the product of the reaction forms a separate phase this is indicated by the symbol \downarrow , and when an extended defect, such as a grain boundary or dislocation, is a reactant it is indicated by ED . Mass-action equations similar to

(12) and (13) can be written for reactions (15) through (19). The most significant characteristic of the defect chemistry of ionic compounds is that the various intrinsic and extrinsic-defect reactions are coupled through sharing common defect or impurity species. This feature makes it crucial that the quality of the crystals used in the study of physical- or chemical-properties dependent on defect species be very carefully controlled, and contributes greatly to the remarkable diversity in the magnitude of thermodynamic parameters separated as experimental evidence for impurity-related properties in alkali halides.

c. Characteristic Impurity Behavior. In alkali halides, ν seldom exceeds 1 because of the energy required to form the additional vacancies necessary to compensate the impurity charge. It has been shown that Ce^{3+} (i.e. $\nu = 2$) is neither very soluble nor mobile in KCl.²³ However, others²⁴ reported that Bi^{3+} diffuses with a remarkably low migration energy and suggest an interstitial diffusion mechanism. However, the D_0 (which is proportional to the square of the jump distance) is inconsistent with interstitial diffusion. In general, impurities with $\nu > 1$ should not be found in alkali halides unless intentionally added.

Experimental measurements of ζ are not sufficiently sensitive to distinguish various values of ζ . A common method of assigning binding energies to nearest neighbors ($\zeta = 0$) and next-nearest neighbors ($\zeta = 1$) for impurity/vacancy complexes $[\text{MV}_c(\zeta)]$ is from dipole-relaxation times obtained from dielectric relaxation,²⁵ d.c. polarization,²⁶ and ionic thermal currents.²⁷ This work shows that when the impurity radius, r_i , is larger

than or near the radius of the ion for which it substitutes, r_w , the predominate value of v is 0, but when r_i is much smaller than r_n significant concentrations of the complex $[Mv_c(1)]$ are formed.

Recently Catlow and coworkers²⁸ have calculated the binding energies for alkaline earth-vacancy complexes in KCl, NaCl, KBr. They apply a modern version of the Mott-Littleton²⁹ method using a commercial program, Harwell Automatic Defect Evaluation System, commonly denoted HADES,³⁶ to achieve rapid convergence of the large lattice summations required. Their results suggest that next-nearest-neighbor complexes should be much more common with large impurities than experimental work suggests. Unfortunately they can only calculate energies assuming $e \approx h$ and can make no estimate of entropy so that careful comparison of free energies, g , cannot be done as the derivation of h from the experimentally measured g .

Of more importance here is the tendency for these complexes to aggregate into clusters as described by Eq. (16). Clustering was discovered in the 60's.^{30,31,32,33,34,35} Cook and Dryden³⁰ noted that in alkali halides quenched from 350 to 400°C all the impurity ions are initially present as dipoles (two to five percent dissociated into isolated M^+ and V_c^- ions), then aggregate into trimers as the crystal ages. Trimers were reported to form by third-order kinetics. As third-order reactions are extremely rare, considerable controversy has resulted.^{37,38} These kinetic arguments are not of immediate importance here, except to note that these aggregation processes can occur at storage temperatures for crystals. Cappelletti and DeBenedetti³⁹ have found direct evidence from ionic thermal current

measurements that some second-order reaction occurs. Crawford³⁵ has developed a model utilizing binary reactions to form trimers that would appear to be a third-order reaction. The rate constant is given by

$$k_3(\text{apparent}) = 4\pi N_L e^{-Sr/k} D_0 r_D e^{-E_M/kT} e^{-(E_M - E_B)kT} \quad (20)$$

The activation energy for the reaction as measured from the temperature dependence of k_3 is E^* and

$$E^* = E_M - E_B \quad , \quad (21)$$

where E_B is binding energy for dimer formation, r_D is the capture radius of dimers, D_0 is the temperature independent preexponential and E_M the migration energy for diffusion of monomers.

Assuming no lattice relaxation about the defect and assuming that E_a , the formation energy of the impurity-vacancy complex is 1 eV we can easily estimate the relative electrostatic energy of the various configurations.³⁵

The trimer is postulated^{30,33,34,41,51} to be a six-sided complex on the {111} planes of the cation sub-lattice with an isolated cation in its center. The total electrostatic energy³⁵ of such an array is given by

$$E_T^{(3)} = -\frac{q^2}{\kappa r_0} \left[6 + \frac{3}{2} - \frac{6}{\sqrt{3}} \right] = -4.036 \frac{q^2}{\kappa r_0} \quad (21a)$$

and

$$E_I^{(3)} = E_T^{(3)} - 3E_a = 1.063 e^2/\kappa r_0$$

where $-q$ is the electronic charge, κ the static dielectric constant, and r_0 is the cation-cation distance in the $\{111\}$ plane. For KCl $r_0 = 4.44 \times 10^{-8}$ cm and $\kappa = 4.64$ which yields $E_I^{(3)} = 0.73$ eV and for NaCl ($r_0 = 3.94 \times 10^{-8}$ cm, $\kappa = 5.62$) $E_I^{(3)} = 0.668$ eV.

The dimer, as a planar quadripole lying in the $\{100\}$ planes, has a total electrostatic energy given by

$$E_T^{(2)} = \frac{-2q^2}{\kappa r_0} \left[2 - \frac{1}{\sqrt{2}} \right] = 2.586 q^2/\kappa r_0, \quad (22)$$

and

$$E_I^{(2)} = E_T^{(2)} - 2E_a = 0.586 q^2/\kappa r_0.$$

The values for KCl and NaCl of $E_I^{(2)}$ are 0.413 and 0.377 eV, respectively.

If the dimers form by loosely coupling as a linear arrangement along $\langle 110 \rangle$ directions the pair of impurity-vacancy complexes may be adjacent ($z = 0$) or next-nearest neighbor ($z = 1$) or $z = 3$ etc. Such a pair of complexes has a total electrostatic energy given by

$$E_T = \frac{-e^2}{\kappa r_0} \left[\frac{1}{n} + \frac{1}{n+2} - \frac{2}{n+1} + 2 \right], \quad (23)$$

where n is the number of unit r_0 's the pair is separated along the $\langle 110 \rangle$

row. The interaction energy is, then, given by

$$E_I = \frac{-e^2}{\kappa r_0} \left[\frac{1}{n} + \frac{1}{n+2} - \frac{2}{n+1} \right] .$$

For $n = 1$, $E_I = 0.235$ eV; $n = 2$, $E_I = 0.059$ eV; $n = 3$, $E_I = 0.024$ eV in KCl and in NaCl similar spacings give 0.214 eV, 0.054 eV and 0.021 eV, respectively.

On the basis of this crude estimate if we neglect the contribution of the entropy to the free energy, the concentration of hexipoles and quadripoles should not differ greatly in concentration in the temperature range of 50-100°C.

Manganese in sodium chloride is the most extensively studied system,^{37,38,41,48,55} followed by cadmium in NaCl.^{27,60,61,62,63} Unfortunately there is little agreement on the enthalpies or entropies derived from the various experiments, or even universal agreement on the species that exist. Most workers accept trimers as the stable species and assume very rapid formation of dimers followed by a slightly slower buildup of trimers. However, Lilley^{58,59,60,64} puts forth strong arguments that cast doubt on their existence. Our concern is only the fraction of typical impurities found in aggregates or in large defects and their rate of formation. One would expect that with the large amount of work done on such systems, concentrations could be calculated with some confidence. Unfortunately that is not true. In Table IV a selection of thermodynamic parameters are presented for a few impurity systems. These large species must be formed by

diffusion of the divalent ion and the vacancy to adjacent sites. This occurs with remarkable speed. Table V gives frequency factors and activation energies for formation rates of the species assumed to be $\{MV_c(0)\}_3$.

The salient feature of these large impurity species is the remarkable speed with which they form at low temperatures. Symmons^{38,56} notes that in NaCl containing less than 10^{-4} molar fraction of Mn^{2+} (below the concentration at which Mn^{2+} forms visible precipitates), the equilibrium between $\{MnVc(0)\}$, and $\{MnVc(1)\}$, was established in 15 days at $-120^\circ C$. At $40^\circ C$ equilibrium would be achieved in 70 seconds. Symmons finds less than 0.02 of the Mn^{2+} in NaCl present as single dipoles when the system has reached equilibrium at $21^\circ C$. Cappelletti and Fieschi²⁷ claim that it requires 100 hours for equilibrium with "microprecipitates" in KBr: Sr at $61^\circ C$. To achieve equilibrium between nearest neighbor and next-nearest neighbor species requires a host cation to exchange positions by one jump. The jump frequencies from nearest neighbor and next-nearest neighbor is given by

$$W_4 = 1.059 \times 10^{14} e^{-0.6711/kT} \quad (24)$$

and the jump from next-nearest neighbor to nearest neighbor is given as

$$W_3 = 7.357 \times 10^{13} e^{-0.6319/kT} \quad (25)$$

Clearly, a one-jump process can achieve equilibrium rapidly.

Species such as trimers or microprecipitates that require the migration of impurity ions into a cluster form in much shorter

times than would be expected if the impurities are reasonably uniform in their distribution in the host and they migrate by normal diffusion processes.²² Unless a very special effort is made, it is almost impossible to grow an alkali halide with a uniform distribution of impurities. The nonuniform distributions have caused problems in many experiments.⁶⁹

General reaction 17 represents association reactions among cations and anions within a lattice. These have been observed to affect most measurements made on ionic crystals. Here are a few examples to illustrate this: ionic conductivity,⁷⁰ ionic thermal currents,²⁷ perturbed optical absorption,⁷¹ dielectric relaxation,²⁶ increased solubility of impurities,⁷² and anomalous diffusion.⁷² In addition to direct reactions, cation-cation or anion-anion interactions that markedly affect the properties being measured⁴³ can occur.

A related process that does not occur entirely within the host crystal is the modification of an impurity within a crystal by a reactive gas in the external phase.^{73,74,75} Typical of this type reaction is the apparent anomalous diffusion in KCl of OH^- in the presence of Cl_2 .⁷⁴ While such reactions are known, no thermodynamic data is available and only for the system KCl: OH: Hg have all the products been identified.⁷¹

Precipitation of an impurity to form a metastable phase is represented by reaction (18). As written ξ ion pairs of impurity compound M_iA_i precipitate with ϕ ion pairs of host M_hA and ξv cationic vacancies to form a separate phase. The best known examples are the Suzuki

phases which form with some divalent impurities in the alkali halides with the stoichiometry $[M_iA_2 \cdot (M_hA_h)_6 \cdot V_{c2}]^{2-}$ as a cubic phase.⁷⁶ Frequently these are written as $6 NaCl \cdot CdCl_2$, but here it is written as a lattice anionic impurity because its structure requires two cationic vacancies in the normal alkali-halide lattice which are compensated by two cations in the host lattice. This phase is stable below 500°C in NaCl.⁷⁶ Many similar phases have been identified in sodium chloride: NaCl: SrCl₂, NaCl: MnCl₂, NaCl: BaCl₂, NaCl: CaCl₂, LiF: MgF₂.^{77,78,79,80,81} Most early work was done by x-ray diffraction; but now such phases have been observed by optical microscopy,^{82,83} by gold decoration replication^{84,85} and by direct transmission electron microscopy.⁸⁶ Most studies of Suzuki phases involve crystals containing the impurity ion in a concentration far in excess of its low-temperature solubility. However, it seems to be the species that forms as a precursor to precipitation of regions of MA₂. The distributions of precipitate sizes has been determined by replication measurements⁸³ and is generally in accord with that predicted for a surface-reaction limited Ostwald-ripening mechanism.⁸⁷ In this mechanism, the $6NaCl \cdot MnCl_2$ was best fit by an $F_1(u)$ except for the small number of particles in which R/R_c was less than 0.5, where R is the radius of the particle considered and R_c is the radius of a particle which is instantaneously in equilibrium with the average solute concentration, that is the radius of a particle that is neither growing nor shrinking.

A carefully grown and well treated alkali halide can be relatively free of extended defects [reaction(19)]. If such crystals are strained, as in machining or polishing, dislocations are introduced. Rapid or

rough growth from mechanical vibrations or from thermal stresses will also introduce significant numbers of dislocations. When a crystal is periodically deformed, dislocations sweep through it collecting vacancies as they traverse it, thus, becoming charged.^{88,89,90} The dislocations will not only collect free V_c but will remove associated vacancies, i.e. decompose $\{MV_c(0)\}$. Charges as high as one ionic charge per two cation sites on the dislocation core have been reported.⁸⁸ If no jogs are formed, the dislocation can come to equilibrium only by migration of V_c at temperatures too low for anion diffusion.

The equilibrium concentration f of cation vacancies on the core will be given approximately by

$$\frac{f}{1-f} = \alpha e^{\left(\frac{1}{kT} (g_{+d} - \frac{\partial E}{\partial M})\right)} \quad , \quad (26)$$

where α is the concentration of free cation vacancies in distant parts of the crystal, g_{+d} is the free energy of binding of a cation vacancy to a core site and $\partial E/\partial M$ is the increase in the electrostatic energy of the whole system resulting from the addition of one vacancy to the core.^{92,93} The charge cloud satisfies the Debye-Hückel equation and in NaCl has a radius of a few hundred lattice spacings. When divalent impurity cations are mobile they may diffuse to the dislocation core, but they can't move with the dislocation as it glides. They act as pinning points and their accumulation can be studied by internal friction,⁹⁴ but not by experiments that detect moving charged dislocations. When processes occur that produce free electrons,

such as photoionization of a monovalent impurity, they may collect on dislocations. Ohkura found a trap depth of 0.26 eV for a dislocation and 0.48 eV for a jog in KBr.⁹¹

Another type of extended defect in alkali halides is the grain boundary. These macroscopic defects are present in poorly grown crystals, especially Stockbarger-grown crystals that have seeded poorly. They are introduced by gross deformation of crystals, and are present in the pressed windows used for preparation of infrared windows. Grain boundaries are very active defects chemically. They collect impurities and provide charge anomalies in otherwise reasonably good crystals. Whipple⁹⁵ has developed the theory of diffusion along grain boundaries. Harris^{96,97,98,99,100,101} has extensively studied the properties of grain boundaries in alkali halides. Diffusion measurements are in reasonable agreement with Whipple's theory.⁹⁵ Diffusion can contribute significantly to the deterioration of the optical properties of crystals containing grain boundaries.¹⁰² Impurity concentrations along grain boundaries far exceed the bulk impurity content.¹⁰¹ At present, little has been reported on the charge anomaly that accompanies the grain boundary, but in gold-decoration experiments Harris and Cutmore⁹⁸ found that the influence of the grain boundary could extend 250 to 300 μm from the grain boundary plane. Even grain boundaries formed at such small angles that they are difficult to detect produce a major disruption in the properties of the crystal.

While the major chemical properties are determined by the long-range electrical forces, these alone do not explain the behavior of defects and impurities in alkali halides or other ionic crystals.

Certainly one more localized force is the displacement of the host ions about such defects. Typical of this type of problem is the volume of formation of Schottky defects in alkali halides. Faux and Lidiard¹⁰³ calculated these volumes using an extended Mott-Littleton approach and predicted that the volumes of formation were less than the molecular volumes. For example, in NaCl, $-0.69 V_m$; KCl, $-0.73 V_m$; KBr, $-0.51 V_m$; i.e. the volumes of relaxations are negative. Experimentally, both contractions and expansions have been reported. Early work based on density changes in KCl to which CaCl_2 and SrCl_2 had been added indicated DV was negative.¹⁰⁴ However, recent experiments on the pressure dependence of ionic conductivity in both the extrinsic and intrinsic regions^{105,106,107,108} gave volumes of formation greater than V_m , i.e. an expansion of the lattice around the vacancies due to relaxation of the lattice. For simple substitutional monovalent impurities, even those that produce "off-center" defects such as Li^+ in KCl can be calculated with reasonable success,¹⁰⁹ but later results have differed somewhat from experimental results for divalent highly ionic impurities.²⁸ These seem to overestimate the fraction of next-nearest neighbor complexes formed with impurities near the size of the host cation. Clearly the experimental data should be reevaluated using a slightly different model. As yet no modern work has been done on impurities that form only partially ionic bonds with the host anion. Nor is there any theoretical explanation of the enhanced solubility of divalent cations in alkali halides containing OH^- or other anionic species, or of the unusual stability of these impurity compounds.

IV. DEFECT SCATTERING

Only Theimer and his associates have attempted to study defect scattering from alkali halides.^{16,17,18,19} At the time of their work, neither good crystals nor a very satisfactory understanding of the nature of impurities in alkali halides was available. Apparently many of their crystals contained rather large quantities of dislocations, grain boundaries, and impurities in undefined states of aggregation.

In a crystal with a low dislocation content and no grain boundaries, but with a small content of divalent impurity, the defect species will be small compared to the wavelength of the incident light. The defect species act as independent scattering centers. At low impurity concentrations the intensity of the Brillouin scattering will not be greatly changed and provides a convenient reference so that a modified Landau-Placek ratio provides a useful experimental measure of defect scattering.

This scattering ratio is given by

$$\eta = \eta_{WK} + \frac{8\pi^2 N}{\beta_B \lambda^4} \sum_K x_K \tilde{g}_K \tilde{\alpha}_K^2, \quad (27)$$

where λ is the wavelength of the light incident on the scattering center K , N is the number of ion pairs per unit volume, x_K is the mole fraction of defects of species K , $\tilde{\alpha}_K$ is the effective polarizability tensor of defect K in a particular host lattice and \tilde{g}_K selects the elements of $\tilde{\alpha}_K$

that contribute to the light scattered at an angle θ from the incident beam of specific polarization from each of the allowed orientations of defect K that are optically distinguishable. Equation (27) applies to constant temperature measurements because χ_K depends on the temperature at which the defect system was equilibrated and the time since the system was equilibrated. $\tilde{\alpha}_K$ has the values corresponding to the temperature of the scattering measurement, as does β_B and N . At a particular analytical concentration C_i of impurity i the magnitude of η will depend on how the impurity is distributed among the various defect species K because each has a different value of α_K .

Equation (27) must also contain a distribution function, $\rho(\underline{x}, K)$, to account for the inhomogeneous distribution of defect species K within the crystal. In general $\rho(\underline{x}, K)$ is unknown and unique to each crystalline sample as it depends on the host substance, \underline{x} , and the thermal treatment to which the crystal has been subjected. Except at phase boundaries, such as precipitates, $\rho(\underline{x}, K)$ must be continuous with the gradients established by the balance of diffusional forces and the lowering of the free energy of the host-impurity system by forming aggregate species. Scattering experiments should be useful in studying the distribution of impurities in alkali halides.

Many estimates of the polarizability α_K assume it is proportional to the volume of the simple defect or to the volume of the ion removed from the site which forms the defect.¹⁹ This probably underestimates α_K because it neglects the relaxation of the ions surrounding the defect. Of concern in estimating α_K for a particular defect is the

extent of the perturbation of the electronic distribution around the defect. This problem has not yet been treated, although much effort has been spent on electronic centers. If it is assumed that the anomaly in the polarizability that causes scattering is proportional to the relaxation volume around the defect, a more realistic estimate should be obtained.

For sodium chloride using $1 \mu\text{m}$ light, Eq. (27) reduces to

$$\eta = 0.244 + (6 \times 10^{38} \text{ cm}^{-6}) \sum_K \chi_K g_K \alpha_K^2 \quad (28)$$

For a symmetric defect such as an isolated vacancy or impurity ion, g_K is unity. If a 20 percent change in η can be measured, then for symmetric defects, $\sum_K \chi_K \alpha_K^2$ must be $8 \times 10^{-41} \text{ cm}^6$. Small defects such as isolated vacancies would not contribute much scattering at normal concentrations, but the larger aggregates can. Consider the example of one part per million isolated vacancies in sodium chloride or another chloride. Assuming that α_K^2 of the vacancy is equal to that of the missing chlorine ion gives $\alpha_K^2 = (3.7 \times 10^{-24} \text{ cm}^3)^2$. Thus, $\sum_K \chi_K g_K \alpha_K^2 = 10^{-6} (3.7 \times 10^{-24})^2 = 1.4 \times 10^{-53} \text{ cm}^6$, which is a factor of 6×10^{12} smaller than the value of $8 \times 10^{-41} \text{ cm}^6$ required to give a 20 percent change in η .

V. SUMMARY AND DISCUSSION

Intrinsic Brillouin- and intrinsic Rayleigh-scattering, which determine the lowest possible scattering that can be attained in fiber materials, have typical scattering coefficients $\beta_{sc} = \beta_B + \beta_{int R}$ of $1 \times 10^{-9} \text{ cm}^{-1} = 4 \times 10^{-4} \text{ dB/km}$ for lithium to $8 \times 10^{-7} \text{ cm}^{-1} = 0.4 \text{ dB/km}$ for zinc selenide, both at a wavelength $\lambda = 1 \mu\text{m}$. The ratio 2η of intrinsic Raman scattering to the intrinsic Brillouin scattering is non-negligible in general, in contrast to the tacit assumption made in the standard practice of using the Brillouin scattering as that of the V curves for crystalline materials. The total intrinsic scattering coefficient $\beta_B + \beta_{int R}$ can be much greater, by a factor of 40 in the examples considered, than the Brillouin scattering. The scattering curves in the V curves in Sec. G, which include only Brillouin scattering for crystalline materials, should be recalculated with intrinsic Raman scattering included. The extrinsic scattering in fibers can, of course, be orders of magnitude greater than the intrinsic scattering as discussed in Sec. B.

Electronic scattering from vacancies or impurity ions that are either isolated or in small clusters is negligible, but electronic scattering from extended imperfections, such as precipitates, grain boundaries, Suzuki phases, and dislocations can be great.

The substantial variations in both the laser breakdown thresholds and the amount of scattering that is observed as various regions of crystal are probed can be understood as follows: Even though the brief review in Sec. III of the current state of impurity chemistry

in the simplest ionic solids, the alkali halides, is far from extensive, it should dispell the common view that simple point defects are the predominate impurity species in alkali halides. Furthermore, most textbooks create the impression that these "simple point defects" are frozen in some reasonably homogeneous distribution at room temperature. There is ample evidence that this is just not true.

At high temperatures, an alkali halide contains most of its impurities distributed as simple point defects, but their geometric distribution is not uniform enough to allow a measurement of the Soret effect.⁶⁹ Even if quenched to low temperatures, dimers and trimers of impurity/vacancy complexes are very quickly the predominate impurity species, and in three months to a year, microprecipitates will have formed and OH^- and H_2O will have substantially penetrated the crystal if it contains a few parts per million of divalent ions. Annealed crystals, even if relatively pure, contain regions of abnormally high impurity concentration because clusters and precipitates are a lower total-energy state for the system.

In crystals specially purified to remove impurity cations as well as anions, the highest breakdown thresholds and lowest scattering should be observed in quenched crystals, provided the dislocation density can be kept reasonably low. However, the high breakdown thresholds and low scattering would be reasonably short lived because smaller impurity species would grow slowly as the crystal ages.

Molecular ions, with their permanent dipole moments, are expected to be strong scatterers because they are strong absorbers. A study of molecular-ion scattering would be useful.

REFERENCES FOR SEC. C

1. L. D. Landau and G. Placzek, Z. Phys. Sowjetunion 5, 172 (1934).
2. A. Munster, "Statistical Thermodynamics," (English Ed.) Academic Press, N.Y., Vol. I, (1969) p. 199, S 3.6.
3. Ibid. Vol. II, (1974) p.468, S 16.8.
4. H. C. van de Hulst, "Light Scattering by Small Particles," Wiley, N.Y. (1957).
5. I. L. Fabelinski, "Molecular Scattering of Light," Plenum, N.Y. (1968).
6. M. Kerker, "The Scattering of Light," Academic Press, N.Y. (1969).
7. G. Benedek and G. F. Nardelli, J. Chem. Phys. 48, 5242 (1948).
8. G. Benedek and K. Fritsch, Phys. Rev. 149, 647 (1966).
9. L. D. Landau and E. M. Lifshitz, "Electrodynamics of Continuous Media," Pergamon, N.Y. (1969) p. 391.
10. R. K. Wehner and R. Klein, Physica 62, 161 (1972).
11. D. W. Pohl and S. E. Schwarz, Phys. Rev. B. 7, 2735 (1973).
12. F. Wooten, "Optical Properties of Solids," Academic Press N.Y.(1972) p.49.
13. E. E. Havinga and A. J. Bosman, Phys. Rev. 146, A292 (1965)
14. H. Matsuura and T. Tatsuo, Bull. Chem. Soc. Japan. 46, 3031 (1973).
15. J. G. Collins and G. K. White, "Progress in Low Temperature Physics," Vol. IV, ed. C. J. Gorter, North Holland, Amsterdam (1964) p. 450.
16. O. Theimer and C. Plint, Ann. Phys. 3, 408 (1958).
17. C. A. Plint, O. Theimer, and W. A. Sibley, Ann. Phys. 5, 342 (1958).

18. O. Theimer, C. A. Plint, and W. A. Sibley, *Ann. Phys.* 9, 475 (1960).
19. M. D. Daybell, O. Theimer, and K. O. White, "Thermal Light Scattering by Ionic Crystals," Technical Report ONR. Contract Nonr-3531(02), New Mexico State University (1967).
20. A. B. Lidiard, *J. Appl. Phys.* 33, 414 (1962).
21. R. E. Howard and A. B. Lidiard, *Repts. Prog. Phys.* 27, 164 (1964).
22. W. J. Fredericks, "Diffusion in Solids," eds. Burton, Academic Press, San Francisco (1975) p. 381 and p. 410.
23. F. J. Keneshea and W. J. Fredericks, *J. Phys. Chem. Solids* 26, 1787 (1965).
24. R. Reisfeld and A. Honigbaum, *J. Chem. Phys.* 48, 5565 (1968).
25. R. W. Dreyfus, *Phys. Rev.* 121, 1675 (1961).
26. R. E. Chaney and W. J. Fredericks, *J. Solid State Chem.* 6, 240 (1973).
27. R. Cappelletti and R. Fieschi, *Cryst. Lattice Defects* 1, 69 (1969).
28. C. R. A. Catlow, J. Corish, J. M. Quigley and P. W. M. Jacobs, *J. Chem. Phys. Solids* 41, 231 (1980).
29. N. F. Mott and M. J. Littleton, *Trans. Kanaday Soc.* 34, 485 (1938).
30. J. S. Cook and J. S. Dryden, *Proc. Phys. Soc. London*, 80, 479 (1962).
31. J. S. Dryden and G. G. Harvey, *Proc. Phys. Soc. London*, 2, 603 (1969).
32. Y. Chiba, K. Ueki, and M. Sakamoto, *J. Phys. Soc. Jap.* 18, 1092 (1963).
33. Y. Chiba and M. Sakamoto, *J. Phys. Soc. Jap.* 20, 1284 (1965).
34. H. F. Symmons and R. C. Kemp, *Brit. J. Appl. Phys.* 17, 607 (1966).
35. J. H. Crawford, Jr., *J. Phys. Chem. Solids* 31, 399 (1969).
36. A. B. Lidiard and M. J. Norgett, "Computational Solid State Physics," ed. Herman et. al. Plenum, N.Y. (1972) p. 385.

37. C. H. Burton and J. S. Dryden, J. Phys. C. 3, 523 (1970).
38. H. F. Symmons, J. Phys. C. 4, 1945 (1971).
39. R. Cappelletti and E. DeBenedetti, Phys. Rev. 165, 981 (1968).
40. W. H. Stewart and C. A. Reed, J. Chem. Phys. 43, 2890 (1965).
41. J. S. Dryden, J. Phys. Soc. Jap. Suppl. III 18, 129 (1963).
42. T. Ikeda, J. Phys. Soc. Jap. 19, 858 (1964).
43. J. L. Krause and W. J. Fredericks, J. Phys. (Paris) 34, C-9-13 (1971).
44. S. N. Banasevich, B. G. Lure, and A. N. Murin, Sov. Phys., Solid State 2, 72 (1960).
45. H. Machida and W. J. Fredericks, J. Phys. (Paris) 37, C-7-385 (1976).
46. A. N. Murin, S. N. Banasevich, and Grushko, Sov. Phys., Solid State 3, 1762 (1962).
47. F. Beniere, M. Beniere, and M. Chemla, C. R. Acad. Sci. Paris 268, 1461 (1969).
48. J. S. Dryden and Hardy, J. Phys. C. 2, 603 (1969).
49. R. Cappelletti, R. Fieschi, G. Martegani, and L. Pirola, J. Phys. 28, C4-130 (1976).
50. A. R. Allnatt and P. Pantelis, Trans. Faraday Soc, 64, 2100 (1968).
51. Y. Chiba, K. Ueki, and M. Sakamoto, J. Phys. Soc. Jap. 18, 1092 (1963); *ibid.* 20, 1284 (1965).
52. H. Machida and W. J. Fredericks, J. Chem. Phys. Solids 39, 797 (1978).
53. F. Keneshea and W. J. Fredericks, J. Chem. Phys. 41, 3271 (1964).
54. J. Krause and W. J. Fredericks, J. Phys. (Paris) 34, C-9-25 (1973).
55. R. W. Dreyfus and R. B. Larbowitz, Phys. Rev. 135, A1413, (1964).
56. H. F. Symmons, J. Phys. C 3, 1846 (1970).

57. R. Capelletti and Emico Okuno, J. Electrochem. Soc. 120, 555 (1973).
58. E. Lilley and J. B. Newkirk, J. Mat. Sci. 2, 567 (1967).
59. E. Lilley, "Proc. Sixth Int'l Conf. Reat. Solids (ed. J. W. Mitchell et. al.), J. Wiley, New York (1969), p. 631. (also *ibid* (1973)).
60. E. Lilley, J. Phys. (Preis) to be published (1980).
61. Y. Haven, Rec. Trav. Chim. Pays-Bas, 69, 1505 (1950).
62. A. R. Kahn, Ph.D. thesis, Imperial College, London (1967).
63. V. Trnovcová, Fyzikalny Casopis, 18, 211 (1968).
64. E. Lilley, Private communication of preprint.
65. Y. Haven, "Defects in Crystalline Solids," Phys. Soc. London, (1955) p.261.
66. J. Rolfe, Can. J. Phys. 42, 2195 (1964).
67. R. W. Dreyfus and A. S. Nowick, Phys. Rev. 126, 1367 (1962).
68. N. Brown and I. M. Hoodless, J. Phys. Chem. Solids 28, 2297 (1967).
69. A. R. Allnatt and A. V. Chadwick, Trans. Faraday Soc. 63, 1929 (1967).
70. B. Fritz, F. Luty, and J. Anger, Z. Phys. 174, 240 (1963).
71. C. A. Allen and W. J. Fredericks, Phys. Stat. Sol.(a) 3, 143 (1970).
72. C. A. Allen and W. J. Fredericks, Phys. Stat. Sol.(b) 55, 615 (1973).
73. C. A. Allen and W. J. Fredericks, J. Solid State Chem. 1, 205 (1970).
74. T. Ikeda, Jap. J. Appl. Phys. 14, 1383 (1975).
75. T. Ikeda, J. Phys. Soc. Jap. 41, 1968 (1976).
76. K. Suzuki, J. Phys. Soc. Jap. 16, 67 (1961).
77. A. I. Sors, Thesis, Sussex Univ., England (1973).
78. K. Yagi and G. Honjo, J. Phys. Soc. Jap. 19, 1892 (1964).
79. *ibid*, 22, 610 (1967).

80. C. J. J. Van Loom and D. J. W. Ijdo, *Acta Cryst.* B31, 770 (1975).
81. J. A. Chapman and E. Lilley, *J. Mater. Sci.* 10, 1154 (1975).
82. A. I. Sors and E. Lilley, *Phys Stat. Sol. (a)* 32, 533 (1975).
83. D. L. Kirk, A. R. Kahn, and P. L. Pratt, *J. Phys. D*, 8, 2013 (1975).
84. A. J. Bannaghan, D. R. Hayman, and P. L. Pratt, "Reactivity of Solids," (ed. J. J. Anderson et. al.) Chapman Hall, London (1972) p.1.4.
85. D. L. Kirk and R. M. Innes, *Thin Solid Films*, 28, 243 (1975).
86. M. J. Yacaman, M. J. Goringe and L. W. Hobbs, UKAEA Research Report AERE-R8486 (1976).
87. S. C. Jain and A. E. Hughes, *J. Phys. (Paris)* 37, C-7-463, (1976).
88. R. M. Turner and R. W. Whitworth, *Phil. Mag.* 21, 1187 (1970).
89. A. Huddart and R. W. Whitworth, *Phil. Mag.* 27, 107 (1973).
90. R. W. Whitworth, *J. Phys. (Paris)* 34, C9-243 (1973).
91. H. Ohkura, *J. Phys. Soc. Jap.* 16, 881 (1961).
92. F. Bassani and R. Thomson, *Phys. Rev.* 102, 1264 (1956).
93. R. W. Whitworth, *Phys Stat. Sol. (b)* 54, 537 (1972).
94. D. C. Phillips and P. L. Pratt, *Phil. Mag.* 21, 217 (1970).
95. R. T. P. Wipple, *Phil. Mag.* 45, 1225 (1954).
96. L. B. Harris and J. Fiasson, *Phy. Stat. Sol. (a)* 33, 697 (1976).
97. L. B. Harris, *J. Phys. (Paris)* 37, C7-365, (1976).
98. L. B. Harris and N. G. Cutmore, *Surface Science* 65, 1 (1977).
99. L. B. Harris, *Phil. Mag.* B40, 175 (1979).
100. L. B. Harris, *J. Phys. (Paris)* to be published (1980).
101. L. B. Harris, *J. Am. Ceramic Soc.*, to be published (1980).

102. W. J. Fredericks, NBS Special Publication 509, 24 (1977).
103. I. D. Faux and A. B. Lidiard, Z Naturforsch. 26a, 62 (1971).
104. H. Pick and H. Weber, Z. Phys. 128, 409 (1950).
105. W. Biermann, Z. Phys. Chem., Frankfurt, 25, p. 90 and p. 253 (1960).
106. M. Lallemand, C. R. Acad. Sci. B, 267, 715 (1968).
107. M. Beyeler and D. Lazarus, Solid State Comm. 7, 1487 (1969).
108. D. Lazarus, D. N. Yoon and R. N. Jeffery, Z Naturforsch, 26a, 56 (1971).
109. C. R. Catlow, K. M. Diller, M. J. Norgett, J. Corish, B. M. C. Parker, and P. W. M. Jacobs, Phys. Rev B 18, 2739 (1978).

TABLE I: Room Temperature Values (a) of η_{WK} .

Substance	$r^{(b)}$	$\alpha^2 \times 10^6 (b)$ (K^{-1})	$c_{11} \times 10^{-11} (b)$ (dyn/cm ²)	$\rho^{(c)}$ (gm/cm ³)	$c_p \times 10^{-6} (d)$ (erg/gmk)	η_{WK}
Si	+150	2.5	16.6	2.32	7.11	37.4
C	+ 12	1.1	102.	3.51	5.02	0.227
MgO	- 19	10.4	29.2	3.65	9.20	10.1
LiF	- 0.35	32.6	11.2	2.295	16.11	0.157
NaF	+ 0.48	31.0		2.79	11.16	~0.4
NaCl	- 0.5	39.5	4.85	2.165	8.64	0.244
KCl	- 0.4	36.7	4.05	1.984	6.88	0.210
KBr	- 0.06	38.1	3.46	2.75	4.39	0.125
KI	- 0.2	40.5	2.75	3.13	4.36	0.128
CaF ₂	- 0.01	18.8	16.4	3.18	8.78	0.0568
ZnS	- 57	7.6	9.76	4.10	4.72	26.25

(a) Calculated from Eq. (2).

(b) Values from reference 10, except NaF from reference 11.

(c) "Handbook of Chemistry and Physics," Chem. Rubber. Publishers.

(d) Calculated from D. R. Stille, H. Prophet, et. al., J.A.N.A.F. Thermochemical Tables, N.S.R.D.S.-NBS-37.

TABLE II: Estimated^(a) Values of β_B and β_R at 298K.

Substance ^(b)	ϵ (dimensionless)	λ (nm)	$C_{12} \times 10^{-11}$ (dyn/cm ²)	P_{11} (dimensionless)	P_{12} (dimensionless)	β_B (10^{-9} cm^{-1})	β_R (10^{-9} cm^{-1})
Si	12.0	3390	6.4	0.081	-0.01	1.78	66.8
C	5.7	583	25	-0.31	0.09	300	68.2
MgO	3.02	589	9.1	-0.25	-0.01	28.5	288
LiF	1.93	589	4.5	0.02	0.13	7.0	1.1
NaF ^(c)	1.93	633		0.08	0.20		
NaCl	2.33	600	1.25	0.11	0.153	29.1	7.09
KCl	2.17	589	0.66	0.215	0.159	42.3	8.88
KBr	2.36	500	0.56	0.22	0.171	114	14.3
KI	2.65	546	0.45	0.21	0.169	154	19.7
CaF ₂	2.06	589	4.7	0.026	0.198	14.3	0.81
ZnS	5.5	630	5.9	0.091	-0.01	191	5020

(a) R_B calculated from Eq. (8) with C_{44} and P_{44} calculated from $(C_{11} - C_{12})/2$ and $(P_{11} - P_{12})/2$ for these cubic crystals. ϵ and P were not always measured at same λ , nor were the differential coefficients used in Wehner and Kleins¹⁰ estimate of r . Here the order of priority for λ used in Eq. (8) was $\lambda(\epsilon)$, $\lambda(P)$. β_R was calculated from Eq. (9) using η_{WK} from Table I.

(b) Values of constants taken from reference (10).

(c) Values for NaF taken from reference (11) except C_{12} .

TABLE III: Experimental Migration, E_M , and Aggration E^* Energies and Dimer Formation Energies E_B from Crawfords Model.

System	$E^*(\text{eV})$	$E_M(\text{eV})$	$E_B(\text{eV})$
NaCl:Mn	0.83 (30)	0.95 (40)	0.12
	$0.78 \pm .05$ (41)		0.17
NaCl:Cd	$0.50 \pm .04$ (39)	0.92 (41)	0.42
		0.857 (43)	0.36
		0.64 (42)	0.14
NaCl:Ca	0.92 (41)	0.96 (44)	0.04
		0.90 (46)	-0.02
		0.851 (45)	-0.07
		1.15 (47)	0.23
NaCl:Pb	0.80 (48)	0.982 (43)	0.18
NaCl:Co	0.61 (49)	1.06 (50)	0.45
KCl:Sr	0.73 (30)	0.871 (52)	0.14
KCl:Ba	0.74 (30)		
KCl:Pb	0.85 (53)	0.908 (54)	0.06

TABLE IV: Enthalpies and Entropies of Solution of Divalent Impurities in Alkali Halides.

Host→ Impurity	NaCl		KCl		KBr	
	h(eV)	S(k)	h(eV)	S(k)	h(eV)	S(k)
Ca	0.64	-0.7(65) ¹	0.086(27) ³		0.72	- 4.8(66) ¹
	1.0	(67) ²				
Sr	1.80	15 (68) ¹			1.14	7.3(66) ¹
	1.4	(68) ²			0.204	(27) ³
Ba	2.0	9.4(68) ¹			1.88	13 (66) ¹
	1.6	(68) ²				
Pb					0.190	(27) ³
Cd	0.71	(63) ¹				
	0.66	(27) ¹				
	1.24	10.6(65) ¹				
	1.14	(67) ²				
	0.992	0.81(60) ^{1,6}				
	0.378	1.56(60) ^{3,6}				
	1.195	0.95(60) ^{5,6}				
	0.24	(27)(57) ³				
Mn	0.816	-2.92(60) ^{1,6}				
	0.386	-2.48(60) ^{3,6}				
	0.347	-2.42(60) ^{4,6}				
	0.984	-2.34(60) ^{5,6}				

- Notes: 1. Solute assumed to form M^+ and V_C^- only in crystal.
 2. h_c , the enthalpy of formation of V_C assumed to be 0.7 eV.
 3. Solute assumed to form $\{MV_C(0)\}$.
 4. Solute assumed to form $\{MV_C(1)\}_1$.
 5. Solute assumed to form $\{MV_C(0)\}_3$.
 6. Species in 1,3,4,5 in equilibrium with $6NaCl \cdot MCl_2$.

TABLE V: Activation Energy and Frequency Factor for Formation of Trimers.

$$dn/dT = -\nu_0 n^3 e^{-E/kT}$$

M^{2+}	KCl		NaCl	
	E(eV)	$\nu_0(s^{-1})$	E(eV)	$\nu_0(s^{-1})$
Sr	0.73	4×10^{13} (30)		
Ba	0.74	8×10^{15} (30)		
Mn			0.83	8×10^{17} (30)
Cd			0.5	2.8×10^{16} (39)
			$\sim 1.0^1$	6×10^{11} (57)
			$\sim 0.8^1$	3×10^6 (57)

D. LIGHT SCATTERING BY POINT DEFECTS IN INSULATING CRYSTALS^{*}

The scattering by point imperfections and clusters is often characterized by an effective particle size, which is obtained formally by equating the Mie-scattering result to the result for the point imperfection or cluster. This effective radius r_e is typically greater than the actual radius. In this section it is shown that the scattering by the strain field around an impurity ion is negligible and cannot account for the difference between the effective radius and the actual radius. The difference between the effective radius and the actual radius does not constitute an unresolved theoretical problem because the macroscopic theoretical Mie results is not expected to hold at such small volumes that the assumption of many atoms within the volume is violated.

I. INTRODUCTION

There is currently interest in the elastic scattering of light from point defects in alkali halides, since these materials may prove useful for fabrication of optical fibers with ultra-low absorption near $1\text{ }\mu\text{m}^1$. This requires that all sources of absorption or scattering be eliminated, save that from intrinsic processes. In materials presently available, quasi-elastic scattering of light is observed with intensity one or two orders of magnitude greater than expected from theoretical considerations applied to the pure material. Experimentally, one verifies this by comparing the integrated intensity of the Brillouin doublets, and that of light scattered by quasi-elastic processes. From the Landau-Placzek ratio, as modified recently by Wehner and Klein², one expects the quasi-elastic peak to be two orders of magnitude weaker than the Brillouin doublets in alkali halide crystals, while in practice the two features are found to have comparable intensity even in crystals of high nominal purity.

A point defect in the crystal scatters light elastically because, when its influence is viewed in macroscopic terms, the dielectric constant within the unit cell that contains the impurity differs from that of the surrounding medium. This leads to Rayleigh scattering, with cross section proportional to ω^4 , where ω is the frequency of the light. Thus, point defects such as impurity ions or vacancies lead to scattering which contributes to the intensity of the quasi-elastic peak.

In addition to the scattering mechanism described above, there is a second means by which even an isoelectronic point defect may scatter

light elastically. When an impurity or vacancy is introduced into the crystal, the nearest neighbors shift off lattice sites appropriate to the perfect crystal, with the result that a macroscopic strain is induced in the surrounding material. This strain is long-ranged, and has the potential of substantially increasing the cross section for scattering from the defect. When it is noted that the dielectric constant is affected by this strain field, the impurity is surrounded by a "halo" of substantial effective radius. Even if the local change in dielectric constant within the halo is small, its large effective radius may render it effective in scattering light.

One aim of this paper is to derive an expression for the light scattering cross section from a point defect, with the "strain halo" effect included. Then we apply the resulting formula to the alkali halides, with emphasis on potassium bromide, which has been studied extensively by Edwards and Fredericks³, to isolate the contribution of particular impurities to the quasi-elastic central peak. Our simple model is applicable to isoelectronic defects in alkali halides, and here we reach conclusions compatible with the data: that isoelectronic impurities at the part per million level fail to contribute significantly to the central peak.

II. THE CALCULATION

Let the defect produce a perturbation in the dielectric tensor of the crystal we designate as $\Delta\epsilon_{ij}(\vec{x})$. We assume that the crystal is optically isotropic, but the strain field induces local anisotropy in the dielectric tensor. We suppose $\Delta\epsilon_{ij}(\vec{x})$ is non-zero only in the neighborhood of the defect, although we may proceed without specifying its form in detail.

If $E_i^{(0)}(\vec{x})$ is the i^{th} Cartesian component of the incident electric field, which has frequency ω , then to first order in $\Delta\epsilon_{ij}(\vec{x})$ the scattered field is given by

$$E_i^{(s)}(\vec{x}) = -\left(\frac{\omega}{c}\right)^2 \int d^3x' \sum_{jk} D_{ij}(\vec{x} - \vec{x}') \Delta\epsilon_{jk}(\vec{x}') E_k^{(0)}(\vec{x}') \quad (1)$$

where $D_{ij}(\vec{x} - \vec{x}')$ is the Green's function matrix associated with Maxwell's equations. Far from the impurity, as $|\vec{x}| \rightarrow \infty$ with \vec{x}' fixed, one has

$$D_{ij}(\vec{x} - \vec{x}') = -\frac{e^{iK_0|\vec{x}|}}{4\pi|\vec{x}|} (\delta_{ij} - \hat{n}_i^{(s)} \hat{n}_j^{(s)}) e^{-i\vec{k}^{(s)} \cdot \vec{x}'} \quad (2)$$

where $K_0 = \omega\epsilon^{1/2}/c$, with ϵ the optical frequency dielectric constant of the unstrained crystal. Here we assume the material is transparent, so ϵ is real and positive. We have $\hat{n}^{(s)}$ a unit vector from the impurity to the point of observation \vec{x} , and $\vec{k}^{(s)} = K_0 \hat{n}^{(s)}$ is the wave vector of the scattered light. If for $E_k^{(0)}(\vec{x}')$ we take the form $\delta_{kx} E^{(0)} \exp[i\vec{k}^{(0)} \cdot \vec{x}']$, corresponding to an electric field parallel to the x-axis with wave vector $\vec{k}^{(0)}$ directed parallel to \hat{z} , then we have

$$E_i^{(s)}(\vec{x}) = \frac{\omega^2 e^{iK_0 x}}{4\pi c^2 x} \sum_j \left\{ \delta_{ij} - \hat{n}_i^{(s)} \hat{n}_j^{(s)} \right\} \Delta \epsilon_{jx}(\vec{Q}) \quad (3)$$

where we have defined

$$\Delta \epsilon_{ij}(\vec{Q}) = \int d^3 x' e^{-i\vec{Q} \cdot \vec{x}'} \Delta \epsilon_{ij}(\vec{x}') \quad (4)$$

with $\vec{Q} = \vec{k}^{(s)} - \vec{k}^{(o)}$ the scattering vector. The magnitude of \vec{Q} is $2K_0 \sin(\theta/2)$ where θ is the angle between the \hat{z} -axis and the wave vector of the scattered light.

By forming the Poynting vector associated with the scattered radiation, then dividing by the incident energy flux, one can form an expression for the cross section σ for scattering from the point defect. One has

$$\sigma = \frac{\omega^4}{16\pi^2 c^4} \int d\Omega(\hat{n}_s) \sum_{jj'} (\delta_{jj'} - \hat{n}_j^{(s)} \hat{n}_{j'}^{(s)}) \Delta \epsilon_{jx}(\vec{Q}) \Delta \epsilon_{j'x}(\vec{Q}) \quad (5)$$

where the integration is over all directions of the scattered light.

We now turn to our explicit model of $\Delta \epsilon_{ij}(\vec{x})$. Suppose the impurity cell perturbs the matrix by changing the dielectric constant within the impurity unit cell by the amount $\Delta \epsilon_0$. If V_c is the volume of the unit cell, approximated by a sphere of radius R_0 , we then have

$$\Delta \epsilon_{ij}(x) = V_c \Delta \epsilon_0 \delta(\vec{x}) \delta_{ij} + \tilde{\Delta \epsilon}_{ij}(\vec{x}) \quad (6)$$

where $\Delta\tilde{\epsilon}_{ij}(\vec{x})$ is the part that comes from lattice strains outside the unit cell. Thus

$$\Delta\epsilon_{ij}(\vec{Q}) = V_c \Delta\epsilon_{ij} + \int_{|\vec{x}'| > R_0} d^3x' e^{-i\vec{Q}\cdot\vec{x}'} \Delta\tilde{\epsilon}_{ij}(\vec{x}') \quad (7)$$

The first term in Eq. (7) taken alone gives for the cross section the Rayleigh result σ_0 which, in our present model is

$$\sigma_0 = \frac{\omega^4 (V_c \Delta\epsilon_0)^2}{6\pi c^4} \quad (8)$$

We next turn to the form of $\Delta\tilde{\epsilon}_{ij}(\vec{x})$. We model the strain field around the defect as follows. Imagine the unit cell which surrounds the defect is a sphere of nominal radius R_0 . After introduction of the defect, the impurity cell will contract or expand, to change the radius by the amount Δ . This produces a displacement $\vec{U}(\vec{x})$ of the material outside the unit cell and elasticity theory for an isotropic material allows us to write

$$\vec{U}(\vec{x}) = \hat{x} \Delta \left(\frac{R_0}{x} \right)^2 \quad (9)$$

where \hat{x} is the unit vector in the radial direction. The expression in Eq. (9), and of course the results deduced from it, are valid only in the limit where Δ is small compared to R_0 , so linear elasticity theory may be used to describe the lattice deformation outside the unit cell.

In the presence of strains described by the strain tensor $e_{ij}(\vec{x}) = 1/2(\partial U_i / \partial x_j + \partial U_j / \partial x_i)$, we have for $e_{ij}(\vec{x})$ the forms

$$\delta\epsilon_{xx}(\vec{x}) = -\epsilon^2 \left[p_{11}e_{xx} + p_{12}(e_{yy} + e_{zz}) \right], \quad (10a)$$

$$\delta\epsilon_{xy}(\vec{x}) = -\epsilon^2 p_{44} e_{xy} \quad (10b)$$

with the remaining elements of $\delta\epsilon_{ij}(\vec{x})$ obtained by permutation. In Eqs. (10), ϵ is again the optical frequency dielectric constant, while p_{11} , p_{12} and p_{44} are the Pockels elasto-optic tensors. For convenience, we adopt the isotropy assumption $p_{44} = p_{11} - p_{12}$, which allows Eq. (10a) and Eq. (10b) to be combined into the statements

$$\delta\epsilon_{ij}(\vec{x}) = P_1 \delta_{ij}(\nabla \cdot \vec{U}) + P_2 \left[e_{ij} - 1/3 \delta_{ij}(\nabla \cdot \vec{U}) \right] \quad (11)$$

where $P_1 = -\epsilon^2(p_{11} + 2p_{12})/3$ and $P_2 = \epsilon^2(p_{12} - p_{11})$.

Now for the displacement pattern in Eq. (9), one has

$$\vec{\nabla} \cdot \vec{U} = 0 \quad (12)$$

and there is no local dilation in volume outside the defect cell. Thus, the scattering from the "strain halo" comes entirely from the second term in Eq. (11). If we let $A = P_2 R_0^2 \Delta$, then this gives us

$$\delta\epsilon_{ij}(\vec{x}) = \frac{A}{x^3} \left(\delta_{ij} - 3 \frac{x_i x_j}{x^2} \right) \quad (13)$$

so the strain field falls off slowly with distance as x^{-3} . With this form, one has

$$\Delta\epsilon_{ij}(\vec{Q}) = \epsilon_1(Q)\delta_{ij} + \epsilon_2(Q)\hat{Q}_i\hat{Q}_j \quad (14)$$

where

$$\epsilon_1(Q) = V_c\Delta\epsilon_0 + \frac{4\pi A}{(QR_0)^2} \left(\cos(QR_0) - \frac{\sin(QR_0)}{QR_0} \right) \quad (15a)$$

and

$$\epsilon_2(Q) = -\frac{12\pi A}{(QR_0)^2} \left(\cos(QR_0) - \frac{\sin(QR_0)}{QR_0} \right) \quad (15b)$$

For our purposes, the limit $QR_0 \ll 1$ is appropriate, so we may replace these forms by

$$\epsilon_1(Q) = V_c\Delta\epsilon_0 - \frac{4\pi A}{3} \quad (16a)$$

and

$$\epsilon_2(Q) = +4\pi A \quad (16b)$$

It is a straight forward, but tedious matter to use Eq. (14) combined with Eqs. (16) to work out an explicit expression for the light scattering cross section. We introduce a parameter r that provides a dimensionless measure of the role played by the "strain halo". We thus define

$$r = \frac{P_2\Delta}{R_0\Delta\epsilon_0}, \quad (17)$$

which enables the cross section to be written in the form

$$\sigma_{TOT} = \sigma_0 S \quad (18)$$

where

$$S = 1 - \frac{5}{4} r + \frac{5}{2} r^2 \quad (19)$$

and where the quantity σ_0 is the Rayleigh cross section defined in Eq. (8).

We see that inclusion of scattering from the strain halo alters the magnitude of the Rayleigh cross section, but leaves the well-known ω^4 frequency dependence unaltered. We do not find the latter result obvious, in view of the long ranged nature of the strain field around the defect. In the next section, we estimate the value of r for a typical alkali halide, along with the scattering power of a defect in such a crystal.

The principle results of the present paper are contained in Eq. (18) and Eq. (19). Since these results were obtained within the context of a simple model which treats the medium outside the defect as an isotropic elastic continuum, it is useful to comment on what features will remain in a more general treatment of the problem.

It can be shown quite generally, even if the material outside the defect cell is not isotropic, that inclusion of the scattering from the "strain halo" leaves the ω^4 variation of the Rayleigh cross section unaltered. This is true within the framework of a calculation that treats the medium outside the defect cell as an elastic continuum, but not necessarily isotropic in character. What is required to demonstrate this is that the displacement field $\vec{U}(\vec{x})$ falls off inversely with x^2 , though in general there will be an angular variation of the displacement pattern more complex than displayed in Eq. (9). A discrete lattice calculation will show deviations from the

x^{-2} behavior close in to the defect, but such short range modifications of the displacement field will also leave the ω^4 dependence unaltered, as the leading contribution to the cross section. Thus we believe that Eq. (18), with S independent of frequency, to be valid quite generally when the strain halo scattering is incorporated into the theory.

Of course, the specific form given for S in Eq. (19) is dependent on our use of the isotropic continuum picture to model the medium outside the defect cell. It is possible to obtain formal expressions for $\Delta\epsilon_{ij}(\vec{Q})$ for more general models, and in specific cases it should be possible to carry these through to the calculation of S . But these forms are cumbersome and not enlightening, so we have confined our attention to the simple isotropic continuum model, which we believe provides reliable semi-quantitative estimates of the magnitude of S .

We have also confined our attention to an isolated defect in a medium of infinite extent, since for the very low impurity concentrations present in the high purity materials that motivate this work, the total scattering cross section is simply the cross section per impurity multiplied by the numbers of impurities exposed to the beam. This is so as long as the impurities are distributed randomly in the host. If a defect is placed in a finite sample, the strain field must be synthesized from the direct strain field from the defect itself (considered here), and that from an array of image defects arranged to insure satisfaction of the stress free boundary conditions. The strain fields from the image defects are small, and will lead to no major modifications of our results, save for defects located near the surface. In highly transparent media, these are only a small fraction of those sampled by the beam.

III. DISCUSSION

In this section, we comment on the implications of the result displayed in Eq. (18), which is the principal result of the present paper. We first assess the possible importance of scattering from the "strain halo" effect contained in the factor S in Eq. (18).

For a number of crystals, Wehner and Klein² have tabulated values of p_{11} and p_{12} , along with the optical frequency dielectric constant. This enables us to calculate the constant P_2 , which is dimensionless and depends on only the properties of the host crystal. Both Δ/R_0 and $\Delta\epsilon_0$ depend on the nature of the particular defect under consideration. Here we choose $|\Delta/R_0| = 0.1$ and $|\Delta\epsilon_0| = 1.0$ as typical order of magnitude estimates for these quantities. For a lattice vacancy in an alkali halide, where the optical frequency dielectric constant is near 2.0 in value, we expect $\Delta\epsilon_0 \approx -1.0$ and the lattice should collapse locally into the defect cell. Then we have $r \approx 0.1 P_2$ for this picture.

For the alkali halides, with the exception of lithium flourine, p_{11} and p_{12} do not differ greatly. For potassium bromide, for example, $|p_{11} - p_{12}| \approx 0.04$ so with $\epsilon = 2.36$ we estimate $|r| \approx 0.02 \ll 1$. The scattering from the "strain halo" is thus quite negligible.

The reason for this is clear upon noting that for the displacement pattern in Eq. (9), $\nabla \cdot \vec{U} = 0$. Thus, outside the impurity cell, the lattice distortion leads to no local change in density, but it simply lowers the local symmetry from cubic to tetragonal. The dielectric constants of the alkali halides is described rather well by the Clausius -

Mosotti relation combined with free ion polarizabilities; this is a reflection of the highly ionic character of the alkali halides. The consequence is that the dielectric constant of the alkali halides depends on the density of the ions, but is insensitive to ionic rearrangements which leave the average density unchanged.

The above argument suggests that in covalent materials, the "strain halo" scattering may be much more significant in magnitude. Consider silicon, for example. Here $|p_{11} - p_{12}| \approx 0.09$, and $P_2 = 12.9$, so we estimate $|r| \approx 1.29$ with the above value of (Δ/R_0) and $\Delta\epsilon_0$. Thus, here the "strain halo" scattering is estimated to be of equal importance, or possibly larger than, that produced by the local change in electronic polarizability. A similar estimate for barium titanate gives $|r| = 1.42$, so again the "strain halo" scattering contributes importantly to the cross section⁵.

Our conclusion is that in the alkali halides, our parameter r is small compared to unity always, and the cross section provided by the Rayleigh theory is quite adequate. In less ionic materials, such as silicon or barium titanate, where the dielectric tensor is sensitive to local changes in symmetry, then scattering produced by the strain field outside the impurity cell is of comparable importance to that from the local change in electronic polarizability produced by the defect.

Edwards and Fredericks⁽³⁾ have carried out an extensive series of light scattering studies of the Landau-Placzek ratio in potassium bromide of high nominal purity, to determine whether point defects are responsible for the large intensity of the quasi-elastic central peak. While their samples contain rubidium at the part per million level, present as an

isoelectronic substitutional impurity which replaces potassium, this impurity has no effect on the intensity of the central peak. They do find that Fe^{2+} , present at much lower concentration than rubidium, does give a contribution to the central peak linear in the Fe^{2+} concentration.

Our model applies to rubidium, and with r chosen to be zero, and $\Delta\epsilon \approx -1$, we find the Rayleigh cross section assumes the value $\sigma_0 \approx 5.9 \times 10^{-25} \text{ cm}^2$. This estimate applies to the 5145 \AA Ar^+ laser line, and we take $R_0 = 3.28 \text{ \AA}$, the nearest neighbor distance in potassium bromide. If rubidium impurities are present at the one part per million level, then with $n \approx 1.4 \times 10^{16}$ defects per cm^3 , we estimate the extinction length associated with Rayleigh scattering from rubidium impurities to be $\ell \approx 1.2 \times 10^8 \text{ cm}$, a value comfortably higher than the values of $10^6 - 10^7 \text{ cm}$ typically associated with Brillouin scattering intensities in the alkali halides. Thus, our conclusion is that while rubidium is the most abundant impurity in the samples used by Edwards and Fredericks³, Rayleigh scattering from these ions is too weak to account for the quasi-elastic peaks observed by them. This is in accord with their interpretation of the data, as outlined above.

At this point, we can say little about scattering produced by Fe^{2+} on the basis of our model, which ignores the macroscopic electric field outside the defect unit cell present when an impurity with valence different than the host ion it replaced is present. Also, such impurities have charge compensation centers in their near vicinity, so a simple physical picture of light scattering from the complex involves a number of considerations not contained in the present model.

IV. SUMMARY

We have examined the theory of light scattering by point defects in crystals through use of a model which includes scattering induced by the strain field near the defect, in addition to that caused by the change in electronic polarizability within the unit cell which contains it. The model applies to defects with the same valence as the missing host ion. We find the light scattering-cross section is given by an expression of the Rayleigh form, with overall magnitude influenced by interference between the two mechanisms considered. A rough estimate of the cross section shows, in agreement with recent data, that isoelectronic impurities present in alkali halide crystals at the part per million level should not influence the Landau-Placzek ratio.

V. ACKNOWLEDGEMENTS

We are grateful to Professor W. Fredericks for his useful comments and his interest in the present study. This research was supported by the Defense Advanced Research Projects Agency, with technical administration by the Naval Research Laboratory.

REFERENCES

- * Accepted for publication in the Journal of Applied Physics.
1. A. L. Gentile, M. Braunstin, D. A. Pinnow, J. A. Harrington, D. M. Henderson, L. M. Hobrock, J. Meyer, R. C. Pastor, and R. R. Turk, "Infrared-Fiber Optical Materials," in Fiber Optics: Advances in Research and Development, Bernard Bendow and Shashanka S. Mitra, Eds., Plenum Publishing Corporation, 1979.
 2. R. K. Wehner and R. Klein, *Physica* 62, 161 (1972).
 3. David F. Edwards and W. J. Fredericks, private communication, 1980.
 4. See J. F. Nye, Physical Properties of Crystals (Oxford University Press, England, 1960).
 5. In silicon, and very clearly in barium titanate, our isotropy assumptions must be modified to obtain a proper description of the strain halo scattering.

E. MULTIPLE SCATTERING

In this section it is shown by developing a multiple-scattering formalism and applying the result to scattering by randomly located spherical voids that the multiple-scattering reduction of the individual scattering results is entirely negligible in low-loss fibers because the scattering must be small and multiple-scattering effects are negligible for small scattering.

I. INTRODUCTION

The propagation of light in a medium with randomly distributed inhomogeneities or scattering centers can be usefully treated by the perturbation methods originally developed for quantum field theory. In addition to providing a convenient framework for describing the effects of multiple scattering, the techniques allow important classes of terms appearing in the multiple scattering expansion to be summed in closed form.

Following the work of Tatarski¹, in Sec. II we derive expressions for the ensemble-averaged propagator, which carries information about the effects of multiple scattering on the dielectric properties of the medium. In particular, it provides an estimate of the attenuation. In Sec. III we apply the results to the simple case of randomly located identical spherical inclusions. The calculation leads to simple closed-form expressions for the modification of the dielectric constant by the inclusions.

II. MULTIPLE SCATTERING FORMALISM

Scalar wave propagation in a spatially varying medium is described by the Green's function $G(\underline{r}, \underline{r}')$ between points \underline{r} and \underline{r}' satisfying the equation

$$\nabla^2 G(\underline{r}, \underline{r}') + k_0^2 \epsilon(\underline{r}) G(\underline{r}, \underline{r}') = \delta^3(\underline{r} - \underline{r}') . \quad (1)$$

Here $k_0 \equiv 2\pi/\lambda_0$ is the free space wave number corresponding to wavelength λ_0 and $\epsilon(\underline{r})$ is the stochastic dielectric function for the medium. Defining the ensemble averaged dielectric constant $\langle \epsilon \rangle$ and $k_1^2 \equiv k_0^2 \langle \epsilon \rangle$, Eq. (1) can be written

$$\nabla^2 G(\underline{r}, \underline{r}') + k_1^2 [1 + \epsilon_1(\underline{r})] G(\underline{r}, \underline{r}') = \delta^3(\underline{r} - \underline{r}') \quad (2)$$

where

$$\epsilon_1(\underline{r}) \equiv [\epsilon(\underline{r}) - \langle \epsilon \rangle] / \langle \epsilon \rangle . \quad (3)$$

By construction $\langle \epsilon_1 \rangle = 0$. Defining the operators $L_0 \equiv \nabla^2 + k_1^2$ and $M_0 \equiv L_0^{-1}$, the unperturbed propagation is described by the equation for the free propagator G_0

$$L_0 G_0(\underline{r}, \underline{r}') = \delta^3(\underline{r} - \underline{r}') \quad (4)$$

having the solution satisfying the radiation boundary condition

$$G_0(\underline{r}, \underline{r}') = M_0 \delta^3(\underline{r} - \underline{r}') = -(4\pi)^{-1} \exp [ik_1 |\underline{r} - \underline{r}'|] / |\underline{r} - \underline{r}'|. \quad (5)$$

Substitution into Eq. (2) produces

$$G(\underline{r}, \underline{r}') \equiv -k_1^2 (M_0 \epsilon_1 G)(\underline{r}, \underline{r}') + G_0(\underline{r}, \underline{r}') \quad (6)$$

$$\equiv -k_1^2 \int d^3 \underline{r}'' G_0(\underline{r}, \underline{r}'') \epsilon_1(\underline{r}'') G(\underline{r}'', \underline{r}') + G_0(\underline{r}, \underline{r}'). \quad (6a)$$

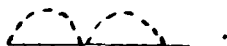
Ensemble averaging Eq. (6) gives in operator notation

$$\langle G \rangle = G_0 - k_1^2 M_0 \langle \epsilon_1 G \rangle. \quad (7)$$

Equation (7) can be formally solved by iteration to produce the usual Born series. Each term in the series can be represented by a diagram as in quantum field theory leading to the diagrammatic representation of Eq. (7)

$$\begin{aligned} \text{---} &= \text{---} + \text{---} \text{---} \text{---} \\ &= \text{---} + \text{---} \text{---} \text{---} + \text{---} \text{---} \text{---} + \dots + \\ &+ \text{---} \text{---} \text{---} + \dots + \text{---} \text{---} \text{---} + \dots \end{aligned} \quad (7a)$$

Instead of solving Eq. (7) by iteration directly it is desirable to separate out the disconnected diagrams such as



Following Tatarski¹, set

$$G = \langle G \rangle + G_F \quad (8)$$

so $\langle G_F \rangle = 0$ and substitute into Eq. (2)

$$L_0[\langle G \rangle + G_F] + k_1^2 \epsilon_1[\langle G \rangle + G_F] = \delta^3(\underline{r} - \underline{r}'). \quad (9)$$

Ensemble averaging gives

$$L_0 \langle G \rangle + k_1^2 \langle \epsilon_1 G_F \rangle = \delta^3(\underline{r} - \underline{r}') \quad (10)$$

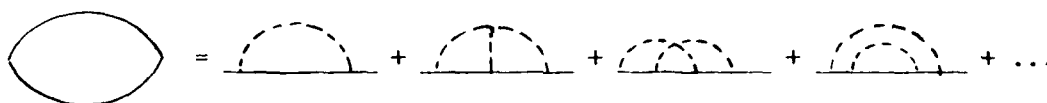
where we have used $\langle \epsilon_1 \rangle = 0$. Subtracting Eq. (10) from (9) and operating with M_0 produces

$$G_F = -k_1^2 M_0 \epsilon_1 \langle G \rangle - k_1^2 M_0 [\epsilon_1 G_F - \langle \epsilon_1 G_F \rangle]. \quad (11)$$

Iteration of this expression followed by multiplication by $k_1^2 \epsilon_1$ and ensemble averaging gives

$$\begin{aligned}
k_1^2 \langle \epsilon_1 G_F \rangle &= [-k_1^4 \langle \epsilon_1 M_0 \epsilon_1 \rangle - k_1^6 \langle \epsilon_1 M_0 \epsilon_1 M_0 \epsilon_1 \rangle \\
&\quad - k_1^8 \langle \epsilon_1 M_0 \epsilon_1 M_0 \epsilon_1 M_0 \epsilon_1 \rangle + k_1^8 \langle \epsilon_1 M_0 \epsilon_1 \rangle M_0 \langle \epsilon_1 M_0 \epsilon_1 \rangle \\
&\quad + \dots] \langle G \rangle \equiv -Q \langle G \rangle .
\end{aligned} \tag{12}$$

Unlike Tatarski, who was calculating the effects of normally distributed refractive index fluctuations with zero mean, we cannot in general neglect the odd order moments of ϵ_1 , except the first. This leads to the appearance of terms such as the one proportional to k_1^6 which are absent in Tatarski's treatment. In diagrams the expression above for Q appears as



This represents the "self-energy" contribution to the propagator and consists of only the connected diagrams of $\langle G \rangle$. Substituting Eq. (12) into (10) gives

$$L_0 \langle G \rangle - Q \langle G \rangle = \delta^3(\underline{r} - \underline{r}'). \tag{13}$$

Operating with M_0 produces

$$\langle G \rangle = G_0 + M_0 Q \langle G \rangle \tag{14}$$

which is Dyson's equation representing the average propagation as an infinite sum of "self-energy" terms coupled by the free propagation.

In diagrams

$$\begin{aligned}
 \text{thick line} &= \text{thin line} + \text{thin line with circle} \\
 &= \text{thin line} + \text{thin line with circle} + \text{thin line with two circles} + \dots
 \end{aligned}
 \tag{14a}$$

Equation (14) can be solved using Fourier transforms once a choice of Q is made; letting $\langle g \rangle$, g_0 , and q devote the respective transforms of $\langle G \rangle$, G_0 , Q a simple calculation gives

$$\langle g(\underline{\kappa}) \rangle = g_0(\underline{\kappa}) + (2\pi)^6 g_0(\underline{\kappa}) q(\underline{\kappa}) \langle g(\underline{\kappa}) \rangle \tag{15}$$

or

$$\langle g(\underline{\kappa}) \rangle = [g_0(\underline{\kappa})^{-1} - (2\pi)^6 q(\underline{\kappa})]^{-1} . \tag{16}$$

If desired, $\langle G \rangle$ can be obtained from Eq. (16) by inverse transformation; however, the most useful information about the averaged propagator concerns the modification of multiple scattering to the dielectric constant which can be obtained directly from the pole structure of Eq. (16) as will be illustrated in the next section.

III. SCATTERING FROM SPHERICAL INCLUSIONS

As an example of the application of the formalism just developed, consider the scattering from a randomly distributed set of identical spherical inclusions of radius a and dielectric constant ϵ_S imbedded in a uniform background of dielectric constant ϵ_0 . The dielectric function for a sample volume Ω is then

$$\epsilon(\underline{r}) = \sum_{i=1}^N W(\underline{r} - \underline{R}_i) \quad (17)$$

where we have assumed there are N inclusions located at random points \underline{R}_i . In this case

$$\begin{aligned} W(\underline{r}) &= \epsilon_S & \text{for } |\underline{r} - \underline{R}_i| \leq a \\ &= \epsilon_0 & \text{for } |\underline{r} - \underline{R}_i| > a \end{aligned} \quad (18)$$

The mean of $\epsilon(\underline{r})$ is

$$\begin{aligned} \langle \epsilon \rangle &= \frac{1}{\Omega} \int d^3r \epsilon(\underline{r}) = \frac{1}{\Omega} \sum_{i=1}^N \int d^3r W(\underline{r} - \underline{R}_i) = \frac{1}{\Omega} \sum_{i=1}^N \int d^3r W(\underline{r}) \\ &= f\epsilon_S + (1 - f)\epsilon_0 \end{aligned} \quad (19)$$

where $f \equiv 4\pi a^3 N / 3\Omega$ is the fractional volume displaced by all the inclusions.

To estimate Q we make the simplest approximation of keeping only the lowest order contribution and assume the spheres do not overlap. Then

$$\begin{aligned}
 Q(\underline{r} - \underline{r}') &\approx k_1^4 \langle \epsilon_1 M_0 \epsilon_1 \rangle \\
 &= k_1^4 \langle \epsilon_1(\underline{r}) \epsilon_1(\underline{r}') \rangle G_0(\underline{r} - \underline{r}') \\
 &= \frac{k_1^4}{\langle \epsilon \rangle^2} [\langle \epsilon(\underline{r}) \epsilon(\underline{r}') \rangle - \langle \epsilon \rangle^2] G_0(\underline{r} - \underline{r}'). \quad (20)
 \end{aligned}$$

Let $B_\epsilon(\underline{r} - \underline{r}') \equiv \langle \epsilon(\underline{r}) \epsilon(\underline{r}') \rangle$ be the correlation function satisfying the requirements $B_\epsilon(0) = \beta \epsilon_S^2 + (1 - \beta) \epsilon_0^2$ and $\lim_{r \rightarrow \infty} B_\epsilon(\underline{r}) = \langle \epsilon \rangle^2$. Expanding $\langle \epsilon \rangle$, it can be shown that

$$B_\epsilon(\underline{r}) = \beta(1 - \beta)(\epsilon_S - \epsilon_0)^2 f(r) + \langle \epsilon \rangle^2, \quad (21)$$

where $f(r)$ is the overlap function for two spheres of radius a . Straight-forward calculation gives

$$\begin{aligned}
 f(r) &= 1 - \frac{3}{2} \left(\frac{r}{2a} \right) + \frac{1}{2} \left(\frac{r}{2a} \right)^2, \quad r \leq 2a \\
 &0, \quad r > 2a. \quad (22)
 \end{aligned}$$

The mathematics is greatly simplified by approximating $f(r) \approx e^{-r/a}$ for all r . With this choice

$$B_{\epsilon_1}(\underline{r}) \simeq \beta(1 - \beta)(\epsilon_S - \epsilon_0)^2 e^{-r/a} / \langle \epsilon \rangle^2 \quad (23)$$

and

$$\begin{aligned} q(\underline{\kappa}) &= \frac{k_1^4}{(2\pi)^3} \int d^3r B_{\epsilon_1}(\underline{r}) G_0(\underline{r}) e^{-i\underline{\kappa} \cdot \underline{r}} \\ &= - \frac{k_0^4}{(2\pi)^3} \beta(1 - \beta) \frac{(\epsilon_S - \epsilon_0)^2}{\kappa^2 + (\frac{1}{a} - ik_1)^2} . \end{aligned} \quad (24)$$

Substituting into Eq. (16) gives

$$\langle g(\underline{\kappa}) \rangle = (2\pi)^{-3} \left[k_1^2 - \kappa^2 + \frac{k_0^4 \beta(1 - \beta)(\epsilon_S - \epsilon_0)^2}{\kappa^2 + (\frac{1}{a} - ik_1)^2} \right]^{-1} \quad (25)$$

For small particles, with $k_1 a \ll 1$, the poles of $\langle g(\underline{\kappa}) \rangle$ occur at

$$\kappa^2 \simeq k_1^2 + k_0^4 \beta(1 - \beta)(\epsilon_S - \epsilon_0)^2 a^2 (1 + i2k_1 a) . \quad (26)$$

Defining $k_1 \equiv p_0$ and $k \equiv n_e p_0 + i\beta_{sc}$, we find

$$n_e \simeq \left[1 + k_0^2 a^2 \beta(1 - \beta) \operatorname{Re}(\epsilon_S - \epsilon_0)^2 / n_{\langle \epsilon \rangle}^2 \right]^{1/2} \quad (27)$$

$$\beta_{sc} \approx \frac{k_0^4 a^3 f(1-f) \operatorname{Re}(\epsilon_S - \epsilon_0)^2}{n_e} \quad (28)$$

Here n_e represents the correction to the average refractive index $n_{\langle \epsilon \rangle}$, defined as $p_0 = k_0 n_{\langle \epsilon \rangle}$, due to multiple scattering from the inclusions and β_{sc} is the scattering coefficient for Rayleigh scattering corrected for multiple scattering through the factor n_e .

The numerator of the second term is essentially the Rayleigh scattering result, given by Condon and Odishaw² for example. Since $n_e \geq 1$, multiple scattering has the effect of decreasing the single scattering contribution to the extinction coefficient through rescattering into the forward direction.

To estimate the importance of this screening we assume $f \ll 1$ and approximate Eq. (27) as

$$n_e \approx 1 + \frac{(k_0 a)^2}{2} \frac{\operatorname{Re}(\epsilon_S - \epsilon_0)^2}{\epsilon_0} f \quad (29)$$

In order for the Rayleigh model to be valid, the inequality $k_0 a \leq \pi$ must be satisfied. Consider the extreme case of $k_0 a = \pi$ and scattering by vacuum inclusions ($\epsilon_S = 1$). Figure 1 is a plot of n_e as a function of the refractive index n_0 of the host material, taken to be real, for various values of f . We see that in order to observe a ten percent reduction in the extinction coefficient for $n_0 = 2$, f must be about 10^{-2} ; since f can be expressed as $(a/s)^3$ where s is the average spacing between inclusions, this implies $a/s = 0.2$ which is quite large.

AD-A092 264

SCIENTIFIC RESEARCH CENTER SANTA MONICA CA
THEORETICAL STUDIES OF LOW-LOSS OPTICAL FIBERS. (U)
SEP 80 M SPARKS, W FREDERICKS, D MILLS

F/6 20/6

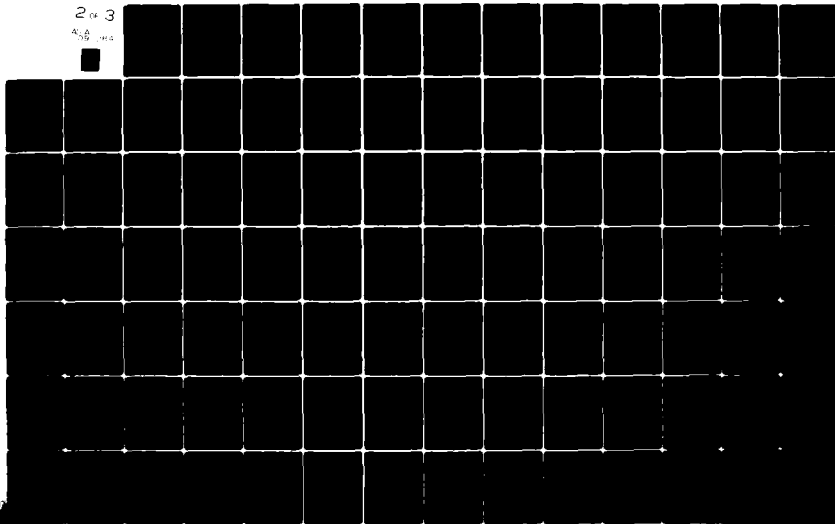
N00173-79-C-0361

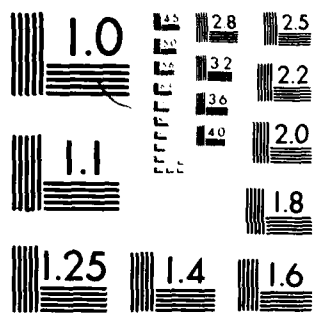
NL

UNCLASSIFIED

2 of 3

4-8 1984





MICROCOPY RESOLUTION TEST CHART
NATIONAL BUREAU OF STANDARDS-1963-A

We conclude that for $a/s \ll 0.2$ multiple scattering is not likely to change the first order Rayleigh result appreciably. For the case of low-loss fibers, the multiple-scattering reduction of the individual scattering results is entirely negligible because the scattering must be extremely small, and $n_e \approx 1$ for small scattering.

FIGURE CAPTIONS FOR SEC. E

- Fig. 1 Refractive-index dependence of correction factor n_e for multiple Rayleigh scattering from spherical vacuum inclusions imbedded in a material of refractive index n_0 . The parameter f represents the fractional volume displaced by the inclusions.

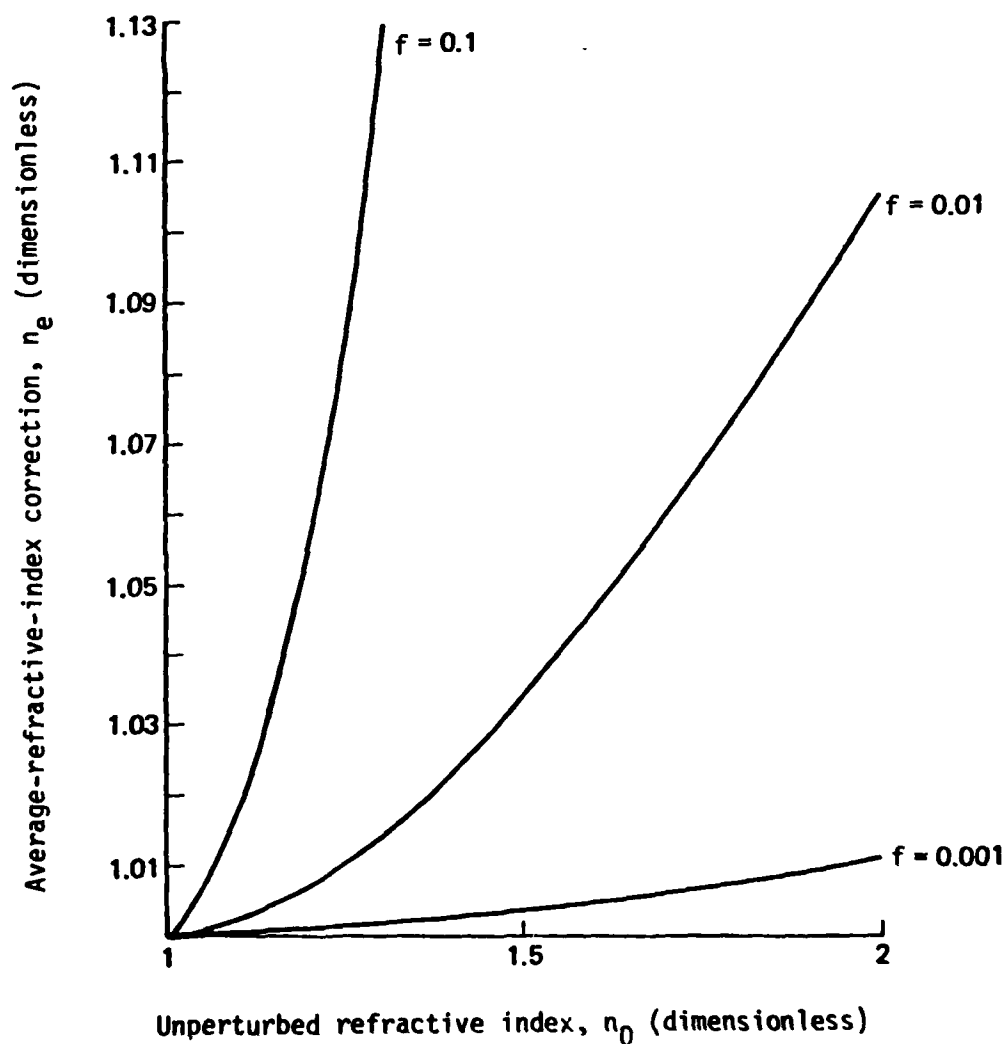


Fig. 1--Refractive-index dependence of correction factor n_e for multiple Rayleigh scattering from spherical vacuum inclusions imbedded in a material of refractive index n_0 . The parameter f represents the fractional volume displaced by the inclusions.

REFERENCES FOR SEC. E

1. V. I. Tatarski, The Effects of the Turbulent Atmosphere on Wave Propagation, translated from the Russian, originally published in 1967 (National Technical Information Service, Springfield, VA., 1971).
2. E. W. Condon and H. Odishaw, eds., Handbook of Physics, 2nd ed., McGraw-Hill, 1967.

F. TABULATION OF INFRARED-ABSORPTION COEFFICIENTS

The lowest experimental values of infrared optical-absorption coefficients from the literature are tabulated as plots of absorption coefficients as functions of frequency. Both intrinsic and extrinsic values are tabulated.

8011 18 027

There has been considerable recent interest in lowering the absorptance of transparent materials for use in high-power laser applications.¹ Both the intrinsic values of the optical-absorption coefficients and the lowest experimental values are useful. Early in the study of high-power infrared laser materials, Sparks² tabulated absorption coefficients that were available in the literature at that time. These absorption coefficients were extremely useful, but that tabulation now includes only a fraction of the measured absorption coefficients because most of the currently available data have been taken since the original tabulation was made. Other properties of laser materials that have been tabulated include the following: ultraviolet and visible-impurity absorption spectra,³ extrinsic absorptance in infrared laser-window materials,^{4,5} and laser-damage thresholds.⁶

Here we tabulate the lowest experimental values of the optical absorption coefficients β reported to date for infrared transparent materials. The results for all materials are plotted on the same scale for convenience of direct comparison. Since the multiphonon absorption mechanism is now well understood,⁷ the curves are more useful in practical applications than in theoretical investigations. Thus, the absorption coefficients are plotted as functions of the frequency ω , rather than the ratio ω/ω_f , where ω_f is the fundamental Reststrahlen frequency. The strong frequency dependence of the real part of the index of refraction near the fundamental resonance at $\omega = \omega_f$ causes some inaccuracy of the values near the fundamental Reststrahlen resonance peaks.

The larger values of β , typically greater than 10^{-2} cm^{-1} , can be measured spectroscopically. Measurement of smaller values of β

requires calorimetric measurements, for which only a limited number of discrete laser frequencies have been available in the measurements to date. Other techniques of measuring small absorption coefficients, such as emissivity, frequency-modulation spectroscopy, and photo-acoustical measurements, have been demonstrated but not used extensively.

The general shape of the $\beta(\omega)$ absorption curves is shown schematically in Fig. 1. The values of β on the frequency range from the Reststrahlen absorption peaks to the values of $\beta \approx 10^{-2}$ to 10^{-5} cm^{-1} (depending on the material and its purity) are generally believed to be intrinsic--that is, a property of a perfect sample. For example, the absorption coefficient for potassium chloride in Fig. 22 for frequencies $\omega < 1000 \text{ cm}^{-1}$ is believed to be intrinsic. The value of the intrinsic absorption coefficient decreases as the frequency increases for $\omega > \omega_f$. This strong, nearly exponential frequency dependence is well explained by multiphonon absorption.⁷ The intrinsic multiphonon absorption becomes so small at high frequencies that extrinsic processes dominate the absorptance. For example, at frequencies $\omega \gtrsim 1000 \text{ cm}^{-1}$ for potassium chloride, the absorptance is extrinsic (up to the intrinsic electronic-absorption edge).

The source of the extrinsic absorption is seldom known. Duthler⁴ has shown that molecular-ion impurities are a major potential source of impurity absorption. Hooper and Uhlmann⁸ and Sparks and Duthler⁹ showed that macroscopic inclusions were important sources of intrinsic absorption.

The conductivity σ , the extinction coefficient k , and the imaginary parts ϵ_1 of the dielectric constant are given in terms of the absorption coefficient β as follows:

$$\sigma = (cn_r/4\pi)\beta ,$$

$$k = (\lambda/4\pi)\beta ,$$

$$\epsilon_I = (cn_r/\omega)\beta ,$$

where ω is the laser frequency, c is the velocity of light, and n_r and the extinction coefficient k are the real and imaginary parts of the index of refraction, $n = n_r + ik$.

The data in Figs. 2 through 53 are from references 10 through 64. The curves and data points are marked with the reference numbers.

Materials in Figs. 2 through 53 are listed in Table I.

We greatly appreciate the assistance of Mrs. Lona Case and Mr. D. F. King in preparing the tables. This research was supported by the Defense Advanced Research Project Agency, administered by the Naval Research Laboratory, the Air Force Office of Scientific Research, and the Air Force Wright Aeronautical Laboratories.

REFERENCES FOR SEC. F

1. See, for example, the proceedings of the Boulder Laser Damage Symposium of the last eleven years. The latest is Tenth NBS-ASTM-ONR-ERDA-DARPA Symposium on Laser Induced Damage in Optical Materials, NBS Special Publication 541, Boulder, Colorado, September 12-14, 1978.
2. M. Sparks, Theoretical Studies of High-Power Infrared Window Materials, Xonics, Inc., Final Technical Report, Contract DAHC 15-72-C-0129, December 1972.
3. M. Sparks, H. Vora, and M. Flannery, Tabulation of Impurity Absorption Spectra--Ultraviolet and Visible, Xonics, Inc., Ninth and Tenth Technical Reports, Contract DAHC 15-73-C-0127, June 1977.
4. C. J. Duthler, J. Appl. Phys. 45, 2668 (1974).
5. M. Flannery and M. Sparks, "Extrinsic absorption in infrared laser-window materials," Ninth NBS-ASTM-ONR-ERDA-DARPA Symposium on Laser Induced Damage in Optical Materials, NBS Special Publication 509, Boulder, Colorado, October 4, 1977.
6. J. Sliney and M. Sparks, "Tabulation of laser breakdown thresholds in solids" (unpublished).
7. M. Sparks and L. J. Sham, Phys. Rev. B8, 3037 (1973); M. Sparks, Theoretical Studies of High-Power Infrared Window Materials, Xonics, Inc., Quarterly Technical Progress Report No. 1, Contract DAHC 15-72-C-0129, March 1972; M. Sparks and L. J. Sham, "Exponential frequency dependence of multiphonon summation infrared absorption," Solid State Commun. 11, 1451 (1972); M. Sparks and L. J. Sham,

"Temperature dependence of multiphonon infrared absorption," Phys. Rev. Lett. 31, 714 (1973); L. J. Sham and M. Sparks, "Explicit exponential frequency dependence of multiphonon infrared absorption," Phys. Rev. B9, 827 (1974).

8. R. W. Hooper and D. R. Uhlmann, J. Appl. Phys. 41, 4023 (1970).
9. M. Sparks and C. J. Duthler, J. Appl. Phys. 44, 3038 (1973).

References continued on following page.

10. T. F. Deutsch, "Absorption Measurements on High Power Laser Window Materials," in Third Conference on High Power Infrared Laser Window Materials, Vol. I: Optical Properties (Nov. 12-14, 1973), edited by C. A. Pitha and B. Bendow, AFCRL-TR-74-0085(1), Special Report No. 174, 14 Feb. 1974, p. 13.
11. A. Hordvik and L. Skolnik, "Photoacoustic Measurements of Surface and Bulk Absorption in HF/DF Laser Window Materials," in High Power Infrared Laser Window Materials (LQ-10 Program), edited by Jane A. Bruce and William S. Ewing, RADC Annual Report for 1976 (ETS Technical Memorandum No. 5), 1 Jan. 1977.
12. Data by A. Hordvik and L. H. Skolnik, as reported by Marvin Hass and Bernard Bendow, "Residual Absorption in Infrared Materials," in High Power Infrared Laser Window Materials (LQ-10 Program), edited by Jane A. Bruce and Wm. S. Ewing, RADC Report for 1976 (ETS Technical Memorandum No. 5), 1 Jan. 1977.
13. A. J. DeLai, C. P. Gazzara, and R. N. Katz, "The Production of Large Sapphire as a Potential Laser Window," in Proceedings of the Fourth Annual Conference on Infrared Laser Window Materials, compiled by C. R. Andrews and C. L. Strecker, sponsored by ARPA, Tucson, Ariz., Nov. 18-20, 1974, pp. 476-491.
14. "Introduction" to High Power Infrared Laser Window Materials (LQ-10 Program), edited by Jane A. Bruce and Wm. S. Ewing, RADC Annual Report for 1976 (ETS Technical Memorandum No. 5), 1 Jan. 1977.

15. W. J. Turner and W. E. Reese, Phys. Rev. 127, 126 (1962).
16. C. T. Moynihan, P. B. Macedo, M. Maklad, and R. Mohr, "Infrared Transmission of As_2Se_3 Glass," in Conference on High Power Infrared Laser Window Materials, Vol. II, AFCRL-TR-73-0372, Special Report No. 162, 19 June 1973.
17. T. M. Donovan and A. D. Baer, " As_2S_3 and ThF_4 Coatings on KCl and NaCl Windows," in Proceedings of the Fifth Annual Conference on Infrared Laser Window Materials, compiled by C. R. Andrews and C. L. Strecker, sponsored by DARPA, Las Vegas, Nev., Dec. 1-4, 1975, pp. 292-300.
18. M. Maklad, R. Mohr, R. Howard, P. B. Macedo, and C. T. Moynihan, Sol. State Comm. 15, 855 (1974).
19. F. A. Horrigan and T. F. Deutsch, Research in Optical Materials and Structures for High-Power Lasers, Raytheon Research Division, Final Technical Report, Contract DA-AH01-70-C-1251, Sept. 1971.
20. P. Denham, G. R. Field, P.L.R. Morse, and G. R. Wilkinson, Proc. Roy. Soc. (London) A 317, 55 (1970).
21. A. D. McLachlan and W.E.K. Gibbs, "A New Chalcogenide-Glass Antireflection Coating for KCl ," in Laser Induced Damage in Optical Materials: 1977, edited by A. J. Glass and A. H. Guenther, NBS Special Publication 509, Proceedings of a Symposium at Boulder, Colo., Oct. 4-6, 1977, pp. 222-228.
22. A. Hordvik, B. Bendow, H. G. Lipson, L. H. Skolnik, and R. N. Brown, "Studies of Absorption in Mid IR Laser Window Materials," in Laser Induced Damage in Optical Materials: 1976, edited by A. J. Glass and A. H. Guenther, NBS Special Publication 462, Proceedings of a Symposium at Boulder, Colo., July 13-15, 1976, pp. 50-57.

23. T. F. Deutsch, J. Phys. Chem. Solids 34, 2091 (1973).
24. Perry Miles, "Ultimates, Pragmatism and New Materials," in Proceedings of the Fifth Annual Conference on Infrared Laser Window Materials, compiled by C. R. Andrews and C. L. Strecker, sponsored by DARPA, Las Vegas, Nev., Dec. 1-4, 1975, pp. 8-16.
25. James W. Davisson, "Chemical Polishing of KBr and Absorption Measurements at 1.06 μm ," in Proceedings of the Fifth Annual Conference on Infrared Laser Window Materials, compiled by C. R. Andrews and C. L. Strecker, sponsored by DARPA, Las Vegas, Nev., Dec. 1-4, 1975, pp. 114-121.
26. J. A. Harrington, D. A. Gregory, and W. F. Otto, "Optical Absorption in Chemical Laser Window Materials," in Proceedings of the Fifth Annual Conference on Infrared Laser Window Materials, compiled by C. R. Andrews and C. L. Strecker, sponsored by DARPA, Las Vegas, Nev., Dec. 1-4, 1975, pp. 872-886.
27. G. Rupprecht, Phys. Rev. Letters 12, 580 (1964).
28. J. S. Loomis and E. Bernal G., "Optical Distortion by Laser Heated Windows," in Laser Induced Damage in Optical Materials: 1975, edited by A. J. Glass and A. H. Guenther, NBS Special Publication 435, Proceedings of a Symposium at Boulder, Colo., July 29-31, 1975, pp. 20-28.
29. F. A. Horrigan and T. F. Deutsch, "Research in Optical Materials and Structures for High-Power Lasers," Raytheon Research Division, Quarterly Technical Report No. 3, Contract DA-AH01-72-C-0194, July 1972.
30. James A. Harrington, "New Materials for Chemical Laser Windows," in Laser Induced Damage in Optical Materials: 1976, edited by A. J. Glass and A. H. Guenther, NBS Special Publication 462, Proceedings of a Symposium at Boulder, Colo., July 13-15, 1976, pp. 45-49.

31. F. A. Johnson, *Progress in Semiconductors* 9, 181 (1965).
32. B. Bendow, H. G. Lipson, and S. P. Yukon, "Frequency and Temperature Dependence of Residual Lattice Absorption in Semiconducting Crystals," in High Power Infrared Laser Window Materials (LQ-10 Program), edited by Jane A. Bruce and Wm. S. Ewing, RADC Annual Report for 1976 (ETS Technical Memorandum No. 5), 1 Jan. 1977.
33. C. P. Christensen, R. Joiner, S.T.K. Nieh, and W. H. Steier, "Investigation of Basic Infrared Loss Mechanism in High Resistivity GaAs," in Third Conference on High Power Infrared Laser Window Materials, Vol. I: Optical Properties, edited by C. A. Pitha and B. Bendow, AFCRL-TR-74-0085(1), Special Report No. 174, 14 Feb. 1974.
34. F. A. Horrigan and T. F. Deutsch, "Research in Optical Materials and Structures," Quarterly Technical Report No. 2 (Raytheon Corp., Waltham, MA, 1972),; T. F. Deutsch, in *Proc. of 1972 Laser Window Conf.*, Ref. (1); and T. F. Deutsch, *J. Elec. Mats.* (to be published).
35. B. Bendow, L. H. Skolnik, and H. G. Lipson, "Limiting Loss Mechanisms in Semiconducting Optical Waveguide Materials," in Optical Phenomena, Materials and Techniques, edited by B. Bendow and P. D. Gianino, AFCRL ETS Tech. Memo. No. 2, Jan. 1, 1976, p. 22.
36. James A. Harrington, Low Loss Window Materials for Chemical Lasers, University of Alabama Research Report No. 177, Contract No. DAAH01-74-C-0437, August 1975.
37. L. Genzel, *Fest Korper Problems* 9, 32 (1969).
38. T. C. McGill, et al., *J. Phys. Chem. Sol.* 34, 2105 (1973).

39. Herbert B. Rosenstock, Don A. Gregory, and James A. Harrington, "Infrared Bulk and Surface Absorption by Nearly Transparent Crystals," in Proceedings of the Fifth Annual Conference on Infrared Laser Window Materials, compiled by C. R. Andrews and C. L. Strecker, sponsored by DARPA, Las Vegas, Nev., Dec. 1-4, 1975, pp. 860-870.
40. Philipp H. Klein, "Growth of Lowloss KBr in Halide Atmospheres," in Proceedings of the Fifth Annual Conference on Infrared Laser Window Materials, compiled by C. R. Andrews and C. L. Strecker, sponsored by DARPA, Las Vegas, Nev., Dec. 1-4, 1975, pp. 983-991.
41. D. L. Stierwalt, "Spectral Emittance Measurements With a Cryogenically Cooled Instrument," in Laser Induced Damage in Optical Materials: 1975, edited by A. J. Glass and A. H. Guenther, NBS Special Publication 435, Proceedings of a Symposium at Boulder, Colo., July 29-31, 1975, pp. 148-156.
42. Marvin Hass and James A. Harrington, "HF and DF Window Absorption," in Proceedings of the High Power Laser Optical Components and Component Materials Meeting, compiled by J. S. Harris and C. L. Strecker, sponsored by DARPA, Boulder, Colo., Oct. 3-4, 1977, pp. 157-162.
43. C. Smart, G. R. Wilkinson, A. M. Karo, and J. R. Hardy, "Lattice Dynamics," Proc. Intl. Conference, Copenhagen, August 1963, edited by R. F. Wallis (Pergamon Press, Inc., 1965), p. 387.
44. S. D. Allen and J. A. Harrington, "Surface and Bulk Absorption of Window Materials at IR Laser Wavelengths," in Proceedings of the High Power Laser Optical Components and Component Materials Meeting, compiled by J. S. Harris and C. L. Strecker, sponsored by DARPA, Boulder, Colo., Oct. 3-4, 1977, pp. 437-448.

45. S. D. Allen and J. E. Rudisill, "Bulk and Surface Calorimetric Measurements at CO Wavelengths," Hughes Research Laboratories, sponsored by DARPA (rec'd. by M. Sparks at Xonics, Inc., on June 8, 1977).
46. C. J. Duthler, J. A. Harrington, F. W. Patten, and M. Hass, "Multi-phonon Absorption of Alkali Halides and Quasiselection Rules," in Proceedings of the Fifth Annual Conference on Infrared Laser Window Materials, compiled by C. R. Andrews and C. L. Strecker, sponsored by DARPA, Las Vegas, Nev., Dec. 1-4, 1975, pp. 760-769.
47. H. G. Lipson, A. Hordvik, and B. Bendow, "Frequency and Temperature Dependence of Residual Infrared Absorption in Mixed Fluoride Crystals," in Laser Induced Damage in Optical Materials: 1977, edited by A. J. Glass and A. H. Guenther, NBS Special Publication 509, Proceedings of a Symposium at Boulder, Colo., Oct. 4-6, 1977, pp. 56-61.
48. J. A. Harrington, et al., "Proc. Laser Window Conf., 1974," (AFML, Wright-Patterson AFB, Ohio, 1975).
49. F. A. Horrigan and T. F. Deutsch, Research in Optical Materials and Structures for High Power Lasers, Raytheon Research Division Quarterly Technical Reports Nos. 1 and 2, Contract DA-AH01-72-C-0194, January and April, 1972.
50. American Institute of Physics Handbook, 3rd Edition, Dwight E. Gray, Coordinating Editor (McGraw-Hill, New York, 1972), pp. 6-48—6-83.
51. D. L. Stierwalt, "Temperature Dependence of the Absorption Coefficient of Some Window Material Samples," Third Conference on High Power Infrared Laser Window Materials, Vol. I: Optical Properties, edited by C. A. Pitha and B. Bendow, AFCRL-TR-74-0085(1), Special Report No. 174, 14 Feb. 1974.

52. Ontario H. Nestor, Improved (K,Rb)Cl Laser Window Materials, Harshaw Chemical Co. Final Technical Report (Contract F33615-76-R-5304), April 1977.
53. Marvin Hass and Bernard Bendow, "Residual Absorption in Infrared Materials," in High Power Infrared Laser Window Materials (LQ-10 Program), edited by Jane A. Bruce and Wm. S. Ewing, RADC Annual Report for 1976 (ETS Technical Memorandum No. 5), 1 Jan. 1977.
54. Yet-Ful Tsay, Bernard Bendow, and S. S. Mitra, "Optical Properties of Density-Disordered Solids," in High Power Infrared Laser Window Materials (LQ-10 Program), LQ Tech. Memo. No. 35, Part II, edited by Bernard Bendow and Peter D. Gianino, Semi-Annual Report No. 2, 1 July 1975 - 31 Dec. 1975.
55. A. Hordvik, "Recent Advances in Measurement Techniques for Small Absorption Coefficients," in High Power Infrared Laser Window Materials (LQ-10 Program), edited by Jane A. Bruce and Wm. S. Ewing, RADC Annual Report for 1976 (ETS Technical Memorandum No. 5), 1 Jan. 1977.
56. H. E. Bennett, "Thermal Distortion Thresholds for Optical Trains Handling High Pulse Powers," in Laser Induced Damage in Optical Materials: 1976, edited by A. J. Glass and A. H. Guenther, Proceedings of a Symposium at Boulder, Colo., July 13-15, 1976, pp. 11-24.
57. Perry Miles, "Limits on the Use of Alkaline Earth Fluorides in High Power Optics," in Proceedings of the Infrared Laser Window Materials Meeting, compiled by C. R. Andrews and C. L. Strecker, sponsored by DARPA, Boulder, Colo., 12 July 1976, pp. 28-37.

58. James A. Harrington, B. Bendow, K. V. Namjoshi, S. S. Mitra, and D. L. Stierwalt, "Low Loss Window Materials for Chemical and CO Lasers," in Proceedings of the Fourth Annual Conference on Infrared Laser Window Materials, compiled by C. R. Andrews and C. L. Strecker, sponsored by ARPA, Tucson, Arizona, Nov. 18-20, 1974, pp. 402-421.
59. A. R. Hilton, H. C. Hafner, and R. L. Rasmussen, "Optical Quality of Chalcogenide Glasses," in Conference on High Power Infrared Laser Window Materials, Oct. 30, 31, and Nov. 1, 1972, edited by C. A. Pitha, AFCRL-TR-73-0372(II), 19 June 1973.
60. T. Deutsch, Proceedings of International Conference on Physics of Semiconductors, Exeter, July 1962 (Inst. of Physics and Physical Society, 1962), p. 505.
61. The Infrared Handbook, edited by William L. Wolfe and George J. Zissis for the Office of Naval Research, Department of the Navy, Washington, DC, 1978.
62. Handbook of Optics, edited by Walter G. Driscoll and William Vaughan, sponsored by the Optical Society of America (McGraw-Hill, New York, 1978).
63. C. M. Baldwin and J. D. MacKenzie, J. Non-Cryst. Solids 31, 441 (1979).
64. J. R. Gannon, J. Non-Cryst. Solids, in press.

TABLE I

List of materials included in the tabulations.

AgCl	KCl	TiO ₂
Al ₂ O ₃	KI	TI20 Glass
AlSb	KMgF ₃	TI 1173 Glass
As ₂ S ₃	KRS-5	TlBr
As ₂ Se ₃	KRS-6	TlCl
BaF ₂	KZnF ₃	YAG (yttrium aluminum garnet)
BaTiO ₃	LaF ₃	YTTRALOX (Y ₂ O ₃ + ThO ₂)
BeF ₂	LiF	ZnS
CaCO ₃ (calcite)	LiYF ₄	ZnSe
CaF ₂	MgF ₂	ZrF ₄ (based ternary glass)
CdTe	MgO	ZrF ₄ - ThF ₄ Glass
CsBr	NaCl	
CsI	NaF	
Diamond	NaI	
GaAs	RbCl	
Gd ₃ Ga ₅ Si ₁₂ (gadolinium-gallium garnet)	Si	
Ge	SiC	
HfF ₄ (based ternary glass)	SiO ₂ (crystalline quartz)	
InAs	SiO ₂ (fused silica)	
KBr	SrF ₂	
	SrTiO ₃	

FIGURE CAPTIONS FOR SEC. F

Fig. 1. Schematic illustration of the frequency dependence of the absorption of a dielectric material, showing the intrinsic multiphonon- and electronic-absorption and the extrinsic absorption range.

Figs. 2 - 53.

Lowest experimental values of absorption coefficients at various frequencies.

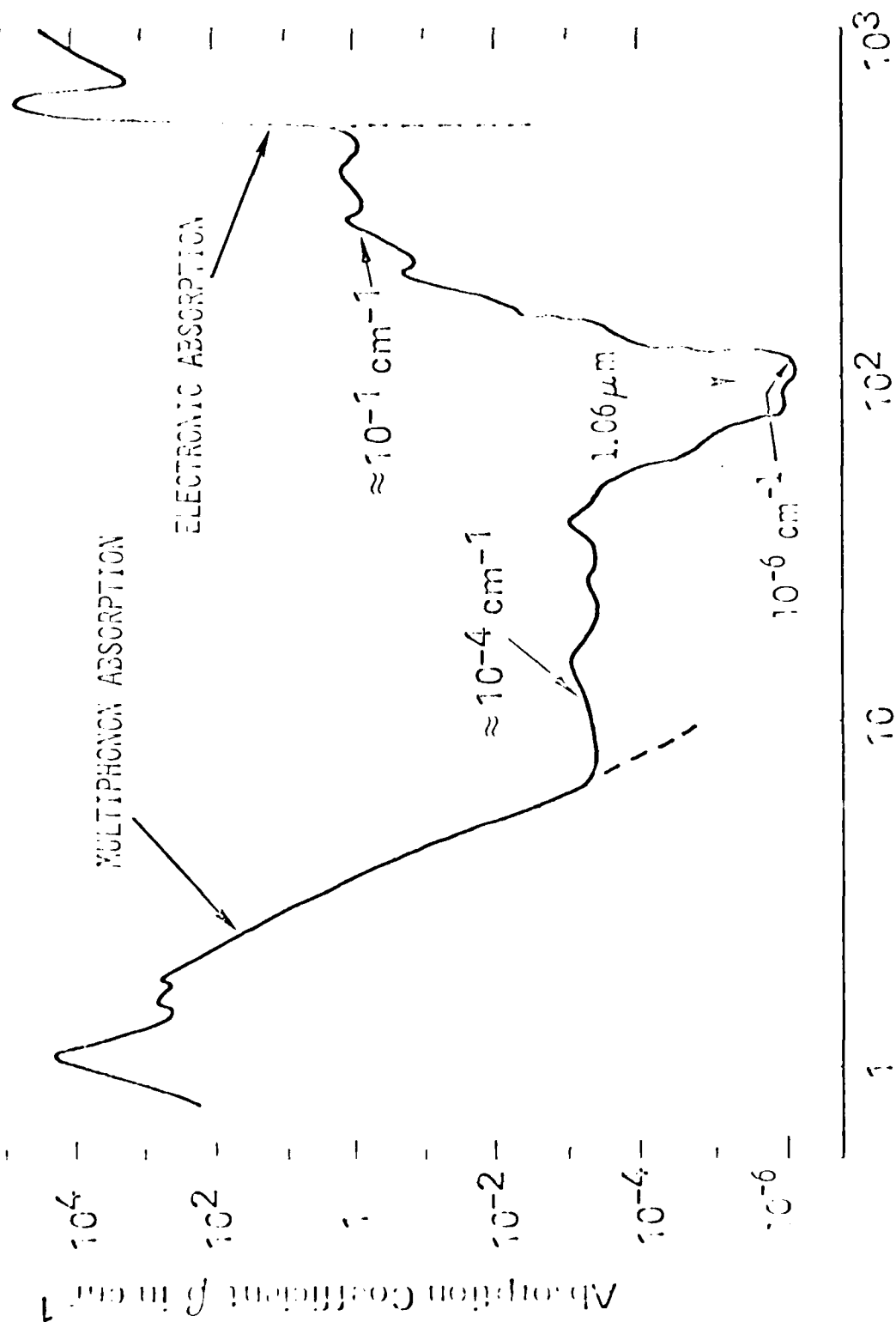


Fig. 1

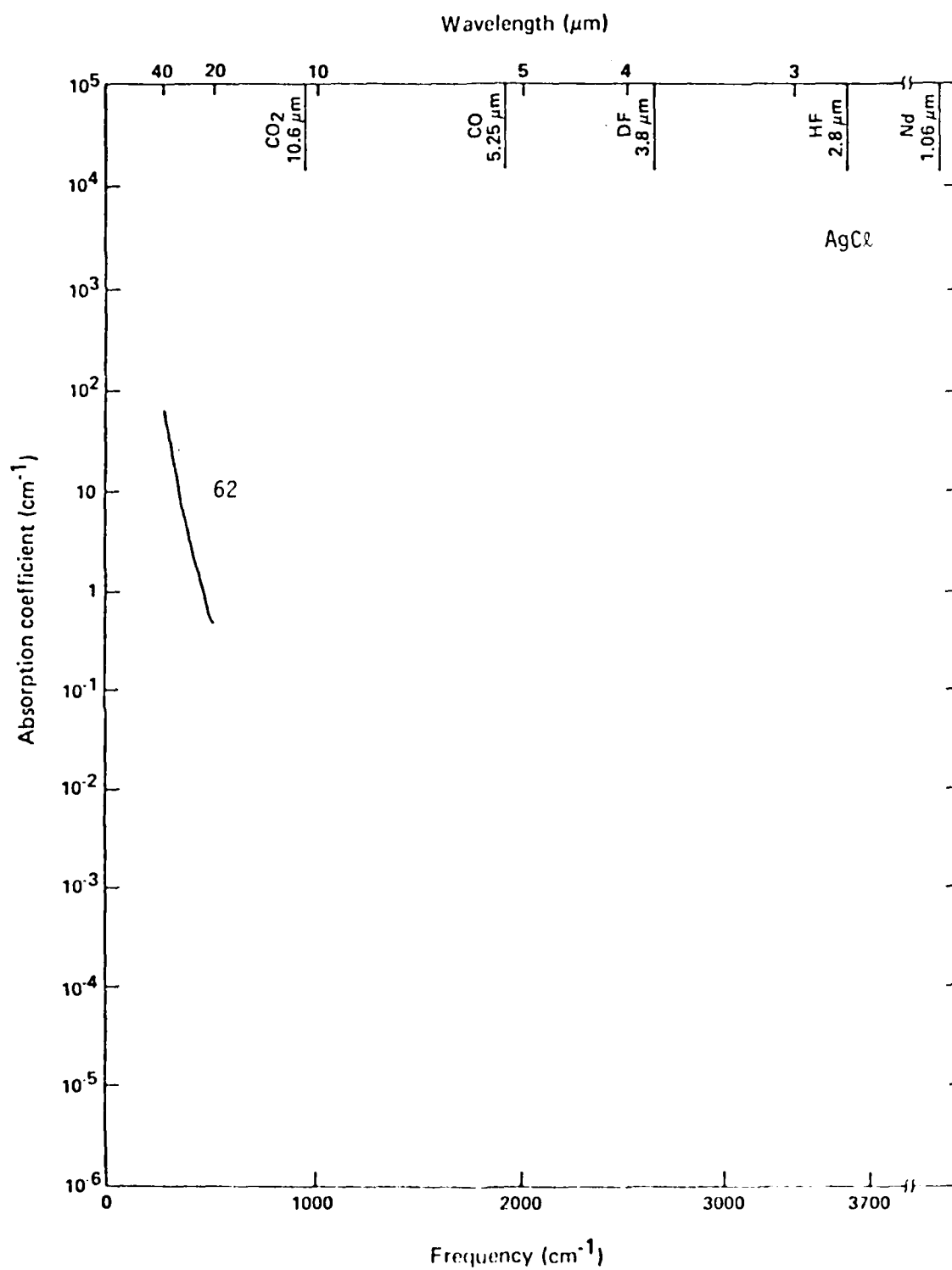


Fig. 2

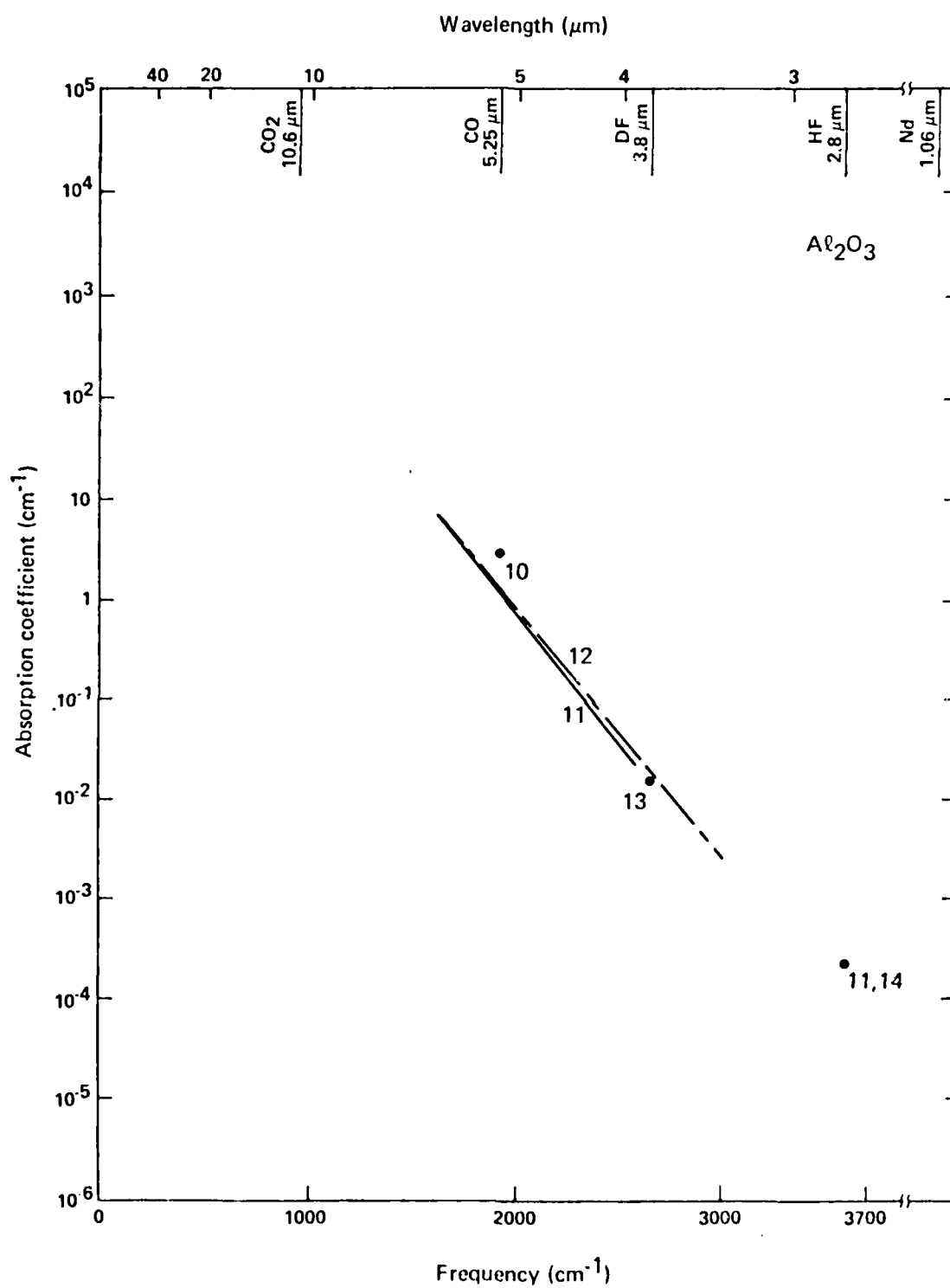


Fig. 3

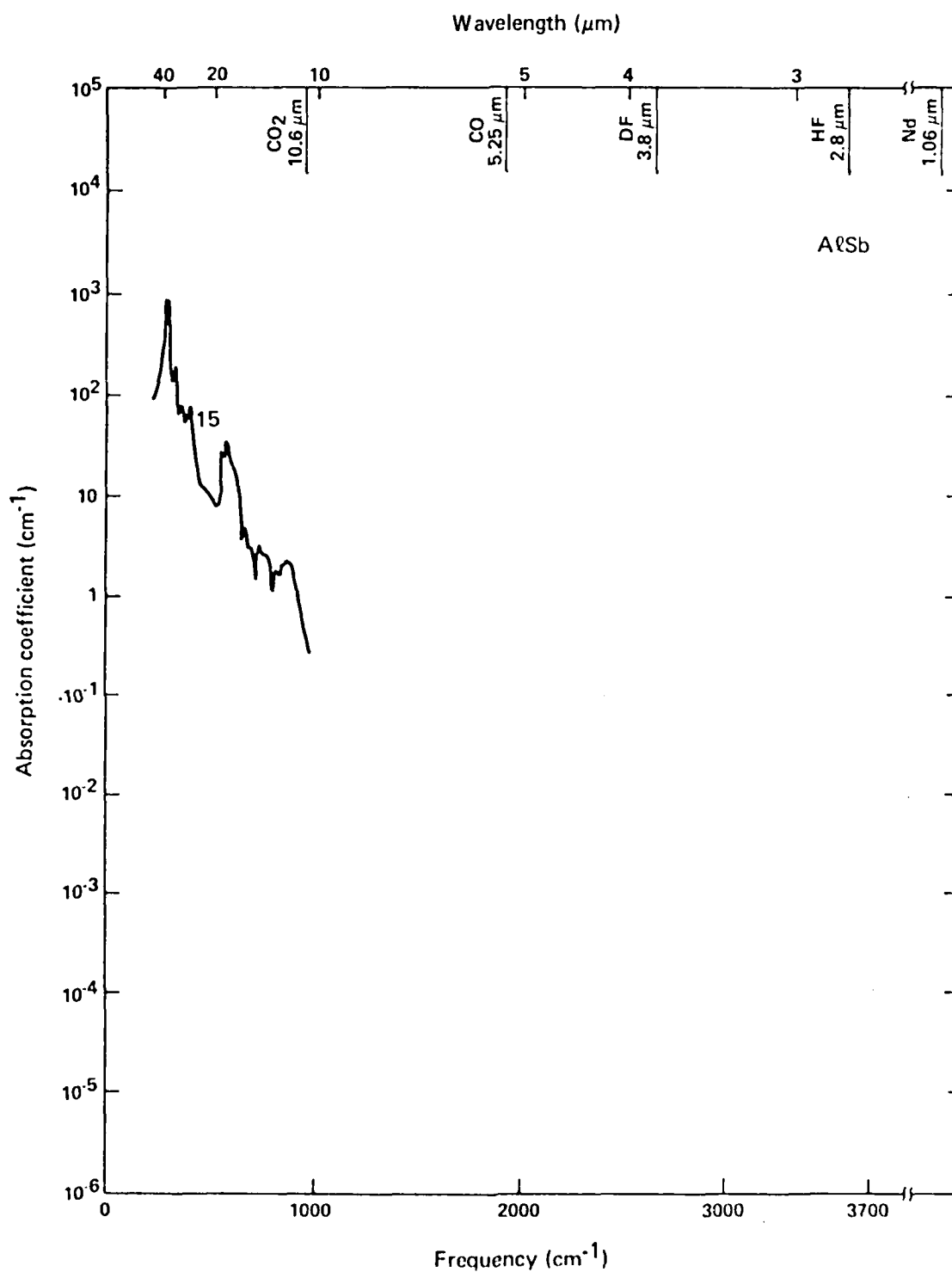


Fig. 4

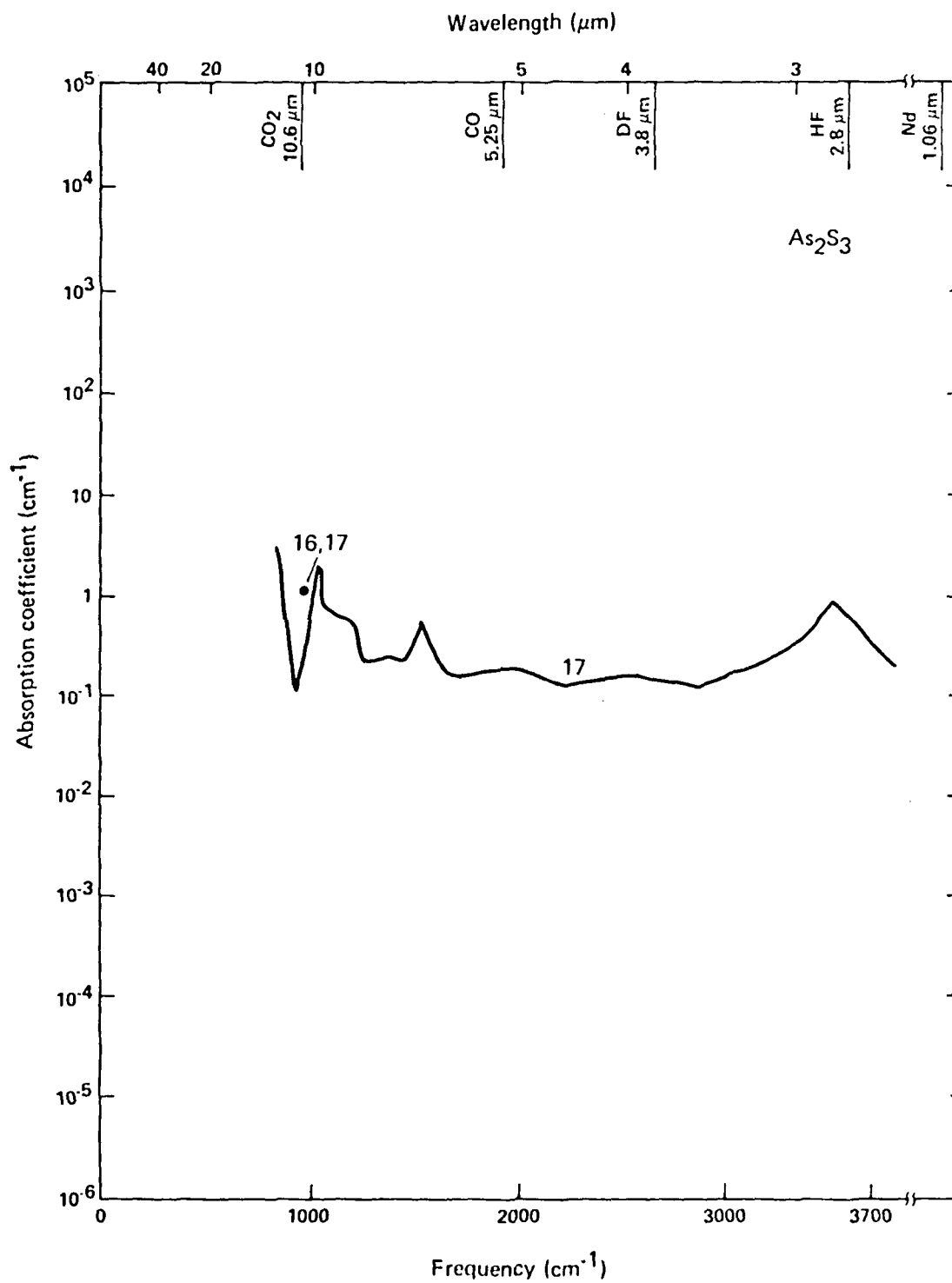


Fig. 5

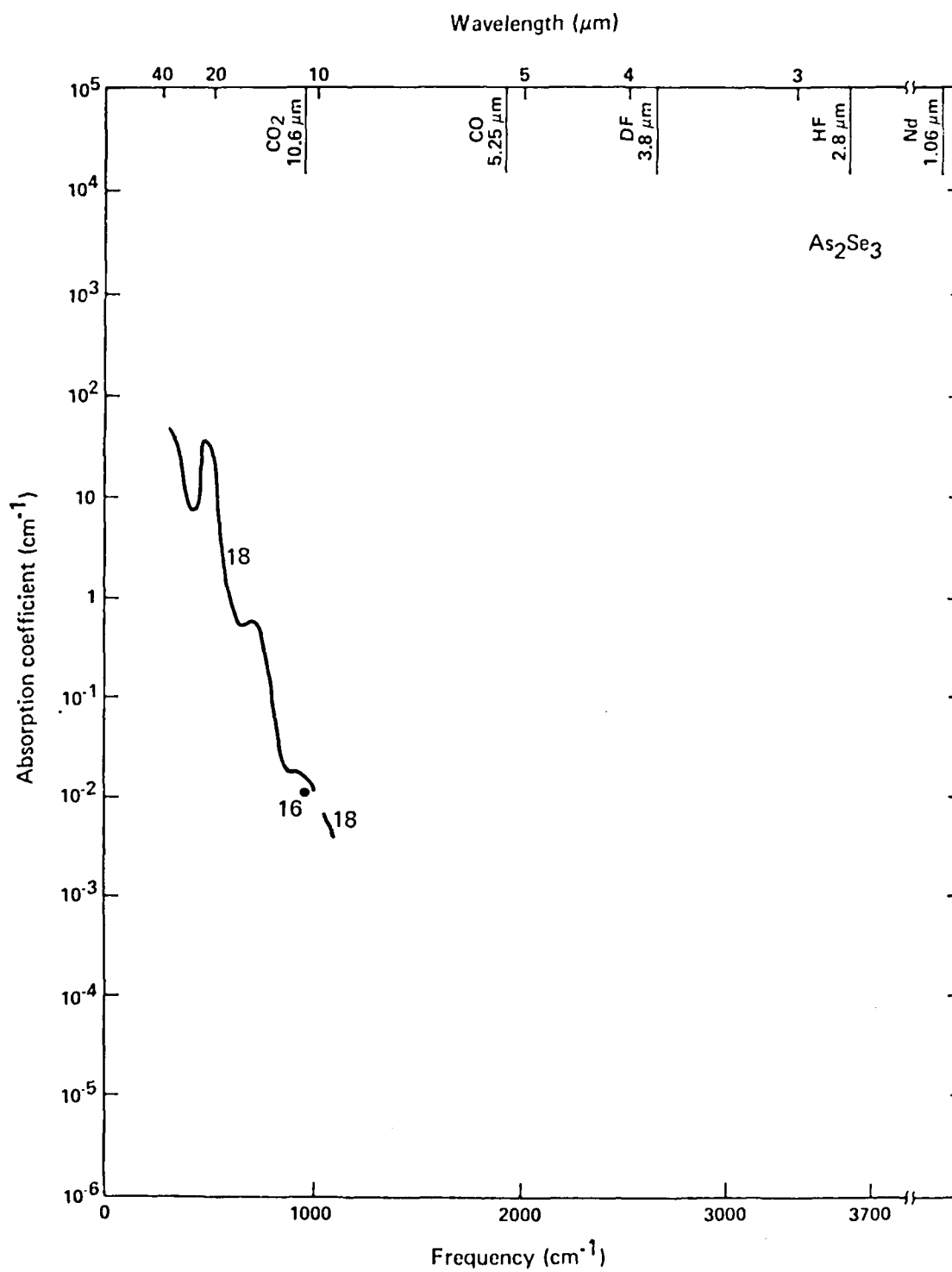


Fig. 6

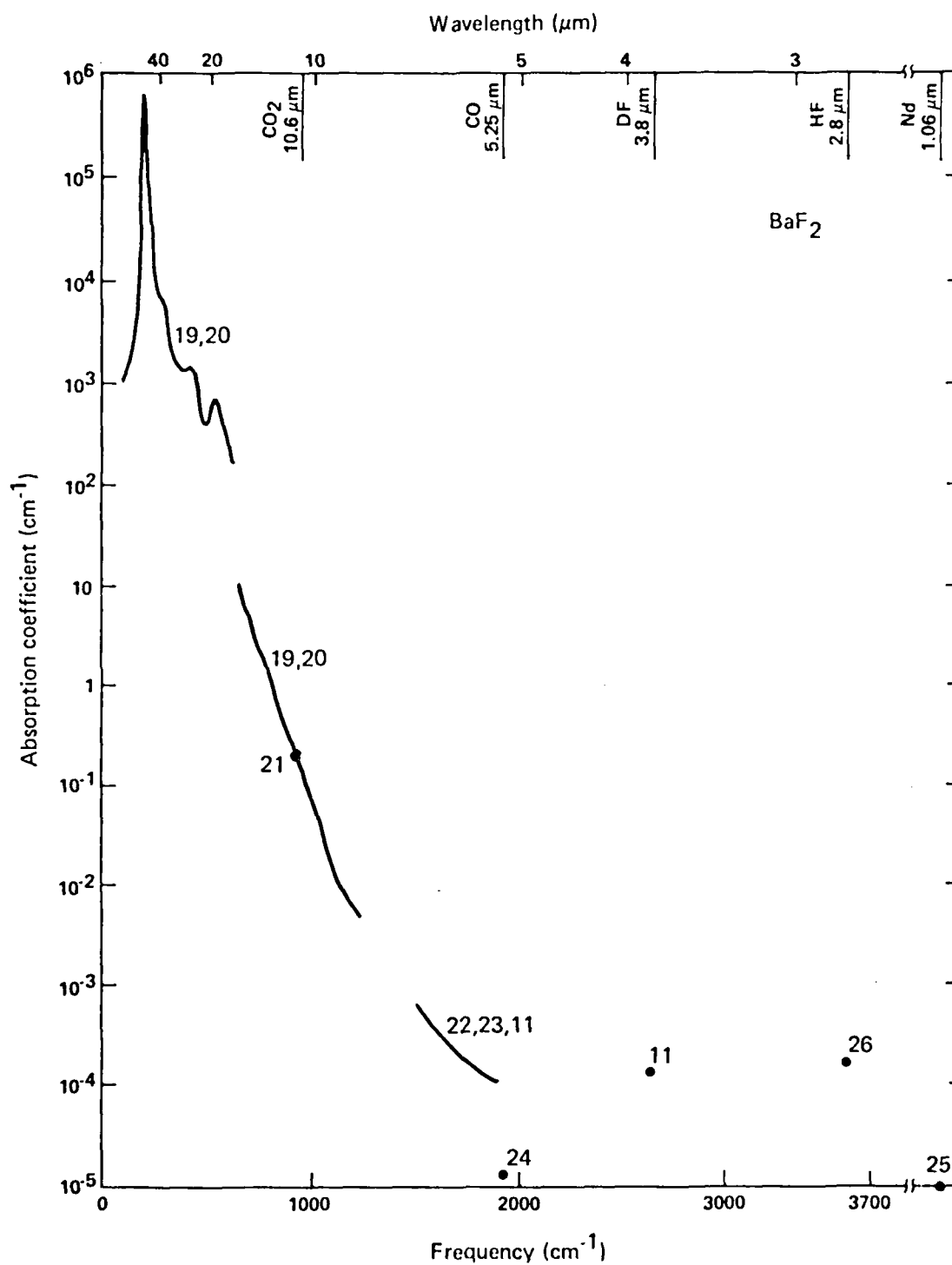


Fig. 7

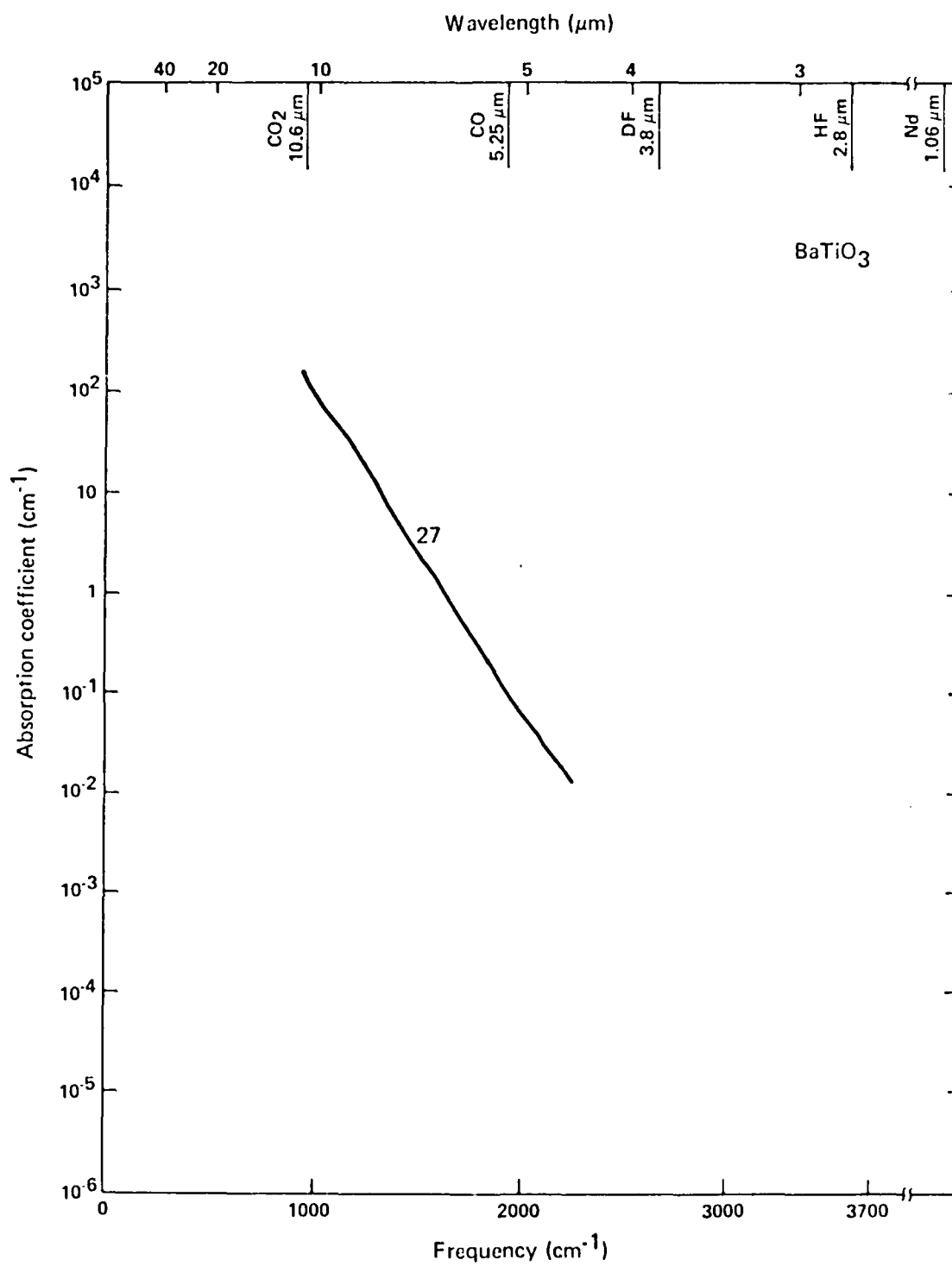


Fig. 8

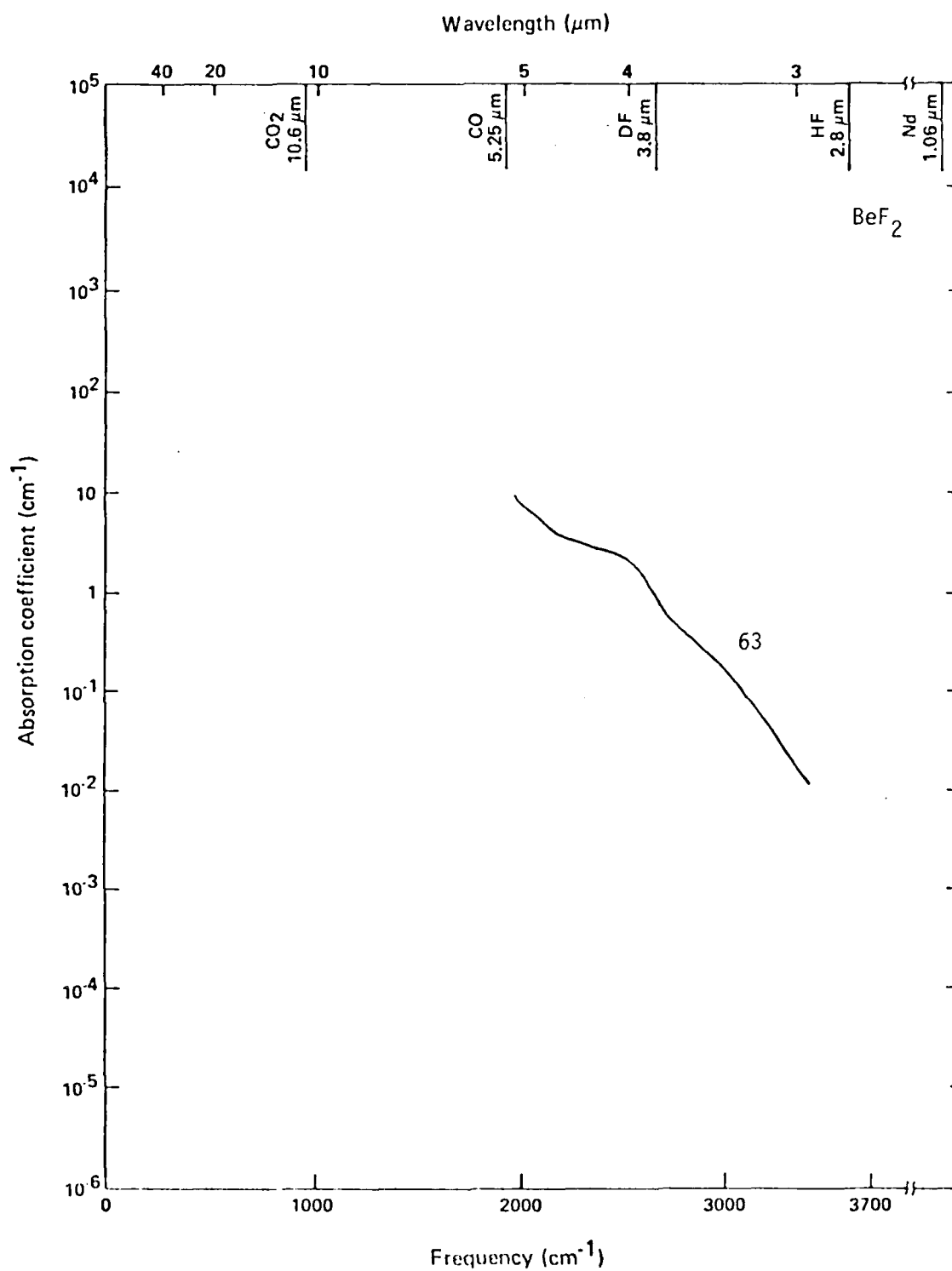


Fig. 9

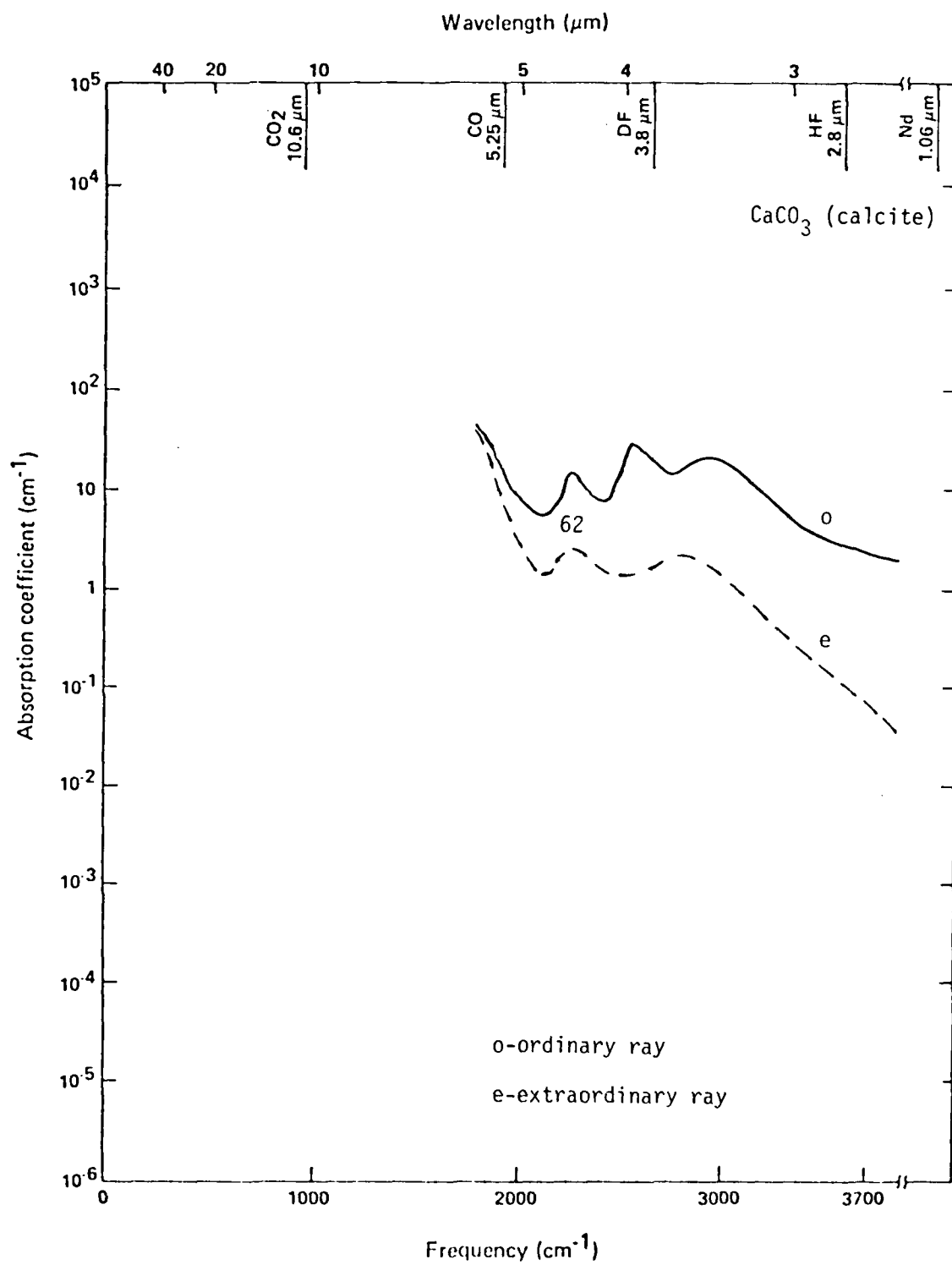


Fig. 10

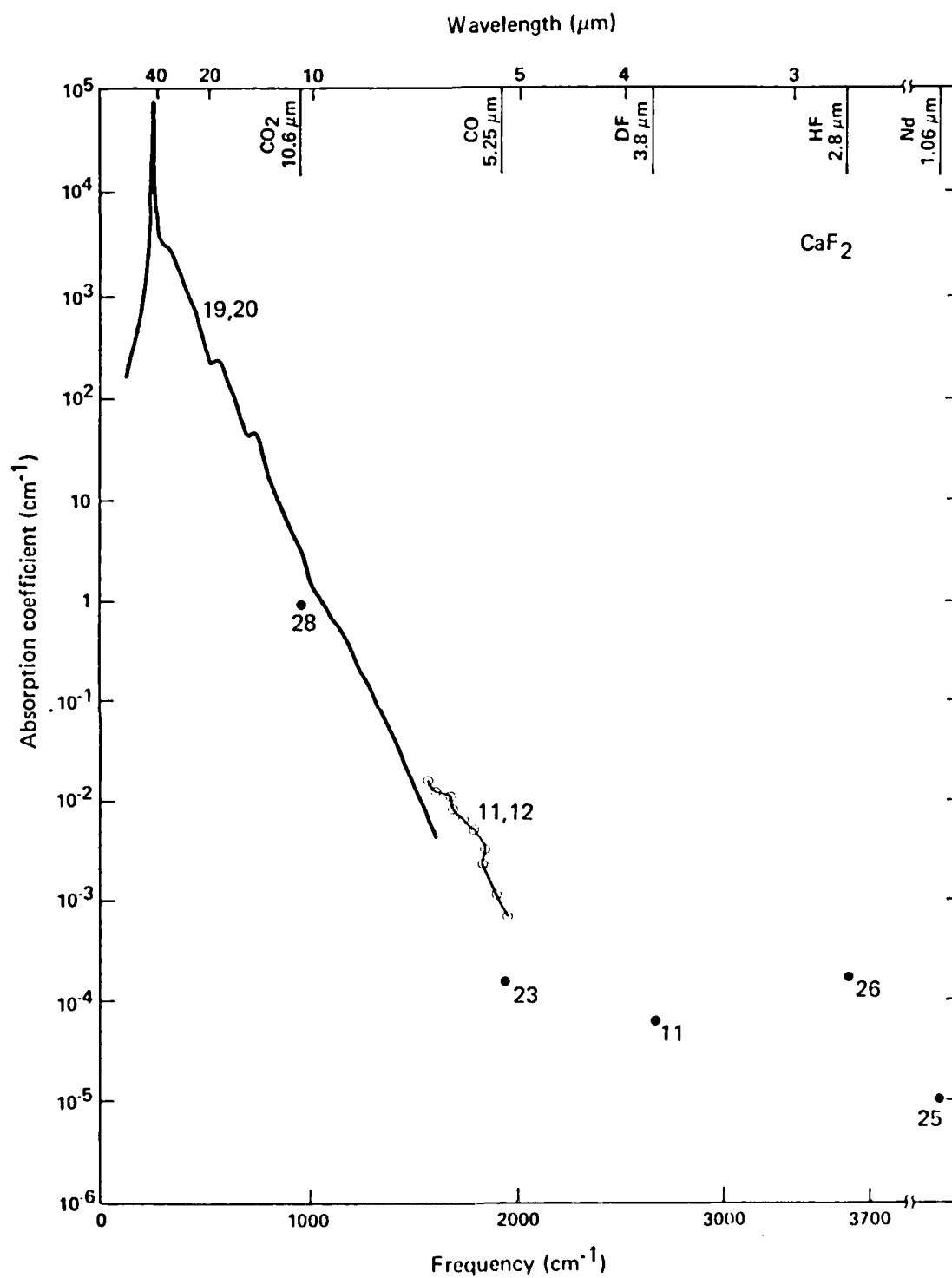


Fig. 11

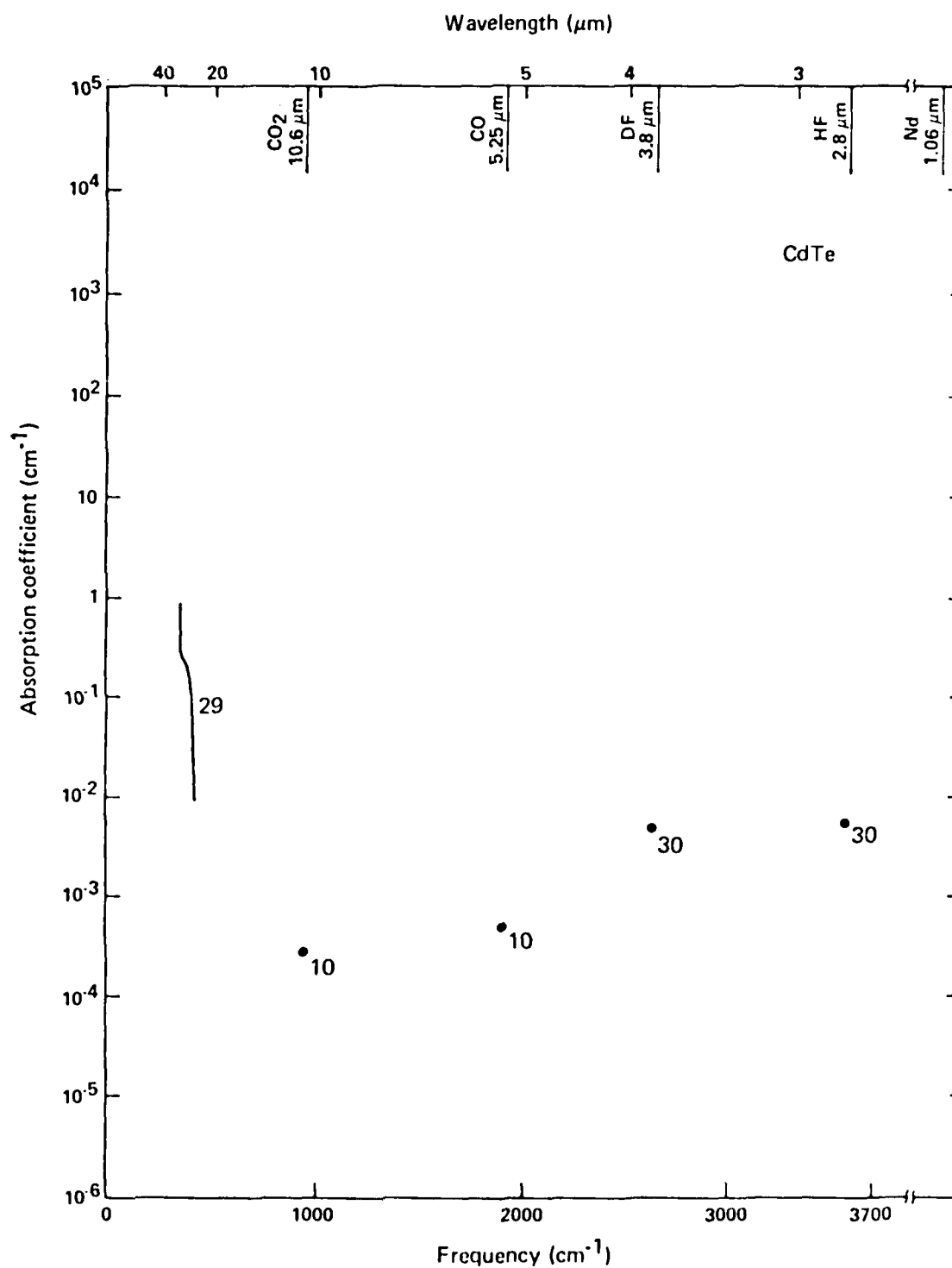


Fig. 12

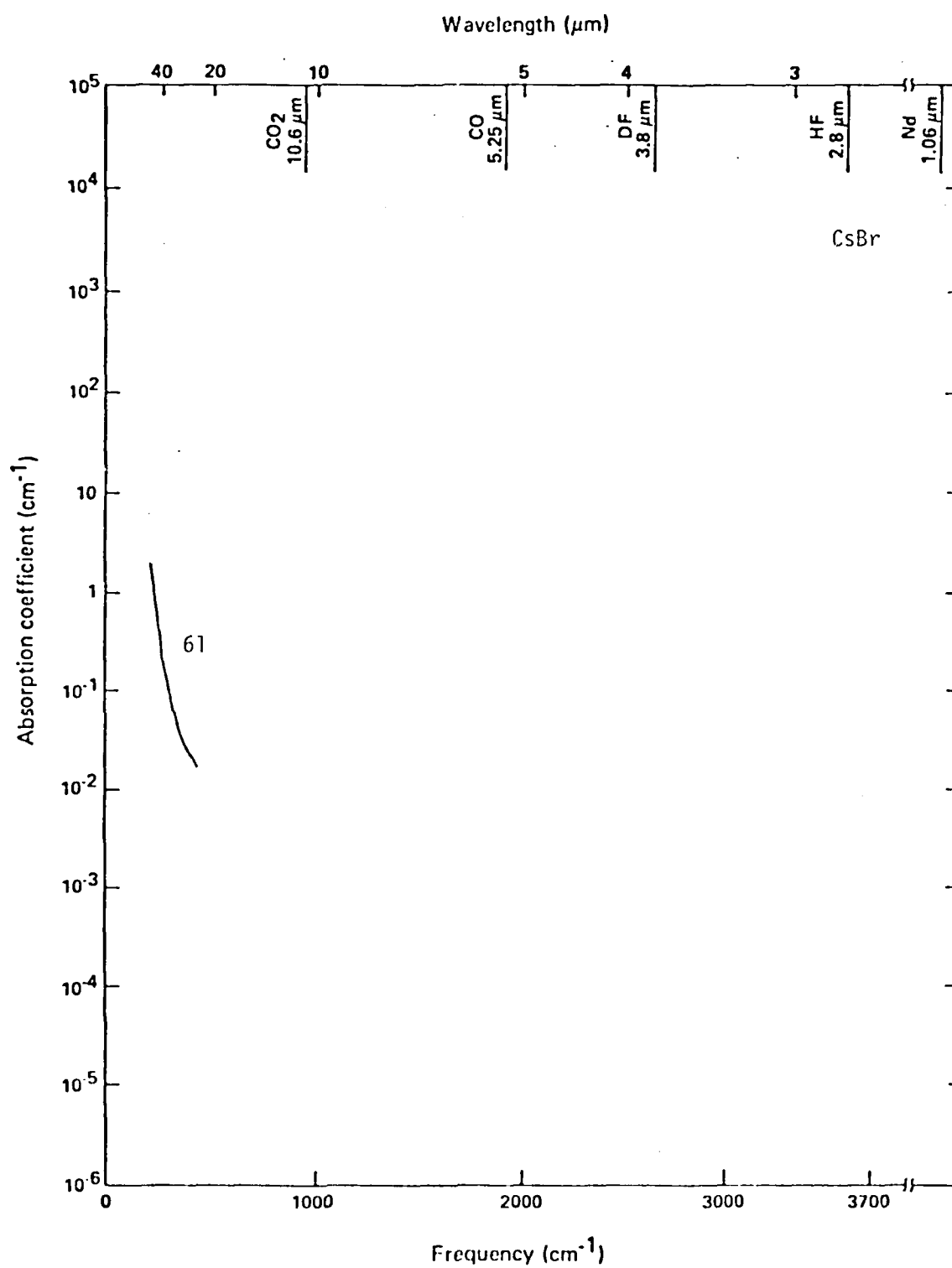


Fig. 13

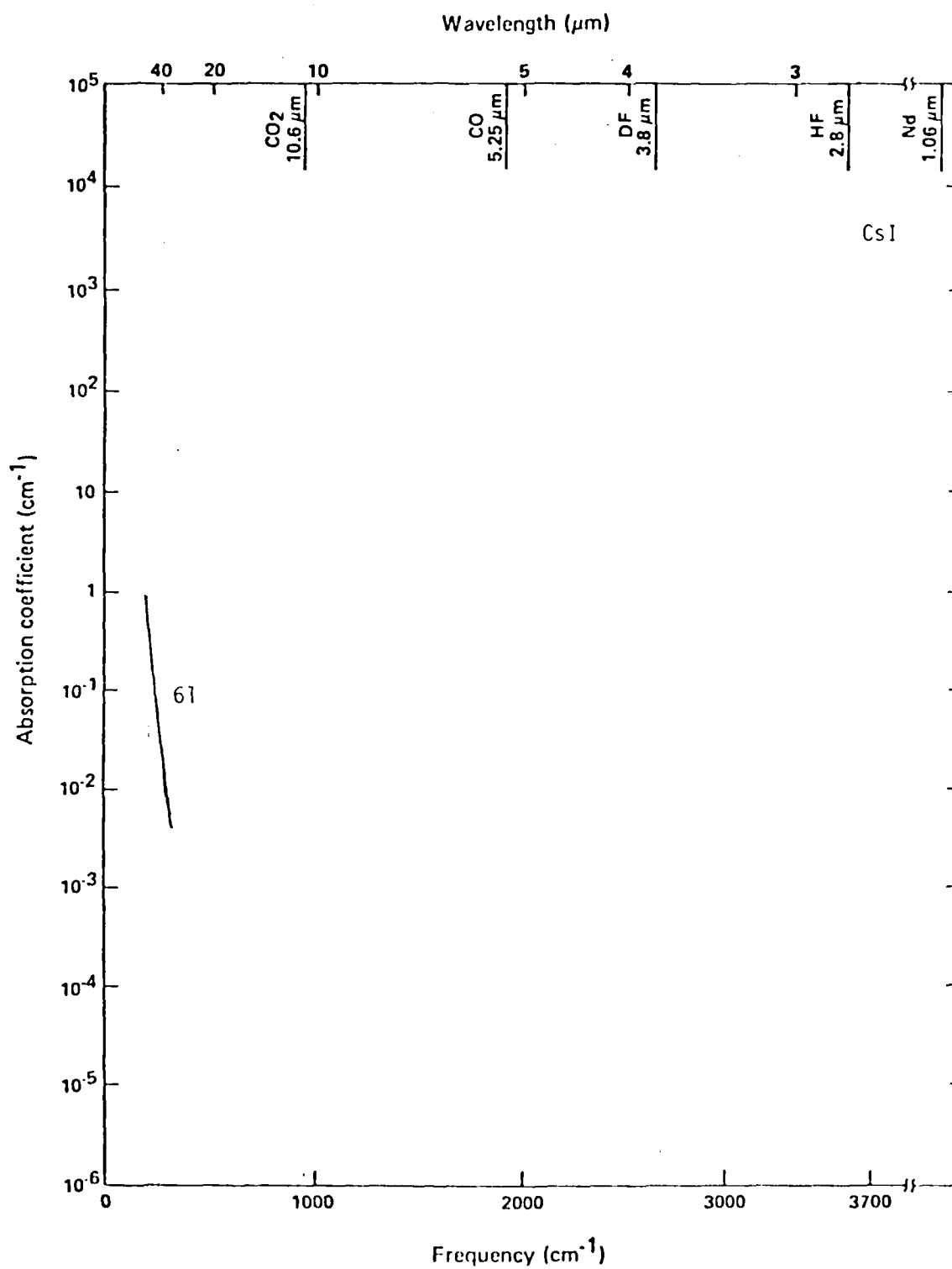


Fig. 14

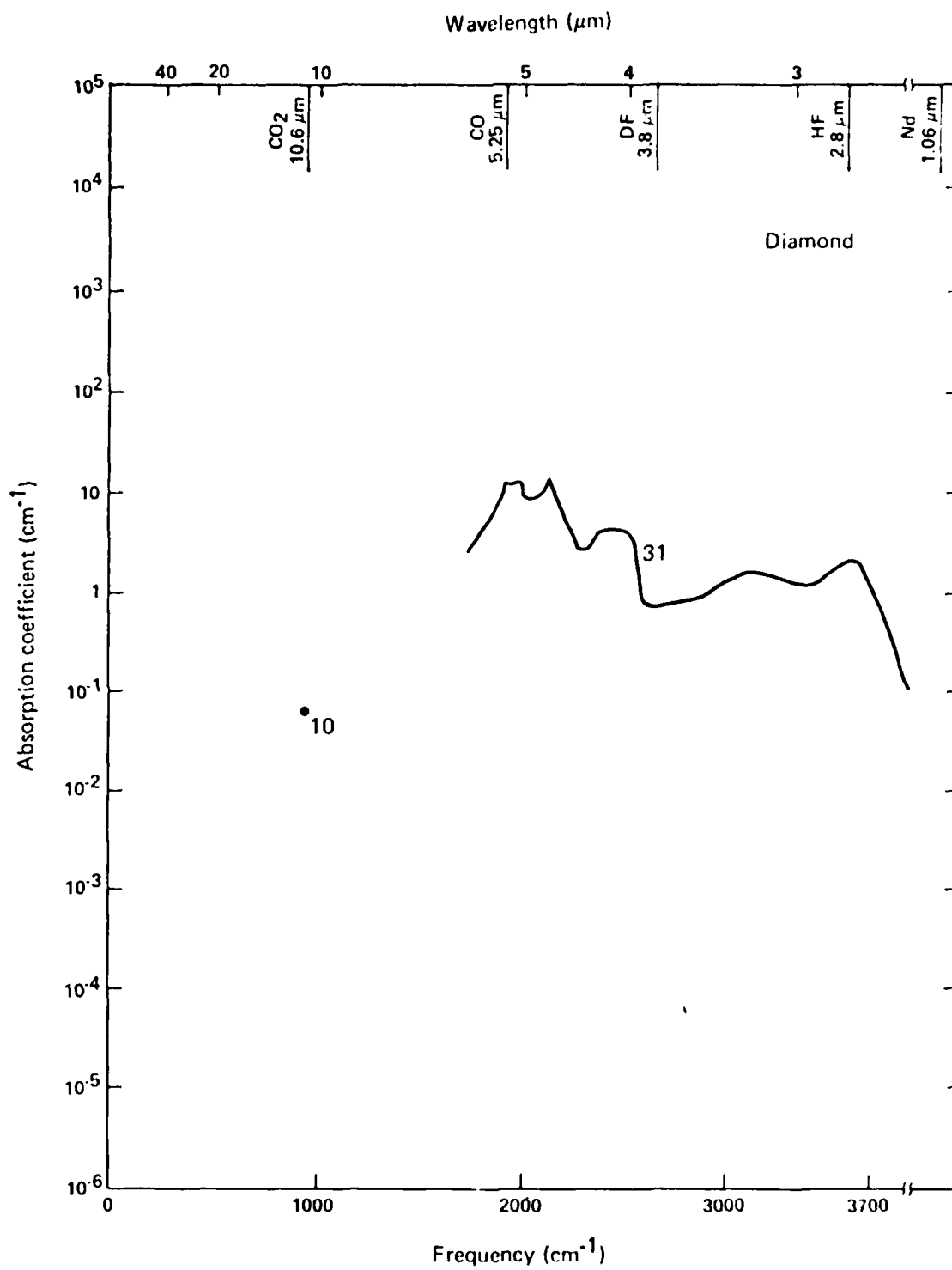


Fig. 15

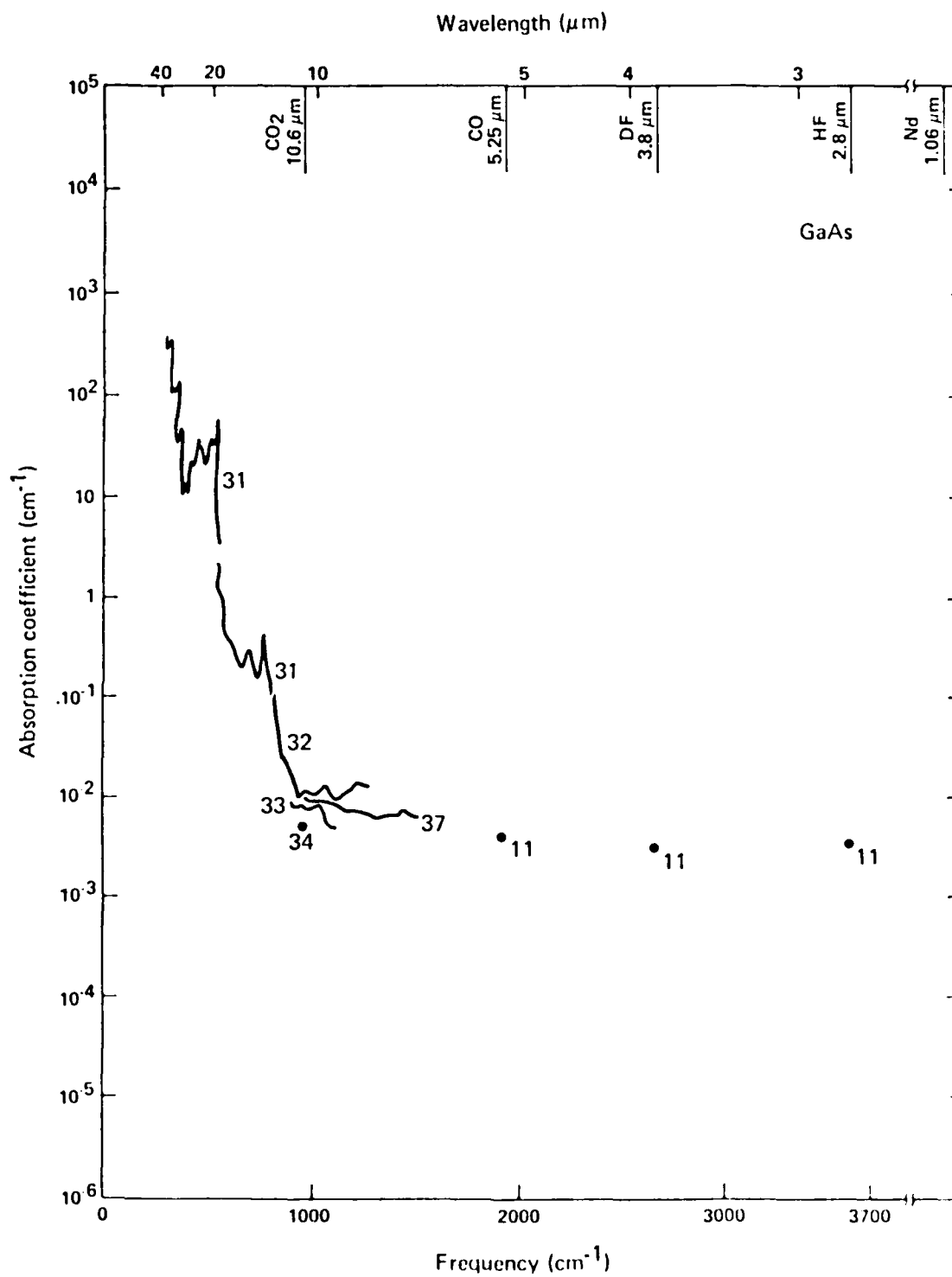


Fig. 16

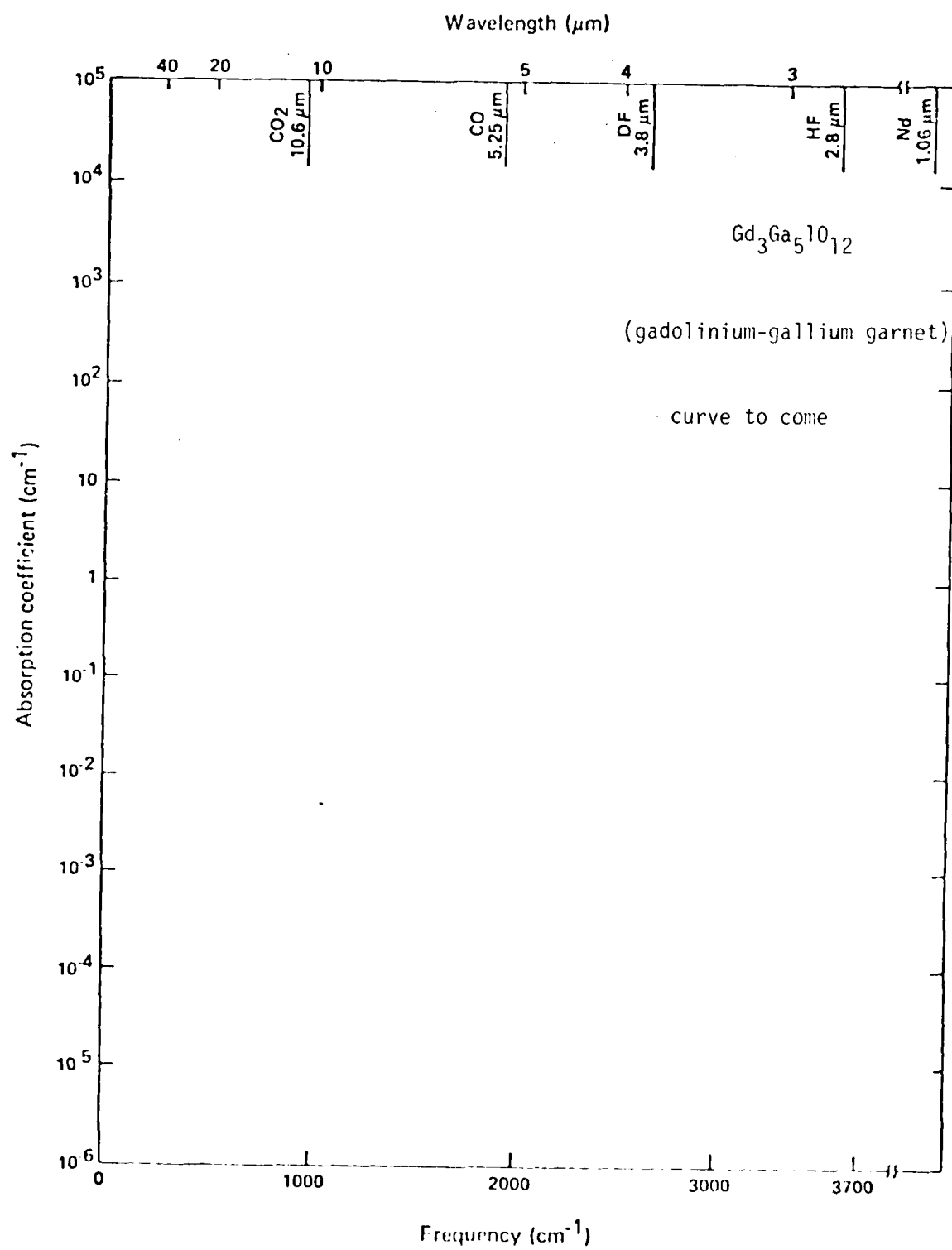


Fig. 17

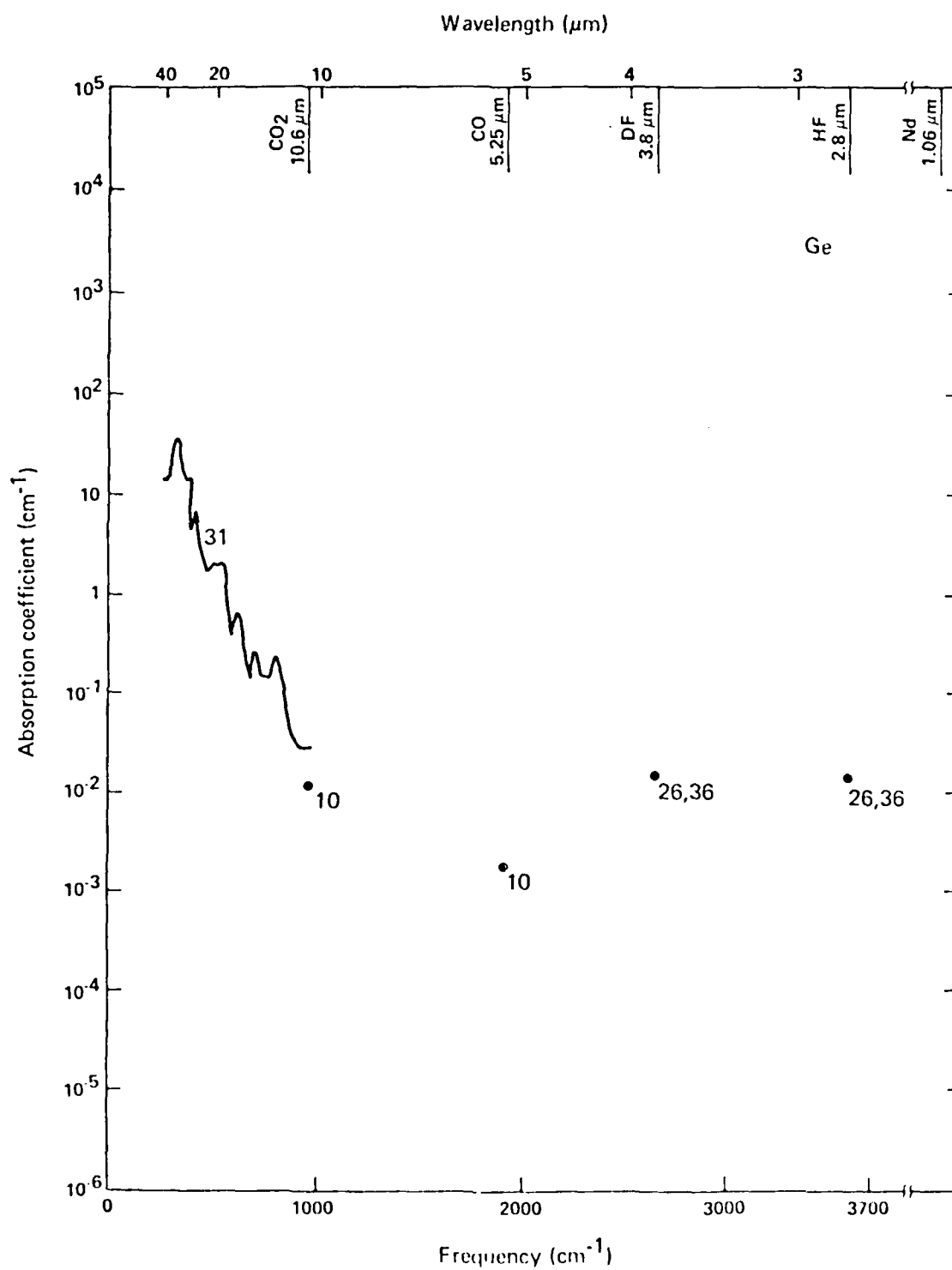


Fig. 18

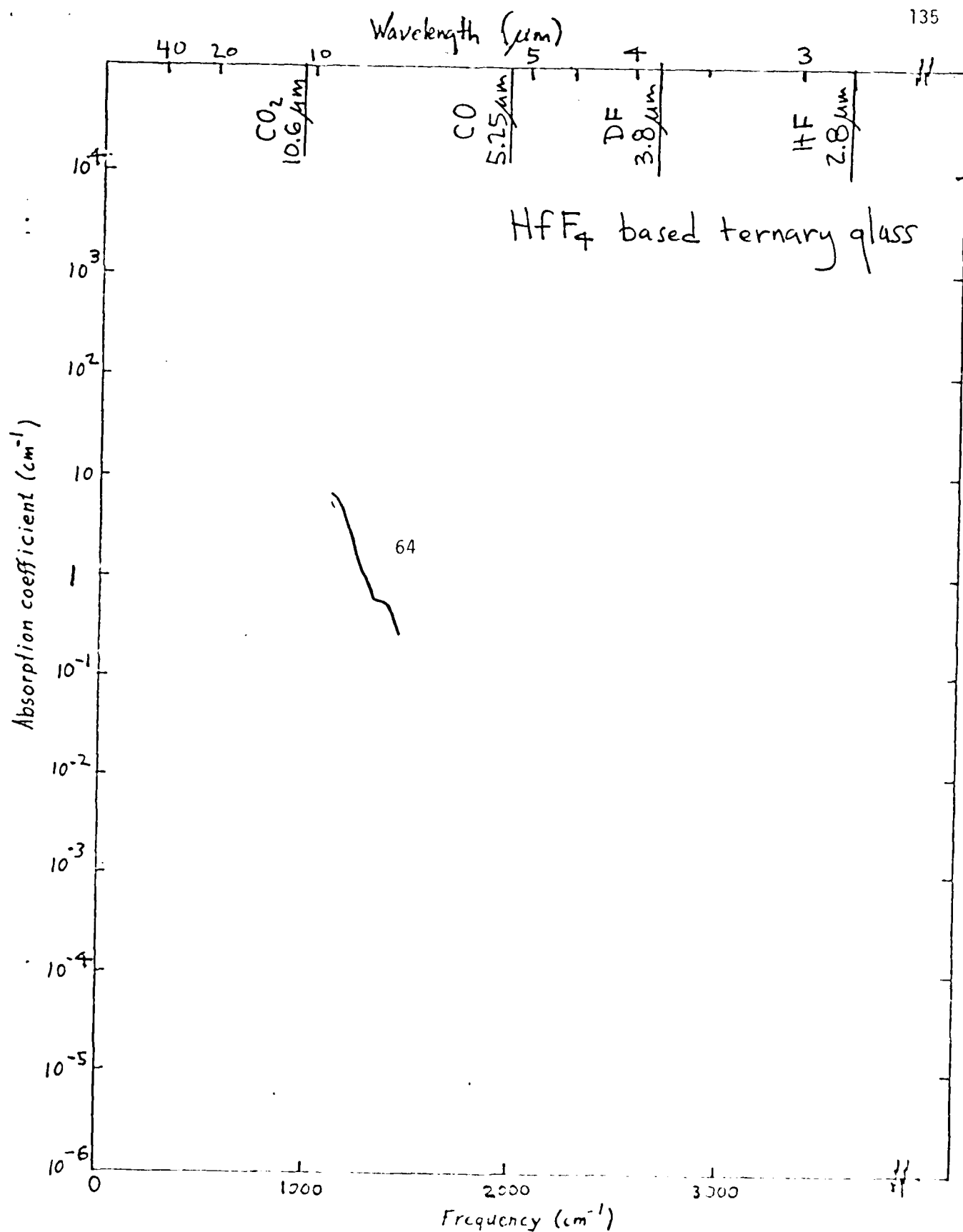


Fig. 19

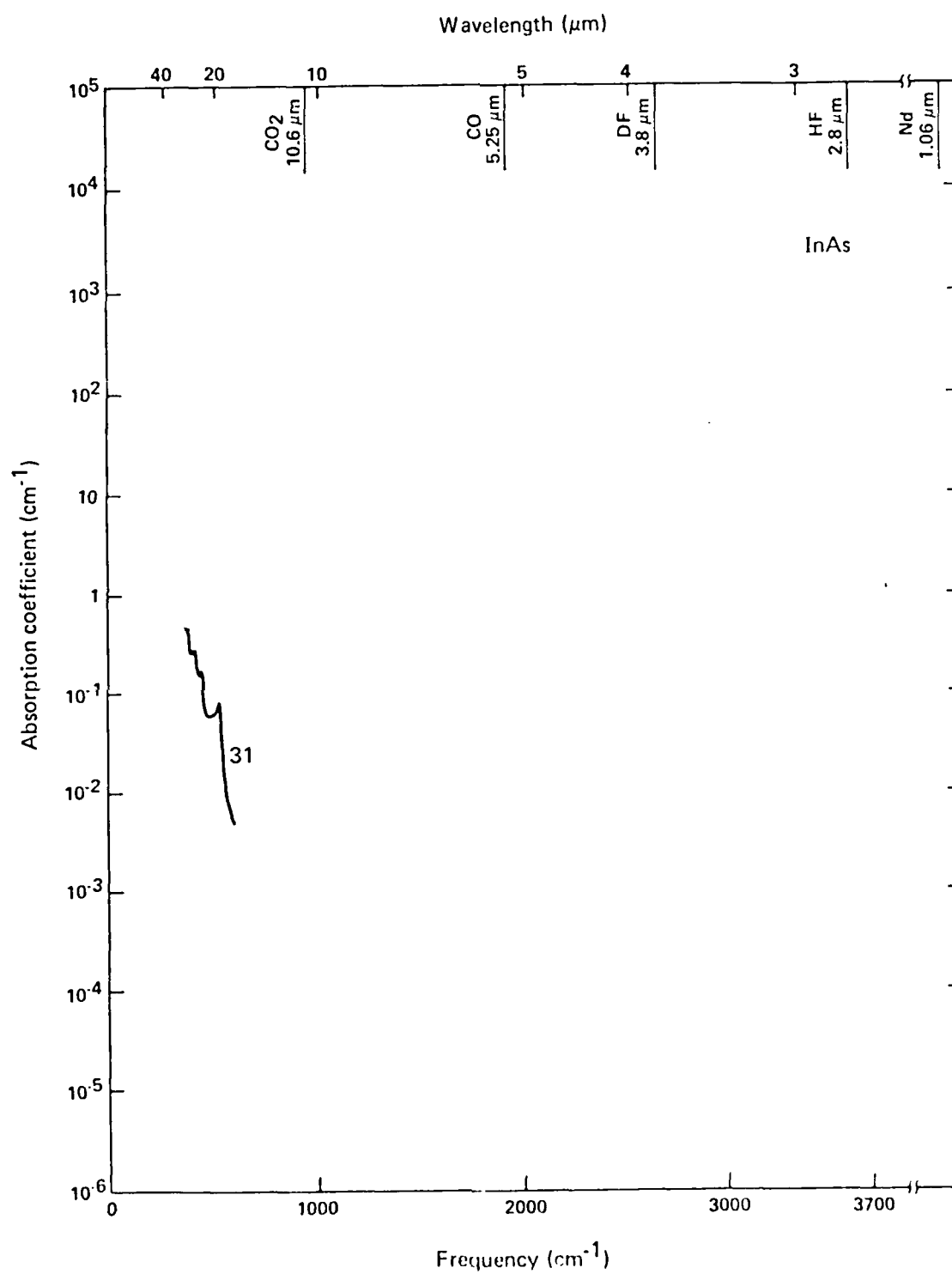


Fig. 20

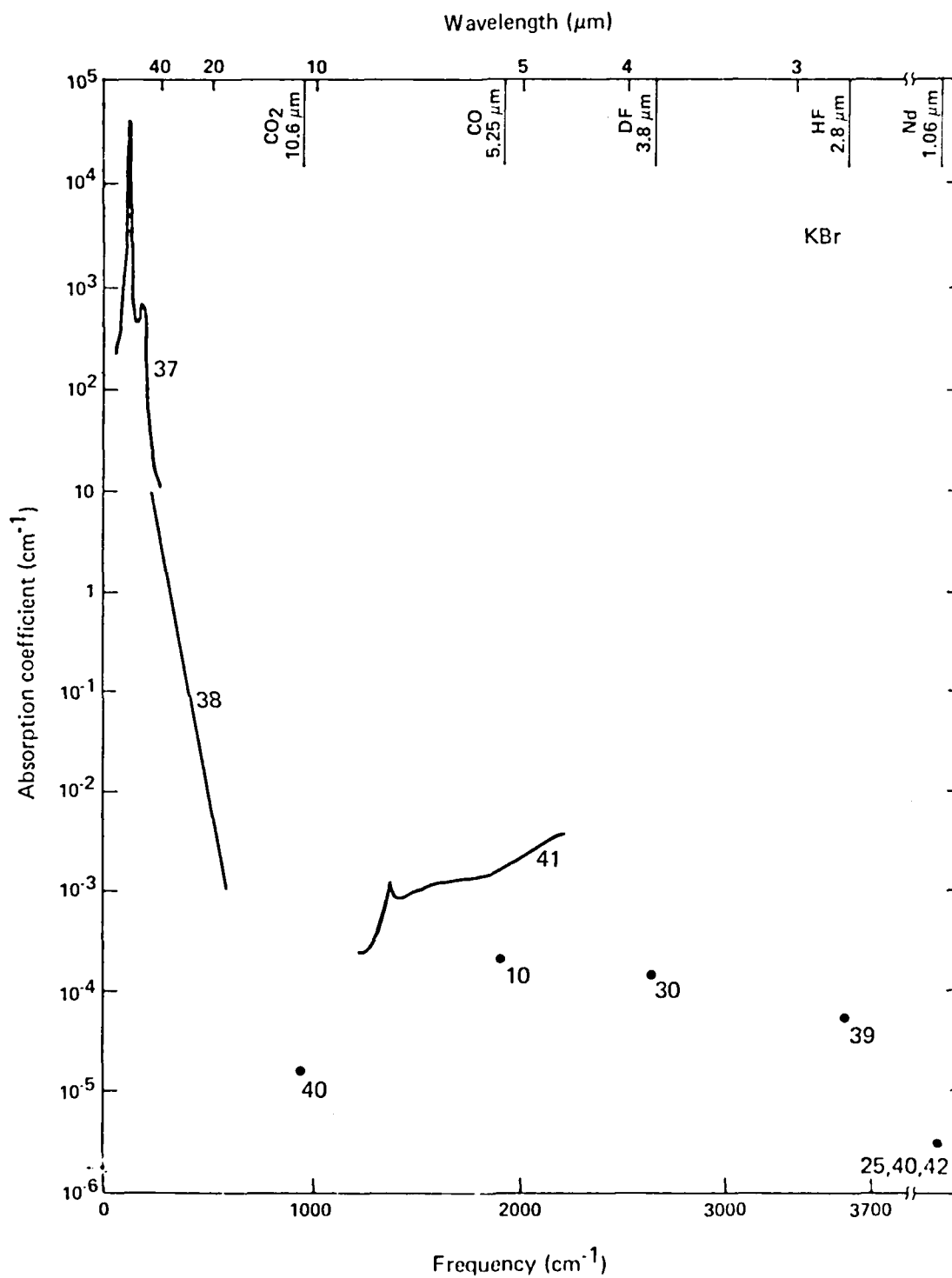


Fig. 21

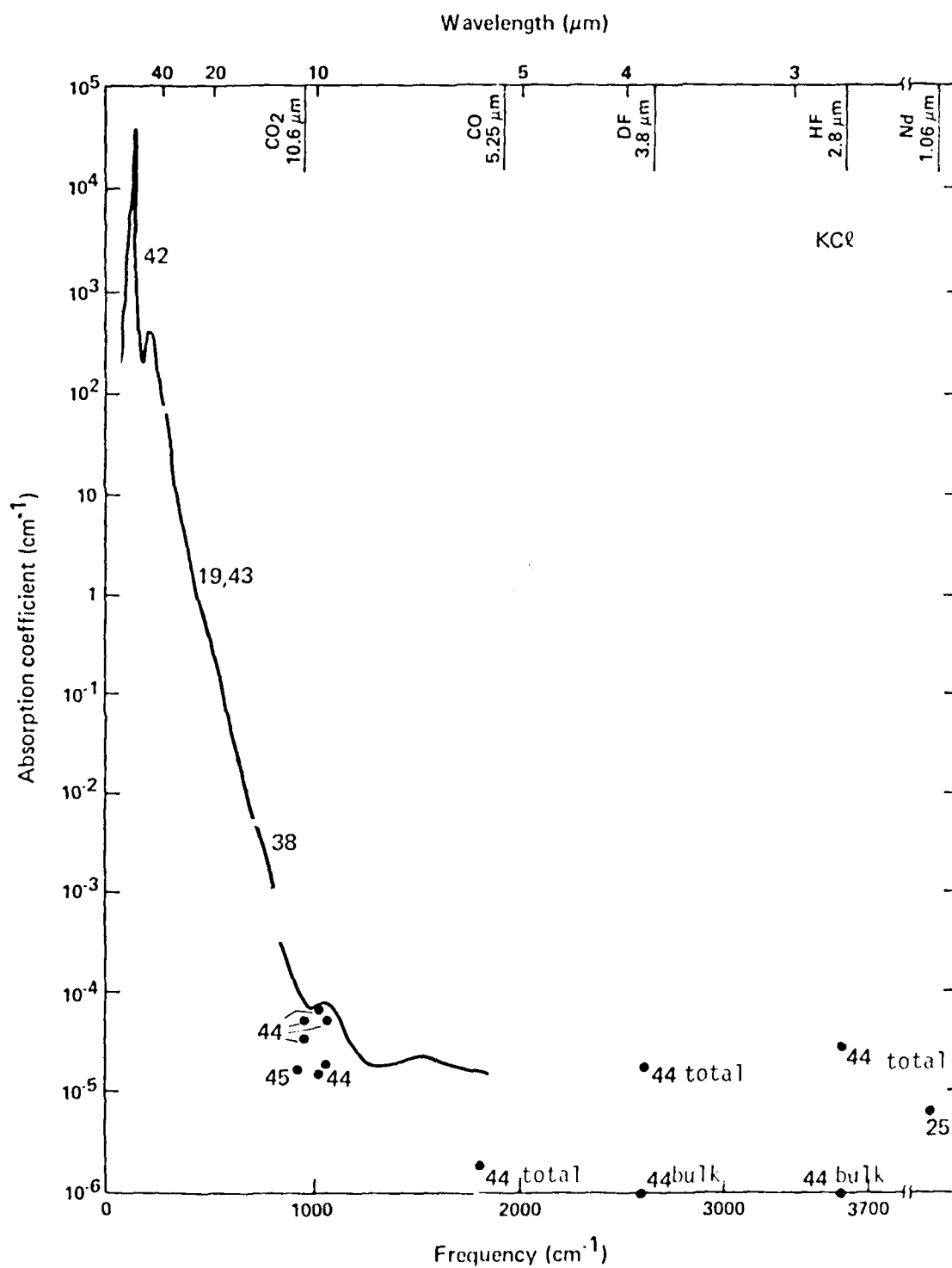


Fig. 22

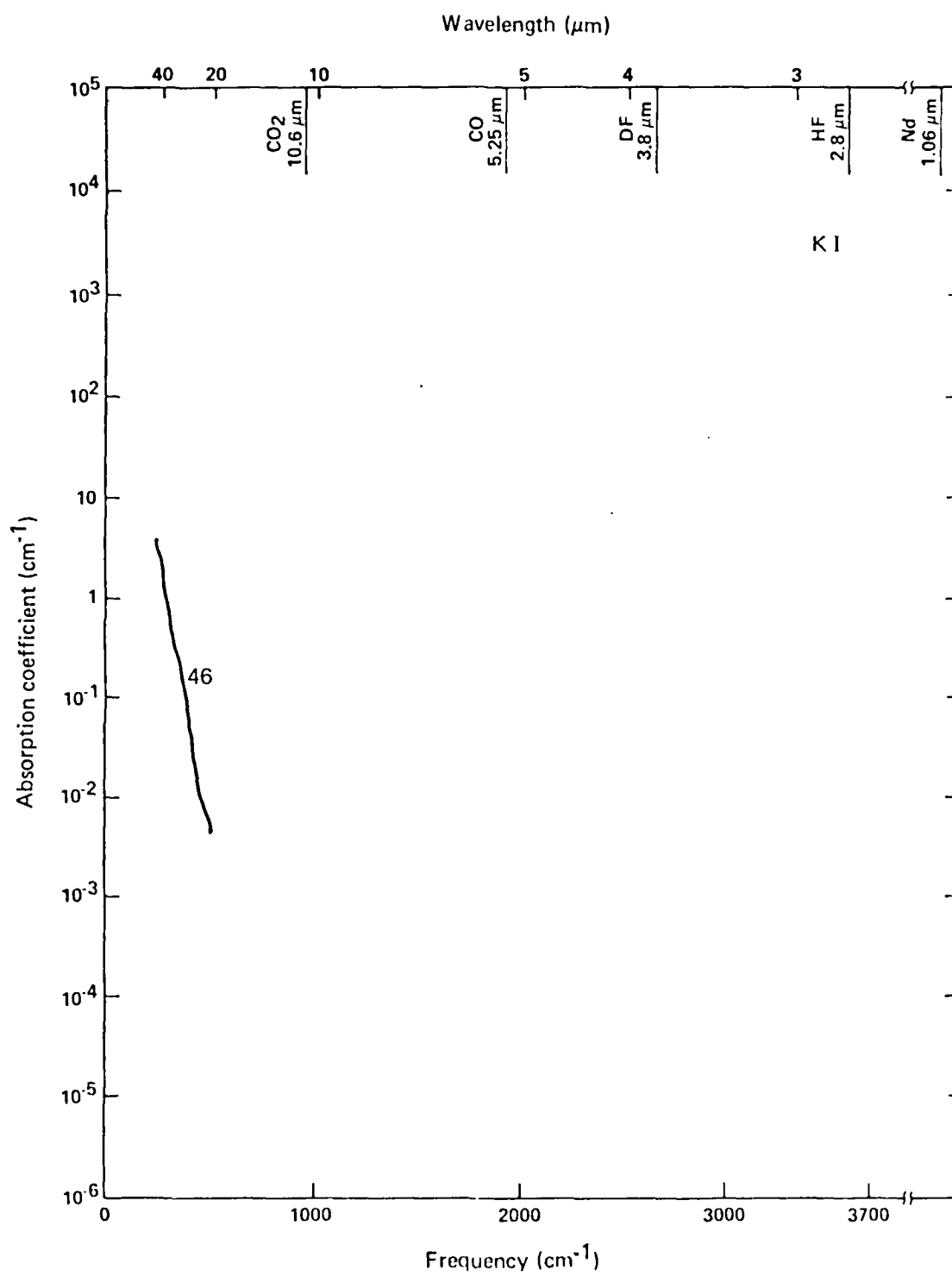


Fig. 23

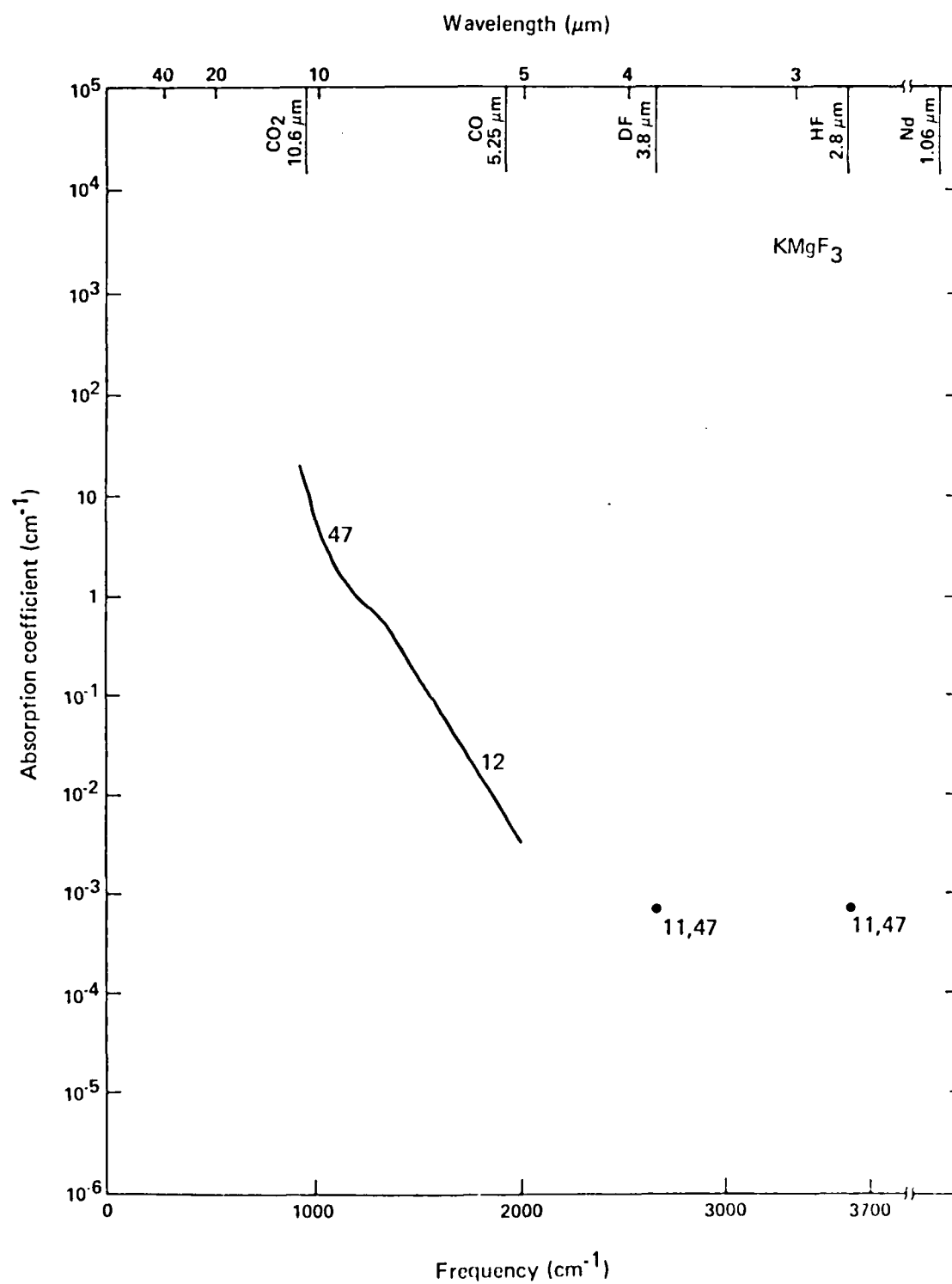


Fig. 24

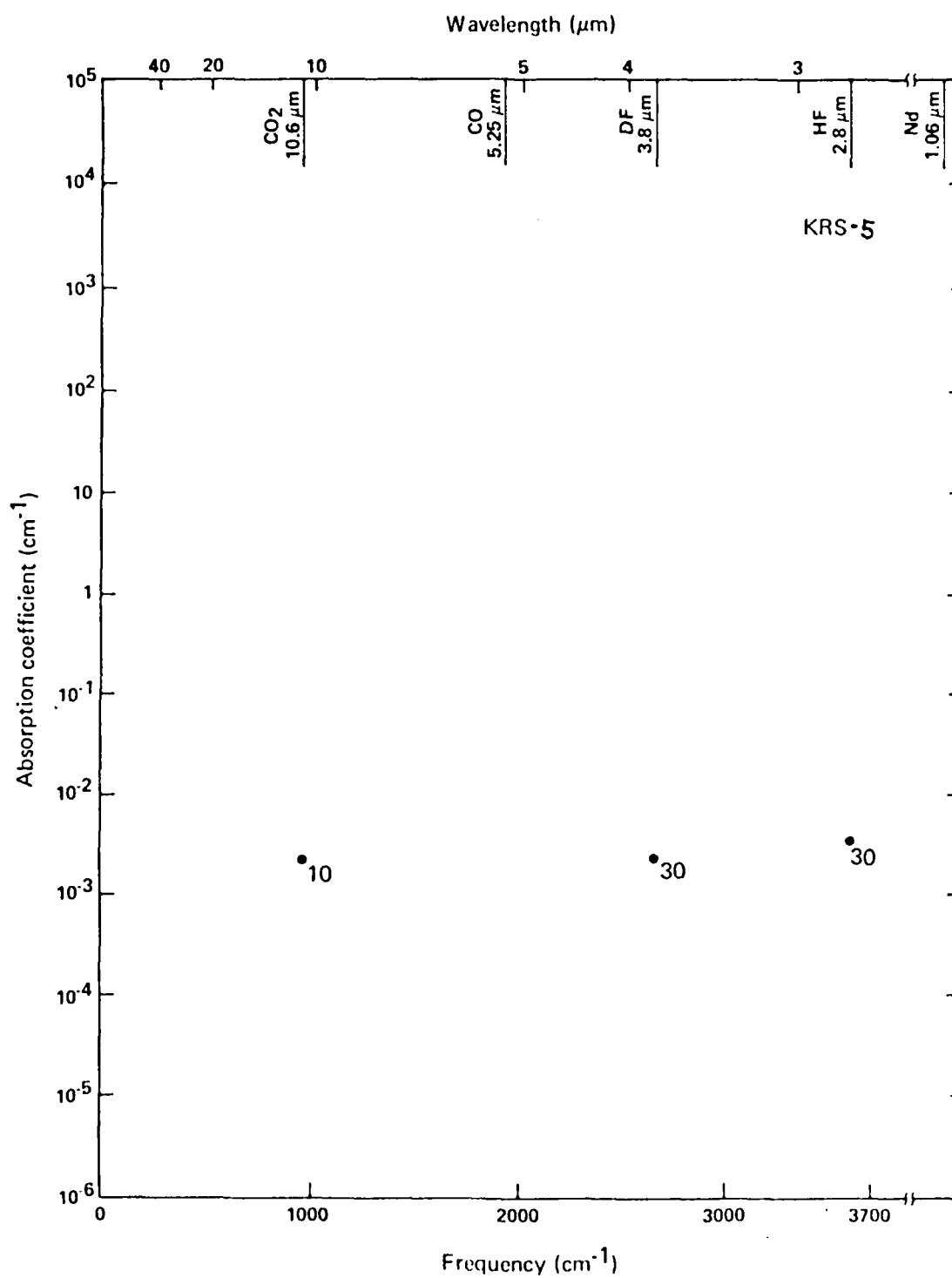


Fig. 25

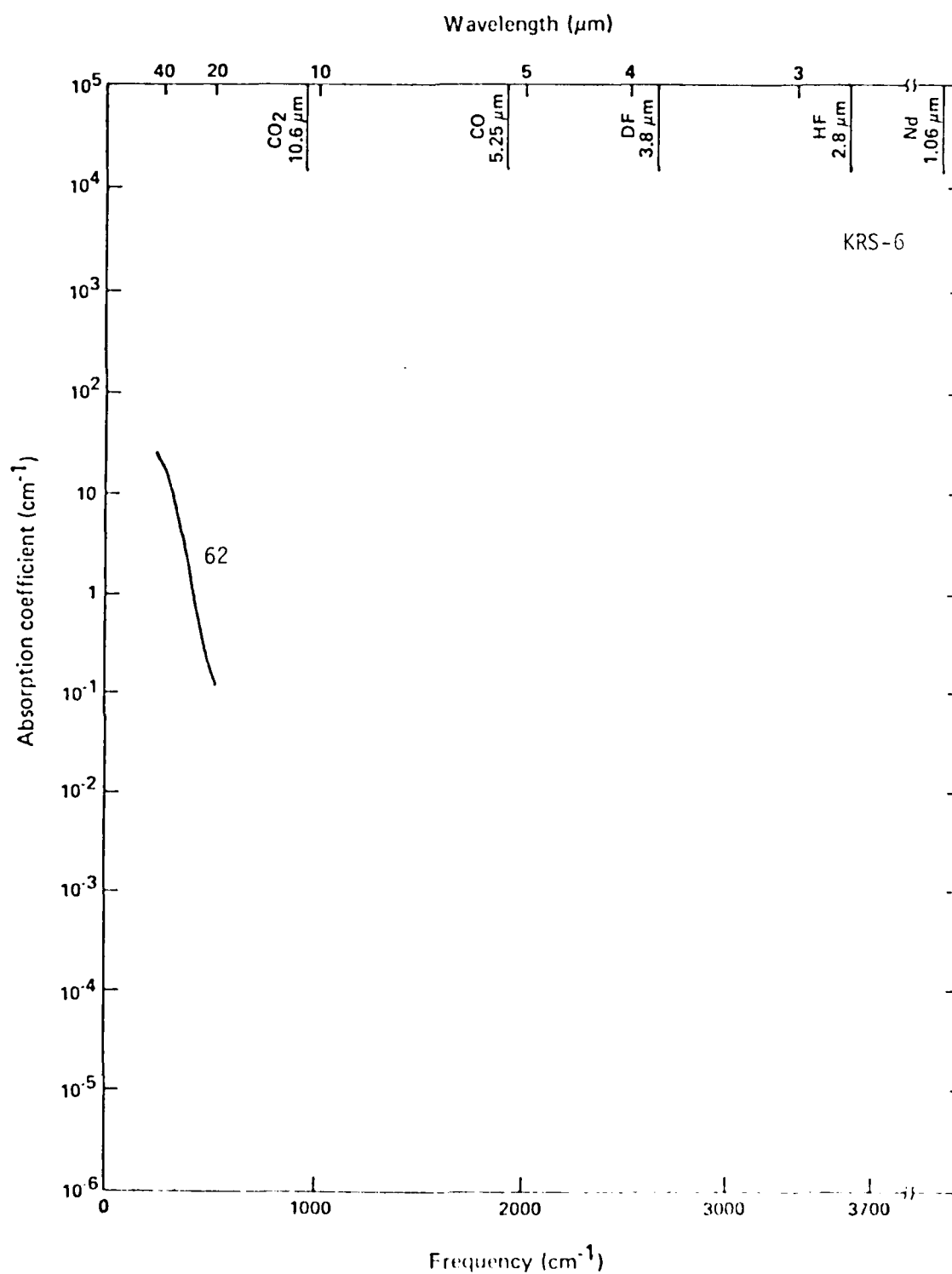


Fig. 26

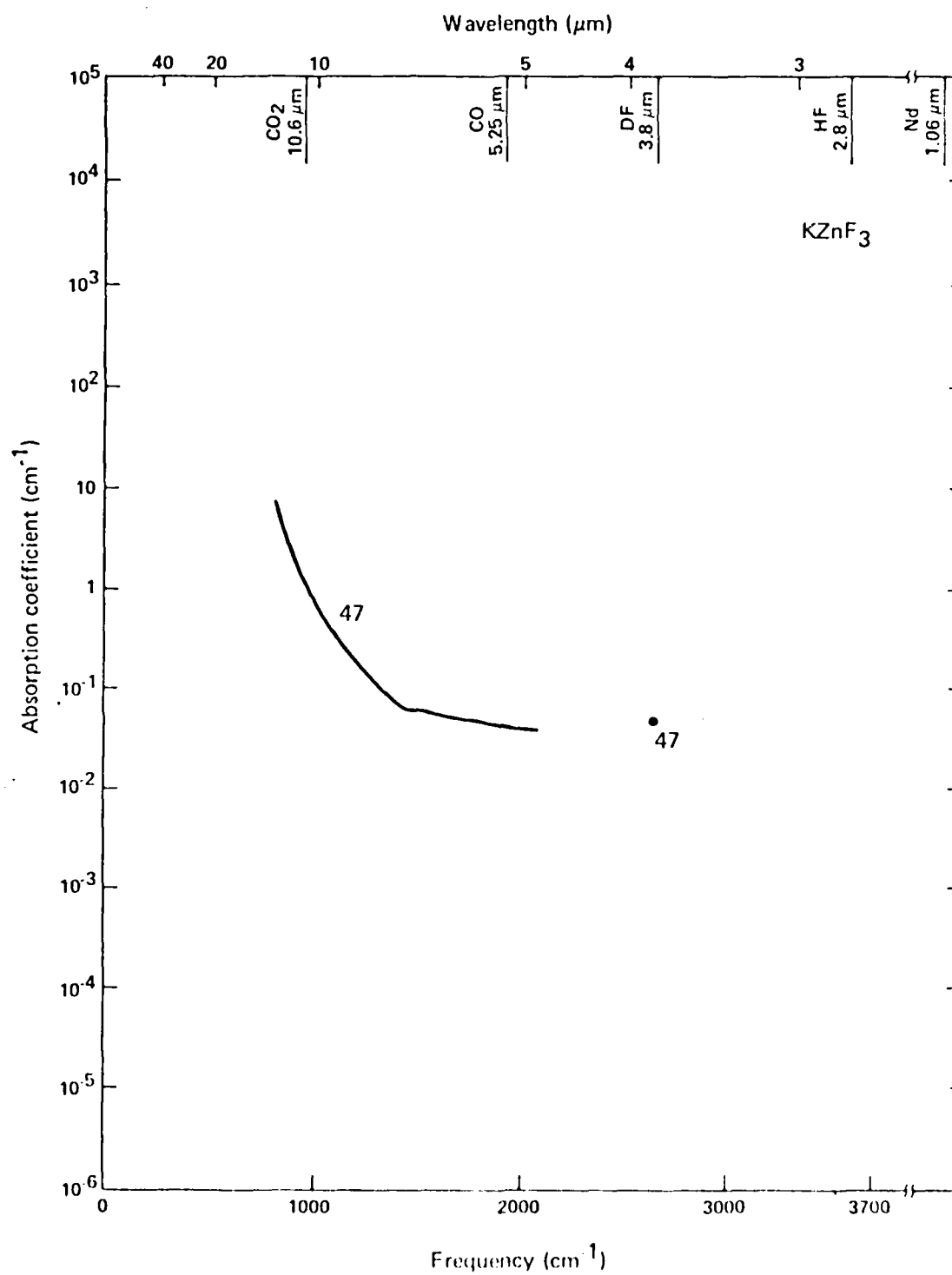


Fig. 27

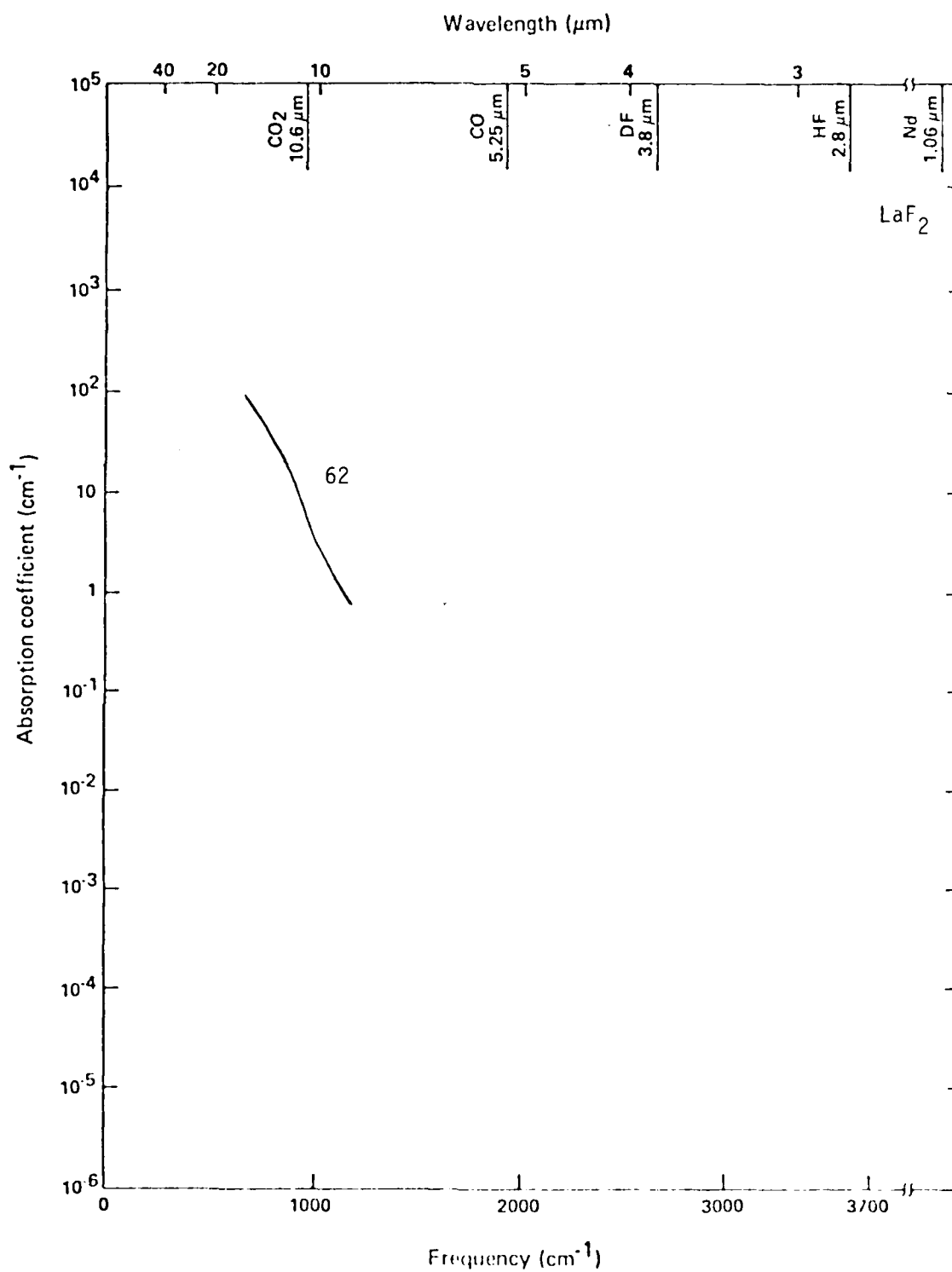


Fig. 28

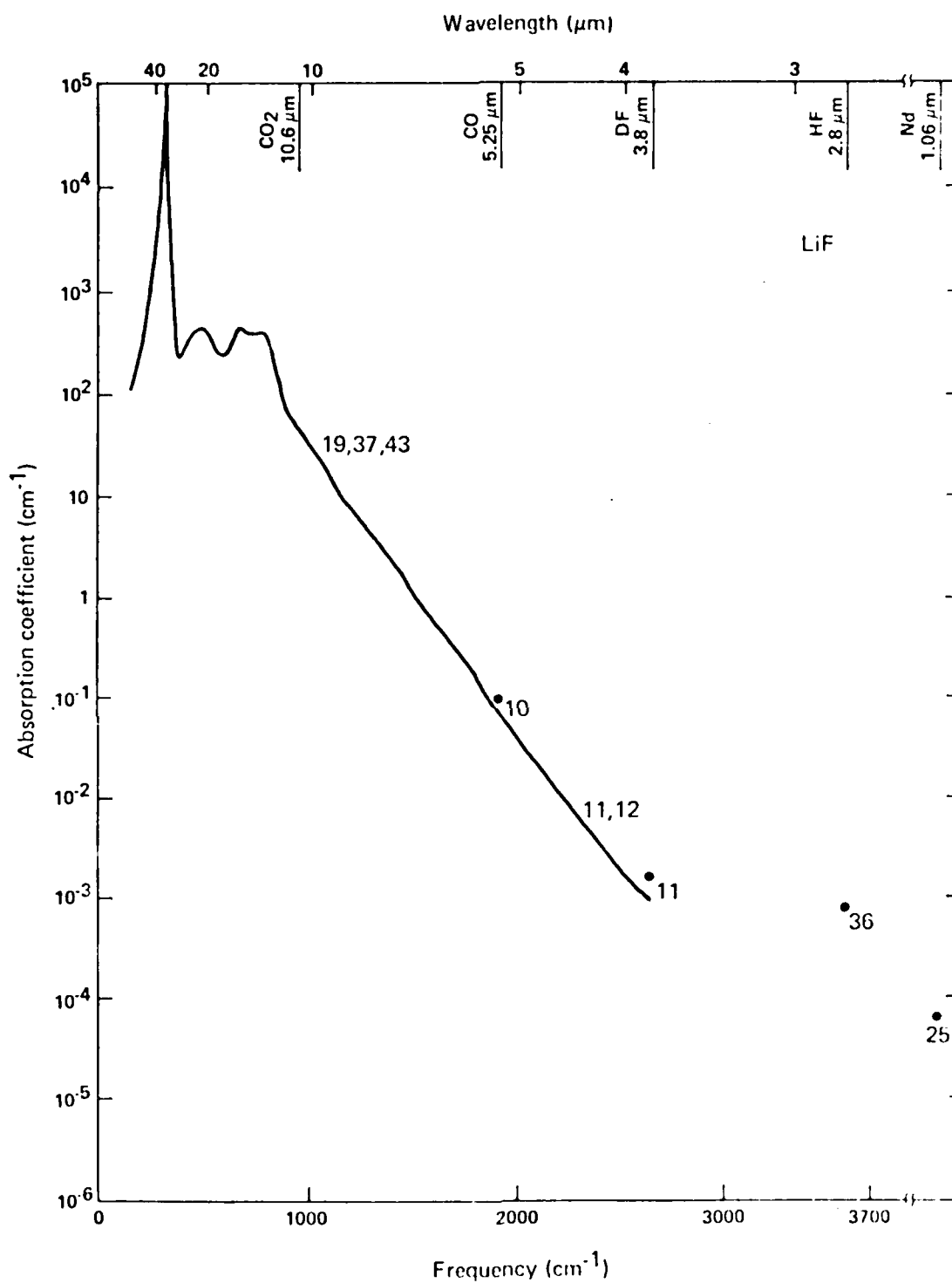


Fig. 29

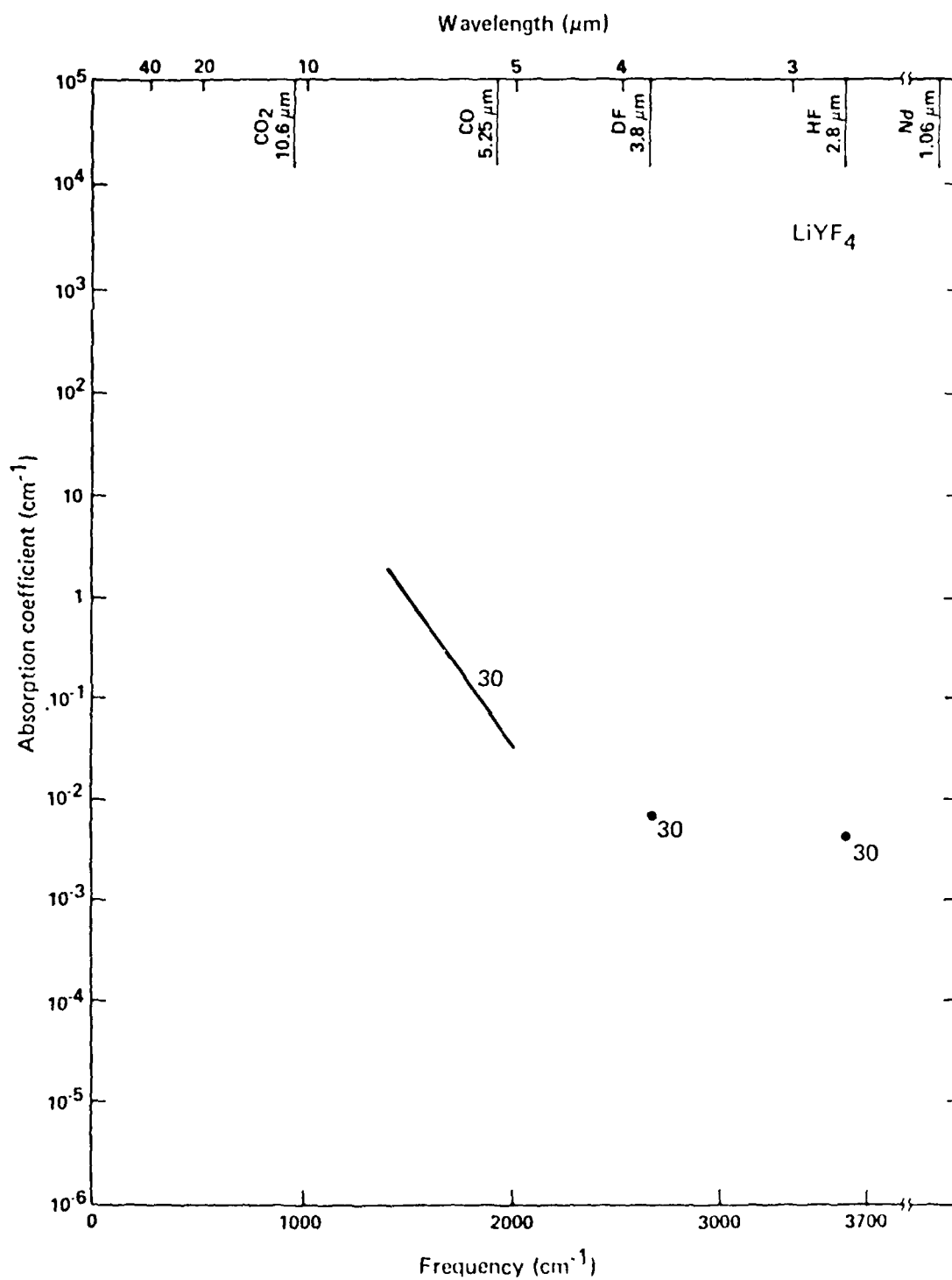


Fig. 30

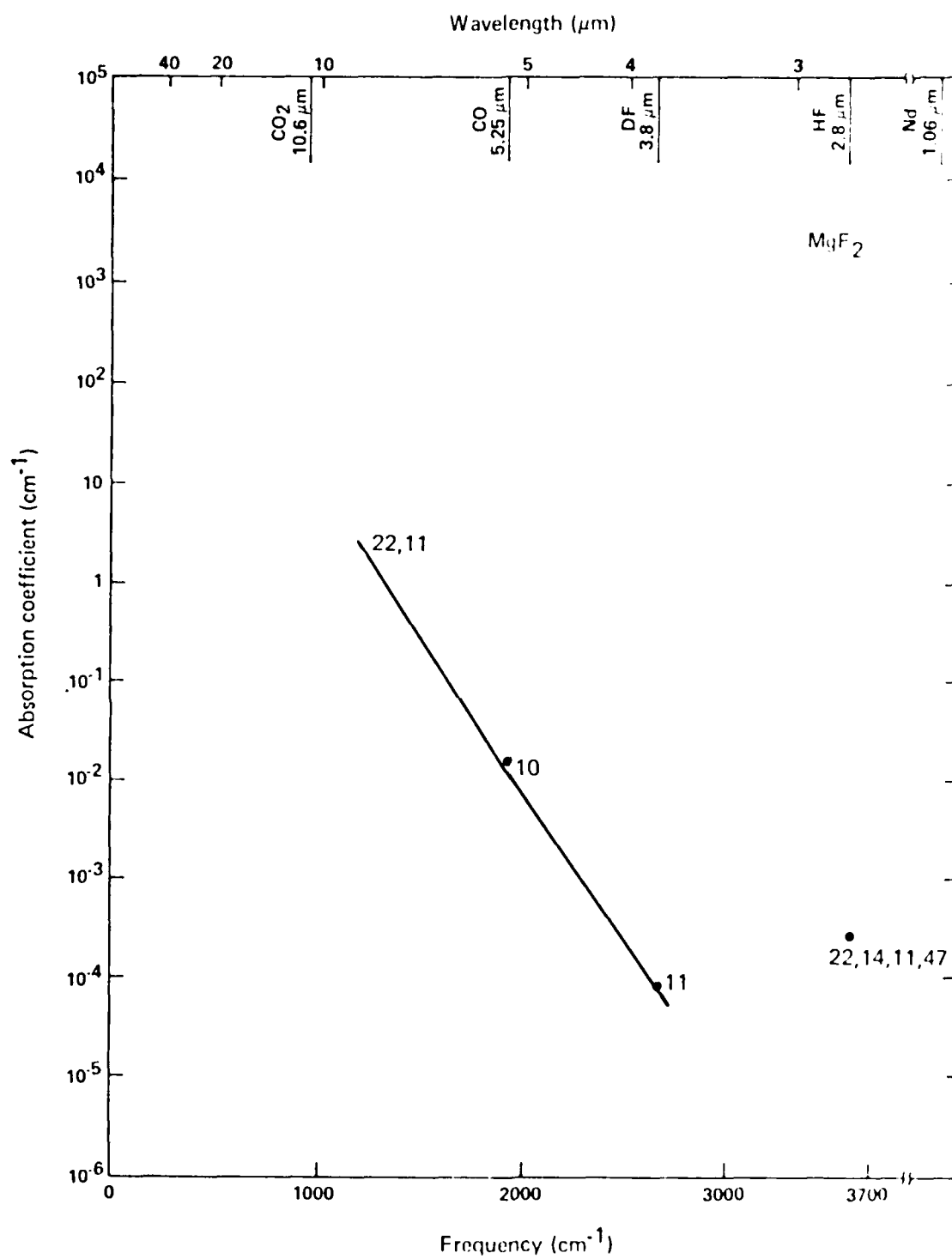


Fig. 31

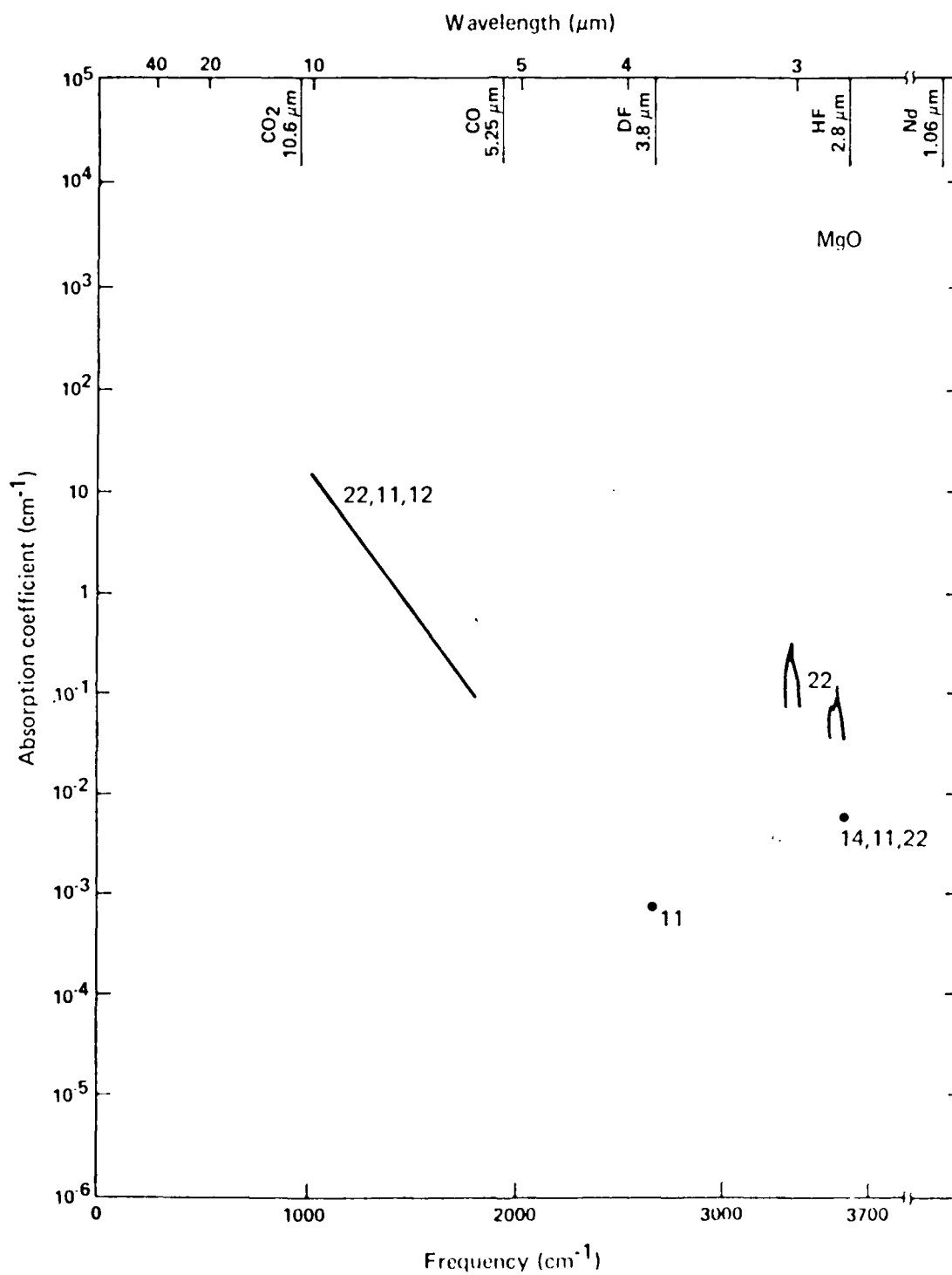


Fig. 32

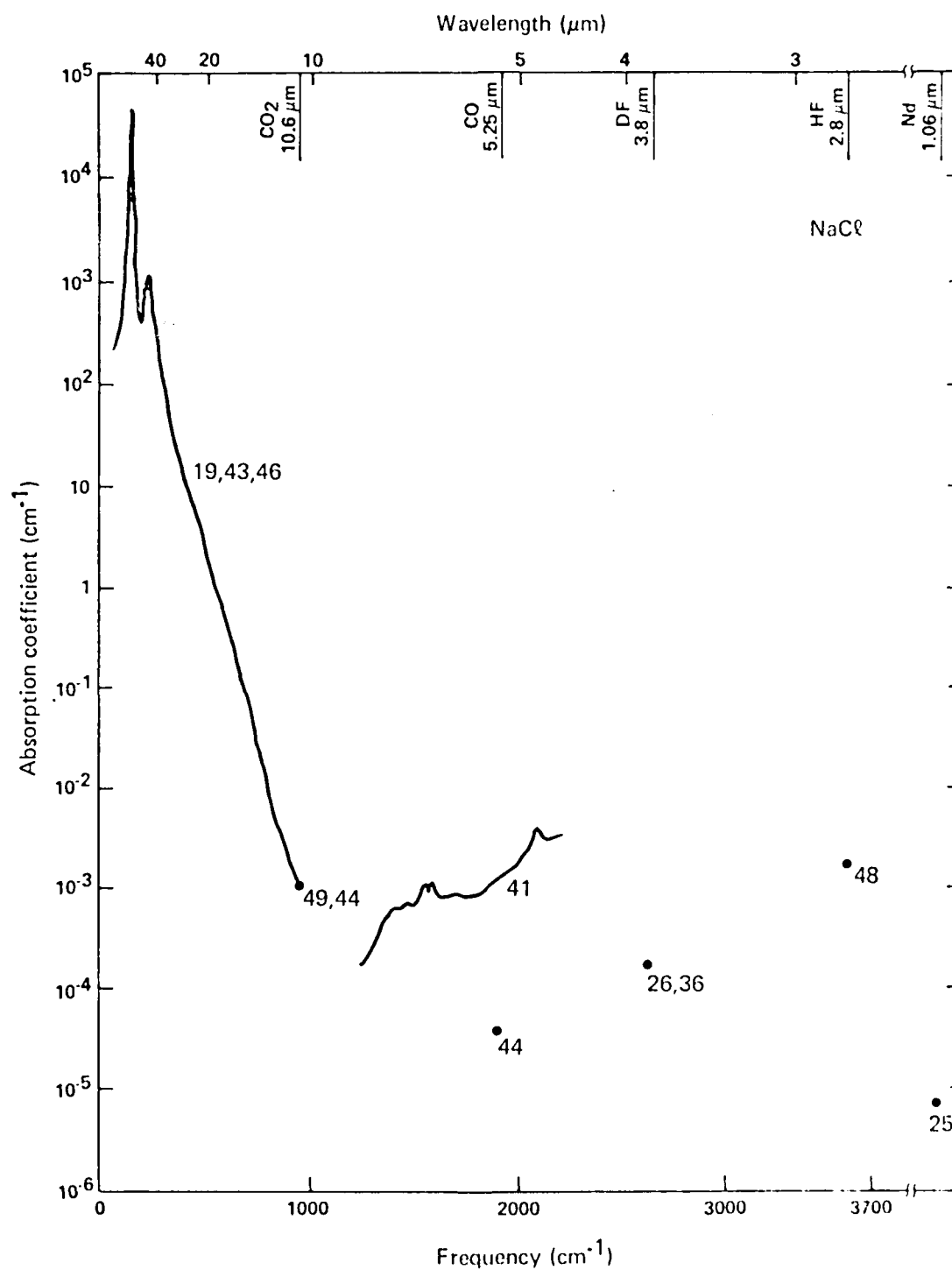


Fig. 33

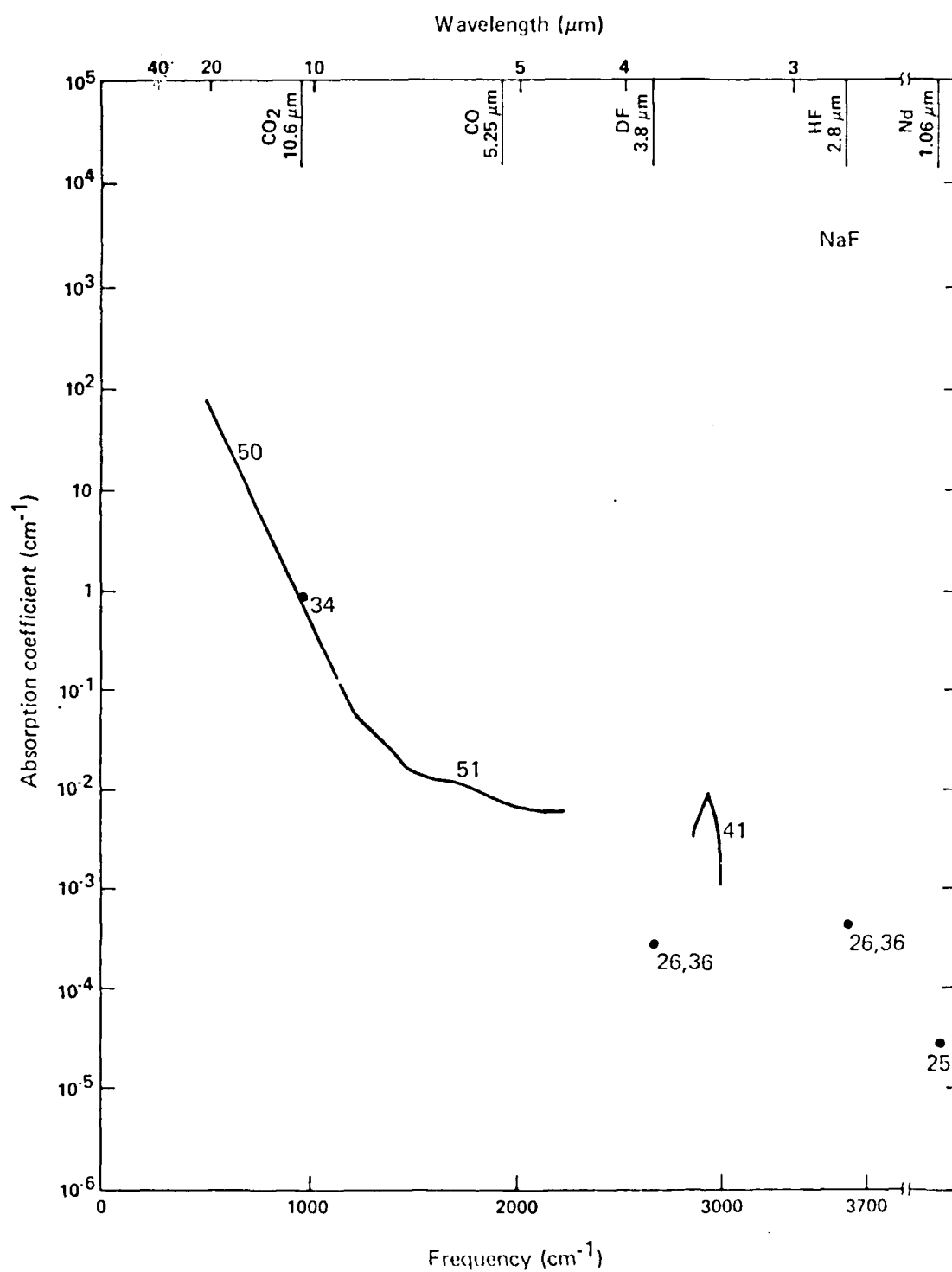


Fig. 34

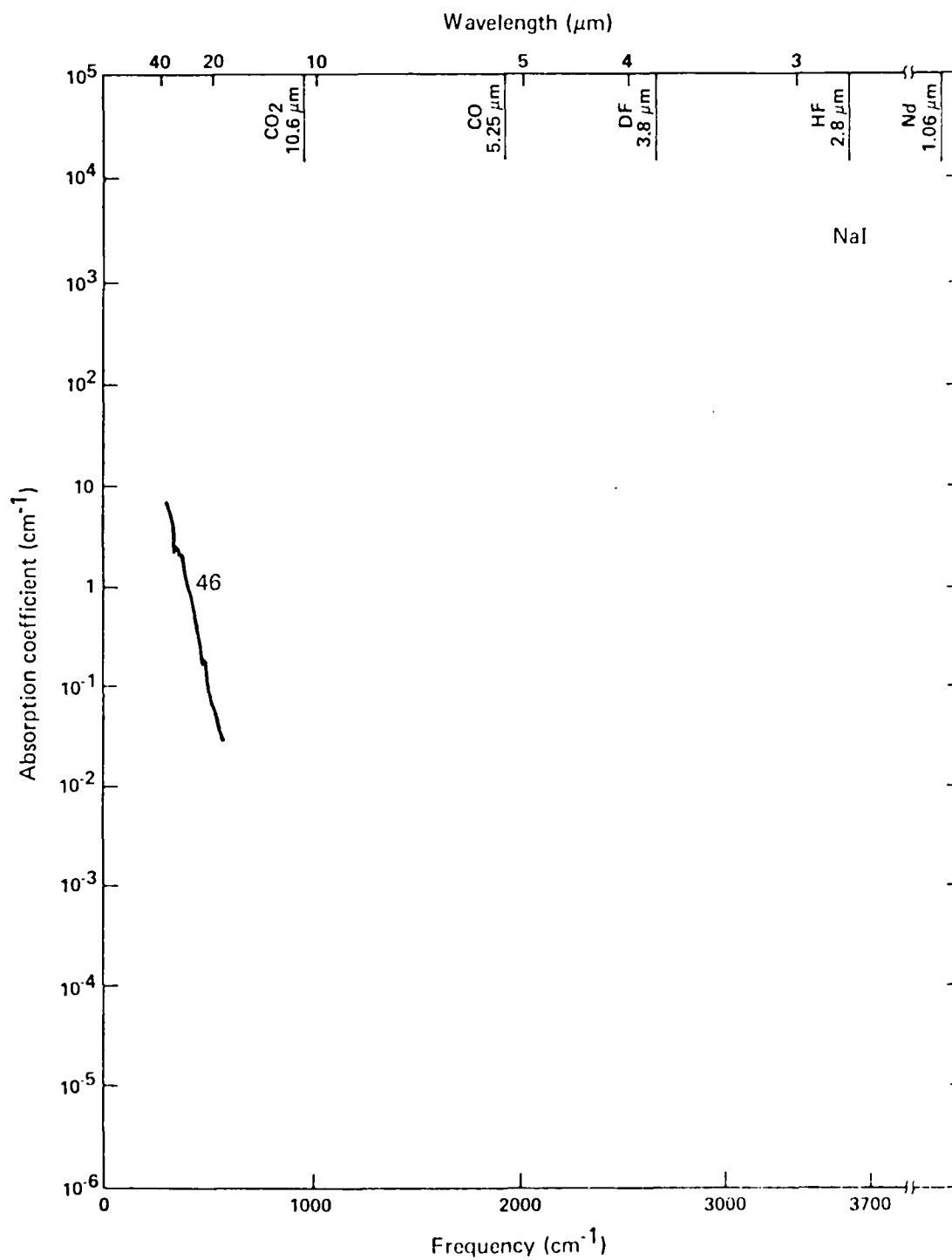


Fig. 35

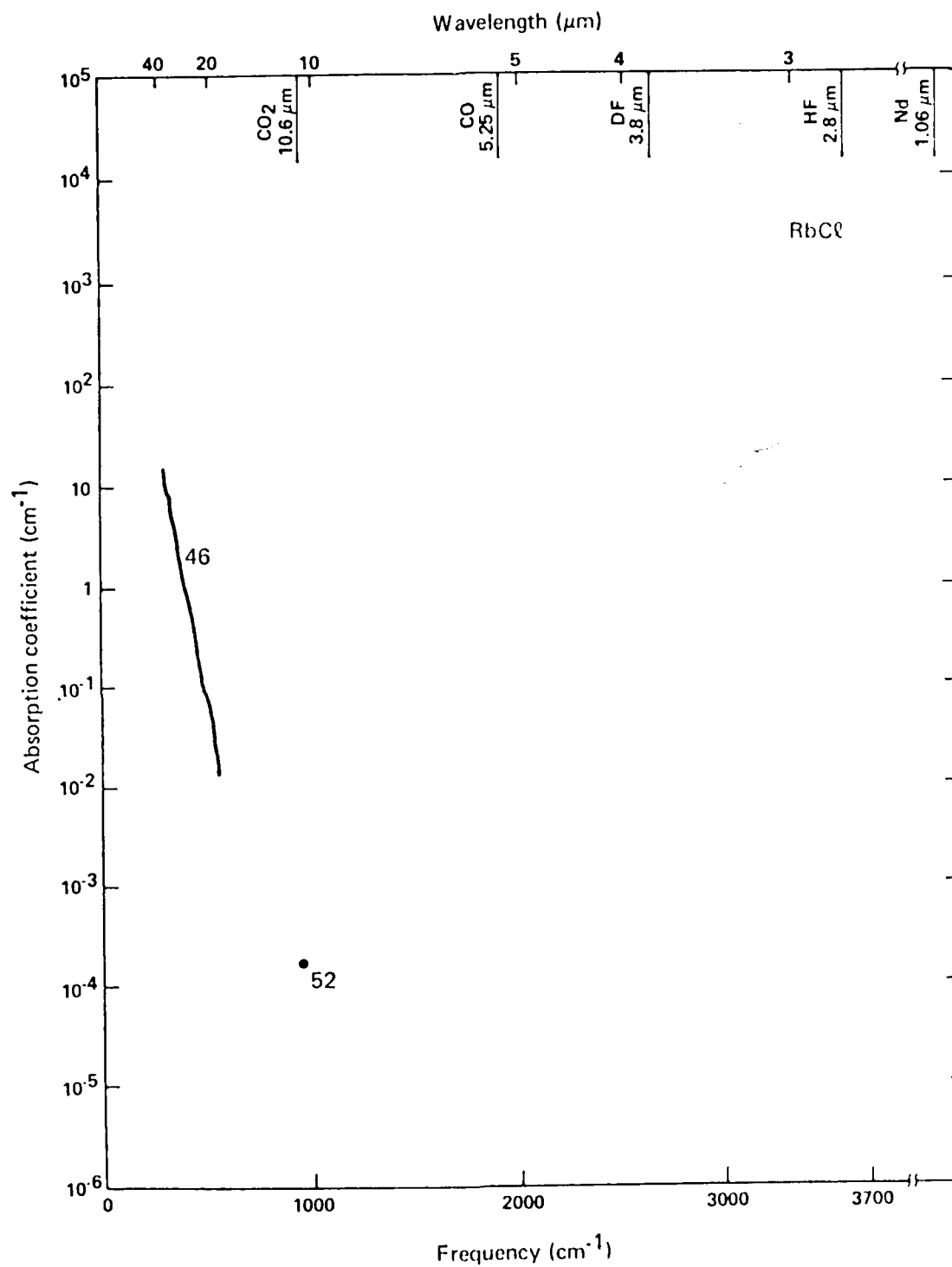


Fig. 36

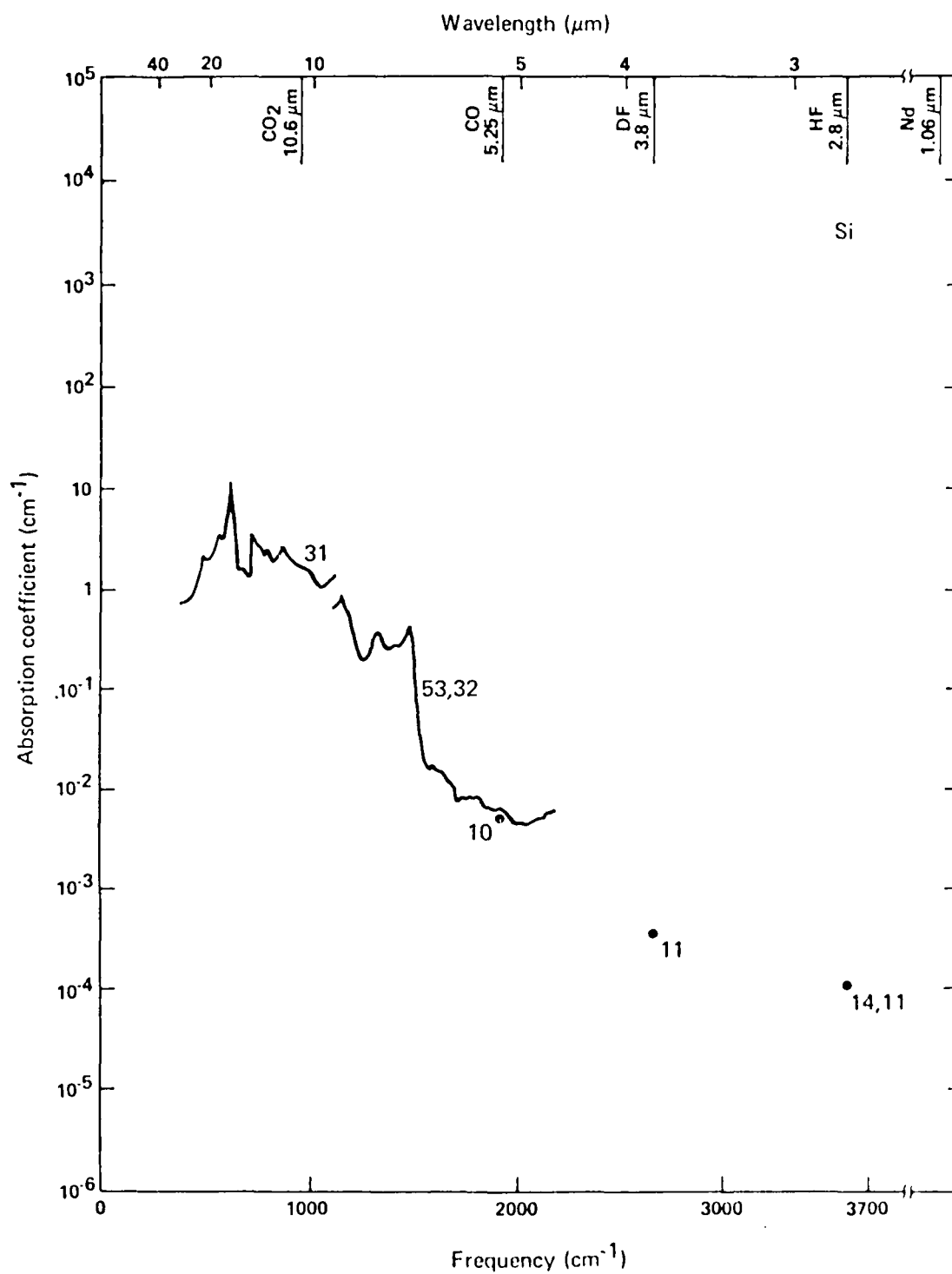


Fig. 37

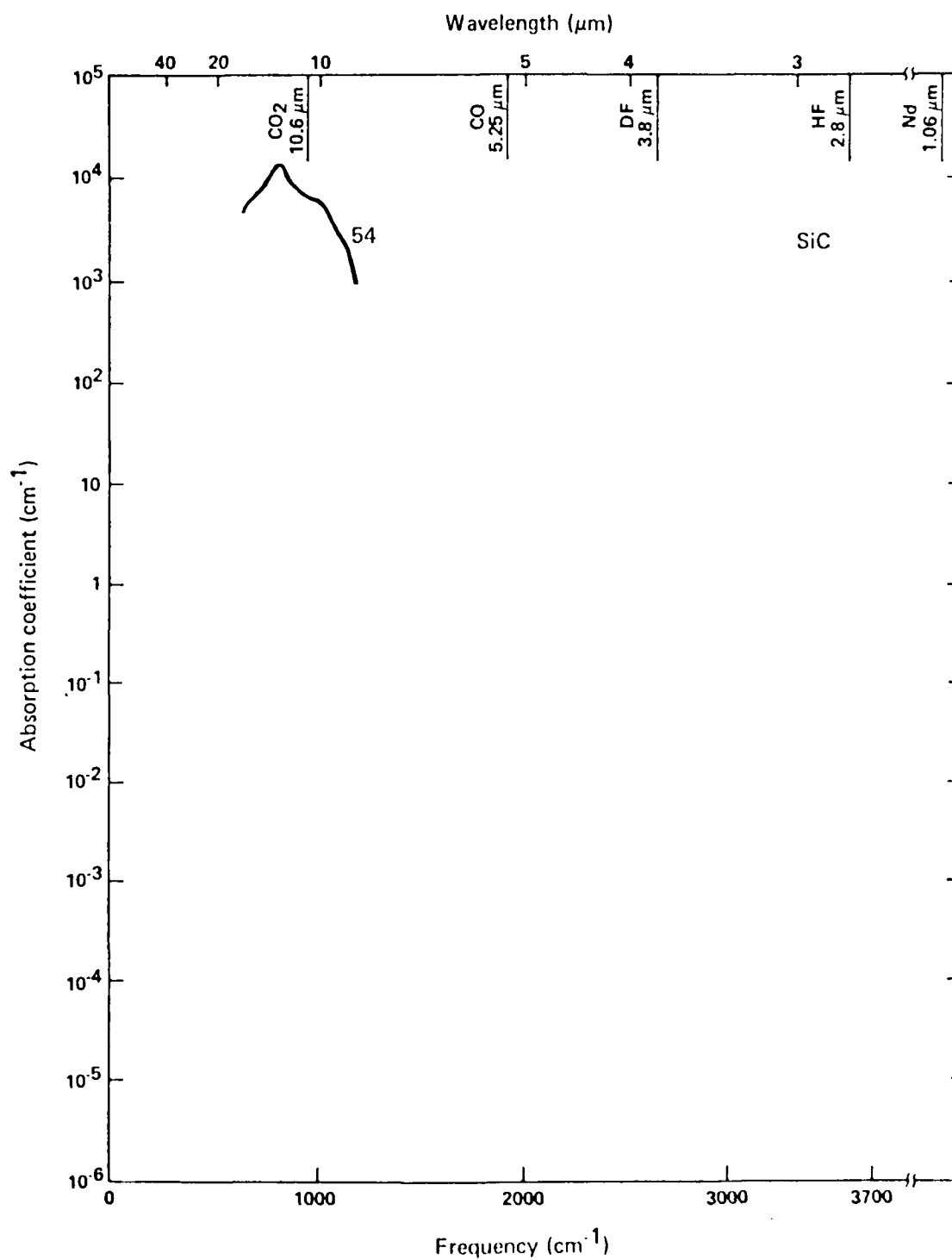


Fig. 38

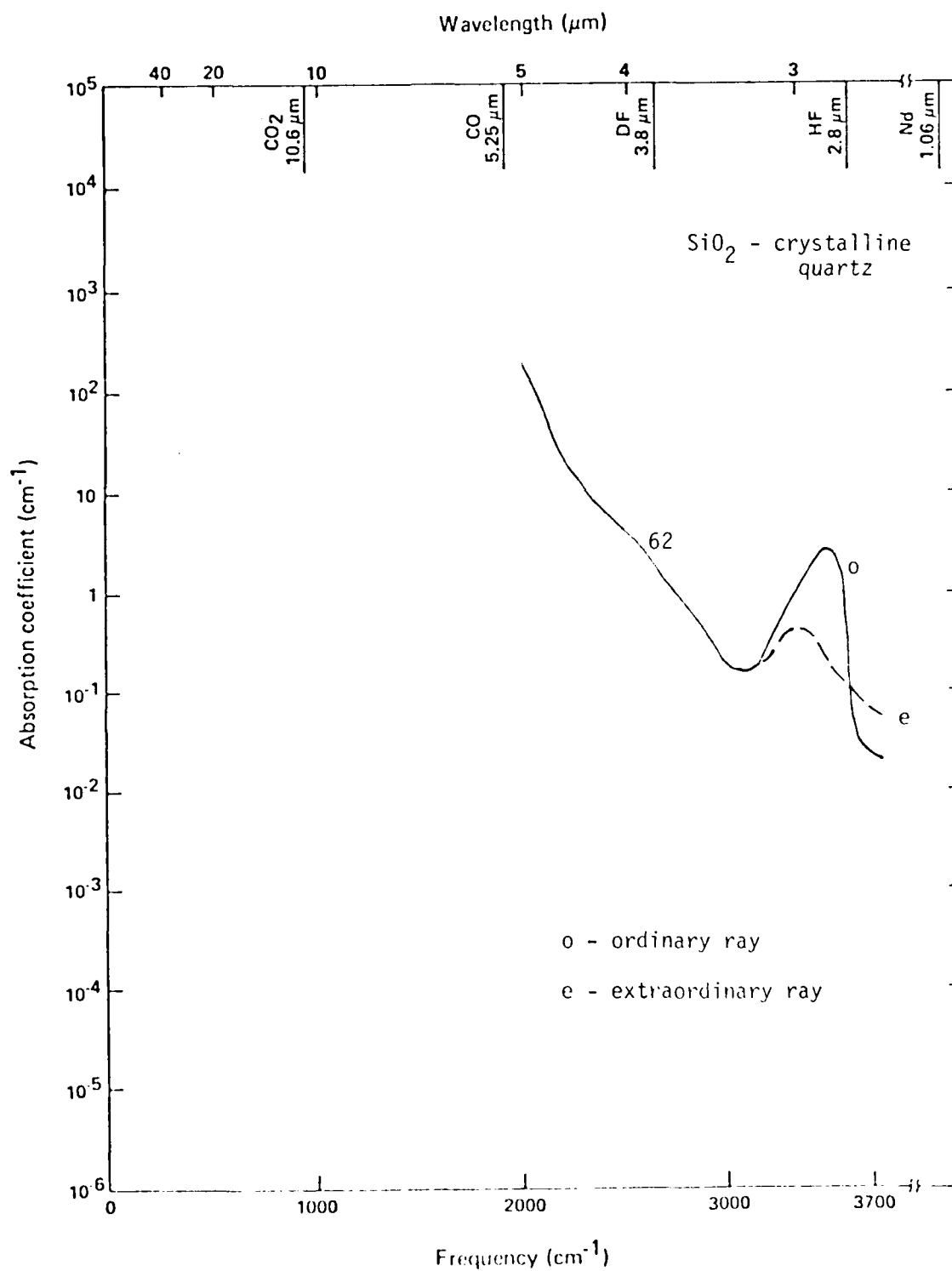


Fig. 39

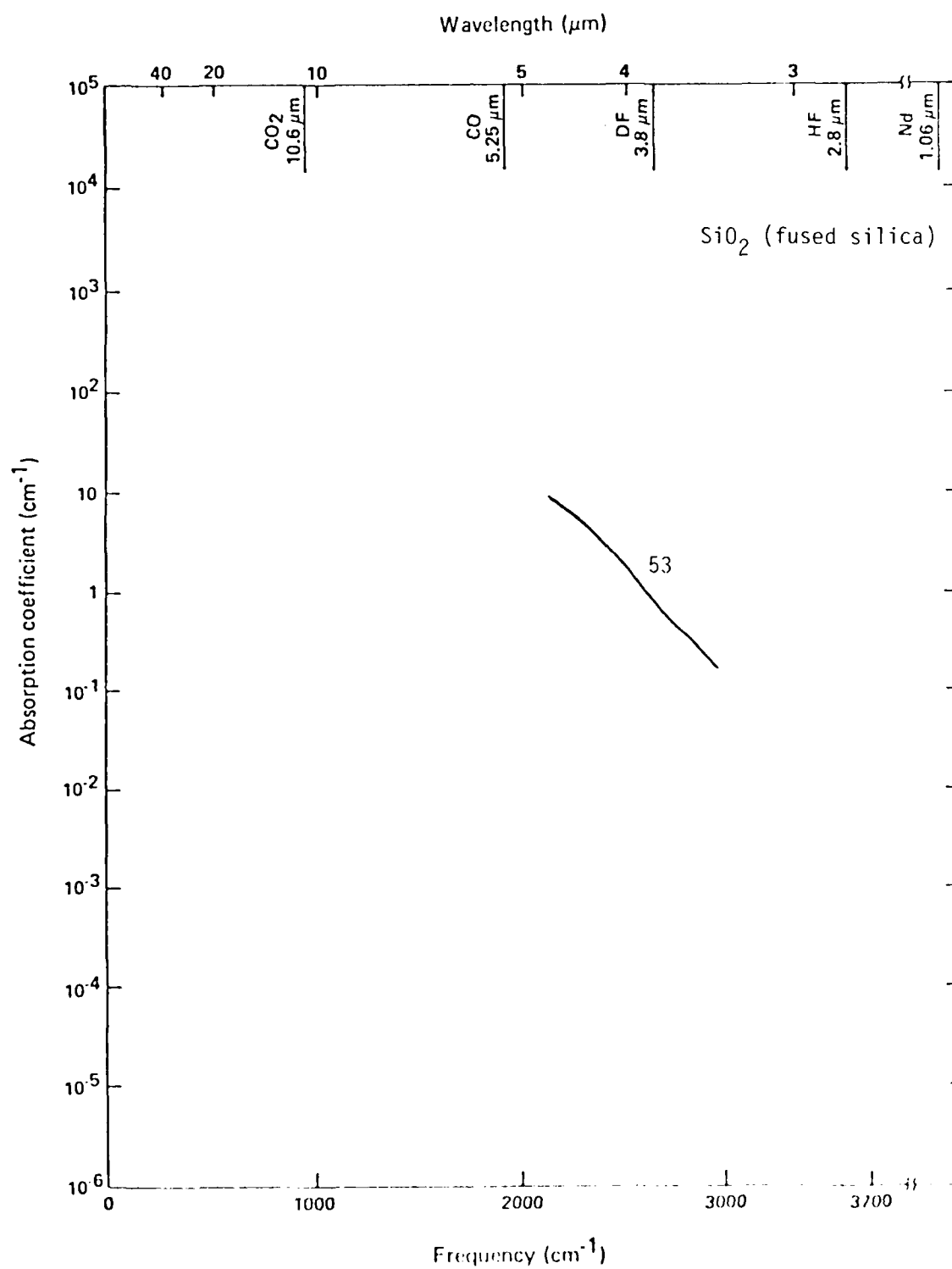


Fig. 40

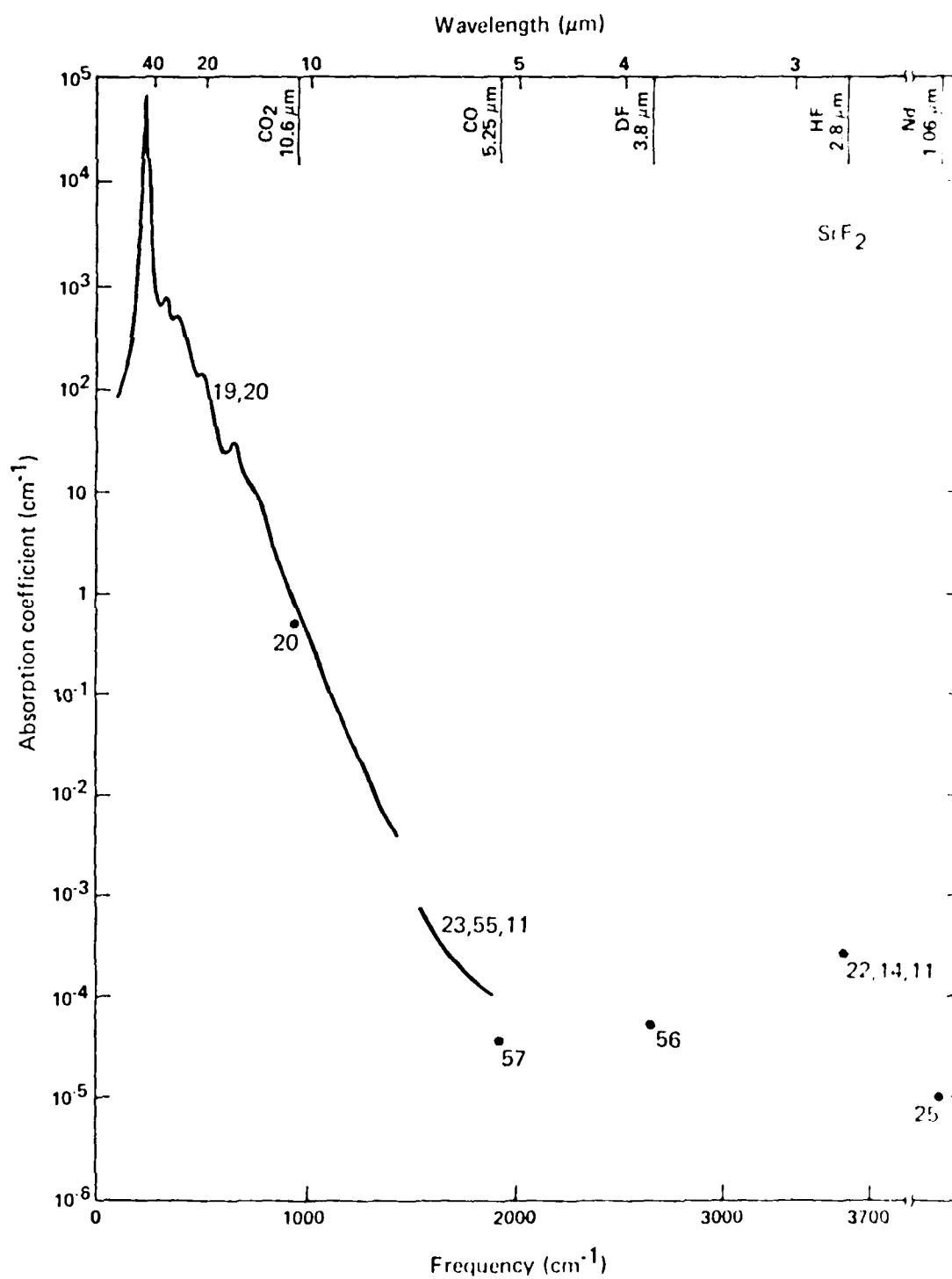


Fig. 41

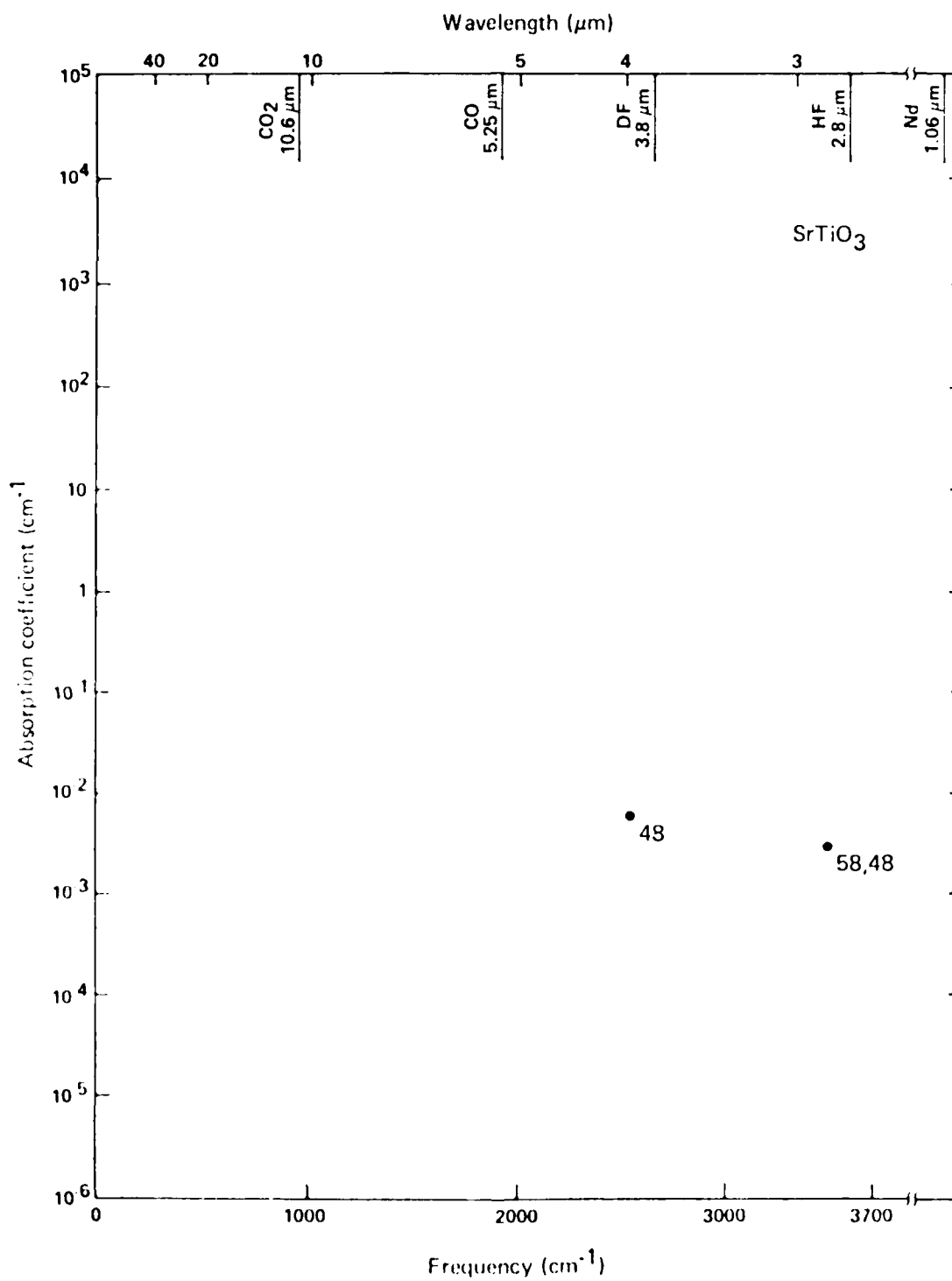


Fig. 42

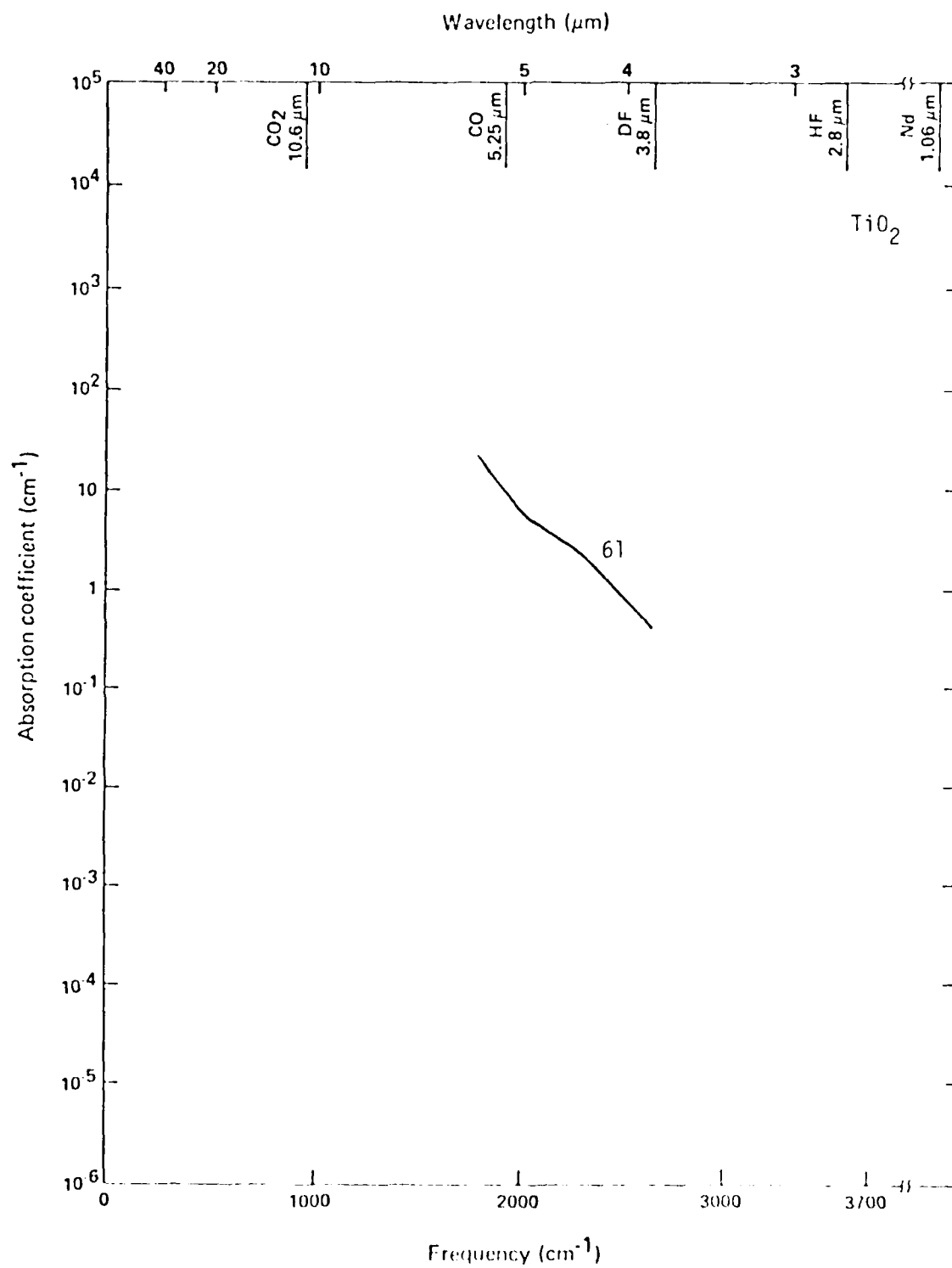


Fig. 43

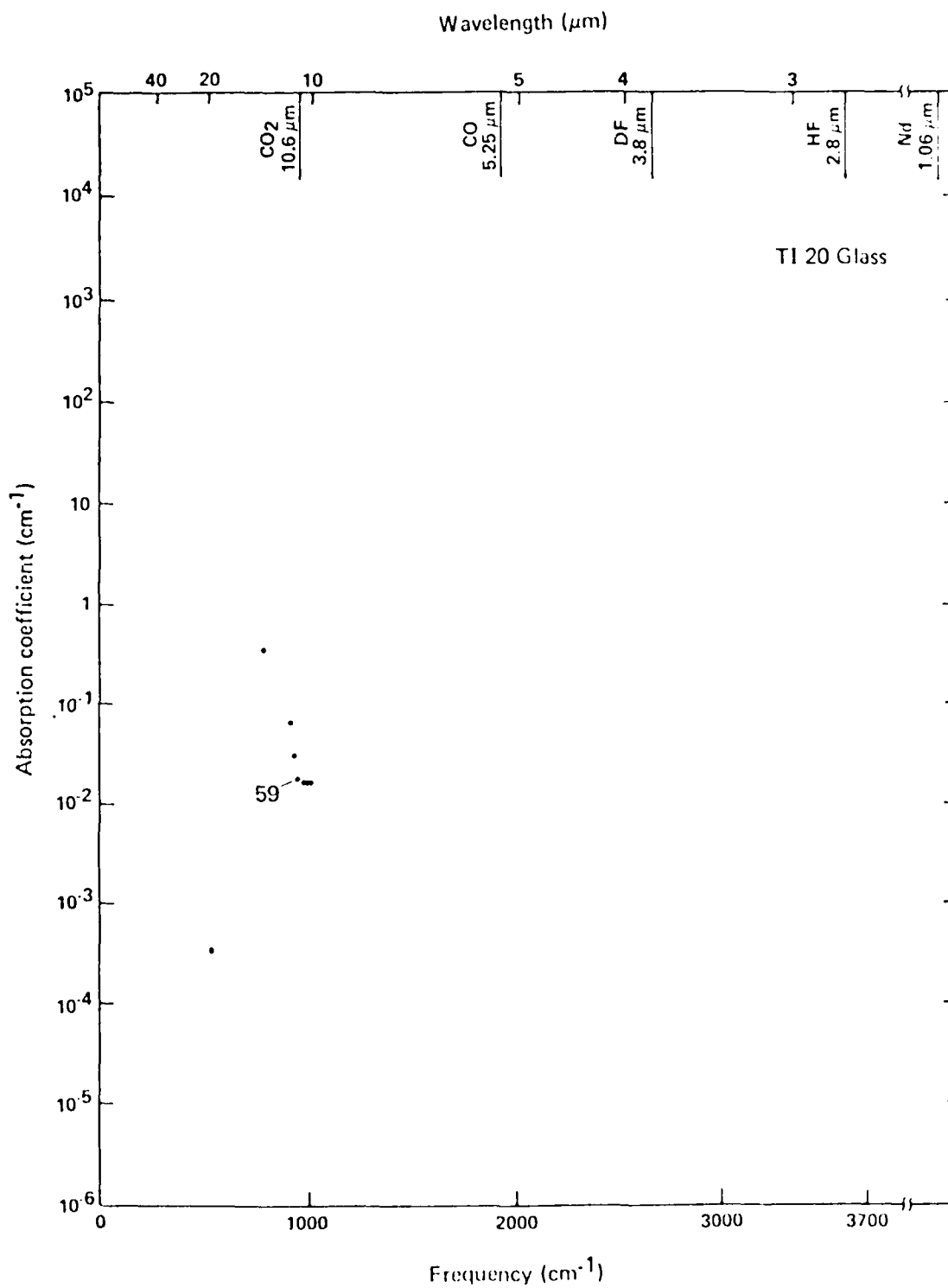


Fig. 44

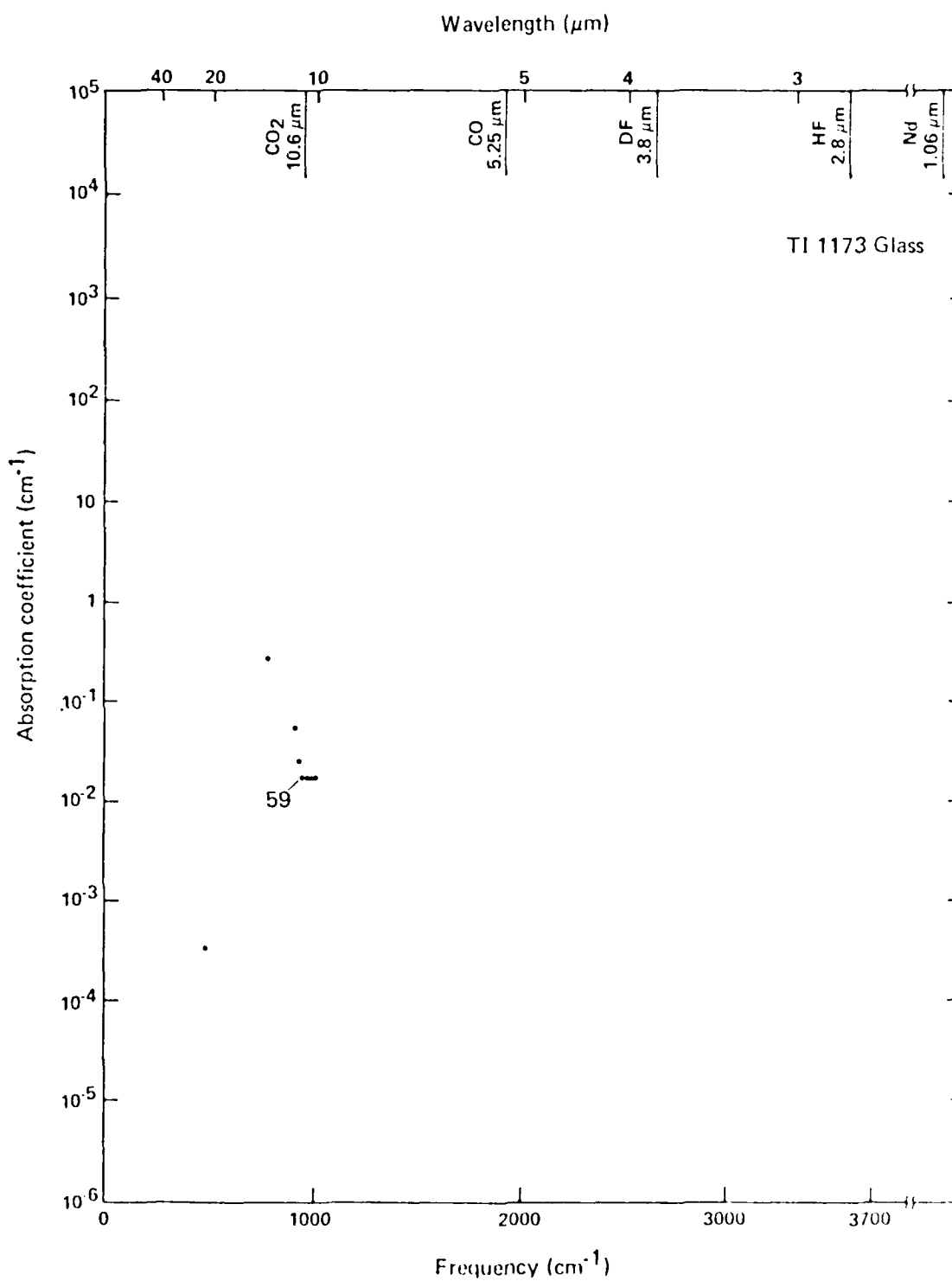


Fig. 45

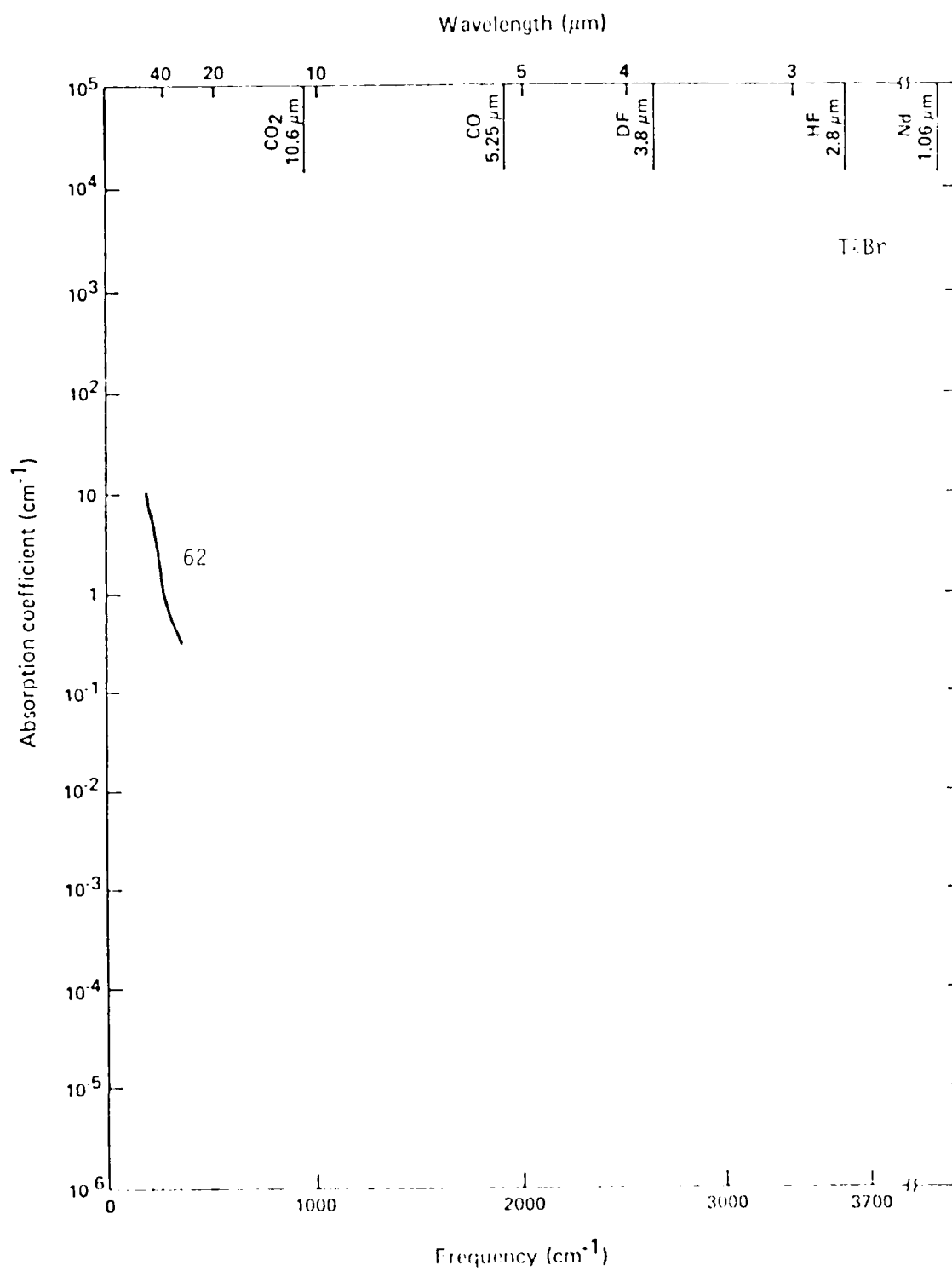


Fig. 46

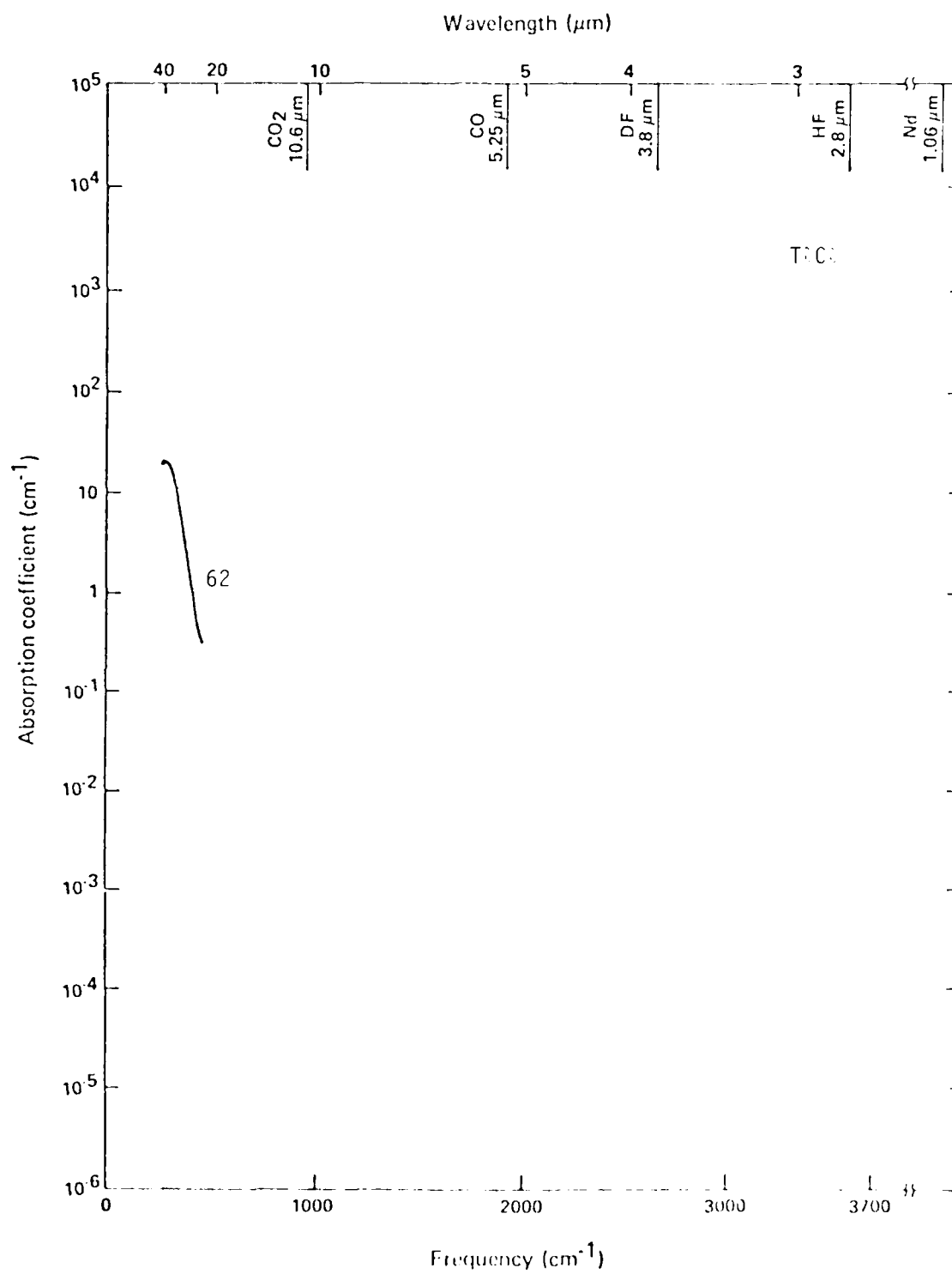


Fig. 47

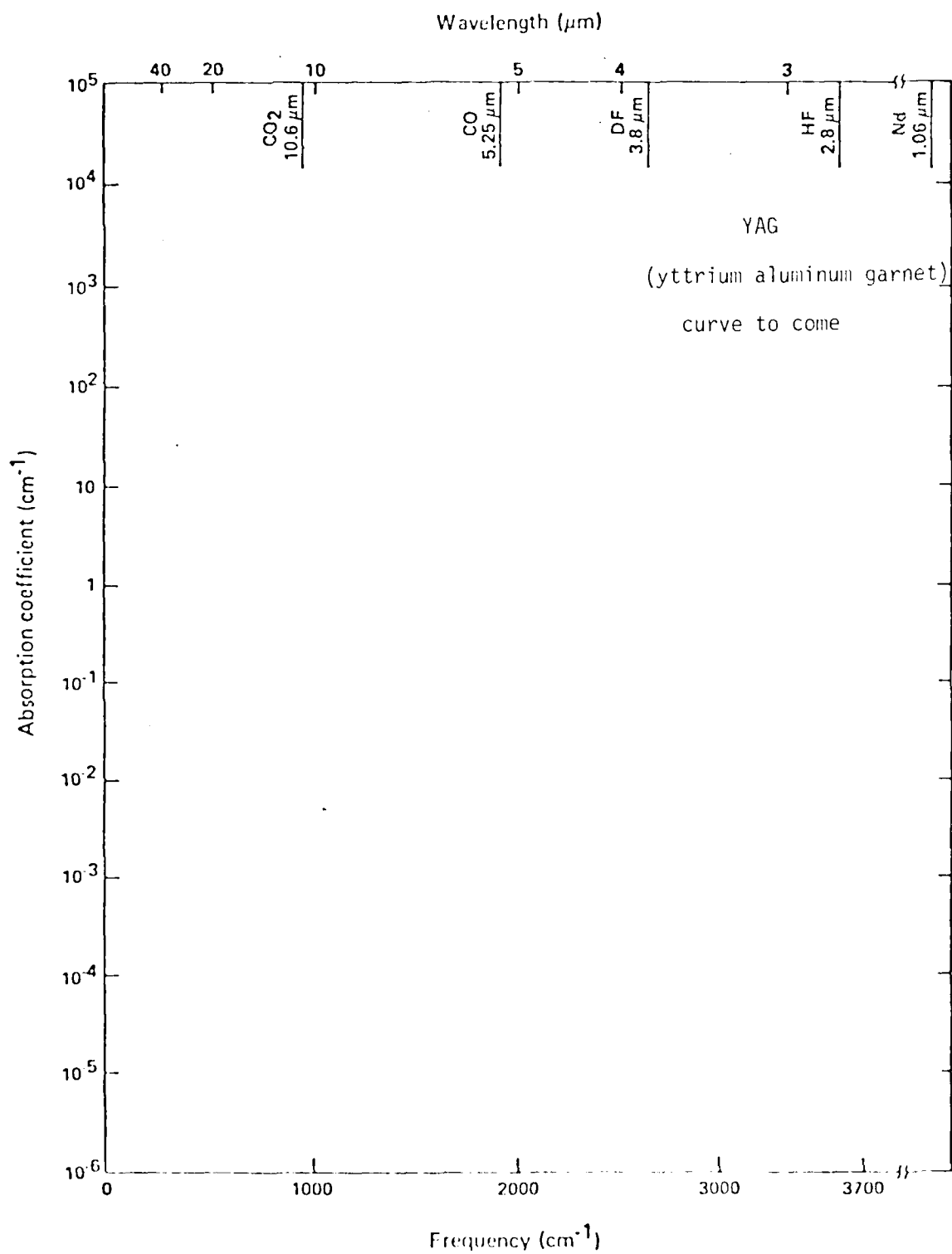


Fig. 48

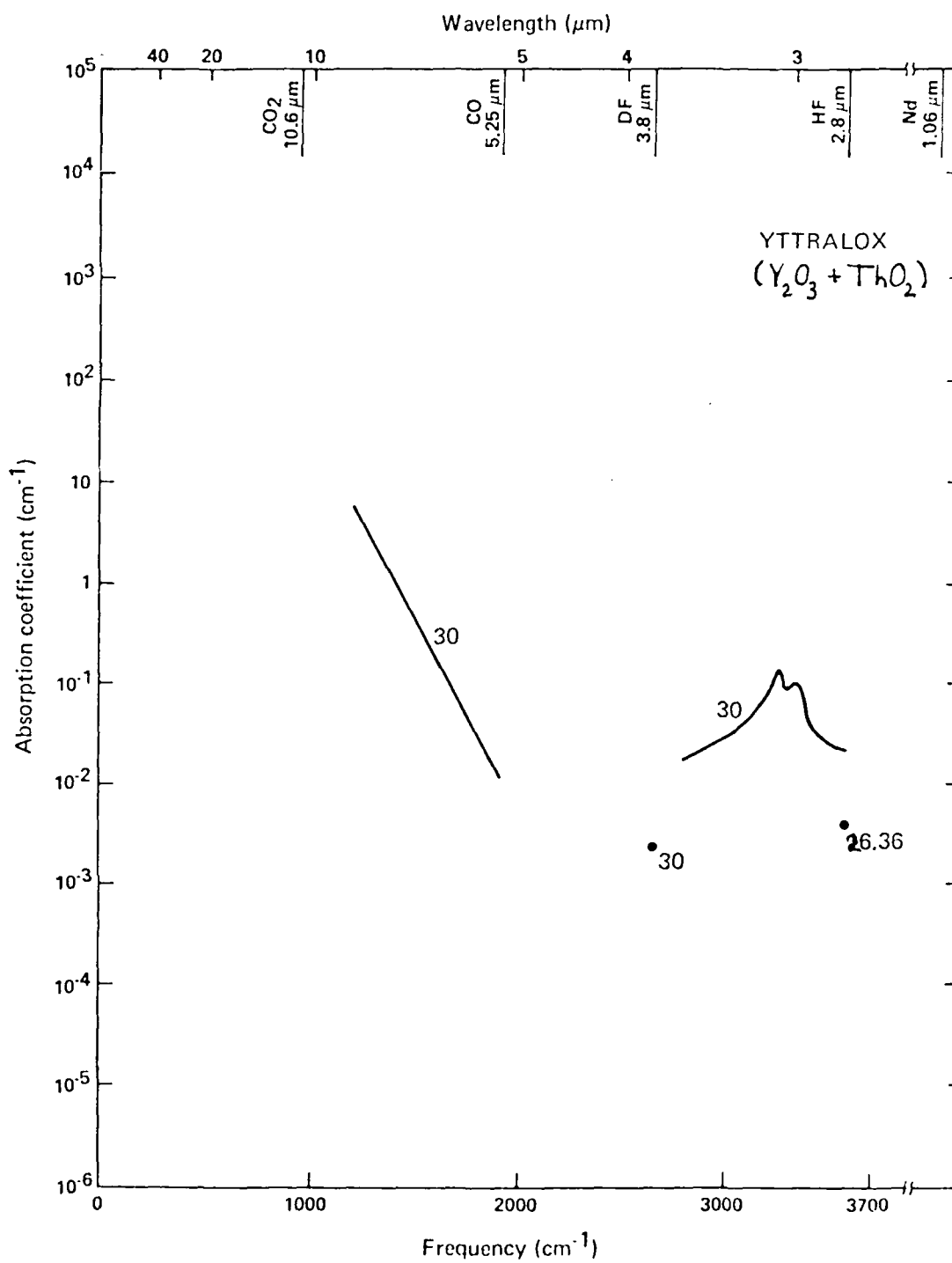


Fig. 49

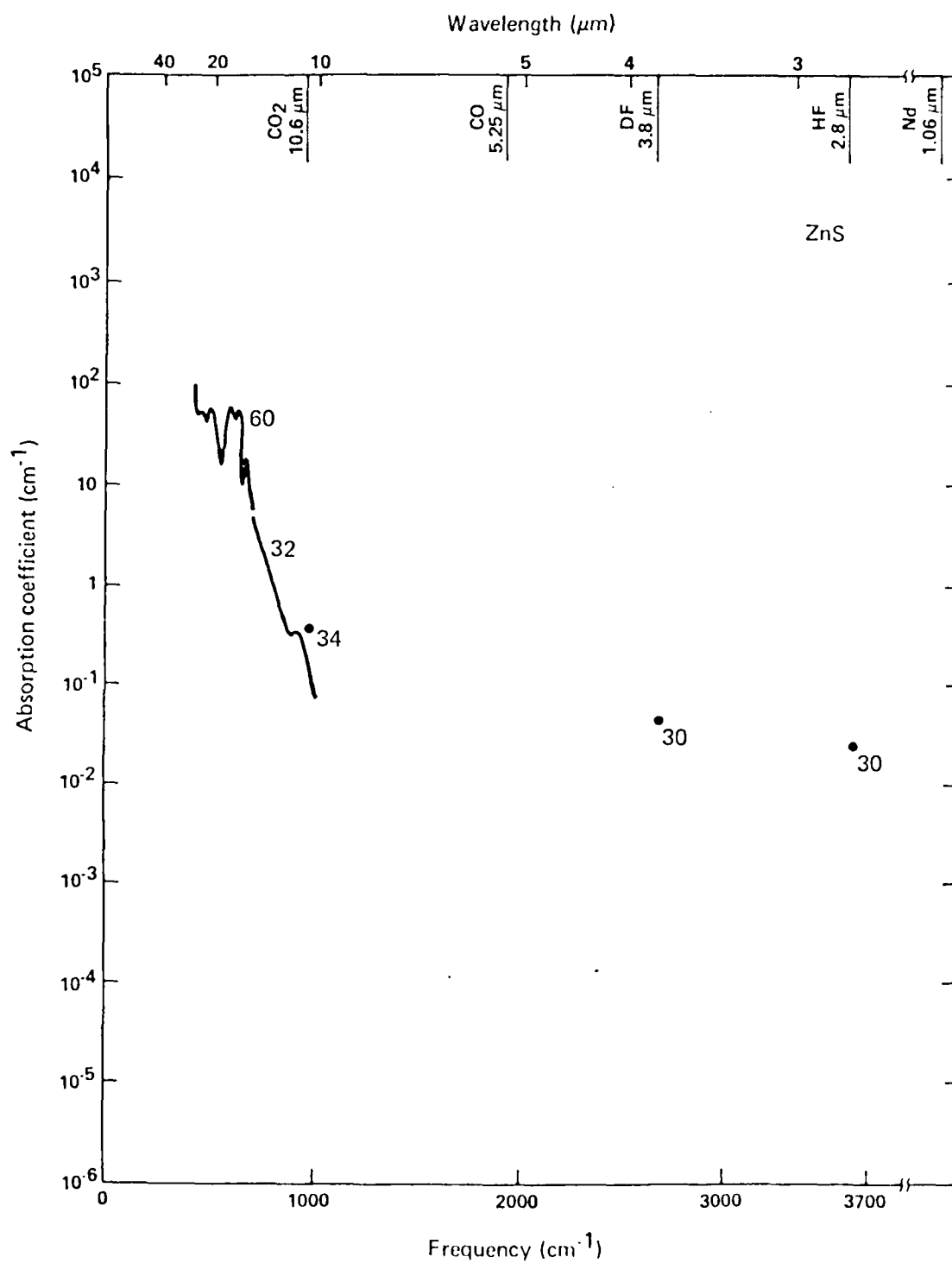


Fig. 50

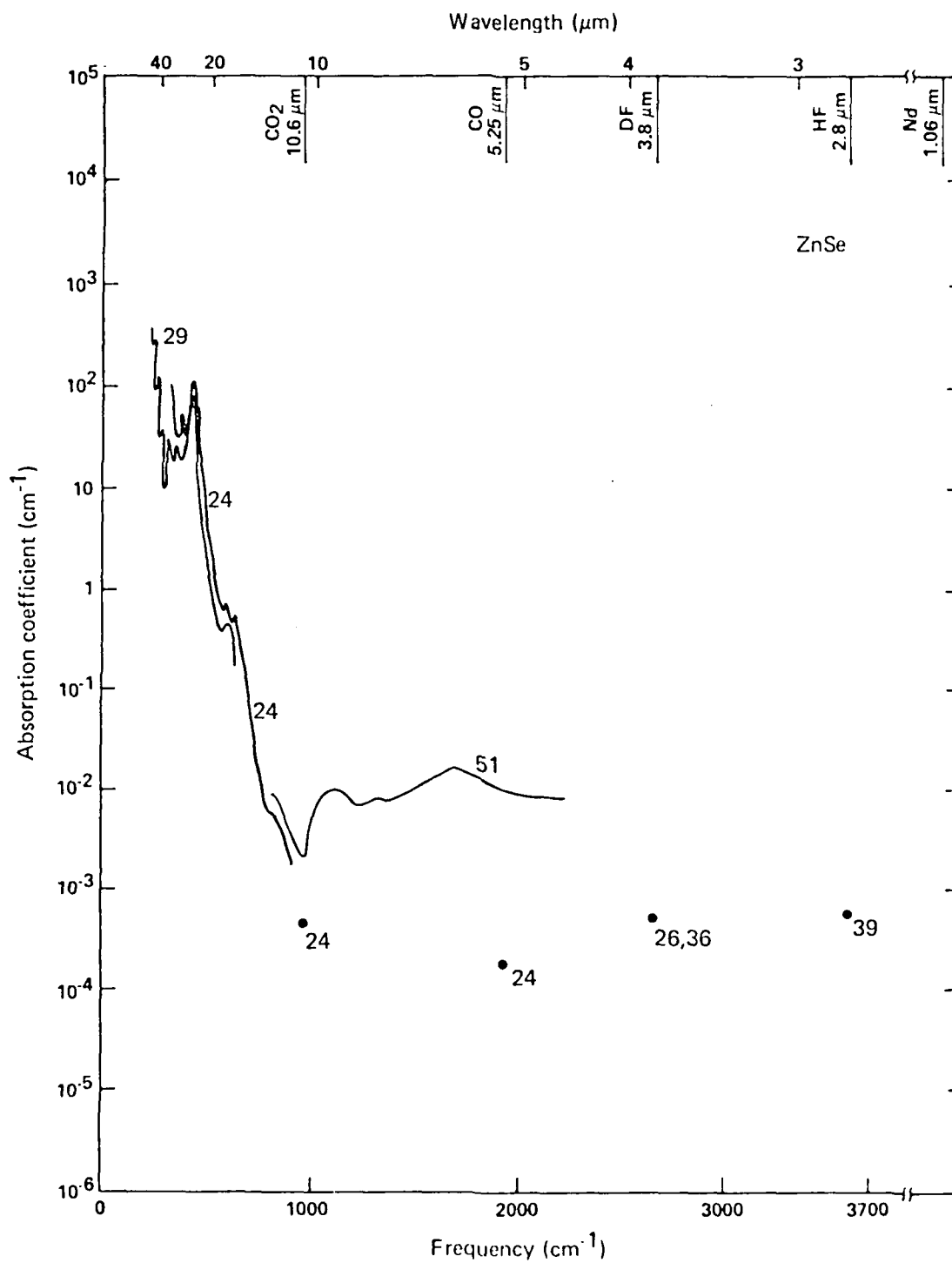


Fig. 51

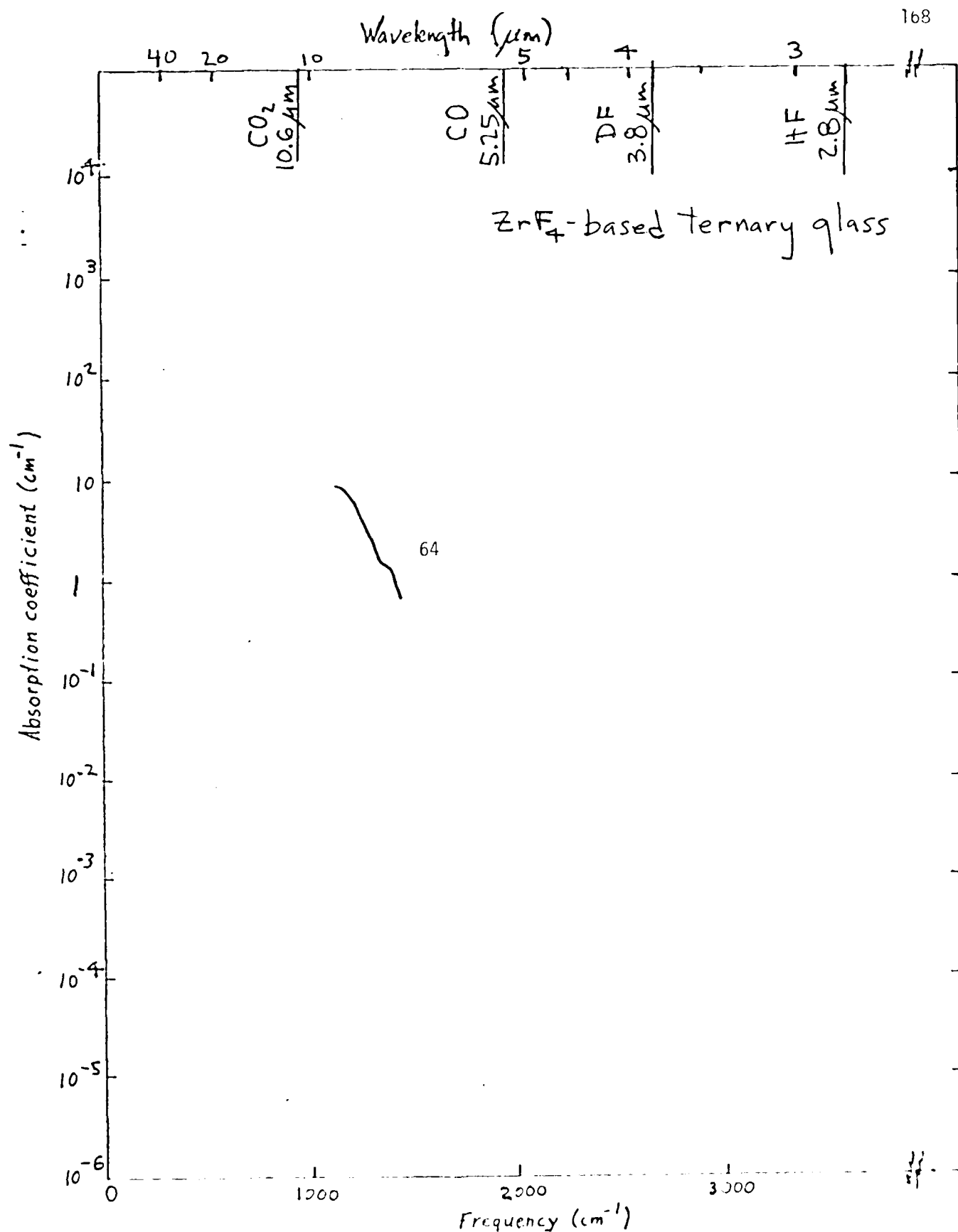


Fig. 52

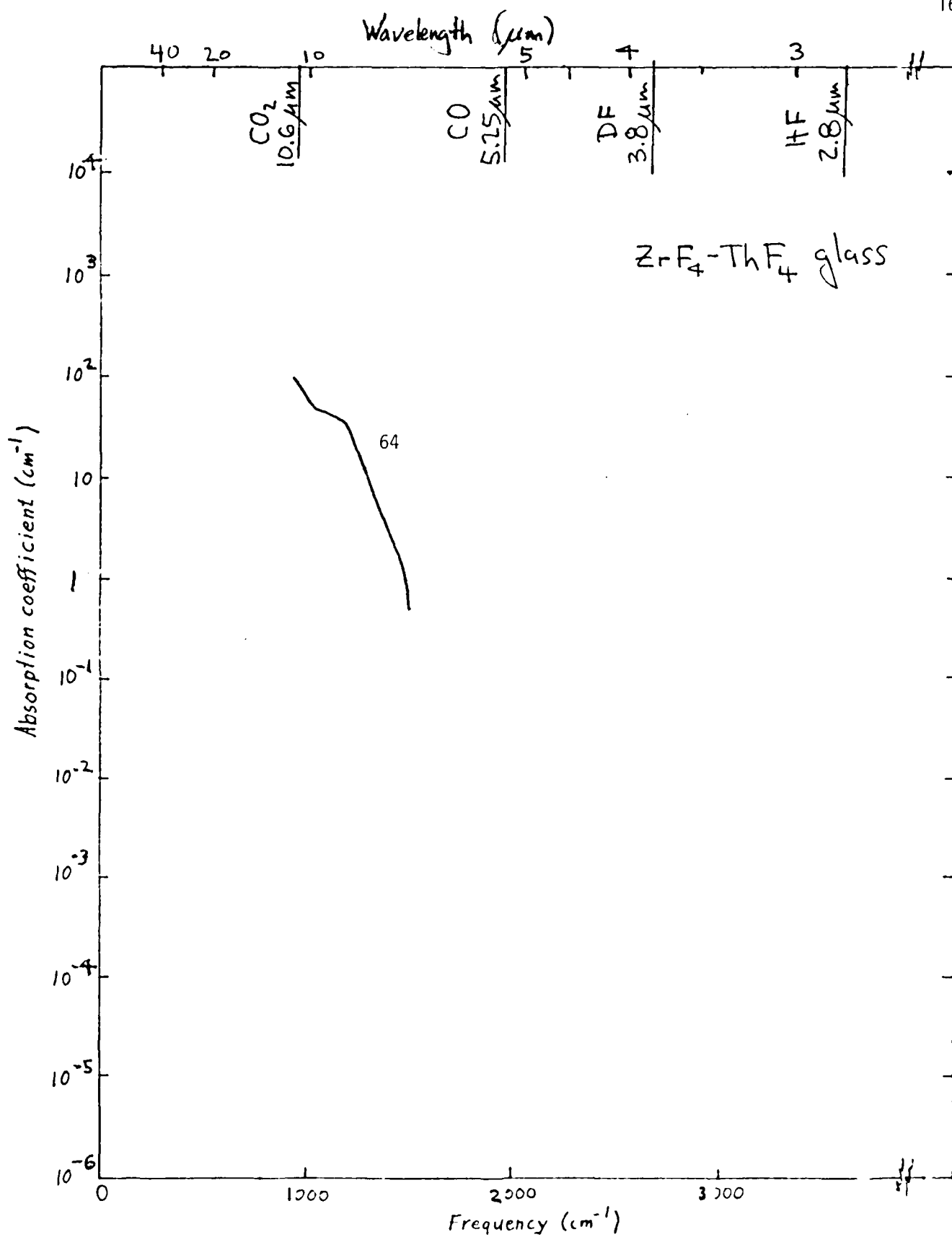


Fig. 53

G. V CURVES OF ABSORPTION AND SCATTERING

Plots of the intrinsic-absorption coefficients and the intrinsic-scattering coefficients have been called V curves. Such curves are useful in displaying the intrinsic limits of the loss in fiber. However, they are likely to be misleading because neither the intrinsic scattering limit nor the intrinsic absorption limit is currently attainable in most cases of current interest. The V curves are more useful in establishing the frequency region in which the intrinsic absorption and scattering will allow operation at a specified loss ($\beta_{ex} = \beta_{ab} + \beta_{sc}$) than in determining the minimum of β_{ex} and the corresponding wavelength. For example, if an extinction coefficient $\beta_{ex} = \beta_{ab} + \beta_{sc} = 10^{-8} \text{ cm}^{-1}$ is required, the useful region--in which $\beta_{ex} \leq 10^{-8} \text{ cm}^{-1}$ --for KI is approximately $1,900 \text{ cm}^{-1} < \omega < 4,800 \text{ cm}^{-1}$ (or $2.1 \mu\text{m} < \lambda < 5.3 \mu\text{m}$), as seen in Fig. 8. It is not necessary to operate at the minimum of the $\beta_{ex}(\omega)$ curve, which occurs near $2,300 \text{ cm}^{-1}$ (or $4.4 \mu\text{m}$) for KI, as seen in Fig. 8. Inaccuracies in extrapolating the absorption curves and in estimating the intrinsic scattering make the operating-region limits quite approximate. With these important reservations, the V curves in Figs. 1 through 8 are presented. The absorption curves, which establish the low-frequency side of the V, are obtained by extrapolating the intrinsic portions of the $\beta_{ab}(\omega)$ curves of Sec. F to high frequencies. The solid portions of the absorption curves are in the region in which the measurements were made, and the dashed portions are extrapolations. A few of the absorptance curves are even more unreliable because they are extrapolations (dotted) of

measured curves (dashed-dotted) that are too short to extrapolate with confidence. The Brillouin-scattering curves, which are all plots of theoretical results, are solid if all the parameters in Eq. (1) below are known and are dashed if any parameters (such as p_{12}) are obtained by formally using values for similar materials.

The Brillouin-scattering curves for the crystalline materials are plots of $\beta_B = \beta_{sc}$, with

$$\beta_B = 8\pi^3 n_r^8 p_{12}^2 k_B T B / 3\lambda^4 \quad (1)$$

where p_{12} is a strain-optic coefficient, k_B is the Boltzman coefficient, and B is the isothermal compressibility.^{1,2} This result is for both the incident- and scattered-radiation polarized along the z axis. In general, $p_{12}B$ is replaced by different combinations of the strain-optic coefficients and elastic constants, depending on the polarizations and measurement geometry. The order of magnitude of the resulting value of β_B does not change in general.

The intrinsic scattering curves for glasses are obtained as follows: The curves for SiO_2 , ZnCl_2 , and BeF_2 are from van Uitert and Wemple.² The curves for As_2S_3 and TI 1173 glass are obtained from Eq. (1) with T replaced by an effective temperature which is approximated by the glass softening temperature, 573 K for As_2S_3 and 643 K for TI 1173 glass. The corresponding values for SiO_2 and ZnCl_2 are 1700 K and 556 K, respectively. Formally replacing the temperature by the effective temperature accounts for the random molecular structure of the glass, which is visualized as phonon-type fluctuations that are frozen into the structure

when the glass solidifies. As an example of the magnitude of the random-molecular-structure scattering, the scattering coefficient for SiO_2 is a factor of $1700/293 = 5.8$ times greater than the Brillouin scattering.

The zero-dispersion crossover wavelengths (at which $d^2n/d\lambda^2 = 0$) are marked on the figures. The values were obtained from the minima of the curves of $dn/d\lambda$ in references 3 and 4. Notice that $d^2n/d\omega^2$ is not zero at the same wavelength at which $d^2n/d\lambda^2 = 0$ in general.

Values of the parameters used in the calculation are listed in Table I. The frequency dependence of the stress-optic coefficients p_{12} are neglected. This is a very good approximation because the scattering is important at short wavelengths, $\lambda \approx 5 \mu\text{m}$ typically, and the wavelength dependence of p_{12} at short wavelengths is quite weak.

REFERENCES FOR SEC. G

1. D. A. Pinnow, T. C. Rich, F. W. Ostermayer, and M. DiDomenic, Jr., Appl. Phys. Lett. 22, 527 (1973).
2. L. G. van Uitert and S. H. Wemple, Appl. Phys. Lett. 33, 57 (1978).
3. W. L. Wolfe and G. J. Zissis, The Infrared Handbook, (Office of Naval Research, Dept. of the Navy, Arlington, VA, 1978).
4. D. E. Gray, American Institute of Physics Handbook, 3rd ed. (McGraw-Hill, 1972).

Table I. Values of parameters used in calculating β_B from Eq. (1).

Material	n (dimensionless)	p_{12} (dimensionless)	ν (dimensionless)	E (10^6 psi)	$B_T^{(5)}$ ($10^{-12} \frac{cm^2}{dyne}$)	$\beta_B(2.8 \mu m)$ ($10^{-10} cm^{-1}$)
SiO ₂	1.45 g	0.281 a	0.376 k(3)	11.0 ℓ	0.981	8.23
As ₂ S ₃	2.41 b	0.272 e	0.3 (2)	2.3 k	7.575	3,470
TI 1173	2.60 c	0.213 a(1)	0.25 k	3.1 ℓ	7.023	3,620
Al ₂ O ₃	1.67 c	0.038 e	0.248 k(3)	50 ℓ	0.439	0.209
BaTiO ₃	2.4 f	0.1 i	0.267 n	23.5 n	0.863	51.7
MgO	1.67 c	-0.04 e	0.232 k(3)	36.1 ℓ	0.646	0.340
Diamond	2.42 b	0.325 e	0.29 g(3)	100 ℓ	0.183	123.7
Ge	4.02 b	-0.130 a	0.273 k(3)	14.9 ℓ	1.326	8,187
Si	3.43 c	0.01 e	0.278 k(3)	19.0 ℓ	1.017	10.6
CdTe	2.69 c	-0.017 d	0.408 k(3)	5.3 ℓ	1.512	1.92
GaAs	3.30 c	-0.140 e	0.311 k(3)	12.3 ℓ	1.344	594
ZnS	2.25 a	-0.01 d	0.385 k(3)	7.73k(4)	1.216	0.128
ZnSe	2.43 a	-0.04 a	0.376 k(3)	10.3 ℓ	1.048	3.27
BaF ₂	1.45 c	0.194 a(1)	0.31 k(3)	7.7 ℓ	2.148	8.59
CaF ₂	1.41 a	0.095 e	0.23 k(3)	11.0 ℓ	2.133	1.64
MgF ₂	1.38 c	0.12 (2)	0.382 k(3)	24.5 ℓ	0.419	0.43
SrF ₂	1.42 a	0.143 a(1)	0.258 k(3)	14.7 ℓ	1.434	2.63
NaF	1.32 b	0.20 d	0.202 k(3)	12.6k(4)	2.060	4.13
LiF	1.39 b	0.130 e	0.272 g(3)	9.3 k	2.133	2.70
NaCl	1.52 c	0.165 e	0.252 j	5.8 ℓ	3.729	15.8
KCl	1.47 a	0.15 a	0.146 k(3)	4.3 ℓ	7.169	19.1
KBr	1.52 b	0.171 e	0.144 k(3)	3.9 ℓ	7.952	36.0
KI	1.67 b	0.169 e	0.138 g(3)	3.7 m	8.518	80.0

REFERENCES FOR TABLE I, SEC. G

- a. A. Feldman, D. Horowitz, R. M. Waxler and M. J. Dodge, Optical Materials Characterizations, Final Technical Report, Feb. 1, 1978-Sept. 30, 1978, NBS Tech. Note 993, U.S. Dept. of Commerce, Nat. Bureau of Standards, Feb. 1979.
- b. M. Sparks, "Optical Distortion by Heated Windows in High-Power Laser Systems," J. Appl. Phys. 42, 5029 (1971).
- c. M. Sparks and C. J. Duthler, Theoretical Studies of High-Power Infrared Window Materials, Xonics Inc., Second Technical Report, Contract No. DAHC15-73-C-0127, Dec. 6, 1973.
- d. Landolt-Bornstein, Numerical Data and Functional Relationships in Science and Technology, New Series, Group III: Crystal and Solid State Physics, Vol. 11, ed. K. H. Hellnege, Springer-Verlag, Berlin, 1979.
- e. Landolt-Bornstein, Numerical Data and Functional Relationships in Science and Technology, New Series, Group III: Crystal and Solid State Physics, Vol. 2, ed. K. H. Hellnege, Springer-Verlag, Berlin 1969.
- f. CRC Handbook of Chemistry and Physics, 59th ed., ed. R. C. Weast, CRC Press, Inc. 1978.
- g. American Institute of Physics Handbook, 3rd ed., McGraw-Hill, 1972.
- h. L. G. van Uitert and S. W. Wemple, Appl. Phys. Lett. 33, 57 (1978).
- i. Bill Fredricks, private communication.
- j. S. K. Dickinson, Infrared Laser Window Materials Property Data for ZnSe, KCl, NaCl, CaF₂, SrF₂, BaF₂, Air Force Cambridge Research

Laboratories, Physical Sciences Research Papers, No. 635, AFCRL-TR-75-0318, 6 June 1975.

- k. C. S. Sahagian and C. A. Pitha, Compendium on High Power Infrared Laser Window Materials (LQ-10 Program) Air Force Cambridge Research Laboratories, Special Report No. 135, AFCRL-72-0170, 9 March 1972.
- l. M. Sparks and C. J. Duthler, Theoretical Studies of High-Power Infrared Window Materials, Xonics Inc., Second Technical Report, Contract No. DAHC15-73-C-0127, 6 December 1973.
- m. From unpublished information kindly supplied by the Harshaw Chemical Company.
- n. The Infrared Handbook, ed. W. L. Wolfe and G. J. Zissis, Office of Naval Research Institute of Michigan, Washington DC, 1978.

Notes:

- (1) Value of P_{12} calculated from q_{11} and q_{12} .
- (2) Value estimated from related materials.
- (3) Value of ν calculated from $\nu = C_{12}/(C_{11} + C_{12})$.
- (4) Value of E calculated from $E = (C_{11} + 2C_{12})(C_{11} - C_{12})/(C_{11} + C_{12})$.
- (5) Value of B_T calculated from $B_T = 3(1 - 2\nu)/E$.

FIGURE CAPTIONS FOR SEC. G

Fig. 1. Extrapolated intrinsic absorption coefficient and intrinsic, random-molecular-structure scattering coefficient for the glasses ZnCl_2 , SiO_2 , and BeF_2 . In this- and the following-figures, the solid portions of the absorption curves are in the region in which the measurements were made, and the dashed portions are extrapolations. Dotted absorption curves are extrapolations of measured curves (dash-dotted) that are too short to extrapolate with confidence. The theoretical Brillouin-scattering curves are solid if all parameters are known and are dashed if any parameters are obtained by formally using values for similar materials.

Fig. 2. Extrapolated intrinsic absorption coefficient and intrinsic, random-molecular-structure scattering coefficient for the glasses As_2S_3 and TI 1173. See the caption of Fig. 1 for the meaning of the various lines.

Fig. 3. Extrapolated intrinsic absorption coefficient and intrinsic Brillouin scattering coefficient for the crystals Al_2O_3 , MgO , and BaTiO_3 . See the caption of Fig. 1 for the meanings of the various lines.

Fig. 4. Extrapolated intrinsic absorption coefficient and intrinsic Brillouin scattering coefficient for the crystals Ge and Si . See the caption of Fig. 1 for the meanings of the various lines.

Fig. 5. Extrapolated intrinsic absorption coefficient and intrinsic Brillouin scattering coefficient for the crystals CdTe , GaAs , ZnS , and ZnSe . See the caption of Fig. 1 for the meanings of the various lines.

Fig. 6. Extrapolated intrinsic absorption coefficient and intrinsic Brillouin scattering coefficient for the crystals BaF_2 , CaF_2 , MgF_2 and SrF_2 . See the caption of Fig. 1 for the meanings of the various lines.

Fig. 7. Extrapolated intrinsic absorption coefficient and intrinsic Brillouin scattering coefficient for the crystals NaF , LiF , and NaCl . See the caption of Fig. 1 for the meanings of the various lines.

Fig. 8. Extrapolated intrinsic absorption coefficient and intrinsic Brillouin scattering coefficient for the crystals KCl , KBr , and KI . See the caption of Fig. 1 for the meanings of the various lines.

H. EXTRINSIC ABSORPTION

In this section it is shown that only very small trace amounts of either absorbing impurities (as low as 10^{-4} parts per billion) or macroscopic inclusion (as low as 10^{-3} parts per billion) can give rise to the typical goal value of $\beta_{\text{ex}} = 10^{-2}$ dB/km. Tabulations of molecular-ion absorption information given in Table I and Figs. 1 through 4 and of visible- and ultraviolet-absorption spectra should be useful in identifying troublesome impurities.

The concentration of absorbing impurities must be kept at extremely low values in order to attain even the typical goal value of $\beta_{\text{ex}} = 10^{-2}$ dB/km. In recent high-power-window investigations, research programs were required for most materials to reduce the absorption coefficient to $\beta_{\text{ab}} = 10^{-4}$ cm $^{-1}$. Calorimetric-measurement techniques had to be developed in order to measure values of β_{ab} less than approximately 10^{-2} cm $^{-1}$. Apart from reducing the absorptance, even the measurements of values of the absorption coefficient less than 10^{-4} cm $^{-1}$ has been difficult. These results put the typical goal value of $\beta_{\text{ab}} = 10^{-2}$ dB/km = 2.3×10^{-8} cm $^{-1}$ in perspective.

Molecular-ions are believed to be a major source of extrinsic infrared absorption, as shown by Duthler.¹ Deutch² showed that molecules on surfaces of windows gave rise to absorption at the level of absorptance $A = 10^{-3}$ to 10^{-4} . Spectroscopists have measured the absorption spectra of molecules for years by doping them into alkali halide crystals.¹ These studies provide a wealth of information on absorption by the molecular-ion impurities. Duthler¹ and Flannery and Sparks³ tabulated such information that related to

impurity absorption. The results of Flannery and Sparks³ are repeated here in Figs. 1 through 4 and Table I for the convenience of the user.

Nominally pure commercial crystals are commonly observed to contain molecular-anion impurities, such as the metaborate ion (BO_2^-)^{4,5} and the carbonate ion (CO_3^{2-})³, using conventional absorption spectroscopy. The hydroxyl ion (OH^-) is especially difficult to remove from alkali halides during purification⁶, and may be the ion limiting absorption at $2.7 \mu\text{m}$. These anion impurities along with divalent metal cation impurities^{6,7} are most likely still present in small concentrations in specially purified materials because concentration at the parts per billion level can give rise to the presently common extrinsic values of $\beta_{\text{ab}} \approx 10^{-4} \text{ cm}^{-1}$.

The severity of the problem of the limit on the loss β_{ex} by trace amounts of molecular ions can be seen from the results of Duthler¹ and of Flannery and Sparks.³ Scaling the result that parts per billion can give rise to $\beta_{\text{ab}} \approx 10^{-4} \text{ cm}^{-1}$ to the typical goal of $\beta_{\text{ex}} = 10^{-2} \text{ dB/km} = 2.3 \times 10^{-8} \text{ cm}^{-1}$ shows that 10^{-4} parts per billion of absorbing impurities can give rise to 10^{-2} dB/km .

This result can also be seen directly from the following general argument. From the typical value of $\beta_{\text{ab}} = 10^5 \text{ cm}^{-1}$ at Reststrahlen absorption peaks in solids, with typical densities of $N_{\text{sol}} = 10^{22}$ ions per cm^3 , a typical infrared absorption cross section of a strong absorber at resonance is

$$\sigma_{\text{ab}} = \beta_{\text{ab}}/N_{\text{sol}} = 10^5 \text{ cm}^{-1}/10^{22} \text{ cm}^{-3} = 10^{-17} \text{ cm}^2. \quad (1)$$

The corresponding concentration N required to give rise to $\beta_{\text{ab}} = 10^{-2} \text{ dB/km} \approx 2 \times 10^{-8} \text{ cm}^{-1}$ is

$$\begin{aligned} N &= \beta_{\text{ab}}/\sigma_{\text{ab}} = 2 \times 10^{-8} \text{ cm}^{-1}/10^{-17} \text{ cm}^2 \\ &= 2 \times 10^9 \text{ cm}^{-3} \end{aligned} \quad (2)$$

For $\sim 10^{22}$ ions/cm³ in solids, the impurity density $N = 2 \times 10^9$ cm⁻³ corresponds to the concentration $2 \times 10^9 / 10^{22} = 2 \times 10^{13} = 2 \times 10^{-4}$ parts per billion. Even the measurement of such low concentrations of important impurities is impossible at present.

- > Another source of extrinsic absorption is macroscopic inclusions.^{8,9} Platinum particles in laser glass is a well known example. Other examples include nonstoichiometric regions in crystals, contaminated grain boundaries or dislocations, and clusters of impurities. Sparks and Duthler⁹ showed that fractional volumes as low as 10^{-8} can give rise to an absorption coefficient of $\beta_{ab} = 10^{-4}$ cm⁻¹. Formally scaling linearly gives a fractional volume of $2 \times 10^{-12} = 2 \times 10^{-3}$ parts per billion for $\beta_{ab} = 10^{-2}$ dB/km $= 2 \times 10^{-8}$ cm⁻¹.

REFERENCES FOR SEC. H

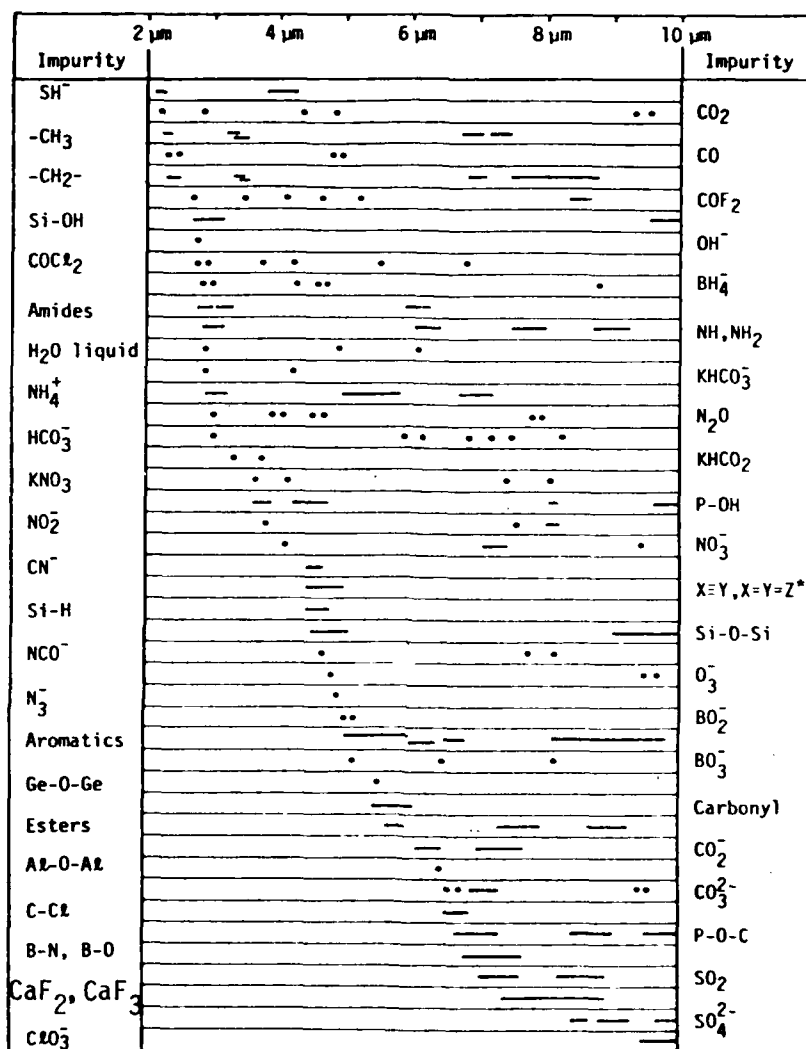
1. C. J. Duthler, "Extrinsic Absorption in 10.6 μm Laser Window Materials Due to Molecular-Ion Impurities," J. Appl. Phys. 45, 2668 (1974); "Impurity Absorption in Halide Window Materials," 4th ARPA Conference on Infrared Laser Window Materials, Tucson, AZ, Nov. 18-20, 1974.
2. T. F. Deutch, J. Phys. Chem. Solids 34, 2091 (1973).
3. M. Flannery and M. Sparks, "Extrinsic Absorption in Infrared Laser-Window Materials," NBS Spec. Publ. 509, 9th NBS-ASTM-ONR-ERDA-DARPA Symposium on Laser Induced Damage in Optical Metals, Boulder, CO, Oct. 4, 1977.
4. H. W. Morgan and P. A. Staats, J. Appl. Phys. 33, 364 (1962).
5. J. C. Decius, J. L. Jacobson, W. F. Sherman, and G. R. Wilkinson, J. Chem. Phys. 43, 2180 (1965).
6. R. C. Pastor and M. Braunstein, Hughes Research Laboratories Technical Report No. AFWL-TR-72-152, Vol. II, 1973 (unpublished).
7. T. L. Maksimova, Phys. Status Solidi 33, 547 (1969).
8. R. W. Hopper and D. R. Uhlmann, J. Appl. Phys. 41, 4023 (1970).
9. M. Sparks and C. J. Duthler, J. Appl. Phys. 44, 3038 (1973).

Table 1. Experimentally observed absorption frequencies of some impurity ions isolated in KCl crystals with the estimated impurity concentration to produce $\beta = 10^{-4} \text{ cm}^{-1}$ at the HF, DF, CO, and CO₂ laser frequencies at 300 K. Estimated concentrations in square brackets are more than ten full line widths from any impurity absorption line.

ION	FREQUENCIES (cm^{-1})	$\nu = 3704 \text{ cm}^{-1}$ $\lambda = 2.7 \mu\text{m}$	$\nu = 2632 \text{ cm}^{-1}$ $\lambda = 3.8 \mu\text{m}$	$\nu = 1905 \text{ cm}^{-1}$ $\lambda = 5.25 \mu\text{m}$	$\nu = 943 \text{ cm}^{-1}$ $\lambda = 10.6 \mu\text{m}$
H ⁺	500	[40]	[20]	[10]	[1]
OH ⁻	3610, 3640	0.03	[5]	[20]	[40]
SH ⁻ ^a	2578, 2590	[5]	0.01	[3]	[10]
CN ⁻	2089, 4151	> 100	[20]	2	[80]
BO ₂ ⁻ ^a	590, 1964, 1972	> 100	[70]	0.5	[70]
CO ₂ ⁻ ^a	1676	> 100	[30]	[2]	[20]
H ₃ ⁺	442, 2049	> 100	[40]	3	> 100
HCO ⁺ ^a	631, 1211, 1297, 2182, 2403, 2499, 2613, 3373, 3459	1	0.03	[5]	[10]
NO ₂ ⁻	806, 1287, 1327, 2580	[20]	0.5	[1]	0.3
NO ₃ ⁻	843, 1062, 1396, 7446, 2789	[10]	0.5	[3]	0.3
CO ₃ ²⁻ ^b	680-720, 883, 886, 1058, 1264, 1378, 1416, 1488, 1518	> 100	[80]	[10]	5
BO ₃ ³⁻ ^a	736, 949, 1222, 1247, 1944	[3]	[1]	0.1	0.01
SeO ₃ ²⁻	~ 780, ~ 850	> 100	[100]	[30]	0.3
AsO ₃ ⁻	589, 672, 713, 840, 971, 1218, 1346, 1701, 3339	[5]	[5]	0.5	0.1
Br ₄ ⁻ ^a	1142, 2256, 2321, 2425	[5]	0.3	[0.3]	0.3
SO ₄ ²⁻ ^a	978, 1083, 1149, 1186	> 100	[90]	[20]	0.01
CrO ₄ ²⁻ ^b	862, 890, 930, 941	> 100	> 100	> 100	0.05
SeO ₄ ²⁻ ^b	834, 861, 904, 924	> 100	> 100	> 100	0.3
ReO ₄ ²⁻ ^b	899, 909, 914, 925	> 100	[80]	[30]	0.02
ClO ₃ ⁻	640, 940, 970	[10]	[5]	[1]	0.001
Br ₄ ⁻	1405, 3100	[0.1]	0.05	0.3	[1]

a. Intensity for the most intense band assumed to be $\beta = 10 \text{ cm}^{-1}$ for 100 ppm of impurity.

b. Exact frequencies and intensities very dependent on compensating Mg^{2+} ion.



*X, Y = C, N; Z = C, N, O, S; X≡Y means C≡C, C≡N, etc.

Figure 1. Correlation chart showing the absorption lines between 2 and 10 μm of some chemical bonds, molecular ions, radicals, and compounds.
Key: • peak positions; — range of peak positions in various materials.

Figure 2. Correlation chart showing the absorption lines between 0.5 and 15 μm of some chemical bonds, molecular ions, radicals, and compounds.

• peak positions

— range of peak positions in various materials

Absorption strength:

S strong

M medium

W weak

V variable

Absorption line width:

B broad

Sh sharp

Numbers associated with an absorption band indicate the number of peaks occurring within that band.

If several designations apply to one peak, they are separated by commas.

If a designation applies to two adjacent peaks, it may be written between them.

aliph. = aliphatic

arom. = aromatic

Me = metal atom.

Impurity	1	2	3	4	5	6	7	8	9	10	11	12	13	14
Phenols	• •	—	S, 1-2	—	Bonded (B)			M	S					
Alcohols	• •	—	Monomer (Sh) M, S	—	Dimer (B)		—	W		S	—	Unbonded		
Tertiary alcohols	• •	—	M, S, B	• • •				M	S					
Secondary alcohols	• •	—	M, S, B	• • •				M		M				
-CH ₃	• • • •	—	S				S	M						
-CH ₂	• • • •	—	S				S	W	—	CH ₂ chains	—	M		
Aromatic C-H	• •	—	W-M											
Allene: >C=C=CH ₂	• •	—			S, 1-2									
>C=CH ₂	• •	—	M, 1-2			M	V	S		S	S			
Amines: NH, NH ₂	•	1-2	1-2			M		S	M			M, B		
-C≡C-H	• •		Sh		M			M, B						S, B
Epoxides, oxiranes	• • •	—						S				M		

Impurity	Wavelength (μm)													
	1	2	3	4	5	6	7	8	9	10	11	12	13	14
$\equiv\text{CN}$...		<u>M</u>				<u>W</u>							
$-\text{C}\equiv\text{N}$	-	-												
H_2O (liquid)	..		<u>S, B</u>		<u>M, B</u>	<u>S, B</u>							<u>S, B</u>	
Imides: $-\text{CO}-\text{NH}-\text{CO}-$..		-		<u>S</u>	.								-
$-\text{HC}=\text{CH}-$..		<u>M</u>			<u>V</u>	<u>M</u>		<u>S</u>					<u>M</u>
$>\text{P}-\text{H}$	-			<u>M</u>										
$>\text{C}=\text{O}$.				<u>S</u>									
Aromatic aldehydes		<u>S</u>		<u>M</u>				<u>M</u>			
Aliphatic aldehydes		<u>S</u>		<u>M</u>		<u>M</u>		<u>M</u>			
SH^-	-		<u>W</u>									<u>W</u>		
CO_2		<u>W</u>	<u>S</u>		<u>S</u>	<u>W</u>				<u>W</u>	<u>W</u>		<u>M</u>	
CO		<u>W</u>			<u>S</u>									

Impurity	Wavelength (μm)													
	1	2	3	4	5	6	7	8	9	10	11	12	13	14
$-\text{C}\equiv\text{N}$.		<u>S</u>									
$-\text{F}-\text{H}$			-											
COF_2			.	.	.	<u>S</u>			<u>S</u>					
Benzene			<u>W</u>	<u>S</u>	<u>M</u>		<u>S</u>	<u>W</u>	<u>M</u>	<u>W</u>	<u>M</u>	.	<u>S</u>	
C_3O_2									
$\text{Si}-\text{OH}$										<u>W</u>		<u>S</u>		
SD^-			<u>W</u>		<u>M</u>									
OH^-			.											
COCl_2			<u>S</u>	<u>W</u>							<u>S</u>
Acetone			<u>W</u>	<u>M</u>	<u>W</u>	<u>S</u>	<u>S</u>	<u>S</u>	<u>M</u>		<u>W</u>		<u>W</u>	
BH_4^-			<u>W</u>		<u>S, B</u>				<u>S, B</u>					
Amides: $-\text{CO}-\text{NH}_2$			<u>M</u>			<u>S</u>	<u>M</u>							




Impurity	Wavelength (μm)													
	1	2	3	4	5	6	7	8	9	10	11	12	13	14
KHCO_3			.	.										
SO_2NH_2			<u>M</u>			<u>M</u>								
Amides: $-\text{CO}-\text{NH}-$			<u>M</u> <u>W</u>			<u>S</u> <u>M</u>								
HCO^-			<u>W</u>		<u>S</u>			<u>S</u>						
n-butyl alcohol			<u>S</u> , <u>B</u> <u>S</u>				<u>M</u>	<u>W</u>	<u>M</u> <u>S</u> <u>M</u>			<u>W</u>		<u>M</u> , <u>B</u>
NH_4^+			<u>S</u>		<u>W</u>		<u>S</u>							
Formamide			<u>S</u> , <u>B</u> <u>M</u> <u>W</u>			<u>S</u> , <u>B</u>		<u>S</u> , <u>B</u>	<u>M</u>				<u>M</u> , <u>B</u>	<u>S</u> , <u>B</u>
N_2O			<u>W</u>	<u>M</u> <u>S</u>				<u>S</u>						
HCO_3^-			<u>B</u>			<u>B</u>	<u>B</u>							
NH_3^+ salt			<u>S</u>		<u>W</u>		<u>M</u>							
K_2CO_3			.	.										
P-NH ₂			<u>M</u>			<u>M</u>			<u>M</u>					

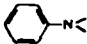


Impurity	Wavelength (μm)													
	1	2	3	4	5	6	7	8	9	10	11	12	13	14
Lactams: $-\text{CO}-\text{NH}-$			<u>M</u> <u>W</u>			<u>S</u>								
Isopropyl: $(\text{CH}_3)_2\text{CH}-$			<u>M</u> <u>W</u>				<u>S</u> <u>M</u> <u>W</u>	<u>M</u>		<u>W</u>				
Carboxylic acid dimer			<u>S</u> <u>M</u>			<u>S</u>	<u>M</u>	<u>S</u>			<u>M</u> , <u>B</u>			
Ethyl: CH_3CH_2-			<u>S</u> <u>M</u>				<u>S</u> <u>M</u>		<u>M</u>	<u>W</u>		<u>M</u>		
Ethyl ether			<u>S</u>	<u>W</u> <u>W</u>			<u>M</u> <u>S</u> <u>M</u>	<u>S</u> <u>S</u> <u>M</u>	<u>W</u>	<u>M</u>				
Toluol			<u>S</u> <u>W</u>		<u>M</u>	<u>S</u> <u>M</u>	<u>M</u>	<u>S</u>		<u>M</u>				<u>S</u>
$(-\text{O}-\text{Si}(\text{CH}_3)_2-\text{O}-\text{Si}(\text{CH}_3)_2-)_n$			<u>M</u> <u>W</u>				<u>W</u> <u>S</u>		<u>S</u> , <u>B</u>		<u>M</u>	<u>S</u>		<u>W</u>
KHCO_2			.	.										
Tetrahydrofuran			<u>S</u> <u>W</u>	<u>W</u>			<u>M</u> <u>W</u> <u>M</u>	<u>S</u> <u>M</u>	<u>S</u>					
HCCl_3			<u>M</u> <u>W</u>				<u>W</u>	<u>S</u>	<u>W</u>	<u>W</u>		<u>S</u> , <u>B</u>		<u>M</u>
NH_2^+ salt			<u>S</u>			<u>M</u>								
NO_3^-			<u>W</u>				<u>S</u>					<u>M</u>		

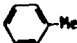

Impurity	Wavelength (μm)													
	1	2	3	4	5	6	7	8	9	10	11	12	13	14
KNO ₃				.	.		S, B					M		W
P-OH				S, B				W		S				
NH ⁺ salt				S										
NO ₂ ⁻				.			.	S				.		
KNO ₂				.			.	S, B				W		
C-D, CD ₂				M					S				M	M
PH ₂				M					M					
-C≡C-				W										
X≡Y, X=Y-Z X, Y = C, N; Z = C, N, O, S				S										
Si-H				V, S										
Si-O-Si				W					S					
B--H--B bridge														

Impurity	Wavelength (μm)													
	1	2	3	4	5	6	7	8	9	10	11	12	13	14
Diborane: B ⁺ -H ⁻ :B					M	W	M	S						
Ge-H														
O ₃ ⁻					W				S					W
N ₃ ⁻					.									
BO ₂ ⁻														
Mo(CO) ₆					S, B				W		W		W	
Aromatic rings					W, 2-7	M			W, 2-6				S-W, 2-3	
BO ₃ ³⁻				
Sn-H														
Thiol esters					S				S		S			
Cyclic anhydrides					S			S						
Anhydrides: -CO-O-CO-					S				S					

Impurity	Wavelength (μm)													
	1	2	3	4	5	6	7	8	9	10	11	12	13	14
Ge-O-Ge						.						_____		
$\text{AlH}_3, \text{AlH}_4$						—								
$>\text{C}=\text{CF}_2$						S								
Esters: $-\text{CO}-\text{O}-$						S			S					
Diene esters: $-\text{CO}-\text{O}-$						S		S						
Aromatic esters: $-\text{CO}-\text{O}-$						S		S						
Ketones						S	arom.	M						
Nitrites: $-\text{O}-\text{NO}$						S							S	
$\text{C}=\text{C}$						S, V								
$\text{C}=\text{N}, \text{N}=\text{N}$						V								
FHF^-						S, B								
Nitrates: $-\text{O}-\text{NO}_2$							S					S		

Impurity	Wavelength (μm)													
	1	2	3	4	5	6	7	8	9	10	11	12	13	14
Carboxyl salt: $-\text{CO}_2^-$						S	M							
CO_2^-						S								
Furans: 						—	—	—						
Triazine ring: 						S, 1-2						M-W		
Nitro-: NO_2						S	M							
Nitroso-: $-\text{N}=\text{N}=\text{O}$						—								
$\text{Al}-\text{O}$.								
Thiophenes: 						—	—	—						
CO_3^{2-}						S					1-2			
Azoxy: $-\text{N}=\text{NO}-$						—	—							
$\text{C}-\text{Cl}$													S	
$\text{P}-\text{O}-\text{C}$						M, 1-4	M, 1-3	S				M, V		

Impurity	Wavelength (μm)													
	1	2	3	4	5	6	7	8	9	10	11	12	13	14
B-N, B-O							—							
SO ₂							—	S	—					
Aromatic amines: 							—	S	—					
CF ₃							—	S	—					
Cyclic P=N							—	S	—					
Aromatic ethers							—	S	—		M			
Inorganic PO ₂ ⁻ salts							—	S	—					
P=O							—	S	—					
CF ₂							—	S	—					
P-O 							—	S	—		S	—		
S=O							—	S	—					
Pyridine ring: 							—	S	—				S,2	

Impurity	Wavelength (μm)													
	1	2	3	4	5	6	7	8	9	10	11	12	13	14
C-S									<u>V, S</u>					
SO ₄ ²⁻									<u>S V, S</u>	<u>W</u>		<u>S</u>		<u>M</u>
Organic PO ₂ ⁻ salts									<u>S</u>					
Aliphatic ethers									<u>S</u>					
 Me									—					
PO ₄ ³⁻									<u>S, B</u>					<u>S, B</u>
Me-O									—					
PO ₃ ²⁻ salts									<u>S</u>	<u>M</u>				
NF ₃									<u>W S W</u>	<u>S, B</u>				
CaO ₃ ⁻									<u>S, B</u>	<u>S</u>				<u>S, B</u>
Pyrimidine ring: 									<u>S</u>			<u>S</u>		
P-F												<u>S</u>		

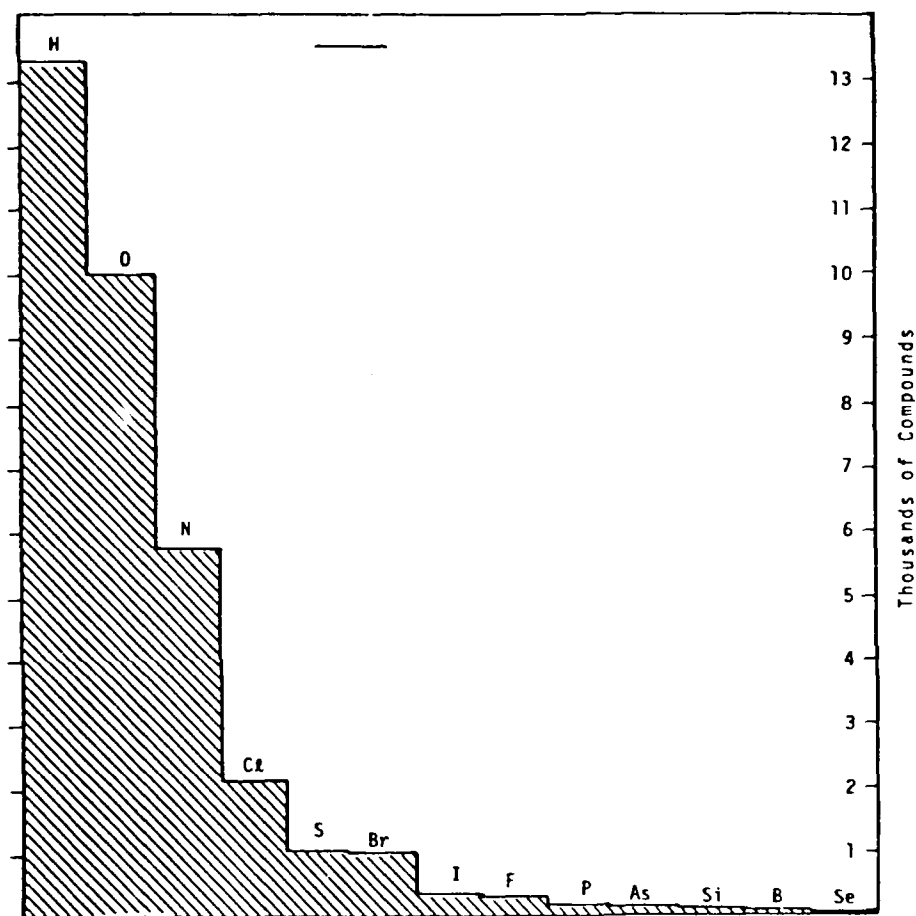


Figure 3. Occurrence frequency of elements in 13,520 organic compounds.
A small number of compounds also contained Na, K, Mg, Sb, Cr, and D.

AD-A092 264

SCIENTIFIC RESEARCH CENTER SANTA MONICA CA
THEORETICAL STUDIES OF LOW-LOSS OPTICAL FIBERS. (U)
SEP 80 M SPARKS, W FREDERICKS, D MILLS

F/6 20/6

N00173-79-C-0361

UNCLASSIFIED

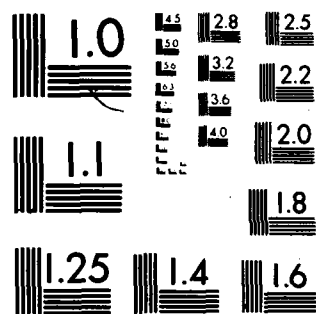
NL

313

4/8/80



END
DATE
FILMED
1-81
DTIC



MICROCOPY RESOLUTION TEST CHART
NATIONAL BUREAU OF STANDARDS-1963-A

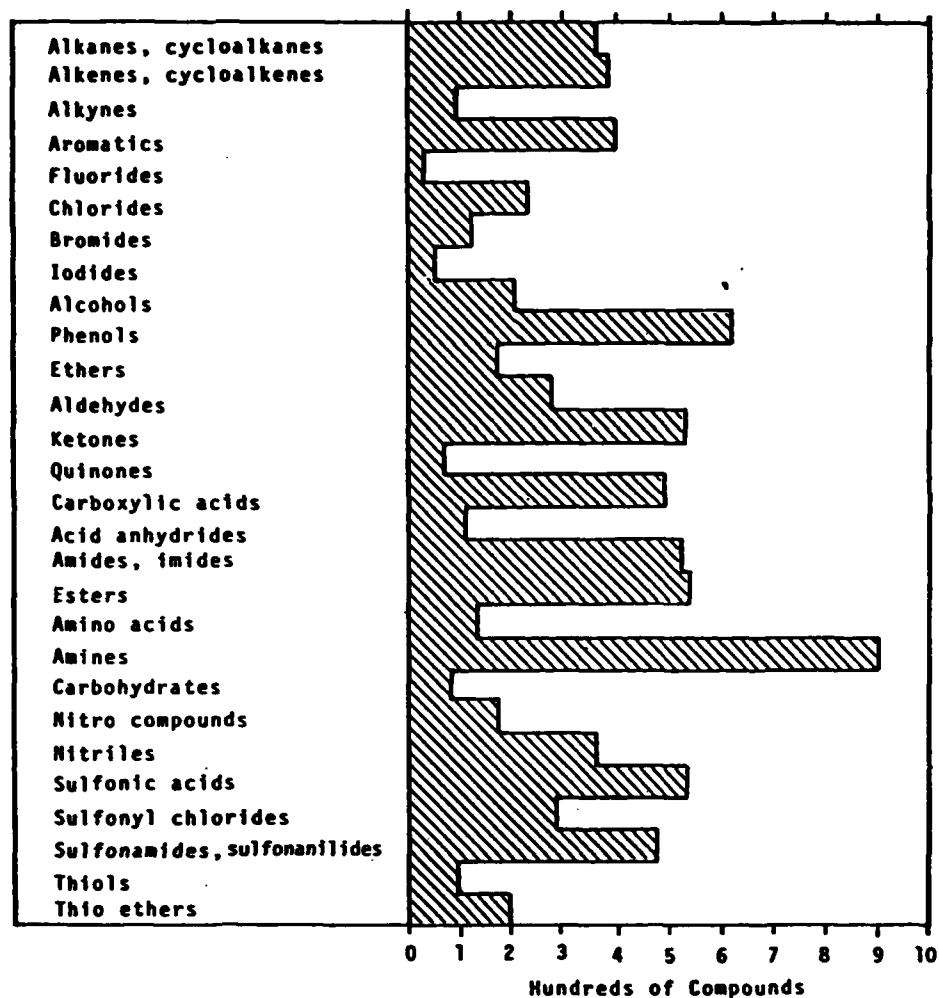


Figure 4. Occurrence frequency of the principal chemical groups in 8462 organic compounds and their derivatives. A compound may include functional groups listed above it, but not those listed below.

I. TABULATION OF LASER-BREAKDOWN THRESHOLDS OF SOLIDS

Even though the present concern with low-loss fibers is reducing the scattering and absorption in order to increase the useful length of fibers, laser damage of fibers is of interest in at least some applications. As seen in the compilation, only a small fraction of the laser-damage studies were specifically concerned with fibers, but the general damage results are also of interest in the study of fiber of course.

There have been so many experimental investigations of laser-damage of solids in recent years^{1,2} that a tabulation of the results should be useful. Smith³ tabulated a number of breakdown thresholds and discussed the theories of breakdown. The present paper is a tabulation of recent work in laser-induced damage. The principle source of information for this tabulation was the annual publication by the U.S. Department of Commerce and the National Bureau of Standards entitled "Laser-Induced Damage in Optical Materials."¹ The purpose of the tabulation is to provide an overview of the vast amount of data in the literature and to identify trends in the data.

The complete tabulation, which is rather long, will be presented elsewhere.⁴ The summary figures are included here as Figs. 1 through 27. The following materials are included in the complete tabulation, but deleted in the summary figures because only a few points were available: KF, RbCl, NaBr, NaI, KI, RbI, CsI, BeF₂, CdTe, GaAsP, GaP, ZnS, Ba₂NbO₁₅, Gd₂Ga₅O₁₂, KH₂PO₄, La₂Be₂O₅, LiIO₃, LiNbO₃, LiTaO₃, MgAl₂O₄, MgO, NH₄H₂PO₄ (ADP), SrTiO₃, TiO₂, YAlO₃, Y₃Al₅O₁₂, Ag₃AsS₃, As₂S₃, BK-7 glass, diamond,

CdCr_2S_4 , Cervit glass, KRS-5, KRS-6, LiYF_4 , and various glasses.

The most obvious feature of the results is large spread in the experiment results for the same material at the same wavelength. Possible sources of the great variation in results include the most likely source--

- extrinsic sources of damage that are different in different samples--

and the following other sources:

- inaccuracies in the irradiance resulting from inaccuracies in the focal-spot size, particularly that resulting from aberrations in the optical system,
- spatial- and temporal-spikes (regions of high irradiance) in the laser beam resulting from mode locking or multimode operation, for example,
- focal-volume dependence of the breakdown energy density resulting from fundamental effects (an unlikely source),
- focal-volume dependence of the breakdown energy density resulting from technical effects (such as a greater probability of having an easily damaged imperfection in the focal volume), and
- effects of different pulse shapes, both as functions of time and space.

The effect of including extrinsic sources of damage, aberration in the optical system, and easily damaged imperfections in large beams is to reduce the breakdown energy density; whereas the effect of regions of high irradiance (spikes) is to increase the breakdown energy density. It is likely that the larger values of the breakdown energy density are closer to the correct intrinsic

values because the samples without extrinsic sources of damage have greater values of the breakdown energy density. Thus, the larger values tend to be more representative of intrinsic results. This tendency is not universally true and can be misleading because larger experimental values can also be caused by spiking and possibly by other effects that have been overlooked.

Trends in the data are difficult to identify because the spread in the values is so great. Thus, the following trends should not be considered as fundamental or indicative of trends expected for a given controlled experiment. The breakdown energy density tends to increase with increasing pulse duration. The spread in data is too great to determine a meaningful relation between It_p and t_p , but the relations $It_p \sim t_p^{1/2}$ and $It_p \sim t_p$ are sketched for copper at $10.6 \mu\text{m}$ in Fig. 9, for fused silica at $1.06 \mu\text{m}$ in Fig. 22, and for sodium chloride at $10.6 \mu\text{m}$ in Fig. 19. For copper and fused silica, the relation $It_p \sim t_p^{1/2}$ is a better fit to the data; whereas, for sodium chloride, $It_p \sim t_p$ is a better fit. The great spread in the data prevents a convincing choice between even the $t_p^{1/2}$ and t_p trend.

The damage energy densities at $2.7 \mu\text{m}$ and $3.8 \mu\text{m}$ tend to be greater than at the other wavelengths. However, this tendency is largely accounted for by the longer pulse durations at $2.7 \mu\text{m}$ and $3.8 \mu\text{m}$. Otherwise, there is not a convincing trend of It_p as a function of wavelength on the region from $0.53 \mu\text{m}$ to $10.6 \mu\text{m}$. The lack of a striking wavelength dependence does not imply that the intrinsic breakdown mechanism is wavelength independent because the data here is believed to be largely determined by extrinsic processes.

In almost all of the pulsed-laser damage studied to date, for values of irradiance near the damage threshold the damage occurs at small isolated-spots within the laser beam rather than uniformly over the beam. The known possible sources of the isolated-spot damage are all extrinsic. Thus, extrinsic mechanisms for damage and for plasma initiation dominate intrinsic processes. In fundamental experimental investigations, intrinsic breakdown is studied by focusing a laser beam into a small volume of the bulk material away from the surface of the material. Many measurements are made, and those with low damage thresholds are ignored. There still is no way to verify that the large thresholds are intrinsic. A dramatic illustration of this uncertainty is the new high damage-threshold data from Manenkov and coworkers⁵ reported at the 1977 Boulder Damage Symposium. If corroborated, their new data implies that most previous damage thresholds measured at $1.06 \mu\text{m}$ were extrinsic, rather than intrinsic as previously believed.

One of the most important results from laser-damage studies, which is often overlooked, is that surface-damage thresholds are consistently low when large beams are used. For small beams, it is possible to obtain larger thresholds for some shots--those which miss the low-damage-threshold isolated spots. For damage by large laser beams, the single-pulse damage thresholds for various pulse lengths are as follows:

$\sim 1-10 \text{ J/cm}^2$,	for $\sim 10\text{ps}$ to $\sim 10\text{ns}$ pulses
few hundred J/cm^2	,	for microsecond pulses

These values are the same for metals, dielectrics, and coatings.

For comparison, the intrinsic, electron-avalanche-breakdown thresholds for alkali halides at $1.0\text{ }\mu\text{m}$ and 10ns are approximately $1.5 \times 10^3\text{ J/cm}^2$, which is two-to three-orders of magnitude greater than most of the large-beam surface damage values above.

REFERENCES FOR SEC. I

1. See for example the proceeding of the Boulder Damage Symposia. The latest published copy: NBS Spec. Pub. 541, 10th NBS-ASTM-ONR-ERDA-DARPA Symposium on Laser Induced Damage in Optical Materials, Boulder, CO, Sept. 12-14, 1978.
2. A. Glass and A. H. Guenther, Electro-Optical System Design, pp. 35-39, April 1979.
3. W. Lee Smith, Optical Engineering, Vol. 17, pp. 489-503, September-October 1978.
4. J. Sliney and M. Sparks, to be published.
5. A.A. Manenkov, New Results on Avalanche Ionization as a Laser Damage Mechanism in Transparent Solids, NBS Spec. Publ. 509 Symposium on Laser Induced Damage in Optical Materials, 1977, pp. 455-464.

FIGURE CAPTIONS FOR SEC. I

Figs. 1-27. Summaries of damage thresholds for materials with more than a few measurements. Very well characterized experiments are denoted • or x, and less well characterized experiments are denoted o or □.

J. OPTIMUM FREQUENCY RANGE

In this section it is shown that the choice of the optimum frequency between the reststrahlen- and electronic-absorption-edges involves compromises. The minimum extrinsic absorption is likely to be near $1\text{ }\mu\text{m}$. The zero-dispersion crossover, as the frequency at which $d^2n/d\lambda^2 = 0$ is called, occurs at longer wavelengths for most materials of interest. Also, the scattering is likely to be excessive at $1\text{ }\mu\text{m}$. Operation at frequencies below the fundamental reststrahlen-absorption peak should be considered.

The V-curves of Sec. G are useful in establishing the range of wavelengths over which a material can be used without being limited by intrinsic absorption or intrinsic scattering. The choice of the optimum wavelength within this region depends on such technical factors as reducing the extrinsic scattering and extrinsic absorption.

The optimum wavelength region between the reststrahlen-absorption peak and the electronic-absorption edge for minimum extrinsic absorption is expected to be near $1\text{ }\mu\text{m}$. The absorption peaks of molecular-ion impurities occur at longer wavelengths, as seen in Figs. 1-4 of Sec. H. Overtones can occur in the $1\text{ }\mu\text{m}$ region, but overtone absorption is weaker than the fundamental absorption. Electronic absorption is strong at wavelengths shorter than $1\text{ }\mu\text{m}$. See the tabulation of visible- and infrared-impurity-absorption spectra by Sparks, Vora and Flannery.¹ The lower absorption at $1.06\text{ }\mu\text{m}$ than at 2.7 , 3.8 , 5.25 , and $10.6\text{ }\mu\text{m}$ is seen in the figures in Sec. F.

The zero-dispersion crossover, in fiber-optics terminology, is the wavelength at which $d^2n/d\lambda^2 = 0$. The term dispersion, when referring to

the index of refraction n , has at least three meanings--the general wavelength dependence of n ; the values of $dn/d\lambda$; and the value of $d^2n/d\lambda^2$.

In order to avoid confusion, the dispersion of fiber optics, which is $d^2n/d\lambda^2$, will be called material dispersion. As explained in Sec. A, the material dispersion, along with the inherent dispersion of the mode that propagates in the fiber, determines the spatial spreading of the different frequency components of the information-carrying laser signal.

The frequencies at which $d^2n/d\lambda^2$ is zero are indicated on the V curves in Sec. G. The values were obtained from the minima of plots of $dn/d\lambda$. Such materials as fused silica, lithium fluoride, calcium fluoride, and sodium fluoride have zero-dispersion crossovers between 1 and 1.5 μm . Covalently bonded materials consisting of light elements tend to have their zero-dispersion crossovers at such short wavelengths, while ionically bonded materials consisting of heavy elements tend to have their zero-dispersion crossovers at longer wavelengths.

For the materials having $d^2n/d\lambda^2 = 0$ at short wavelengths, the extrinsic absorption and material dispersion can both be small in this wavelength region near 1 μm . Unfortunately, the scattering tends to be large at such shorter wavelength, at which the extrinsic absorption and dispersion tend to be greater for these materials. For such other materials as NaCl, KCl, KBr, KRS-5, KRS-6, AgCl, KI, CsBr and CSI that have $d^2n/d\lambda^2 = 0$ at longer wavelengths (between 3 μm and 6 μm for the materials listed), the extrinsic absorption is likely to be greater at the longer wavelength of zero-dispersion crossover.

Simultaneously achieving low material dispersion, low extrinsic absorptance, and low extrinsic scattering will require compromises in the

choice of materials and wavelengths. The intrinsic absorption and intrinsic scattering must be low also, but intrinsic scattering and absorption are expected to be negligible with respect to extrinsic scattering and absorption in most materials of interest, as discussed in Sec. G.

Consider an example. Lithium fluoride has zero material dispersion at $\lambda = 1.2 \mu\text{m}$. At this wavelength, the intrinsic absorption is entirely negligible, as seen in the figures in Secs. F and G, and the Brillouin-scattering coefficient is $\beta_B = 2 \times 10^{-3} \text{ dB/km}$. Thus, lithium fluoride is a candidate material, based on zero-dispersion crossover and intrinsic absorption and scattering, even though the zero-dispersion crossover at $\sim 1.2 \mu\text{m}$ is well away from the minimum of the V curves at $\lambda = 2.1 \mu\text{m}$ (from Sec. G). Such fundamental considerations only establish that lithium fluoride is a reasonable candidate. The more difficult task of determining whether the extrinsic scattering and extrinsic absorption can be reduced to tolerable levels involves technical factors, rather than fundamental ones.

As another example of material candidates, neither TI 1173 glass nor gallium arsenide would be good candidates for fibers with $\beta_{ex} \lesssim 10^{-2} \text{ dB/km}$ because intrinsic absorption and scattering process give $\beta_{ex} > 10^{-2} \text{ dB/km}$ for TI 1173 glass and $\beta_{ex} = 10^{-2} \text{ dB}$ at the minimum of the V curve at $\lambda = 6 \mu\text{m}$ for gallium arsenide.

Finally, operation at frequencies below the fundamental reststrahlen absorption peak should be considered. Extrinsic- and intrinsic-scattering and extrinsic absorption should be much less severe. It must be determined whether sufficiently low frequencies to avoid excessive intrinsic absorption,

especially at room temperature and above, can be used. Other fundamental and technical limitations should be carefully considered.

REFERENCES FOR SEC. J

1. M. Sparks, H. Vora, and M. Flannery, "Tabulation of Impurity Absorption Spectra - Ultraviolet and Visible, Volume I," Xonics, Inc. Ninth Technical Report, Contract DAHC15-73-C-0127, 30 June 1977;
M. Sparks, H. Vora, and M. Flannery, "Tabulation of Impurity Absorption Spectra - Ultraviolet and Visible, Volume II," Xonics, Inc. Tenth Technical Report, Contract DAHC15-73-C-0127, 31 December 1977.

K. CHOICE OF GLASS-, POLYCRYSTALLINE-, OR SINGLE-CRYSTAL-FIBERS.

Silica fibers are believed to be at the intrinsic-loss limit, after many years of investigation. New materials will be required in order to attain a loss less than the lowest silica-fiber value of 0.3 dB/km. It is too early in the low-loss-fiber program to choose between glass-, polycrystalline-, and single-crystal-fibers. The central issues that must be settled in order to make the choice are identified in the present section.

The overwhelming factor at present--the ease of fabrication of glass fibers--favors glass fibers. Any new glass-fiber candidate material must be fabricatable by drawing or by another process that avoids the current difficulties of fabricating crystalline fibers, or the advantages of the glass surely will be lost. This is especially important because some candidate glasses apparently cannot be drawn. Furthermore, the manufacturing of significant quantities of some glasses that can be made in small amounts may be impractical by current techniques.

If the ultimate intrinsic-operation limits could be attained, crystalline fibers would be favored. In particular, the limited number of glasses, the greater intrinsic scattering in glasses compared to crystalline materials, and the lower intrinsic absorption of many crystals favor crystalline fibers. Even though there are several candidate glasses, the small number of candidates is evinced by the statement¹ "...that ZnCl_2 glass, though water soluble, is a reasonable and possibly unique choice for meeting the above objectives [of attaining ultralow losses]." Single-component glasses are believed to be required to avoid excessive scattering.

In order to reap the potential benefits of crystalline fibers, the strong

scattering by several extrinsic processes must be greatly reduced. Scattering by both bulk- and surface-imperfections in current crystalline fibers, both polycrystalline and single-crystal, are shown in Secs. B through E to be extremely strong. A new fabrication method is needed for crystalline fibers. Removing the surface and bulk scattering should be the main goal of fabrication programs.

The problem of whether single-crystal fibers will be required or whether polycrystalline fibers will be satisfactory is currently overshadowed by the problem of whether any crystalline fiber--single-crystal or polycrystalline--can have sufficiently low scattering.

There are several sources of loss in polycrystalline fibers that do not exist in crystalline fibers. It is well known that contaminated grain boundaries are a major source of absorption loss in bulk polycrystalline materials. The original Kodak Irtran materials afford good examples of high loss resulting from contaminated grain boundaries. However, it was established in high-power laser-window studies that internally formed grain boundaries can be sufficiently clean to have negligible absorption, at least at the level of $\beta_{ab} = 10^{-4} \text{ cm}^{-1}$. Thus, grain-boundary contamination is not necessarily a problem, but it is not known whether polycrystalline fibers can be manufactured with sufficiently clean grain boundaries to avoid excessive absorption and scattering, especially at $\beta_{ex} \approx 10^{-8} \text{ cm}^{-1}$.

An important method of strengthening materials is to use polycrystalline materials and reduce the grain size. Thus, small-grain polycrystalline fibers are expected to be stronger than single-crystal fibers. Grain growth is likely to be a problem. However, alkali-halide crystals grown by the reactive-atmosphere process are free of OH^- ions and do not show grain growth. The

strength of polycrystalline- and single-crystal fibers was considered by Harrington, Turk, Henderson, and Myer.²

Fredricks³ pointed out that single-crystal alkali-halide fibers may have a characteristic that will limit their usefulness. When alkali halide crystals bend, they do so by sliding on the $\langle 100 \rangle$ planes, thereby forming a set of steps around the corner. Also, once bent, the fiber is likely to break on the next attempt to bend it. The bonding between adjacent $\langle 100 \rangle$ planes is markedly weaker than any other planes in the sodium-chloride structure. The steps formed in typical bending are large with respect to the wavelength of the light. The resulting scattering will be intolerably great, as shown in Sec. B. Fittings could be used, with straight sections of fiber in between fittings, but this solution would surely be impractical in many applications. Installation would be a problem. The bending effect would limit the size of the take-up reels used in producing the fibers.

Processes other than extrusion are of current interest because current extrusion processes have been unsuccessful. Fredricks has made suggestions to improve extruded fibers. First, it may be possible to extrude crystalline fibers with smooth surfaces. Surface layers of current extruded potassium-chloride fibers² split from the main fiber in a rather regular pattern, somewhat like fish scales or like a banana whose skin had been partially peeled so that the peels form an acute angle with the meat. Fibers are made by extruding a potassium-chloride crystal through a parabolic orifice diamond die at 300-400°C. The potassium-chloride fiber must have $\langle 100 \rangle$ planes parallel to its axis and, of course, transverse to it. This puts the weak crystallographic

directions in the proper orientation to form the surface scales.

If the surface tensions, γ , of potassium-chloride, diamond, and the surrounding atmosphere are such that the inequality

$$\gamma (\text{diamond} - \text{gas}) + \gamma (\text{diamond} - \text{KCl}) < \gamma (\text{KCl} - \text{gas}),$$

is valid, the potassium-chloride will wet the diamond. In addition, a second attractive force between potassium-chloride and the diamond die can be generated if the hydrostatic pressure used to extrude the fiber is sufficient to reduce the $\langle 100 \rangle$ steps, which separate the potassium-chloride - diamond surfaces, to less than 100 nm. This is an induced-dipole force, or van der Waals force. A common example is the attractive force between two Johnson blocks. These highly polished blocks cannot be easily pulled apart, but must be slid along the polished surfaces to be separated.

Data on surface-tension measurements between diamond - potassium-chloride - gas systems has not yet been found. Even if they were available they would have to be used with caution as trace water changes the properties greatly. The induced-dipole forces will be a function of the extrusion force and roughness of the die.

As the potassium-chloride crystal is extruded through the die, it becomes strongly bound to the diamond. As it exits the parabolic orifice it tends to follow the surface of the die until the fiber splits on the $\langle 100 \rangle$ cleavage planes parallel to the fiber axis and then breaks on the transverse $\langle 100 \rangle$ cleavage planes. Since both surface tension and induced-dipole forces tend to retard the surface planes when the surface "peels" back, the scales bend slightly away from the fiber as they attempt to relieve the internal strain. There must be a minimum of four peels around

the fiber. More can be present if grain boundaries occur across the fiber axis.

This scaling effect can be avoided by reducing the attractive forces between potassium-chloride and the die. The surface-tension problem can be avoided by using dry potassium-chloride and a quartz die. The van der Waals attraction can be reduced by lowering extrusion pressures, and the tendency for splitting lessened by removing the parabolic exit on the die. The exit should be cut square or at a small angle above the exit hole of the die.

Molten potassium chloride could be extruded through a quartz orifice and either recrystallized as one does for wire, or for a more practical fiber quenched to a glassy state. A rather simple apparatus could be constructed from a quartz crucible with a quartz capillary attached to its bottom. The capillary is drawn to fiber size and cut square. The top of the crucible and the tube enclosing the orifice must be sealed to allow hydrogen chloride flushing. After flushing, the potassium chloride would be quenched by cooled argon blown against the orifice and down the enclosing tube around the fiber. If these fibers have satisfactorily optical properties, a take-up spool could be added to obtain longer samples.

There is a possibility that Fredricks could carry out an experimental program to obtain improved extrusion at Oregon State University if there is interest.

REFERENCES FOR SEC. K

1. L. G. van Uitert and S. H. Wemple, Appl. Phys. Lett. 33, 57 (1978).
2. J. A. Harrington, R. Turk, M. Henderson, and J. Myer, Infrared Fiber Optics, Interim Technical Report, Contract F19628-78-C-0109, July 1979.
3. Professor William Fredricks, Oregon State University, consultants report on this contract, 1980, unpublished.

L. PUBLICATIONS

- M. Sparks, "Ultralow-loss Optical Fibers," invited paper at the Tenth Winter Colloquium on Quantum Electronics, Snowbird UT, Jan. 13-16, 1980.
- M. Sparks, "Ultralow-loss Optical Fibers-Theory," invited talk and paper at the IRIS Specialty Group on IR Optical Materials, Sand Point Naval Air Station, Seattle, Washington, in conjunction with the 28th National IRIS, May 19-22, 1980.
- D. L. Mills, "Light Scattering by Point Defects," J. Appl. Phys., in press.
- W. Fredricks, Low-Loss Optical Fibers, unpublished.
- M. Sparks, "Tabulation of Infrared Absorption Coefficients," to be published.
- M. Sparks and L. Dixon, "Effects of Temperature-Dependent Absorptance in Optical Materials," to be published.
- J. Sliney and M. Sparks, "Tabulation of Laser-Damage Thresholds of Solids," to be published.
- M. Sparks, "Absorption and Scattering Phenomena in Thin-Film- and Bulk-Materials," invited presentation at the Topical Conference on the Basic Optical Properties of Materials, May 5-7, 1980, held at the National Bureau of Standards, Gaithersburg, MD.

M. SUMMARY & CONCLUSIONS

After many years of research, fused-silica fibers are believed to be at their intrinsic-loss limit, which is an extinction coefficient of $\beta_{ex} = 0.3$ dB/km at the minimum of the V curves at a wavelength near $1.6 \mu\text{m}$. Thus, new materials will be required in order to attain a lower loss.

The V curves, as the plots of the intrinsic-scattering coefficient and intrinsic-absorption coefficient are called, are useful in coarse screening of candidate fiber materials and in establishing the useful wavelength region of a given material, as illustrated in Fig. 8 of Sec. G. For low-loss fibers, with extinction coefficients $\beta_{ex} \ll 0.1$ dB/km $= 2.3 \times 10^{-7} \text{ cm}^{-1}$, both the scattering and absorption for wavelengths within this useful wavelength region are determined by extrinsic processes in most materials of interest.

In communications applications, it is usually necessary to operate within a narrow wavelength region near the zero-dispersion-crossover wavelength λ_{0d} , which is the wavelength at which $dn^2/d\lambda^2 = 0$, where n is the real part of the index of refraction. Thus, the problem of obtaining a satisfactory fiber material is as follows: (1) Find a material with λ_{0d} near the operating wavelength (or conversely, choose the operating wavelength equal to λ_{0d} for the most promising candidate material, if possible). (2) Verify that the intrinsic loss, given on the V curves in Sec. G, is at or below the required value. It is not necessary that the minimum of the V curve fall near λ_{0d} . It is sufficient that λ_{0d} is in the useful wavelength region. (3) Improve the material purity and fiber-fabrication process to obtain the required low value of absorption and scattering.

This last step of reducing the extrinsic absorption and extrinsic scattering is expected to be difficult for low-loss fibers. In Secs. B through E, it is shown that any one of several scattering mechanisms can give rise to a scattering coefficient that is five to eight orders of magnitude greater than the typical goal of $\beta_{\text{ex}} = 10^{-2}$ dB/km. In Sec. H it is shown that impurities at the level of approximately 10^{-4} parts per billion, which is too low to even measure for important impurities, can give rise to an absorption coefficient of $\beta_{\text{ab}} = 10^{-2}$ dB/km.

The success of the low-loss fiber program depends on the ability to solve the technical problems of purifying materials and maintaining their purities during fabrication, installation, and field use in order to obtain low extrinsic absorption and scattering and of fabricating fibers with low scattering loss that will remain low during installation and operation. These severe problems are in addition to usual problems of obtaining claddings, achieving index gradation, coupling fiber sections together, and obtaining sufficiently strong fibers. This pessimistic picture establishes the priorities in the low-loss fiber-optics program, rather than suggesting that the program cannot succeed. After all, a loss of ~ 0.3 dB/km has been attained in spite of the difficulties.

It is too soon in the low-loss fiber program to choose between glasses, polycrystals, and single crystals. The problem of choosing between single-crystal fibers and polycrystalline fibers is overwhelmed at present by the problem of whether any crystalline fiber can have sufficiently low scattering. The choice between polycrystalline- and single-crystal-fibers cannot be made until the excessive scattering problem of crystalline fibers

is solved. Nevertheless, the issues involved in the choice between single-crystals and polycrystals, as well as the choice between glasses and crystals, are discussed in Sec. L.

Ease of fabrication is an overwhelming factor in favor of glasses that can be drawn as successfully as fused silica. The limited number of glasses, the greater intrinsic scattering and absorption in glasses than in crystals, and the difficulty in manufacturing large quantities of some glasses favor crystalline fibers. It is possible that single-crystal alkali-halide crystals may not be useful, even if satisfactorily fabricated, because bending the fiber would result in surface imperfections ($\langle 100 \rangle$ "steps") that would cause excessive scattering, and multiple bendings may cause fracture. An improved extrusion method suggested by Fredricks and discussed in Sec. L possibly could result in greatly improved extruded fibers.

The choice of the optimum frequency, for frequencies between the reststrahlen- and electronic-absorption edges, involves compromises. The minimum extrinsic absorption is likely to be near $1 \mu\text{m}$. The zero-dispersion crossover occurs at wavelengths longer than $1 \mu\text{m}$ for most materials of interest. Also, the scattering is likely to be excessive at $1 \mu\text{m}$. Operation at frequencies below the fundamental reststrahlen-absorption peak should be considered.

Intrinsic-Brillouin and intrinsic-Rayleigh scattering, which determine the lowest possible scattering that can be attained in fiber materials, have typical scattering coefficients $\beta_{sc} = \beta_B + \beta_{int R}$ of $1 \times 10^{-9} \text{ cm}^{-1} = 4 \times 10^{-4} \text{ dB/km}$ for lithium fluoride to $8 \times 10^{-7} \text{ cm}^{-1} = 0.4 \text{ dB/km}$ for zinc selenide, both at wavelength $\lambda = 1 \mu\text{m}$. The total intrinsic scattering coefficient, for Brillouin and intrinsic Raman scattering,

can be much greater, by a factor of 40 in the examples considered, than the Brillouin scattering, in contrast to the tacit assumption made in the standard practice of using the Brillouin scattering as that of the V curves for crystalline materials. Electronic scattering from vacancies or impurity ions that are either isolated or in small clusters is negligible, but electronic scattering from extended imperfections, such as precipitates, grain boundaries, Suzuki phases, and dislocations can be great.

The substantial variations in both the laser-breakdown thresholds and the amount of scattering that is observed as various regions of crystal are probed are explained in terms of the distribution of impurities and imperfections, which change in time. Quenching temporarily reduces clustering, thereby reducing scattering and possibly isolated-spot laser damage; whereas annealing temporarily increases clustering, thereby increasing scattering and possibly isolated-spot laser damage. Clusters are expected to form in time even in quenched crystals, and OH^- and H_2O substantially penetrate alkali-halide crystals if they contain a few parts per million of divalent ions.

The substantial variations in both the laser-breakdown thresholds and the amount of scattering that is observed as various regions of crystal are probed can be understood as follows: Even though the brief review in Sec. C-III. of the current state of impurity chemistry in the simplest ionic solids, the alkali halides, is far from extensive, it should dispell the common view that simple point defects are the predominate impurity species in alkali halides. Furthermore, most textbooks create the impression that these "simple point

defects" are frozen in some reasonably homogeneous distribution at room temperature. There is ample evidence that this is not true.

In Sec. D it is shown that the scattering by the strain field around an impurity ion is negligible and cannot account for the well-known difference between the ion radius and the effective radius for scattering. In Sec. E it is shown by developing a multiple-scattering formalism and applying the results to scattering by randomly located spherical voids that the multiple-scattering reduction of the individual scattering results is entirely negligible in low-loss fibers because the scattering must be small and multiple-scattering effects are negligible for small scattering.

The lowest experimental values of infrared optical-absorption coefficients from the literature are tabulated in Sec. F as plots of absorption coefficients as functions of frequency. Both intrinsic and extrinsic values are tabulated. The intrinsic, multiphonon absorption curves must be extrapolated in order to obtain the low values of current interest because the state of the art in reducing the absorption coefficient of window materials, and even in measuring the absorption coefficients, limits the values of β to approximately 10^{-4} cm^{-1} to 10^{-5} cm^{-1} (44 to 4.4 dB/km). These extrapolated curves are given as the absorption parts of the V curves in Sec. G. Laser-damage thresholds in solids, including fibers, are tabulated in Sec. I. Publications produced in the study are listed in Sec. L.